UNIVERSITY OF SOUTHAMPTON

INVERSE DETERMINATION OF STRUCTURE-BORNE SOUND SOURCES

by

Anand Narasinha Thite

Thesis submitted for the degree of
Doctor of Philosophy

Institute of Sound and Vibration Research
Faculty of Engineering and Applied Science

January 2003

UNIVERSITY OF SOUTHAMPTON

ABSTRACT

FACULTY OF ENGINEERING

INSTITUTE OF SOUND AND VIBRATION RESEARCH

Doctor of Philosophy

INVERSE DETERMINATION OF STRUCTURE-BORNE SOUND SOURCES

Structure-borne sound from installed machinery is often transmitted into the receiver structure via many connection points and several coordinate directions at each of them. In order to quantify the contributions from the various connection points and directions, the operational forces at the interfaces should be determined. If these are determined indirectly, two sets of measurements are required: the operational responses at a series of positions and a set of frequency response functions (FRF's). A matrix of measured FRF's has to be inverted at each frequency in order to obtain the forces. The indirect force determination is prone to errors. The forces can contain large errors introduced by the combination of *errors in the measurement* of operational responses and FRF's and *ill-conditioning* of the FRF matrix at certain frequencies.

Although a lot of work has been carried out in the past to improve force determination some limitations still remain. This thesis will contribute to advancement in the solution of inverse problems in structural dynamics, specifically by the use of regularization techniques and response location selection methods.

Initially existing methods, over-determination and singular value rejection, have been explored for their improvement in reconstruction of forces. Simulations have been carried out to represent measurements on a rectangular simply supported flat steel plate with suitable added noise. The 'measured' data is then used to establish the effectiveness of the various methods. The performance of various thresholds for the rejection of singular values, based on either response errors or accelerance errors, is investigated. Both of these thresholds have been found to perform with varying degrees of success when the noise levels in the measurements are varied. Some improvements such as the

use of a different tolerance level and a cumulative sum of singular values have been proposed for singular value rejection methods.

The relative performance of different FRF estimators has also been studied in this thesis. Out of five estimators considered, the conventional H_1 estimator has been found to be more reliable under all conditions of measurement noise considered.

The resampling of the accelerance matrix has been proposed which is then implemented practically by a perturbation of the accelerance matrix. This method has been found to take account of FRF errors reliably. But it is sensitive to the errors in responses measured. The concept of rejecting perturbed singular values has been developed to take account of shortcomings in matrix perturbation and the singular value rejection. This method has been found to be robust against any level of noise in the measurements of operational responses and the FRF's.

Two regularization techniques, iterative inversion and Tikhonov regularization, have been explored in the next stage. Although these are not new, they have not previously been applied to structural dynamics problems rigorously. A direct comparison is made of Tikhonov regularization and singular value rejection. Initially the regularization parameter is selected based on ordinary cross validation (OCV). The performance of OCV for structural dynamics problems is analysed. A new method called selective cross validation (SCV) for selecting the regularization parameter is then proposed. To take of account of large condition numbers at resonances in conjunction with small response errors, modifications referred to as biased OCV and SCV are proposed to limit the error amplification.

Iterative inversion has been studied and a formulation relevant to structural dynamics is developed. Cross validation techniques based on a single response and multi-responses have been developed to enable selection of the iteration number. Although iterative inversion results in robust performance for all levels of noise in the measurements, it takes much more computing time to arrive at the solution than Tikhonov regularization.

Sensor selection methods from modal testing have been explored to improve the inverse force determination. A new method based on condition numbers of the

accelerance matrix has been developed. This method results in encouraging improvements in force determination.

Experiments have been conducted on a hanging rectangular flat plate and a built-up structure. All the methods studied above have been validated using the experimental data for these experiments.

LIST OF CONTENTS

ACKNOWLEDGEMENT

I would like to express my sincere gratitude to my supervisor Dr. David Thompson for his guidance and encouragement. His inputs and the regular discussions I had with him provided greater depth to the project.

I wish to acknowledge valuable advice and useful comments of Dr. Tim Waters and Dr. Neil Ferguson. Thanks are also to Professor Phil Nelson, Dr. M Blau and staff at TNO TPD Delft for their suggestions.

I am grateful to the ISVR for funding the fees and maintenance grant. Many thanks are also to all ISVR staff and colleagues in the Dynamics Group for all the help and encouragement.

Finally, I would like to thank all my family members, my parents, father- and mother-in-law for their encouragement and constant support. Last but not least I am greatly indebted to my wife Mohini for all the encouragement and sacrifices she has made. The arrival of our son Kartik has encouraged me go that extra step in the work.

LIST OF SYMBOLS

a	true operational response,
	largest dimension of the plate
a_i^r	directly reconstructed i^{th} response
a_{ui}	i^{th} response made independent of orthonormal vector in Chapter 9
$\breve{a}$	directly reconstructed operational response
$\tilde{a}$	directly reconstructed operational response with regularization
$\hat{a}$	measured operational response
$\tilde{a}_{valid}$	validating reconstructed operational response
$\hat{a}_{valid}$	measured operational response
b	smaller dimension of the plate
	$\hat{A}^H \hat{a}$ in Chapter 5
	theoretical bias error in Chapter 6
$\hat{b}$	estimated bias error
c	correlation coefficient
	constant in Chapter 6
	$\hat{a}^H \hat{a}$ in Chapter 5
c_L	longitudinal wave speed in the plate
$\tilde{e}$	the fitting error
$f_{crossover}$	cross over frequency in Hz where added mass of transducer starts to
	influence base structure dynamics significantly
g	complex gradient
h	thickness of the plate
i	index for response measurement location,
	unit imaginary quantity
j	index for force application location
k	sample of time history at response location,
	index of singular values in Chapter 3,
	response index in Chapter 5 and
	iteration number in Chapter 6

m	number of locations for acceleration measurement
m_{ad}	added mass of the transducer
m_{all}	locations that are candidates for measuring the operational response
m_{plate}	mass of the plate
n	number of forces used to represent the source
n_d	asymptotic modal density
n_{av}	number of samples used for averaging to estimate FRF's
n_s	number of samples used to estimate the operational responses
$\hat{p}$	reconstructed response at the receiver location
p,q	mode index, indicators for responses in Chapter 9
r	residual, index of singular values in the reverse order in Chapter 3 and correlation indicator between impulse responses
s	singular value of a matrix
t_k	particular instant of time
u	element in orthonormal row vector
x, y	co-ordinates indicating location of response measurement
x_1, y_1	co-ordinates indicating location of force application
x_{ij}	average of the condition numbers over the frequency range corresponding to responses at locations i and j

A	true frequency response functions (accelerance)
A_{pert}	perturbation matrix used to perturb accelerance matrix
$\hat{A}$	measured frequency response function (accelerance) from forcing location to the response measurement location
B	$\hat{A}^H \hat{A} + I\lambda$ in Chapter 5
C, $C_{1,2}$	constants
D	bending stiffness

E	Young's modulus of the material, FRF error in Chapter 3 and expected value in Chapter 6
F	true estimated force
F_e	reconstructed force error
$\hat{F}$	estimated force
$\hat{H}$	measured frequency response function between the force location and the receiver location
H_1, H_2, H_4 H_v, H_s	frequency response function estimators
^{H}	indicates the Hermitian transpose
I	unit matrix
$L_{\hat{F},j}$	reconstructed j^{th} force in 1/3 octave bands in dB
$L_{F,j}$	actual force in 1/3 octave bands in dB
M_{pq}	modal mass
N	number of 1/3 octave bands b in the frequency range considered, indicates random numbers in Chapter 2
N_{in}	random noise spectrum added to the input (X)
N_{out}	random noise spectrum added to the output (Y)
$N_{nd,1}$, $N_{nd,2}$	normally distributed random numbers with mean 0 and standard deviation 1
$N_{ud,1}$, $N_{ud,2}$	uniformly distributed random numbers in the range 0 to 1
R_e	reconstructed receiver response error
S	matrix of singular values, surface area of the plate
S_{xy}	cross spectrum between X and Y
S_{xx}	power spectrum of X
U	unitary matrix containing eigen vectors of $\hat{A}^H\hat{A}$
V	unitary matrix containing eigen vectors of $\hat{A}\hat{A}^H$
VE	validation error
X	'measured' time history of force,

	amplification factor in Chapter 9
Y	'measured' time history of acceleration
α	band-width determining the confidence limit on measured FRF's
β	convergence parameter
δ_k	$Udiag(\phi_1,.....\phi_n,0_{n+1},...0_m)U^H$
ε	response error
ε_b	bias introduced due to regularization
ε_b'	bias introduced due to regularization
ε_{force}	average force error in dB
ε_k^2	mean square error in reconstructed response for k^{th} iteration
$\varepsilon_{reconst}$	direct reconstruction error
ϕ_i	$1-(1-\beta s_i^2)^{k+1}$ in Chapter 6
γ	square root of the coherence between X and Y, exponential decay rate in Chapter 6
κ	condition number of the matrix based on matrix 2-norm
λ	regularization parameter in Tikhonov regularization
μ	structural damping loss factor for the material
ν	Poisson's ratio of the material
ρ	mass density of the material
σ_p	standard deviation of the underlying process for which forces are determined
σ	standard deviation indicating the 68% confidence on the measured response
ω	rotational frequency in radians
ω_{pq}	natural frequency of the mode (p, q)
ψ_i	$\frac{1-(1-\beta s_i^2)^{k+1}}{s_i}$ in Chapter 6
ψ_{pq}	mode shape function of pq^{th} mode

Δ	square of the deviation in OCV and SCV
Λ	matrix that contains square of singular values as diagonal elements
$\hat{}$	symbol to indicate quantity has been estimated from measurements
$\|\|.\|\|_2$	2-norm of the matrix
$\|\|.\|\|_F$	Frobenius norm of the matrix

CHAPTER 1
INTRODUCTION

1.1 VEHICLE NOISE AND TRANSFER PATH ANALYSIS

The acceptability of the interior and exterior noise levels generated by automotive vehicles is one of the important performance criteria determining their competitiveness and comfort. Numerous mechanisms exist in the vehicle which result in noise in the interior and on the exterior of the vehicle. Over the years the noise level targets for road vehicles have been substantially lowered – exterior noise because of legislation [1] and interior noise because of customer demand. Consequently noise contributions by dominant sources have been reduced significantly. For example, due to developments in the automotive vehicle design, contributions from dominant sources such as the engine have reduced [2]. Therefore, the noise tends to be made up of contributions from multiple sources, all of which play an important role, instead of a single dominant source. These sources transmit noise to the interior of the vehicle through various paths which may be separated into air-borne paths and structure-borne paths [3].

Air-borne noise is transmitted into the vehicle due to acoustic excitation of the various panels. This in turn is due to the disturbance introduced by the source on the surrounding air. On the other hand, structure-borne sound is transmitted as vibrational energy from the source, for example the engine, through mounts and other structural connections, and passes through the structure to interior panels which radiate into the cabin. In both of these cases the source could be at some distance from the receiver and the energy transmission could be through complicated multiple paths. Solving problems of such a high complexity, particularly the structure-borne noise case in which energy can be transmitted in different wave types, requires detailed knowledge of the paths and the relative contribution from each of these paths. In recent years, experimental analysis tools have been developed which help in understanding these paths and their contribution, and which have found wide application in the automotive industry as well as other sectors. Such tools are known by a variety of names, including transfer path analysis or noise path analysis [4-5].

Transfer path analysis (TPA) is a means of quantifying the contribution of sound or vibration, transmitted through various paths from a source to a receiver location. These paths could be either air-borne or structure-borne. Basically, it involves the estimation of source strengths and the contributions due to these sources via different paths to the response at the receiver location. For structure-borne paths, particularly where the source structure is resiliently mounted, the source strength, in the form of the forces applied to structure, can be estimated by measuring the displacements across the mounts and using this together with a known mount stiffness [6]. Alternatively the force applied at the interface between source and receiver structures can be determined indirectly. Responses are measured at a series of locations due to the operational source and these are used in combination with accelerances or mechano-acoustic transfer functions measured from source locations to these response locations [7-8]. Such forces may also be required as inputs to numerical models [9].

Structure-borne sound from installed machinery is often transmitted into the receiver structure via many connection points and several coordinate directions at each of them. In order to quantify the contributions from the various connection points and directions, the operational forces at the interfaces should be determined. Alternatively, an equivalent set of forces at some other locations may be used to characterise the transmission [7]. The accuracy with which these forces can be obtained determines the suitability of the application of experimental methods such as transfer path analysis or numerical simulations as tools in understanding the noise problem at hand and ultimately reducing the noise at the receiver location.

If the forces causing structure-borne noise have to be determined indirectly, two sets of measurements are required. First the responses $\hat{a}$ are measured at a series of locations due to the operational source. Second, frequency response functions (FRF's) $\hat{A}$ are measured from a set of source locations to these response locations. The response measurement locations have to be chosen such that the responses measured there can capture contributions from all possible paths involved. Since the forces F should satisfy $\{a\}=[A]\{F\}$, or for measured quantities $\{\hat{a}\}\cong[\hat{A}]\{\hat{F}\}$, a matrix of measured FRF's has to be inverted at each frequency in order to obtain the forces. On the other hand, no knowledge of the structure is required other than this set of measurements.

It may be seen that indirect force determination is prone to errors. The forces can contain large errors introduced by the combination of *errors in the measurement* of operational responses and FRF's and *ill-conditioning* of the FRF matrix at certain frequencies. It is a prerequisite for effective transfer path analysis that the forces determined are reliable. In this thesis, research has been carried out into methods to improve the reliability of inverse force determination.

1.2 LITERATURE REVIEW

The literature review in this section covering the subject of transfer path analysis is divided into four sections; force determination, errors in forces determined by inverse methods, regularization techniques and measurement location selection.

1.2.1 Force determination

The study of transfer paths, although previously well established for the unidirectional case with soft mountings, was first considered in detail for the full case of multidimensional coupling including the effects of flanking paths by Verheij [6-8]. In [6], each mount of a diesel engine was modelled by 36 transfer functions. Assuming a large impedance mismatch at the mounting surfaces, relative velocity measurements in all six directions across the mount were then used to estimate the forces and moments transmitted across the mount. These forces were assumed to act as point forces at the centre of each mounting surface. The forces could then be used to estimate the sound transmission to the receiver location.

Later Verheij [7] used un-correlated point forces to describe large mechanical sources while compact sources were represented in terms of correlated forces. The equivalent force concept was introduced, in which the forces estimated differ from the actual forces due to the use of different forcing points. These were estimated using inverse methods. The method of singular value rejection was introduced in this work in order to improve the conditioning of the matrix inversion (see Appendix A). Smaller singular values were rejected if they were corrupted by noise. A threshold to reject singular values was established based on accelerance measurement errors based on work by Powell [10]. The equivalent forces method was then applied to studying sound

transmission paths [8] for a ship engine and gearbox. Janssens, Verheij and Thompson [11] applied this method to flanking paths of a diesel engine on a ship, in particular the drive shaft and cooling water pipes. In addition a covariance matrix along with Monte Carlo simulation was used to estimate the error bounds for forces that were determined. A relationship for the propagation of the errors to the receiver responses was established.

It was shown by Janssens and Verheij [12] that the pseudo-forces (or equivalent force) method respects the multi-dimensional interaction between a source and its mounting structure. The importance of the coupling between the source and receiver was emphasized and various indirect force measurement techniques were reviewed. In a recent study, the pseudo-forces method was applied to a study of sound transmission paths from a compressor [13]. Different sources of error and the bounds caused by them were studied. A different singular value rejection threshold was proposed which is based on errors in the operational responses.

Van der Auweraer et al [14] give an introduction to transfer path analysis. Approaches for handling both coherent and in-coherent forces are presented. To allow for incoherent forces, a spectral matrix was used in estimating the forces. As suggested by Verheij [6], each mounting degree of freedom (DOF) was taken to define a transmission path. The singular value decomposition as a tool to understand source identification was extensively studied by Otte [15]. Commercial software, eg [4], has helped further to popularize the transfer path analysis method. Some applications in the automotive industry have also been published in recent years [9,16-21]. Recently sound quality analysis has been incorporated with transfer path analysis to enhance the capability and cover the entire noise and vibration problem [18-19].

In the literature reviewed so far the excitation forces were either calculated by assuming a large impedance mismatch or by inverse methods in the frequency domain. Even if there is a large impedance mismatch at the mounting surface, the measurements required may be considerable and difficult to perform accurately. This difficulty restricts the applicability in many cases. On the other hand, in the inverse methods the forces determined may contain large errors due to ill-conditioning of the accelerance matrix and errors in the measurements. Dobson and Rider [22] reviewed different inverse methods. In particular two methods other than direct inversion were considered; one based on a

modal transformation and the other based on the use of impulse responses in the time domain. No difference in performance was observed by using these methods. The application of inverse methods for other purposes in structural dynamics, in particular structural identification and model updating is reviewed by To and Ewins [23]. In the remainder of this thesis attention is restricted to the inverse method in the frequency domain.

1.2.2 Errors in forces determined by inverse methods

As has been indicated earlier, forces determined by inverse methods often involve large errors. This is due to a combination of measurement errors and high condition numbers of the accelerance matrix to be inverted [63-68]. This is true particularly at frequencies where the condition number of the accelerance matrix is high.

Fabunmi [24] reasoned that the errors in force estimation are due to the number of modes contributing to the response at certain frequencies being less than the number of forces to be determined. In this situation, the condition numbers of the matrix to be inverted become large and the forces determined contain large errors. Over-determination of the system [67], i.e. using a larger number of responses than the number of forces to be determined, does not make any difference for the above situation. Desanghere and Snoeys [25] observed that the errors might be reduced if a modal transformation is used. However, the condition suggested by Fabunmi [24] is still relevant and associated errors remain.

To improve the reliability of force determination it is necessary that the error propagation and amplification due to the inversion is known completely. Mas and Sas [26] explored the errors in force determination due to causes other than condition number of the accelerance matrix. For highly damped structures other causes were found to be more important than the condition number. The error amplification was at most a factor of the condition number. It was observed that the absolute errors in force estimation were the same at a given frequency for all the forces. Thus the smaller forces tend to have larger relative error. It was suggested that over-determination should be used to improve the condition of the matrix. It was also concluded that if any of the inputs (paths) were

neglected, then the errors in the determination of the other forces would be proportional to the neglected force.

Hendricx [27] considered the effect of the accuracy of FRF measurements on force determination. A comparison was also made with the mount stiffness method. Using shaker excitation the results of force determination were found to compare better with those of the mount stiffness method than those obtained using impact hammer excitation.

Karlsson [28] suggested using the reciprocal of the condition number as a measure of the sensitivity of the force determination to errors. He further concluded that over-determination does not make much difference to force determination errors, although the response errors reduce with the use of over-determination. The least square error in the operational responses reconstructed from the forces was suggested as a measure of error in force determination.

Error bounds for force determination were derived statistically by Lee and Park [29] based on the assumption that the error in the FRF was smaller than the FRF itself. It was shown that the force determination error is directly proportional to the Frobenius norm (see Appendix A) of the FRF matrix as well as the errors in the FRF matrix and the response vector. For a square matrix, it was predicted that the force errors would be highest at anti-resonance, while errors at resonance would be dependent on the FRF error rather than rank deficiency, which is contrary to Fabunmi's conclusion [24]. It was concluded that by using over-determination, errors were reduced at anti-resonance while at resonance errors still depend on the FRF error.

Unfortunately, none of the literature reviewed above gives results in terms of objective measures of error that can occur in forces determined by inverse methods or how they propagate in the process. This issue was addressed by Roggenkamp and Bernhard [30-31], who derived quality indicators for forces determined at each frequency. Since the errors in force estimates are due to high condition numbers of the accelerance matrix, which magnify any errors in the responses and FRF's, a relative error bound for force estimates was derived using the condition number and the relative error in the response vector or the FRF matrix. Error bounds were placed on the force vector rather than on individual forces. In fact, it was suggested that bounds could not be placed

on individual forces. Over-determination was recommended only if the FRF matrix condition number is reduced as a result. The error bounds so estimated were found to be very conservative and to result in excessively large error estimates.

In more recent work by Blau [32-34], quantitative models were developed to characterise the contributions from various sources to the sensitivity of the inverse force determination. Unlike in [30-31], the estimations were made on individual forces rather than restricting consideration to the norm of vectors. Force estimates were characterised by their auto and cross spectral densities. Considering the sources of error, it was suggested that improvements should be made to measurement methods and processing in order to reduce the errors in the force estimates. For example, the effect of frequency resolution on error amplification was quantified empirically so that appropriate resolution could be selected. Nevertheless, these recommendations are over-complicated for practical implementation, so that it may be expected that errors will remain; the issue then is to minimize their effect.

1.2.3 Regularization techniques

To improve the force determination, attempts have been made to reduce the ill-conditioning of the accelerance matrix by rejecting singular values. Small singular values are more prone to contamination by noise, and this has a large effect on the matrix inversion. By rejecting these singular values (setting them to zero) the inverse can be 'regularized', that is the solution may be improved. The threshold for rejecting singular values may be based on either accelerance errors [7] or response error [12] or some percentage of the maximum singular value [4]. This usually results in reduced force determination errors. It is difficult, however, to decide which criterion should be used to establish a threshold for the singular values in a specific situation. In [7,10] the error band was based on $\pm$ 3 standard deviations in the case of accelerance error but in [12] a band of $\pm$ 1 standard deviation was used in the case of response error. These error bands may not be optimal for every case. In the process of rejecting singular values, information related to those singular values will also be lost completely. If this loss of information is significant then force determination could still contain large errors.

The accelerance matrix inversion can be converted to a forward solution using an iterative process [35] so that error amplification can be restricted. Such a technique has been used extensively in digital image processing. In this approach the iteration number determines the error amplification. Biemond, Lagendijk and Mersereau [35] determined the optimal iteration number based on estimates of bias and random errors in the solution. More recently, iterative inversion has been implemented in Nearfield Acoustic Holography (NAH) [36-38]. This was shown to improve acoustic source reconstruction considerably. As well as iterative inversion, Tikhonov regularization has also been implemented recently for acoustic problems and found to be successful [39-42]. In this method it is critical to establish an optimal value for the 'regularization parameter'. Ordinary cross validation or its variants have been used extensively for this purpose [43-46]. Other methods such as the use of the 'L curve' [63] have also been used successfully in different applications. Blau [47] gives some guidance about regularization with regards to the structural dynamics problem. Here it was suggested to use signal processing methods to improve error estimation in measurements, which can then be used in determining the regularization parameter. However, the performance of these techniques is not known for structural dynamics problems.

Lee and Park [29] suggest using a form of matrix regularization near both resonance and anti-resonance frequency zones. This was based on the principle that increased damping would reduce the ratio of the error to the FRF magnitude and in turn improve signal to noise ratio. Higher modal damping was used to improve the condition number. This needs curve fitting of experimental FRF's and extraction of modal parameters. The regularization parameter was selected based on a measurement of the damping, errors in the FRF matrix and in the response vector. The expression derived for optimal regularization is not expected to work well at high modal density. In this approach it is difficult to determine the width of the resonance and the anti-resonance zones that should be so treated and, moreover, increased damping would result in a completely different model.

In a modal transformation approach, Kim and Kim [48] designed a modal filter to reduce the error amplification in mode shape matrices. It is difficult in this case to determine suitable filter characteristics. For distributed force excitation the solution can

be regularized by using a spatial window and wave number filter [49]. However, in this case it is necessary to have available an analytical model of the structure.

1.2.4 Measurement location selection

In the inverse force determination it is necessary to select a set of force and response locations. Force locations can be readily identified from the source connection points to the receiver. However, it is difficult to decide on a suitable set of response locations and an appropriate number of them to use. The condition numbers of accelerance matrices may vary considerably over the frequency range because of modal behaviour of the structure under consideration. Again, due to modal behaviour, condition numbers may depend on the spatial location of response measurements. This variation could be quite significant across the structure. Some measurement locations could be worse than others resulting in larger condition numbers at some frequencies. This characteristic suggests an alternative approach to reduce error magnification in inverse methods, by appropriate selection of a set of response locations. Since the force locations are usually fixed, the response locations completely determine the error amplification in conjunction with measurement errors. It is a pre-requisite that 'proper' locations be identified and used in force reconstruction so that errors can be reduced.

The selection of measurement locations is an active topic of research in modal testing and condition monitoring of space structures [50-54]. In modal testing the forcing and acceleration measurement locations that are chosen influence the quality of modal parameters extracted. In some cases modes may be missed completely. It becomes extremely important to select a few good locations because of limitations in the number of channels available in the data acquisition system and the post processing. Even if efficient resources are available some sensor locations could be redundant.

Most of the methods published so far are based on the finite element method (FEM) [50-51, 53-54]. These would be difficult to implement in practical structures for transfer path analysis where the structure is often quite well damped and may contain many modes. Moreover, one of the benefits of TPA is that the structure need not be modelled in detail. These methods are a Guyan reduction approach, methods of maximum modal kinetic energy, maximum average modal kinetic energy, average

driving point residue and the effective independence method. The Guyan reduction approach [51] is the same as used to reduce the number of degrees of freedom in large finite element models to make the solution for the eigen values more manageable. In this, co-ordinates are eliminated which have a large ratio of stiffness to mass (which would depend on the upper frequency limit of the analysis). Since lower frequency modes are of greater relative importance, the co-ordinates left by this process are also the ones where sensors can be located. This process might still result in a large number of locations where sensors can be placed. This, however, does not indicate which locations are optimal and whether any redundancy exists.

The effective independence method [50-51] selects measurement locations that make the mode shapes of interest as linearly independent as possible while retaining as much information as possible about selected modal responses in the measurement data. In the effective independence (EFI) method, modal information from an FE model is used for several locations. Using the Fischer information matrix (see Appendix B), the trace of which indicates optimality, locations are chosen. For the locations to contain completely independent information the trace of the matrix should be equal to the number of locations used. This method has been applied recently to NAH [36] where an acoustic boundary element model was used. It essentially requires a complete definition of the mode shapes at all locations of importance, which is why it is quite hard to implement using experimental data.

Gram-Schmidt orthogonalization has also been used to select measurement locations based on FE results [51]. The basic principle in this method is to make the impulse responses at the sensor locations as independent as possible. The cross-correlation matrix of the impulse responses is used to select the positions. The positions which are least correlated are suitable positions for response measurements. This method can, however, be adapted for use with experimental data. The adaptation involves generating the impulse response from experimental accelerances. This method can be explored to select response positions for use in the reconstruction of forces.

The only method to select measurement locations that is based on experimental data, is the test reference identification procedure [52]. This method is based on singular value decomposition of the accelerance matrix. Originally this was applied to find the

best forcing locations for excitation in modal testing, but this could also be applied to select sensor locations with some modification. However, due to its dependence on graphical interpretation rather than objective indicators, application of this method is expected to be limited to the very low frequency range where the modal density of the structure is very low.

Recently, a sensor placement criterion specifically for inverse force identification was proposed by Blau [55]. Few details were given, but since the parameter presented varies with frequency it is unclear how this method could be implemented for the full frequency range.

1.2.5 Other considerations

In all the methods published so far the H_1 frequency response function estimator [69-71] has been used by default. It is not known how the errors in this estimator affect the inversion of the accelerance matrix. It is well known that this estimator is biased at resonance which is a sensitive frequency zone for inverse force determination. In view of this, different estimators of frequency response functions [56-59] should be evaluated before deciding on which one should be used.

Other than these developments, some literature is also available on finding the number of significant sources [60-61], based on the rank of the response matrix, which is essential before implementing the transfer path analysis. Recently an active noise control approach has been used to monitor the transfer paths in a vehicle [62] in which time domain techniques have been used to determine the source.

1.3 OUTLINE OF THE THESIS

In view of the present status of the research in inverse force determination, this thesis will contribute to advancement in the solution of inverse problems in structural dynamics, specifically by the use of regularization techniques and response location selection.

This study is divided into 10 chapters. Chapters 2 and 3 explore existing methods to improve the reconstruction of forces, that is over-determination and singular value rejection. Simulations are carried out to represent measurements on a rectangular simply

supported flat steel plate. The 'measured' data are then used to establish the effectiveness of the various methods. The performance of various thresholds for the rejection of singular values, based on either response errors or accelerance errors, is investigated. Some improvements to the selection of threshold values are proposed for singular value rejection methods. Also, the relative performance of different FRF estimators is established.

In Chapter 4 a new method, resampling of the accelerance matrix, is proposed which is then implemented practically by a perturbation of the accelerance matrix. Then the concept of rejecting perturbed singular values is introduced, which takes into account both FRF and response errors.

In Chapters 5 and 6 two alternative regularization techniques are studied. Although these are not new, they have not previously been applied to structural dynamics problems rigorously. In Chapter 5 Tikhonov regularization is investigated. A direct comparison is made of Tikhonov regularization and singular value rejection. Initially the regularization parameter is selected based on ordinary cross validation (OCV). The performance of OCV for structural dynamics problems is analysed. A new method, called selective cross validation (SCV) for selecting the regularization parameter is then proposed. To take of account of large condition numbers at resonances in conjunction with small response errors, modifications referred to as biased OCV and SCV are proposed to limit the error amplification. In Chapter 6, iterative inversion is studied and a formulation relevant to structural dynamics is developed. A cross validation technique to enable selection of the iteration number is proposed and evaluated.

In Chapters 7 and 8 experiments are reported that are used to validate the techniques developed in the earlier chapters. Experiments on a hanging rectangular flat plate are covered in Chapter 7. In Chapter 8 experimental force determination on a box structure is carried out.

The sensor selection methods from modal testing are explored in Chapter 9. A new method based on condition numbers of the accelerance matrix is then introduced. It is validated using both numerical simulations and experiments.

The conclusions are summarised in Chapter 10 along with recommendations for further work.

CHAPTER 2
THE PERFORMANCE OF CONVENTIONAL INVERSE FORCE DETERMINATION METHODS

2.1 INTRODUCTION

In this chapter, using numerical simulations to represent measurements, an assessment is made of the problems associated with inverse force determination. In each case the test structure is a rectangular plate, and a wide frequency range is used to include regions of both low and high modal overlap. The effectiveness is studied of over-determination of the accelerance matrix, that is using more response positions than the number of forces to be determined. In addition, the consequences of using different frequency response function estimators and different averaging strategies is assessed.

2.2 FORMULATION FOR SQUARE MATRIX

2.2.1 The inverse problem

A source strength, for example a set of forces, can be estimated using response spectra measured at a series of locations due to the operational source $\hat{a}$ in combination with frequency response functions (FRF's) measured from the source locations to these response locations $\hat{A}$. The response measurement locations have to be chosen such that the responses measured can capture and distinguish contributions from all possible paths involved. The following expression can be used to estimate the strength of the sources, here given as forces acting on the structure due to the source,

$$\{\hat{F}\}_\omega = [\hat{A}]_\omega^{-1} \{\hat{a}\}_\omega \tag{2.1}$$

where $\{\hat{a}\}_\omega$ is a vector containing operational responses (accelerations) measured at positions i, $[\hat{A}]_\omega$ is the measured frequency response functions (accelerance) matrix between forces F_j and accelerations a_i and $\{\hat{F}\}_\omega$ is a complex vector containing forces F_j that act to produce the responses a_i. In each case ^ is used to indicate measured or approximate quantities. The subscript ω indicates that each vector/matrix exists for a range of frequencies. Each contains complex quantities, allowing for relative phase differences. It is assumed here (and throughout this thesis unless stated otherwise) that all forces are fully correlated (Appendix C gives the details of formulations if they are

partially correlated or uncorrelated). For the reconstruction of forces, the accelerance matrix and acceleration vectors have to be assembled as follows for each frequency,

$$[\hat{A}]_\omega = \begin{bmatrix} \hat{A}_{1,1} & \hat{A}_{1,2} & . & \hat{A}_{1,n} \\ \hat{A}_{2,1} & . & . & . \\ . & . & . & . \\ . & . & . & . \\ \hat{A}_{m,1} & . & . & \hat{A}_{m,n} \end{bmatrix} \quad \text{and} \quad \{\hat{a}\}_\omega = \begin{Bmatrix} \hat{a}_1 \\ \hat{a}_2 \\ . \\ . \\ \hat{a}_m \end{Bmatrix} \tag{2.2}$$

where m is the number of locations for acceleration measurement and n is the number of forces used to represent the source. The matrix inversion in equation (2.1) can only be performed if $[\hat{A}]_\omega$ is a square full rank matrix i.e. $m = n$. Otherwise a pseudo-inversion has to be performed to give a least-square solution.

The response at some receiver location(s) can be found by using these forces with a measured set of transfer functions,

$$\{\hat{p}\}_\omega = [\hat{H}]_\omega \{\hat{F}\}_\omega \tag{2.3}$$

where $\{\hat{p}\}_\omega$ is a vector containing reconstructed responses at the receiver locations and $[\hat{H}]_\omega$ is the measured frequency response function matrix between the force locations and these receiver locations.

2.2.2 Matrix condition and singular value decomposition

As the accelerance matrix may be ill-conditioned at many of the frequencies, erratic force predictions may occur at these frequencies due to the presence of small errors in the measurement of accelerances $\hat{A}$ and responses $\hat{a}$. Ill-conditioning of the matrix magnifies errors from $\hat{a}$. The degree of ill-conditioning of any matrix can be assessed by the condition number (details are given in Appendix A). The condition number of a matrix is defined as the ratio of the largest singular value to the smallest of the matrix concerned. To calculate the condition number of a matrix $\hat{A}$, the singular values are required which can be obtained using singular value decomposition of the accelerance matrix as below [63-68].

$$\hat{A} = USV^H \tag{2.4}$$

where,

S = diag(s_1, s_2,...., s_n) , where $s_1 \geq s_2$,...., $\geq s_n$ are the singular values of the matrix. The singular values are the square roots of the eigenvalues of $\hat{A}^H \hat{A}$ with H the Hermitian transpose. They are positive real values.

U = matrix of eigen vectors of $\hat{A}\hat{A}^H$ with $U U^H = I$, i.e. U is a unitary matrix and

V = matrix of eigen vectors of $\hat{A}^H \hat{A}$ with $V V^H = I$, i.e. V is a unitary matrix.

The condition number is then given by

$$\kappa = \frac{s_1}{s_n} \tag{2.5}$$

If the condition number is large the matrix is said to be ill-conditioned. If one or more of the singular values are zero, κ is infinite, the matrix is singular and the inverse does not exist.

2.3 TEST STRUCTURE

2.3.1 Description of the structure

A series of numerical simulations have been carried out, based on a simply supported rectangular plate, to represent measurements, in order to investigate the process of matrix inversion in force reconstruction. The advantage of using simulations is that extraneous inputs, for example moments, can be eliminated, while the errors in measured quantities can be varied and are known. Simulations can also be carried out more rapidly than experiments, allowing many conditions to be considered. Actual experiments will be considered in Chapters 7 and 8.

The simply supported plate has been chosen as a test structure since closed form solutions for the natural frequencies and modeshapes are available, enabling understanding and interpretation of results from different methods of inverse force determination. Only flexural motion is considered in the analysis. The arrangement of the plate, along with indications of typical force and acceleration 'measurement' locations, is shown in Figure 2.1. For clarity only 3 force and 4 response locations are shown on the plate, although the number considered is larger than this.

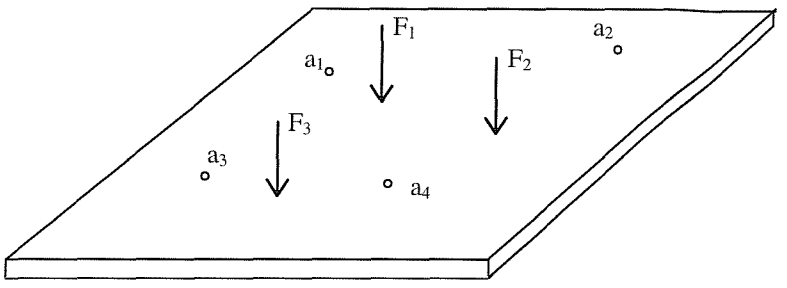

Figure 2.1. Simply supported plate showing force and response positions schematically.

The plate is taken to have dimensions 600mm × 500mm × 1.5mm and to be made of steel. Four (or six) coherent point forces were applied perpendicular to the plate at randomly selected positions. Several locations were chosen for operational response 'measurements', none of which coincided with force locations. The exact locations of the force and acceleration measurement positions are shown in Figure 2.2. A further location, marked **R**, was used as a receiver position. The receiver position is different from those used in reconstructing forces. The locations are also given in Table 2.1 in terms of non-dimensional coordinates.

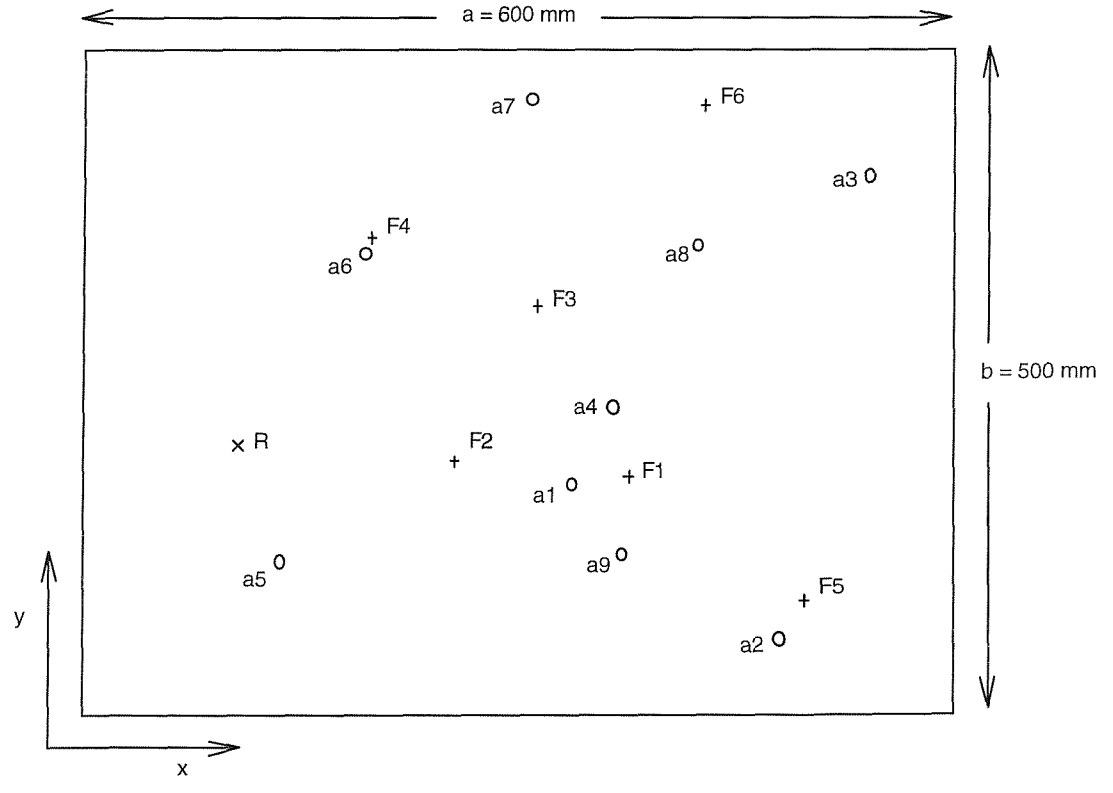

Figure 2.2. Response and force locations on the plate, **R** *is the position of the 'receiver'.*

Table 2.1. Non-dimensional force and response positions measured from the lower left corner.

Force positions				Response positions		
Position	*x/a*	*y/b*	Force[N]	Position	*x/a*	*y/b*
F1	0.62	0.41	27.0	a1	0.55	0.4
F2	0.41	0.43	19.0	a2	0.8	0.2
F3	0.51	0.63	10.0	a3	0.9	0.8
F4	0.31	0.72	6.0	a4	0.6	0.5
F5	0.83	0.25	35.0	a5	0.2	0.3
F6	0.71	0.89	0.1	a6	0.3	0.7
				a7	0.5	0.9
Receiver position				a8	0.7	0.71
R	0.15	0.45		a9	0.62	0.31

The material properties used in the calculations are as follows.

Material of the plate	Steel
Young's modulus	$E = 2.07\text{x}10^{11}$ N/m^2
Poisson's ratio	$\nu = 0.3$
Mass density	$\rho = 7850$ kg/m^3
Damping loss factor	$\mu = 0.03$

Experiments are simulated with different numbers of responses while keeping the number of forces fixed. The combinations of numbers of responses and forces considered are listed in Table 2.2. These different combinations allow for the study of the effect of over-determination ($m > n$) on the force reconstruction and the response prediction. For the various experiments with different numbers of force and response points, the first m response points and n forces from Table 2.1 are used in each case. The force spectra are taken to have constant rms amplitudes, as listed in Table 2.1, when converted to 1/3 octave bands. The phase difference between forces is taken to be zero, i.e. all forces are chosen to be in phase.

Table 2.2 Combinations of number of responses and number of forces.

Number of responses, m	4	5	6	6	9
Number of forces, n	4	4	4	6	6

The frequency range used for the study was from 10 Hz to 3.6 kHz. The plate response is dominated at low frequencies by individual modes and at high frequencies by multiple overlapping modes. The first resonance is at 25 Hz and there are 200 modes up to 3.6 kHz. Figure 2.3 shows an estimate for the modal overlap of the structure under consideration which is given by $\mu\omega n_d$, where n_d is the asymptotic modal density [75]. For a plate, the asymptotic modal density is given by [75]

$$n_d(\omega) = \frac{\sqrt{12}S}{hc_L} \tag{2.6}$$

where S is the surface area of the plate, c_L is the longitudinal wave speed in the plate and h is the thickness of the plate. The modal overlap can be seen to be greater than 1 for frequencies above about 500 Hz.

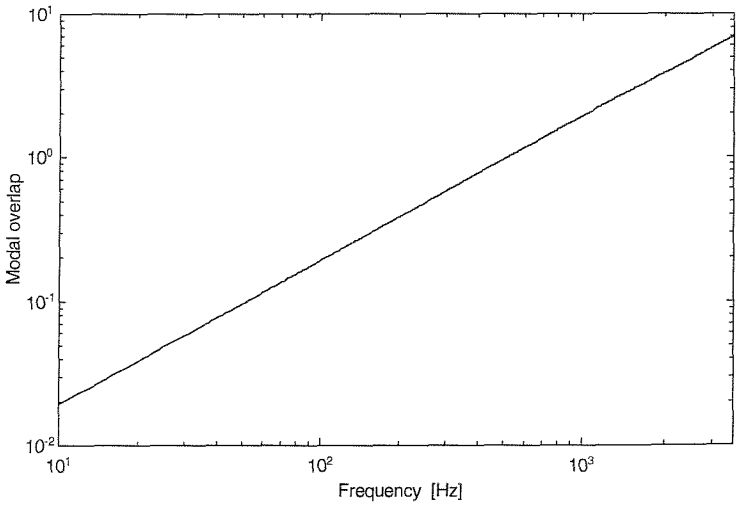

Figure 2.3. Estimated modal overlap for rectangular plate of dimensions 0.6×0.5×0.0015m with hysteretic damping loss factor of 0.03.

2.3.2 Analytical model of the test structure

An analytical model of the flexural vibration of a thin plate has been used to carry out the numerical simulations to represent measurements. For this purpose the accelerance, A, of a simply supported rectangular plate is calculated using [72-74,76]

$$A((x,y),(x_1,y_1)) = \frac{a(x,y)}{F(x_1,y_1)} = \sum_p \sum_q \frac{-\omega^2 \psi_{pq}(x,y)\psi_{pq}(x_1,y_1)}{M_{pq}\left(\left(\omega_{pq}^2 - \omega^2\right) + j\mu\omega_{pq}^2\right)} \tag{2.7}$$

where (x, y) is the response location and (x_1, y_1) is the excitation point. p, q are integers, representing the modes,

$$\psi_{pq}(x,y) = \sin\left(\frac{p\pi x}{a}\right)\sin\left(\frac{q\pi y}{b}\right) \tag{2.8}$$

is the mode shape function, $M_{pq} = \frac{m_{plate}}{4}$ is the modal mass, where $m_{plate} = \rho abh$ is the total plate mass, a and b are the length and width, h is the thickness, ρ is the density. μ is the damping loss factor and ω_{pq} is the natural frequency of the mode (p, q)which is given by

$$\omega_{pq} = \left[\left(\frac{p\pi}{a}\right)^2 + \left(\frac{q\pi}{b}\right)^2\right]\sqrt{\frac{D}{\rho h}} \tag{2.9}$$

where $D = \frac{Eh^3}{12(1-\nu^2)}$ is the bending stiffness, E is the Young's modulus and ν is Poisson's ratio. The summation in equation (2.7) should be carried out over at least all modes in the frequency range of interest.

2.4 NUMERICAL SIMULATIONS

2.4.1 Frequency response function and operational response estimation

Experiments to estimate the accelerance that would be measured in the presence of noise can be modelled as in Figure 2.4. X is the 'measured' force and Y is the 'measured' acceleration. A is the exact accelerance.

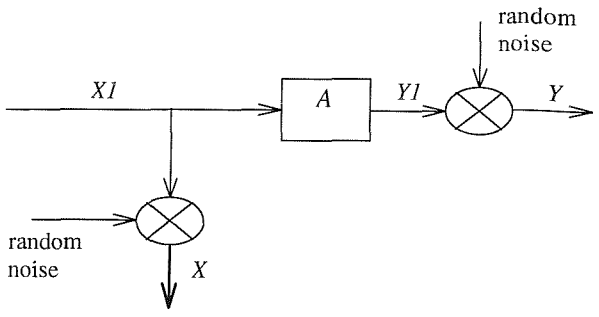

Figure 2.4. Model of experiment for the measurement of accelerance

The measured accelerance as given by the H_1 estimator [69-71] is

$$\hat{A} = \frac{S_{xy}}{S_{xx}} \tag{2.10}$$

where S_{xy} is the cross spectrum between X and Y and S_{xx} is the power spectrum of X. The coherence γ^2 is given by

$$\gamma^2 = \frac{|S_{xy}|^2}{S_{xx}.S_{yy}} \tag{2.11}$$

The coherence indicates the degree of dependence of the input and output signals X and Y. For a single measurement, the coherence is always equal to 1 [69]. However, when an average is taken over a number of samples, the coherence becomes less than or equal to 1.

Based on the above theory, numerical simulations were performed to represent experiments to estimate FRF's as follows. The exact FRF's from each forcing location to the various response locations have been estimated using equation (2.7). The acceleration signals corresponding to 'measured' FRF's were generated using a unit force at each frequency. Both acceleration and force spectra were then corrupted by adding a complex random noise signal in the frequency domain. Then, using the H_1 estimator, the 'measured' FRF's $\hat{A}$ were determined by averaging over a number of samples, n_{av}.

$$\hat{A}_{ij}(\omega) = \frac{\hat{S}_{xy}(\omega)}{\hat{S}_{xx}(\omega)} \tag{2.12}$$

where,

$$\hat{S}_{xy}(\omega)=\frac{1}{n_{av}}\sum_{k=1}^{n_{av}}X_k^{*}(\omega)Y_k(\omega) \tag{2.13a}$$

$$\hat{S}_{xx}(\omega)=\frac{1}{n_{av}}\sum_{k=1}^{n_{av}}X_k^{*}(\omega)X_k(\omega) \tag{2.13b}$$

where n_{av} is the number of samples used for averaging, $X_k = F_j + N_{in,k}$ and $Y_k = A_{ij}F_j + N_{out,k}$. Here F_j is a force spectrum of unit amplitude, N_{in} is the random noise spectrum added to the input and N_{out} is the random noise spectrum added to the output. * indicates the complex conjugate.

Using the principle of superposition, the operational responses $\{\hat{a}\}$ were calculated from the true values of $[A]$ and $\{F\}$ and noise was again added to this response signal in the frequency domain to represent measurement noise. The k^{th} sample of the acceleration at each response location is given by,

$$\hat{a}_{i,k}=\left[\sum_{j=1}^{n}A_{ij}F_j\right]+N_{i,k} \qquad i=1, 2, \ldots\ldots m \tag{2.14}$$

where F_j is the spectrum of the j^{th} force acting on the structure and N is a random noise signal which is a complex quantity as explained in the next section.

The number of averages that have been used in estimating the accelerance and acceleration are as follows:

$\hat{A}$ - 50 samples , $n_{av} = 50$

$\hat{H}$ - 200 samples

$\hat{a}_i$ - 25 samples, $n_s = 25$

The transfer functions $[\hat{H}]$ from the force locations to the receiver location are 'measured' in the same way as the procedure outlined above for FRF estimation.

2.4.2 Noise models

In the simulations, 'measurement noise' was added to the acceleration signals based on a Gaussian additive noise model with a component proportional to frequency and a component constant with frequency. The expression for this is

$$N(\omega)=C_1\omega N_{nd,1}e^{j2\pi N_{nd,1}}+C_2N_{nd,2}e^{j2\pi N_{nd,2}} \tag{2.15}$$

where $C_{1,2}$ are constants, $N_{nd,1}$ and $N_{nd,2}$ are normally distributed random numbers with mean 0 and standard deviation 1 and $N_{ud,1}$ and $N_{ud,2}$ are uniformly distributed random numbers in the range 0 to 1. This noise model is used in corrupting the acceleration signals (both operational responses and FRF's). While estimating the frequency response functions it results in a low coherence at high frequency, depending on the amplitude, C_1. Some constant noise level is also introduced by C_2, which affects the low frequency acceleration. Figure 2.5a shows one of the response signals used in determining the FRF's along with three different noise levels that are used in this thesis. It is shown in the form of a velocity for ease of presentation and is converted to 1/3 octave bands. In converting from acceleration to velocity the factor ω in (2.15) is effectively eliminated. Integration over 1/3 octave bands leads to a $10\log_{10}\omega$ dependence at high frequency. These three noise levels correspond to low, moderate and high signal to noise ratios in the measured FRF's. The noise level is observed to be significant compared with the response signal in the high frequency region for the case of high FRF error. One of the operational responses is shown in Figure 2.5b along with the corresponding noise signals. Again the noise level is significant in the high frequency region for high response errors.

The force signals are corrupted by a Gaussian additive model with an amplitude that is constant with frequency before being used in estimating the frequency response functions. The expression is given below.

$$N(\omega) = C N_{nd} e^{j 2\pi N_{ud}} \tag{2.16}$$

where C is a constant. An example of the noise levels used in these simulations to corrupt the forcing function is shown in Figure 2.6. Note that the spectrum slopes upwards due to the conversion to 1/3 octave bands.

The noise levels added to obtain operational responses and frequency response functions can be quantified by the average signal to noise ratio (S/N) across all 1/3 octave bands. These values for the three levels of noise used are shown in Table 2.3. These three levels of noise have been classified as low, moderate and high.

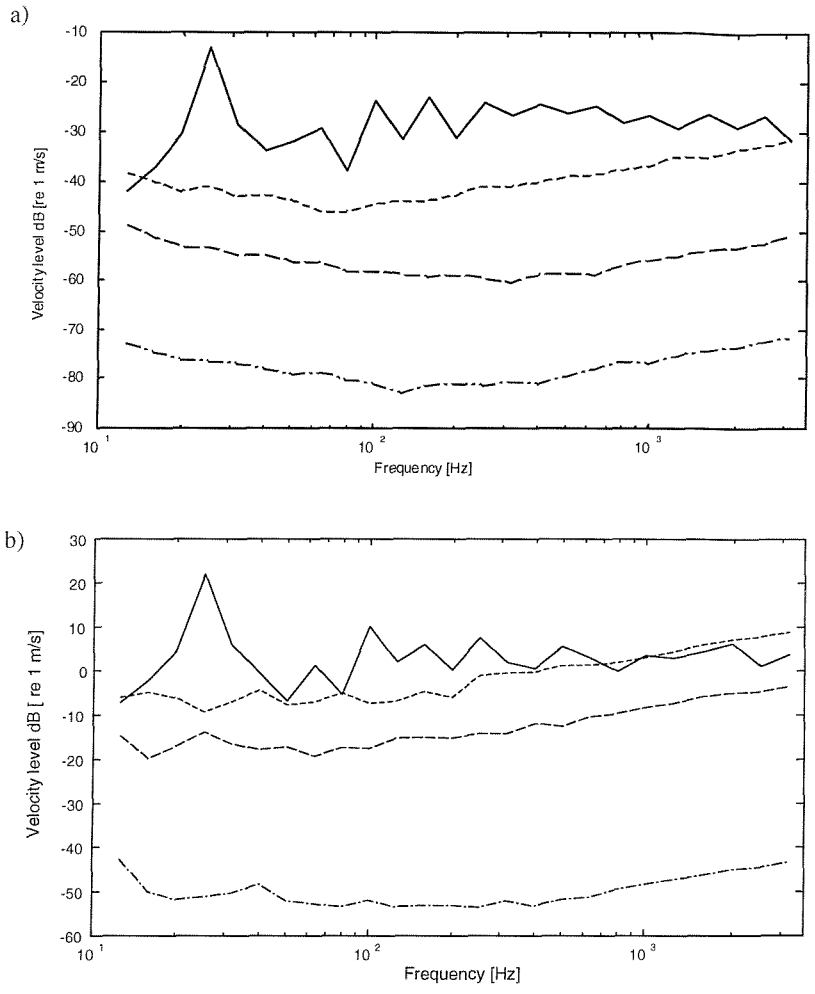

Figure 2.5. Comparison of added noise and original response signal. ———— *response,* – – – – – *high noise,* — — — — *moderate noise,* — · — · — *low noise. (a): example of velocity response used to estimate FRF* A_{11}*. (b): example of operational response, corresponding to position* a_1*.*

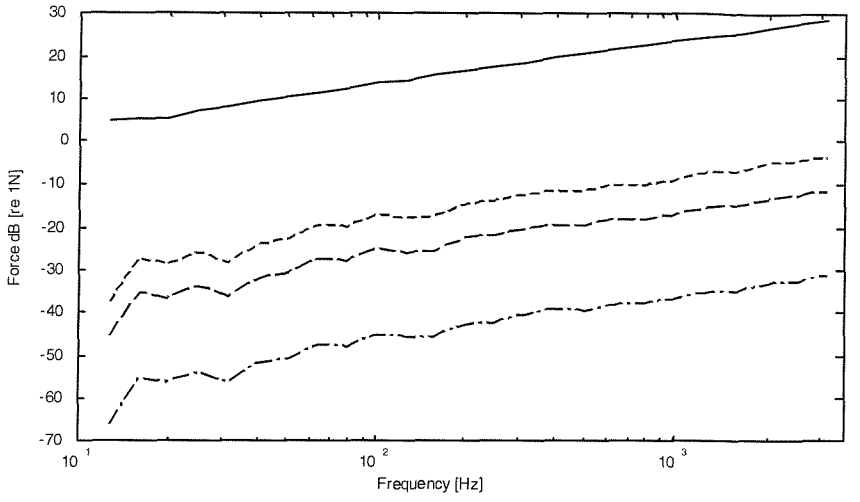

Figure 2.6. 1/3 octave band noise in the measurement of force during accelerance measurement. ——— force, – – – – – high noise, — — — — moderate noise, — · — · — low.

Table 2.3 Average signal to noise ratios in dB indicating the level of noise added to signals to obtain operational responses and frequency response functions.

		Noise level		
		Low (High S/N)	Moderate (Moderate S/N)	High (Low S/N)
Operational response		50.0	13.5	2.6
FRF	Acceleration	49.0	27.3	11.3
	Force	60.0	40.0	32.0

A typical transfer mobility (velocity per unit force FRF) is given in Figure 2.7 which shows the magnitude, phase and coherence for the test structure for one of the response and excitation positions. This figure corresponds to high noise in the FRF. The influence of measurement noise can be seen at high frequencies and is very clear from the fall in coherence.

In this chapter for clarity the forces and responses are often presented in 1/3 octave bands. However, the force reconstruction and receiver position estimations are always carried out in narrow bands (1 Hz spacing) and then converted to 1/3 octaves.

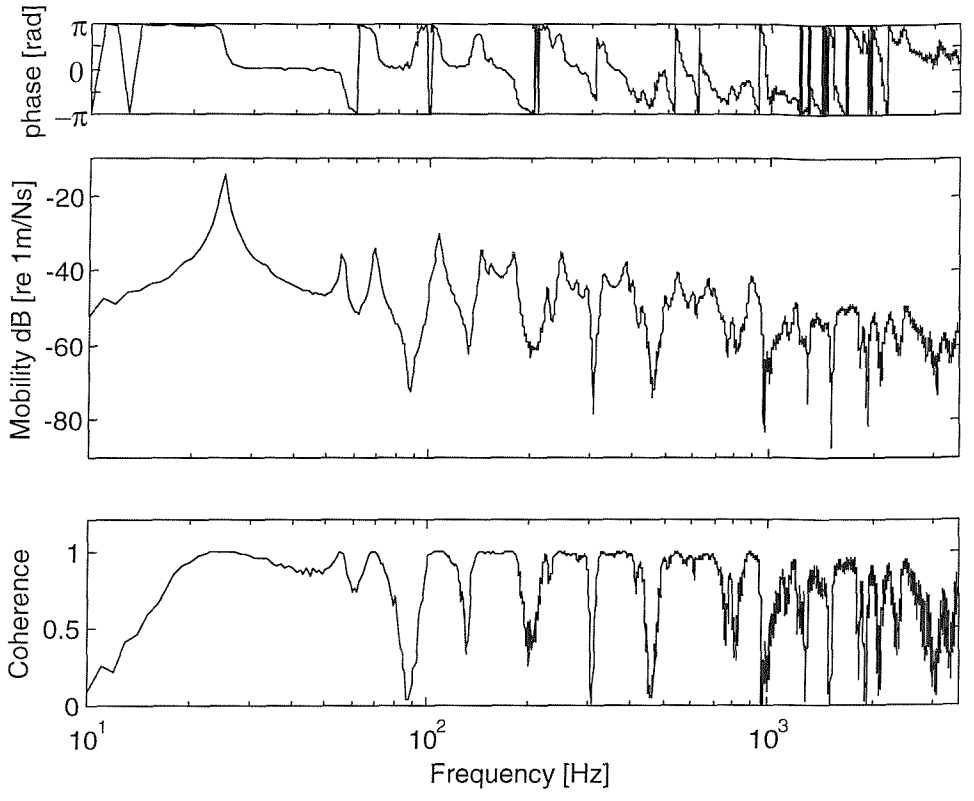

Figure 2.7. Transfer mobility from excitation point 1 to response point 1 for high noise.

2.5 FORCE DETERMINATION AND RESPONSE RECONSTRUCTION

The forces determined by using the inverse method for a square 4×4 matrix are shown in Figure 2.8. Here, the true force levels which apply for all frequencies are shown in the right hand part of the figure. For this case the noise levels in the 'measurements' correspond to high noise in the accelerances and moderate noise in the responses (see Figures 2.5 and 2.6 and Table 2.3). All results are calculated in narrow (1Hz) bands and the results converted to one-third octave bands for ease of presentation. The forces are predicted more reliably at high frequency than at low frequency, and are better for the larger forces than the smaller ones. At low frequencies, as will be seen in section 2.7, high condition numbers combined with measurement errors result in large force determination errors.

Figure 2.9 shows the reconstructed velocity response at the receiver location along with the true response at the same location. The corresponding results in 1/3 octave form are shown in Figure 2.10. Even though considerable errors exist in the forces determined at low frequencies, the reconstructed response is remarkably accurate in the region of the first resonance at 25 Hz. This is a consequence of the fact that the

forces are complex. Although the reconstructed force amplitudes are quite different from the actual forces, when their contributions are added as complex quantities this leads to some cancellation during estimation of the velocity response, resulting in more accurate prediction of responses than forces near the resonances.

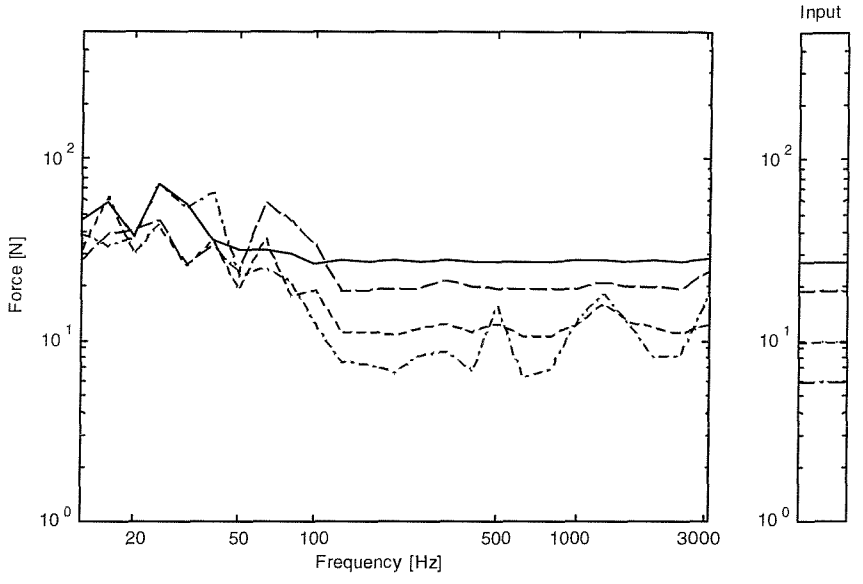

Figure 2.8. Reconstructed rms forces in 1/3 octave bands for 4 forces and 4 responses.
——— force 1, — — — — force 2, – – – – – – force 3, —·—·—· force 4.

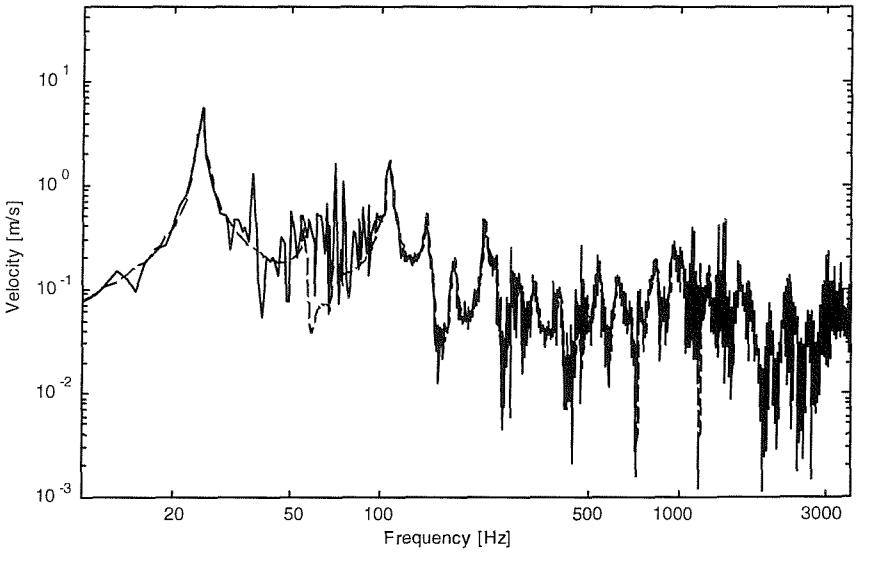

Figure 2.9. Velocity response at the receiver location for 4 forces and 4 responses.
— — — — actual response, ——— reconstructed response.

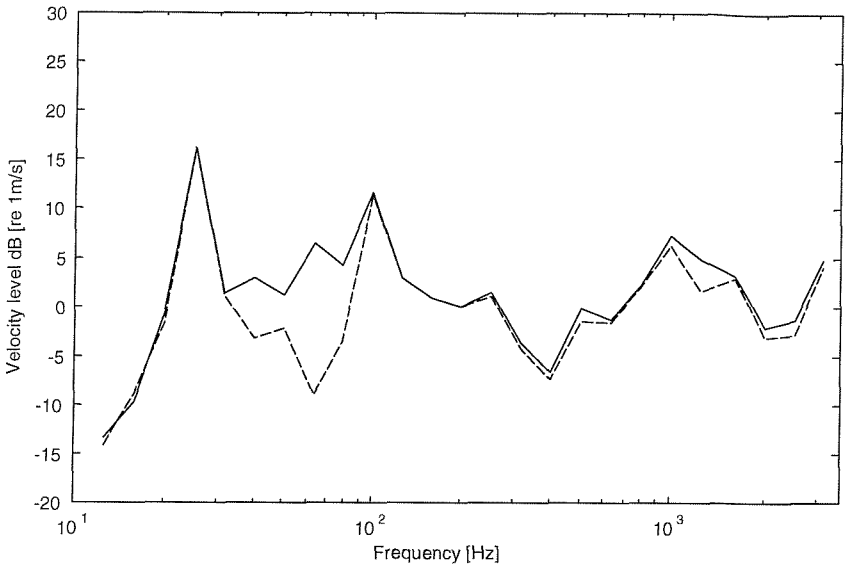

Figure 2.10. 1/3 octave band velocity response. — — — —true response, ———— response predicted using 4 × 4 matrix.

2.6 FORCE DETERMINATION WITH DIFFERENT FRF ESTIMATORS

In most work by different authors, for example [6-8,11-15], the frequency response function estimator H_1 has been used. H_1 is the most popular frequency response function estimator and is designed to minimise the effect of noise on the output signal. It is quite accurate at antiresonances. However, it can underestimate the FRF near resonance (in fact it underestimates the FRF at all frequencies but the difference is small apart from near resonances). As observed in [7] small errors at resonance (when there is a high condition number of the accelerance matrix) can lead to large force reconstruction errors. To overcome this it might be helpful to use an alternative FRF estimator, such as the H_2 estimator which is accurate near the resonances. It is also interesting to explore other estimators which combine the advantages of the H_1 and H_2 estimators. Five different estimators are used in this chapter to reconstruct the forces, and the results from each are compared. These estimators are described in Appendix D. The corrupting noise level used in this section corresponds to high noise in the FRF's and moderate noise in the operational responses.

2.6.1 Frequency response estimators

Figure 2.11 shows the transfer mobility amplitude obtained using the H_1 estimator from forcing point 1 to response point 1. The noise level added corresponds to high noise. The theoretical mobility is also shown in the figure. The H_1 estimator almost matches the theoretical mobility. However, some random variations are observed at high frequency. The H_2 estimator gives a poor mobility in the vicinity of antiresonances and also in the high frequency region as shown in Figure 2.12. The H_4 estimator combines the advantages of H_1 and H_2, as shown in Figure 2.13. This estimator however leads to larger error in the vicinity of antiresonances and at high frequency than H_1. Similar conditions occur with H_v, although the errors are found to be greater than for H_4 (Figure 2.14). The H_s estimator seems to give results that are closest to H_1 (Figure 2.15).

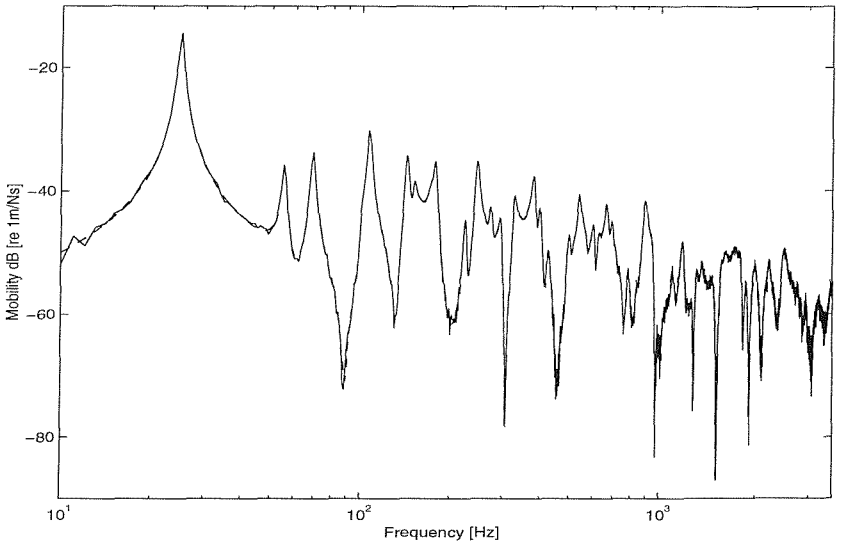

Figure 2.11. Transfer mobility obtained by H_1 estimator from source location 1 to response location 1. — — — — true mobility, ——— 'measured' mobility. Noise added corresponds to high noise.

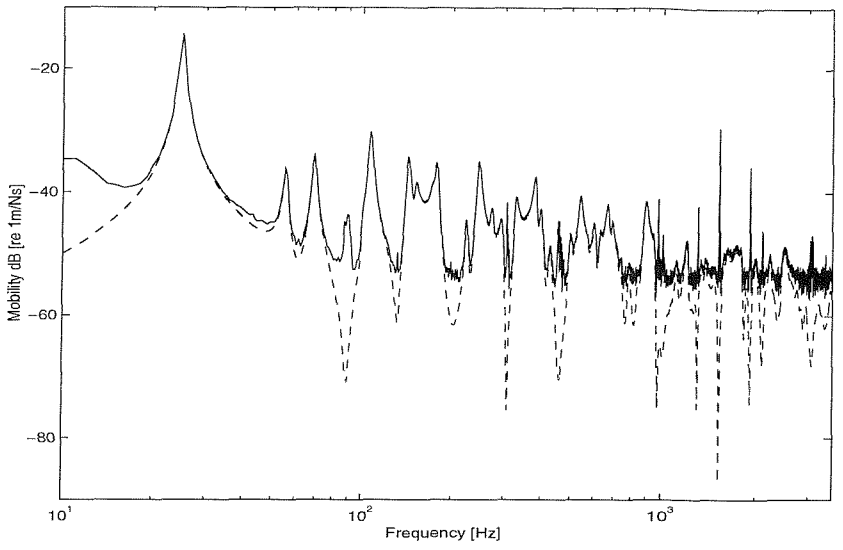

Figure 2.12. Transfer mobility obtained by H_2 estimator from source location 1 to response location 1. — — — — true mobility, ———— 'measured' mobility. Noise added corresponds to high noise.

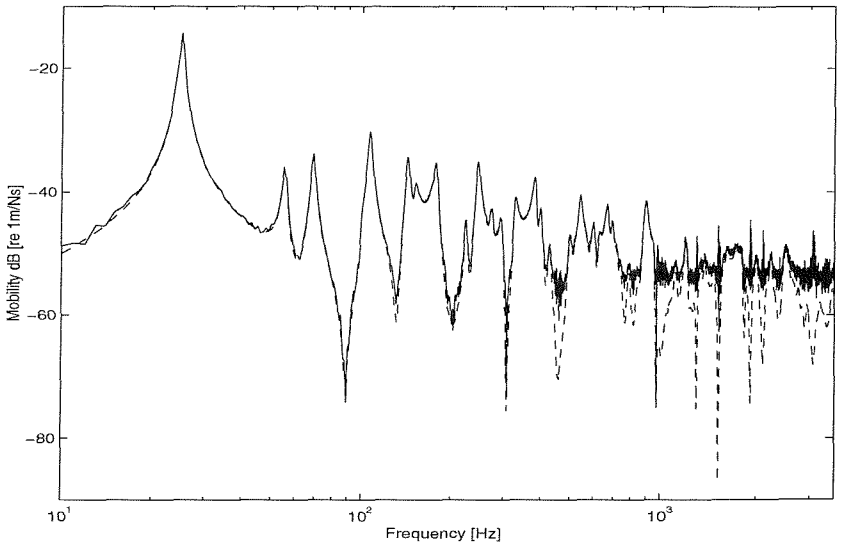

Figure 2.13. Transfer mobility obtained by H_4 - Fabunmi estimator from source location 1 to response location 1. — — — — true mobility, ———— 'measured' mobility. Noise added corresponds to high noise.

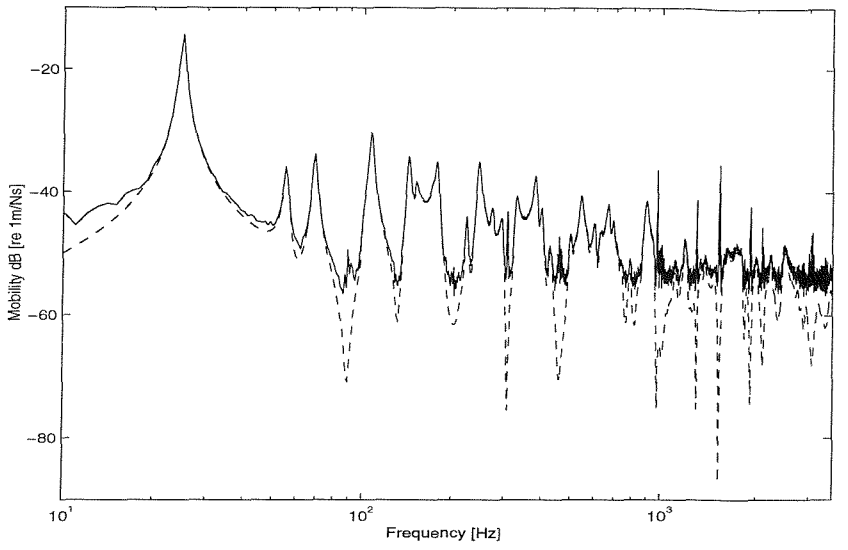

Figure 2.14. Transfer mobility obtained by H_v estimator from source location 1 to response location 1. — — — — true mobility, ———— 'measured' mobility. Noise added corresponds to high noise.

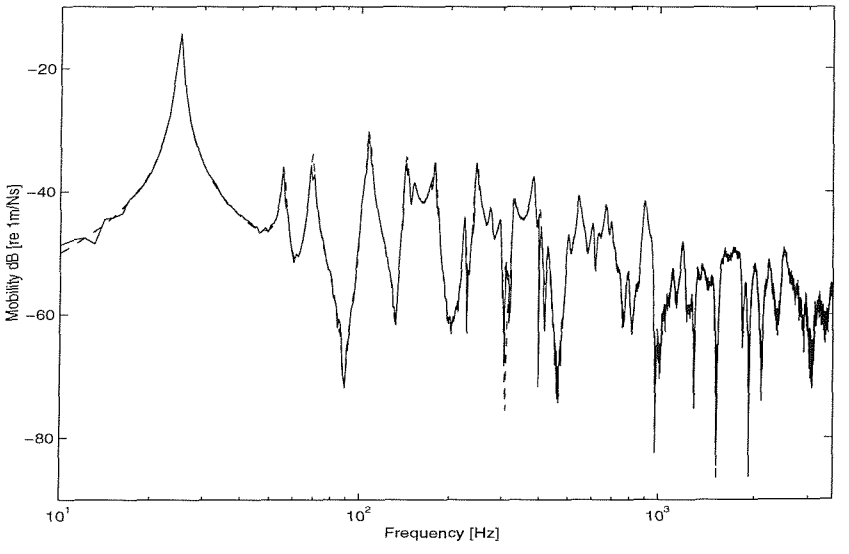

Figure 2.15. Transfer mobility obtained by H_s estimator from force location 1 to response location 1. — — — — true mobility, ———— 'measured' mobility. Noise added corresponds to high noise.

2.6.2 Force reconstruction

These FRF estimators have been used in the construction of the accelerance matrix. Following the procedure given in Section 2.2, forces are reconstructed using each of the estimators.

Figures 2.16-2.19 show the reconstruction of 4 forces from 4 responses based on each of the estimators. The forces determined using H_1 were shown previously in Figure 2.8. Even though the H_1 estimator is biased near the resonances, it reconstructs the forces better than any other estimator considered. Errors near the anti-resonances in other estimators, except H_s, appear to have a significant influence on errors in the forces determined. The H_2 estimator leads to the worst force reconstruction (Figure 2.16). The results for the other estimators lie between those of H_1 and H_2.

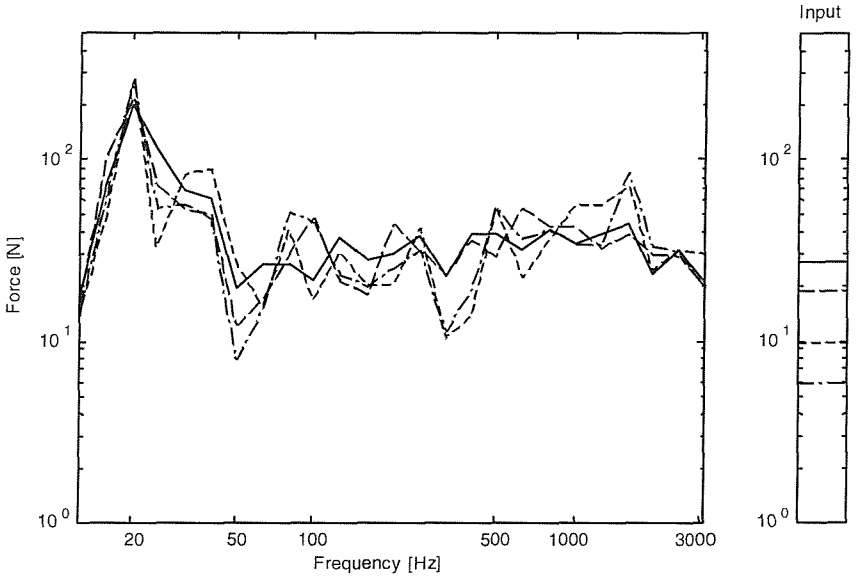

Figure 2.16. Reconstructed rms forces in 1/3 octave bands for 4 forces and 4 responses based on H_2 estimator. ————force 1, — — — —force 2, – – – – – – force 3, —·—·—· force 4.

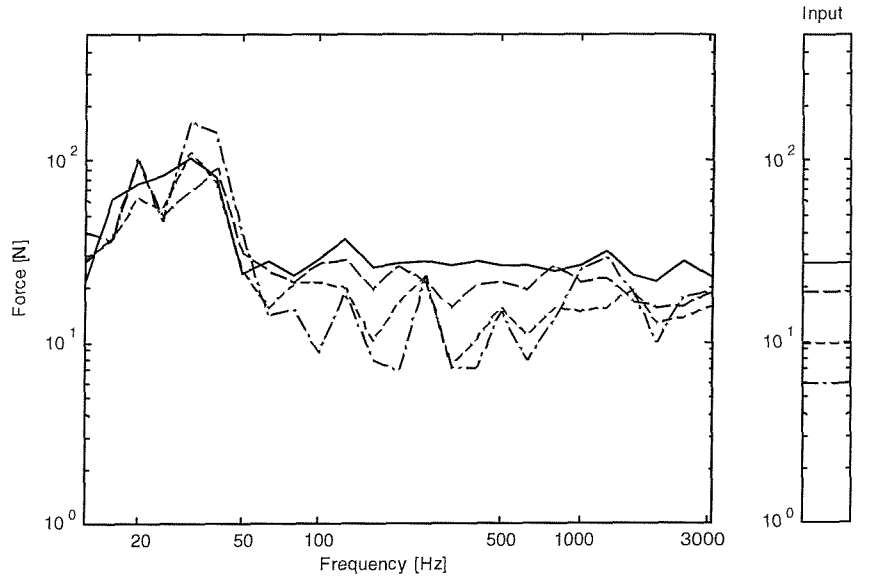

Figure 2.17. Reconstructed rms forces in 1/3 octave bands for 4 forces and 4 responses based on H_4 - Fabunmi estimator. ————force 1, — — — —force 2, – – – – – – force 3, —·—·—· force 4.

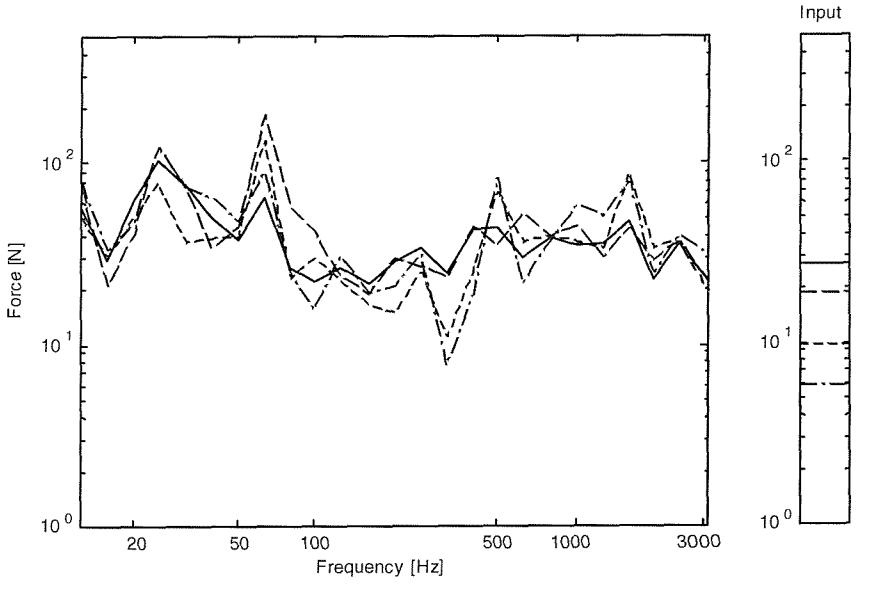

Figure 2.18. Reconstructed rms forces in 1/3 octave bands for 4 forces and 4 responses based on H_v estimator. ————force 1, — — — —force 2, – – – – – – force 3, —·—·—· force 4.

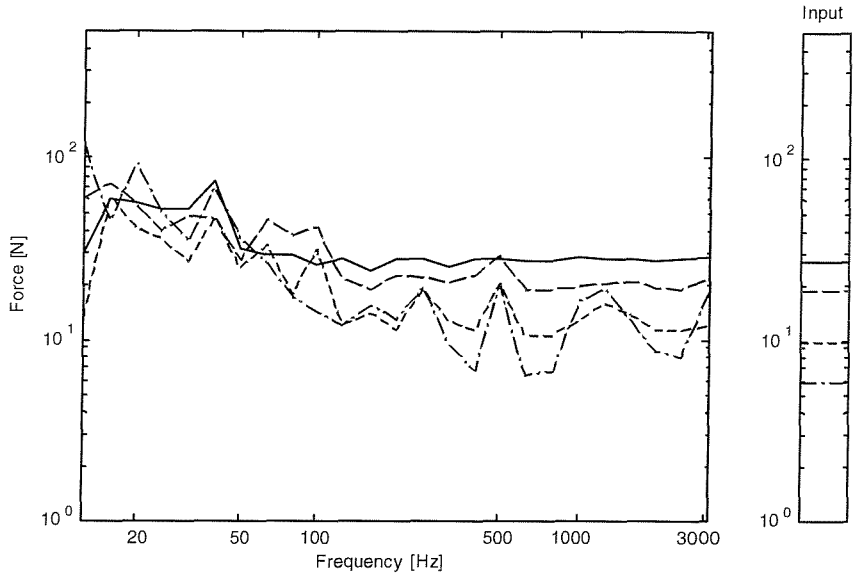

Figure 2.19. Reconstructed rms forces in 1/3 octave bands for 4 forces and 4 responses based on H_s estimator. ————force 1, — — — —force 2, – – – – – – force 3, —·—·—· force 4.

2.6.3 Velocity response at the receiver location

The velocity responses obtained from the forces derived using the various estimators are shown Figures 2.20-2.27 in narrow band and 1/3 octave form. Corresponding plots for the H_1 estimator were shown in Figures 2.9 and 2.10. The predictions based on the H_1 estimator are again better than those from any other estimator considered. The H_2 estimator leads to erratic prediction at many of the frequencies (Figures 2.20 and 2.21). Other estimators predict the responses with an accuracy which lies between those of the H_1 and H_2 based predictions.

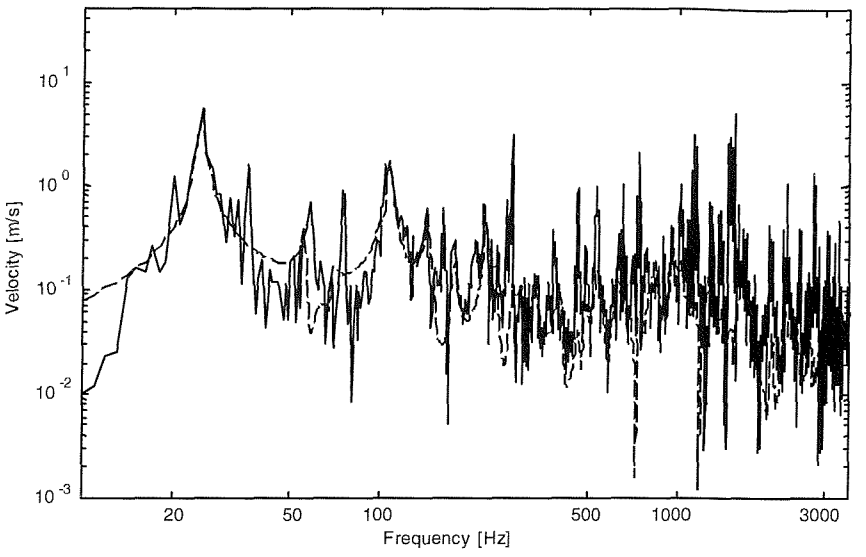

Figure 2.20. Velocity response at the receiver location for 4 forces and 4 responses based on H_2 estimator — — — —actual response, ———— reconstructed response.

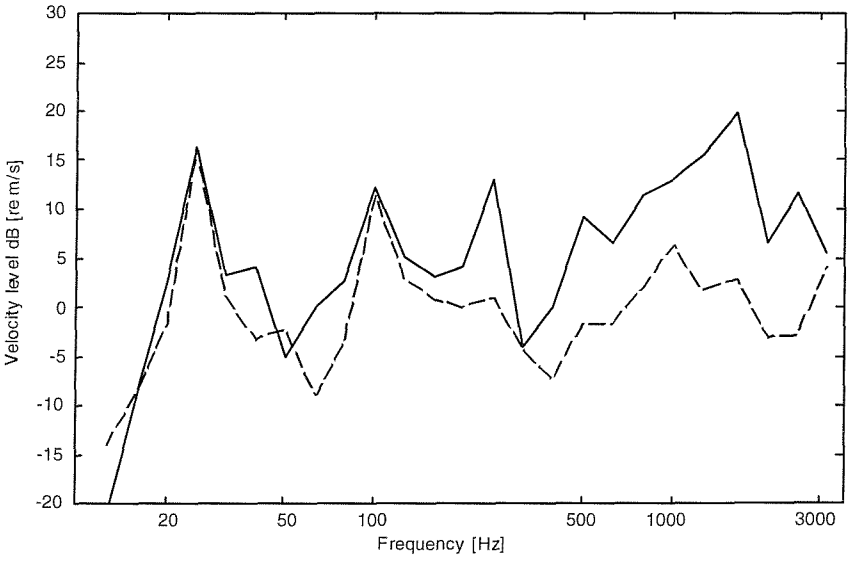

Figure 2.21. 1/3 octave band velocity response at the receiver location for 4 forces and 4 responses based on H_2 estimator — — — —actual response, ———— reconstructed response.

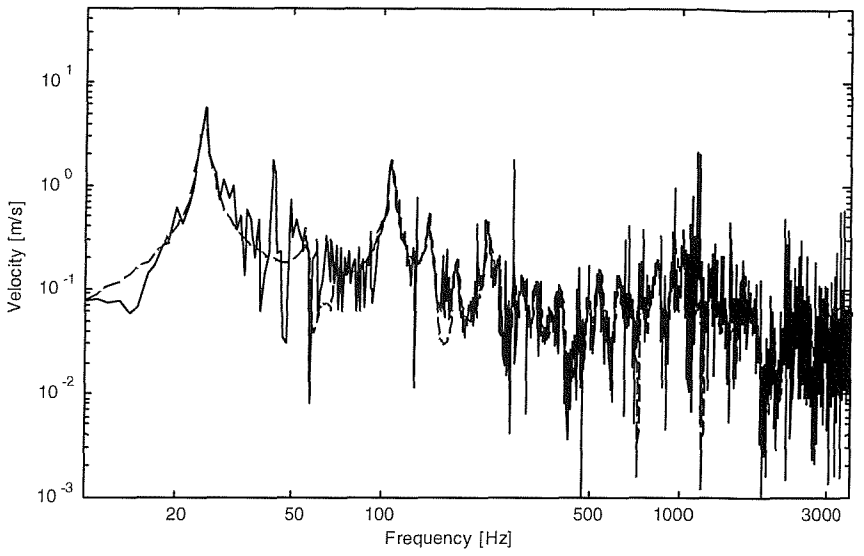

Figure 2.22. Velocity response at the receiver location for 4 forces and 4 responses based on H_4 - Fabunmi estimator. — — — —actual response, ———— reconstructed response.

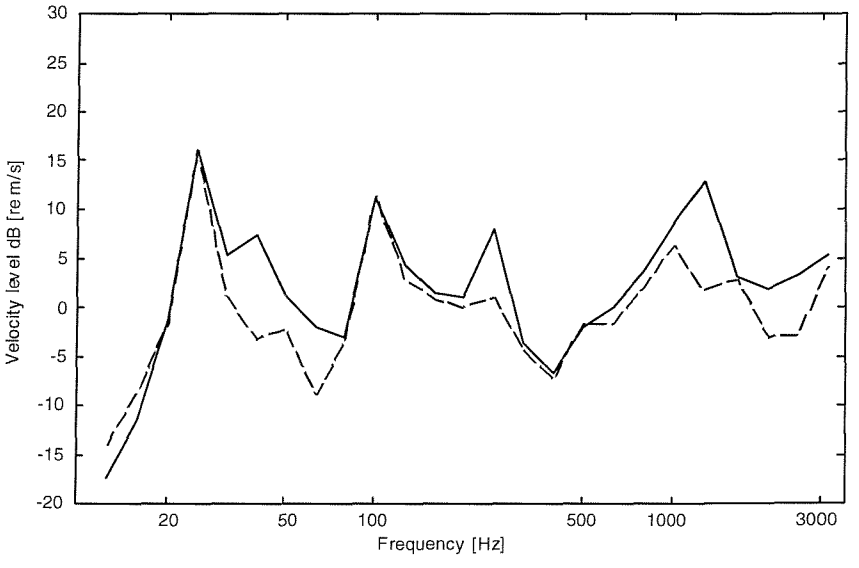

Figure 2.23. 1/3 octave band velocity response at the receiver location for 4 forces and 4 responses based on H_4 - Fabunmi estimator. — — — —actual response, ———— reconstructed response.

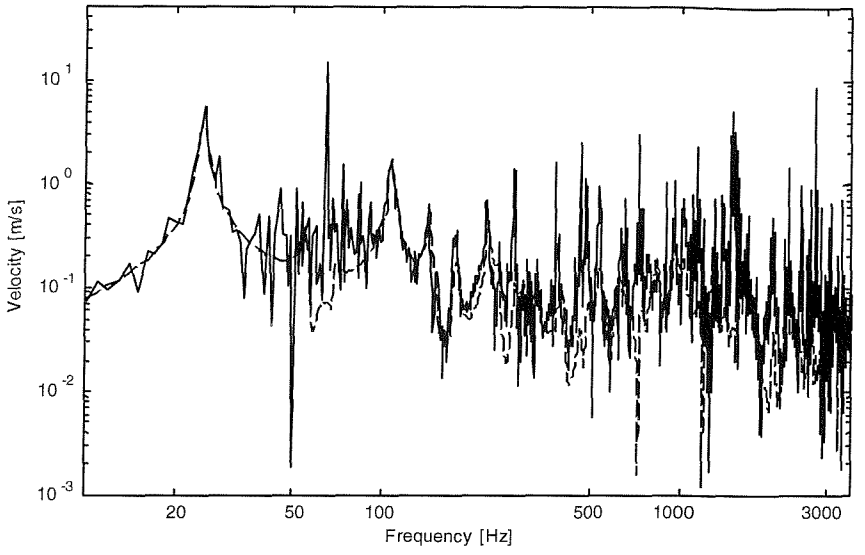

Figure 2.24. Velocity response at the receiver location for 4 forces and 4 responses based on H_v estimator. — — — —actual response, ———— reconstructed response.

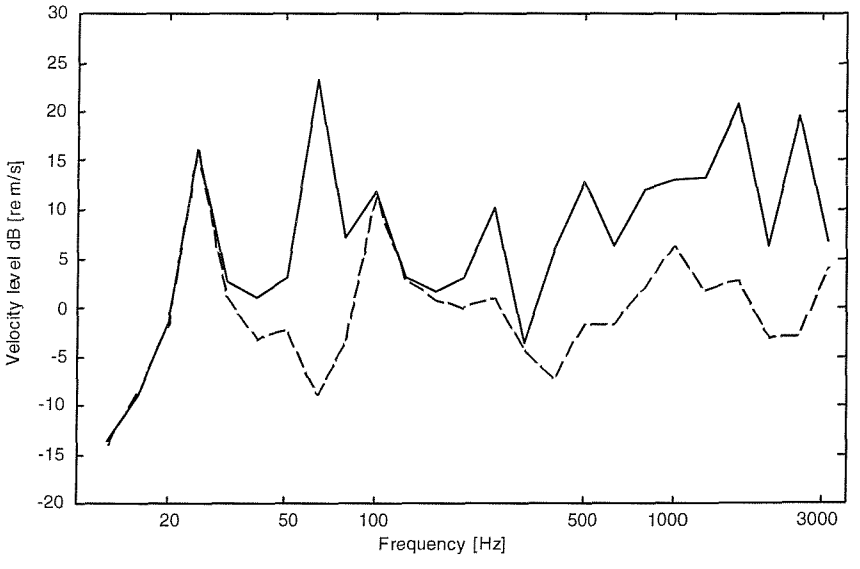

Figure 2.25. 1/3 octave band velocity response at the receiver location for 4 forces and 4 responses based on H_v estimator. — — — —actual response, ———— reconstructed response.

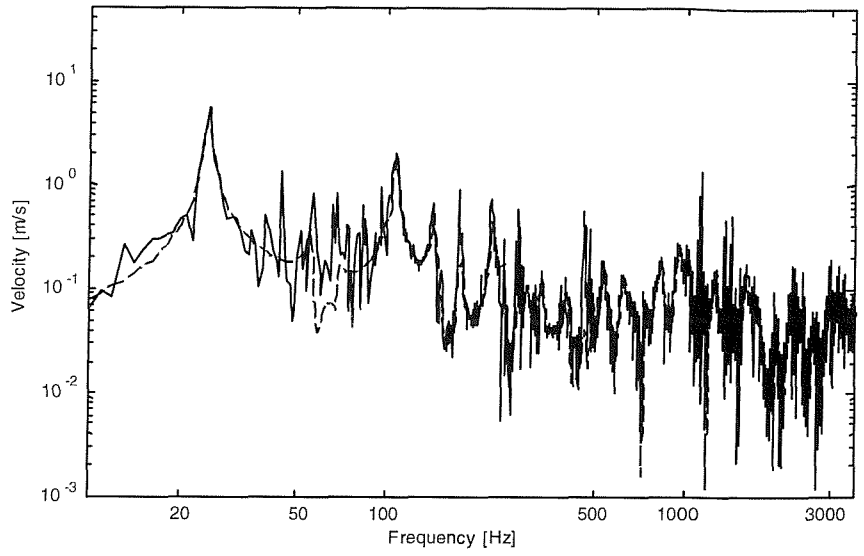

Figure 2.26. Velocity response at the receiver location for 4 forces and 4 responses based on H_s estimator. — — — —actual response, ———— reconstructed response.

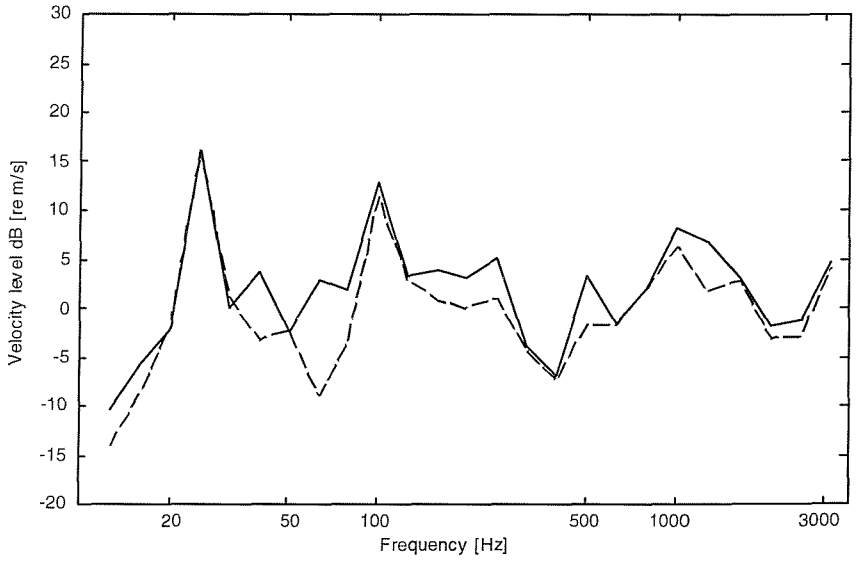

Figure 2.27. 1/3 octave band velocity response at the receiver location for 4 forces and 4 responses based on H_s estimator. — — — —actual response, ———— reconstructed response.

2.6.4 Summary

The H_1 estimator, even though it has differing accuracy at resonance and antiresonance, results in a better force reconstruction across the frequency range in the inversion process than the other estimators considered. It needs to be noted that, for the

noise levels considered (Table 2.3), the relative error at resonance is very small, so the bias in H_1 at resonance is small. The relative error at anti-resonance is greater so the bias in H_2 is large. For other noise models the conclusions drawn here may differ.

2.7 OVER-DETERMINED SYSTEMS

2.7.1 Moore-Penrose pseudo-inverse

As has been discussed by several authors, for example [14,67], force determination errors can generally be reduced by over-determination, i.e. using a larger number of responses than the forces to be identified, and employing a least squared error solution, such as Moore-Penrose pseudo-inversion. This reduction in the error is observed to correspond to improvement in the condition numbers of the matrix $\hat{A}$ at some frequencies. The required least squares solution, Moore-Penrose pseudo-inversion [67], is achieved by minimising the reconstruction errors as given below.

The least squares estimate of forces is based on the assumption that only operational responses contain error. The general direct dynamic problem can be written as

$$\{\hat{a}\}+\{r\}=[\hat{A}]\{\hat{F}\} \tag{2.17}$$

where r is a residual which is zero if the accelerance matrix is square, but otherwise may be non-zero. In the least squares solution to determine the forces, the square of the residual r is minimised. The cost function to be minimised is $\sum_i^m |r_i|^2$. The process followed to obtain least squares solution is given below.

For some variation in the set of forces $\hat{F}$, the differential of the above cost function is equated to zero giving

$$2\sum_i^m r_i^* \, \mathrm{d}r_i = 0 \Rightarrow \{\mathrm{d}r_i\}^H \{r_i\} = 0 \tag{2.18}$$

where * indicates complex conjugate. The expression for the differential $\mathrm{d}r$ can be obtained in terms of the accelerance matrix and the response vector. This is achieved by differentiation of (2.17) with respect to r. Since $\hat{A}$ and $\hat{a}$ are constants for any given measurement, by differentiation

$$\mathrm{d}r = \hat{A}\,\mathrm{d}\hat{F} \tag{2.19}$$

Using this expression in (2.18)

$$(\hat{A}.\mathrm{d}\hat{F})^{H} r = 0 \Rightarrow \mathrm{d}\hat{F}^{H}\hat{A}^{H}(\hat{A}\hat{F} - \hat{a}) = 0 \tag{2.20}$$

For a non-trivial solution

$$\hat{A}^{H}(\hat{A}\hat{F} - \hat{a}) = 0 \tag{2.21}$$

which leads to the following expression for the force vector which minimises the cost function.

$$\hat{F} = (\hat{A}^{H}\hat{A})^{-1}\hat{A}^{H}\hat{a} = \hat{A}^{+}\hat{a} \tag{2.22}$$

The matrix $\hat{A}^{+} = (\hat{A}^{H}\hat{A})^{-1}\hat{A}^{H}$ is termed the Moore-Penrose pseudo-inverse of $\hat{A}$.

2.7.2 Discussion on condition number

Figures 2.28-2.31 show the condition numbers of the $\hat{A}$ matrices for six different experiments. These include the two combinations of m and n considered in Section 2.4, the two cases with m=6, n=6 and m=9, n=6 and the two cases with no 'measurement noise'. The last four cases are used here in the discussion of condition numbers but are not considered further for force determination. In each of the cases, the condition number generally decreases as the frequency increases. At low frequencies the mode shapes are very simple and the modal density is very low so the deflections are closely related at all the locations. The placement of forces at any location would excite the same modes and the responses at any location would be dominated by these same modes. This results in closely dependent columns or rows in the accelerance matrix. Hence the condition numbers are quite high at these frequencies. As the modal overlap increases, the chance of placing forces and response positions at closely related locations is smaller. This results in general in lower condition numbers at high frequencies. However, the condition numbers are still high at some high frequencies.

The effect of over-determination (i.e. $m > n$) on the condition number of the accelerance matrix at different frequencies is clear from Figures 2.28 and 2.29. With over-determination, for example when m=6 and n=4, the condition numbers improve over the whole frequency range. When a larger number of forces are determined by a square matrix, the condition numbers can become quite large. Comparison of Figures 2.28 and 2.29 confirms this behaviour. Particularly in the case of 6 forces the improvement due to over-determination in the low frequency region is small. This can be explained by the fact that the structural behaviour of the plate is dominated by a small

number of modes and little additional information is gained by the further increase in the number of responses considered.

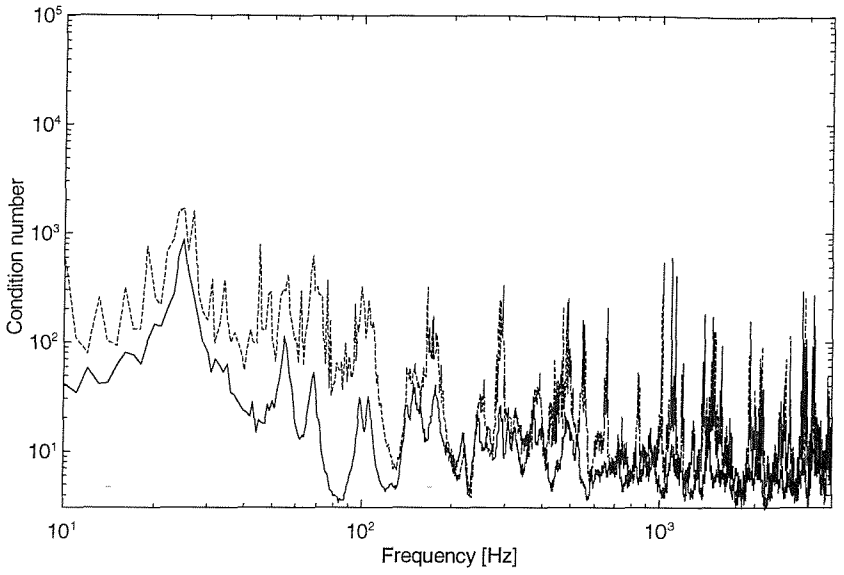

Figure 2.28. Condition numbers for 4 forces and 4 responses — — — — and 4 forces and 6 responses ————.

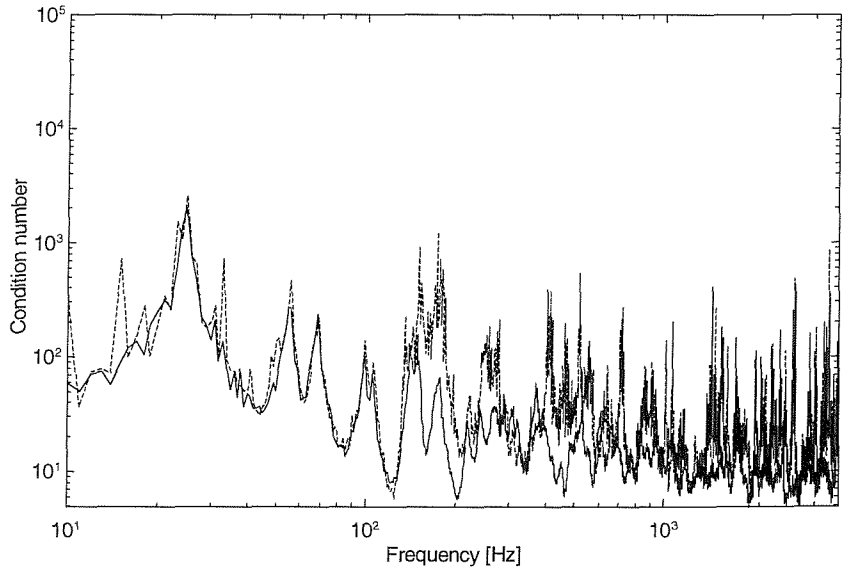

Figure 2.29. Condition numbers for 6 forces and 6 responses — — — — and 6 forces and 9 responses ————.

The introduction of random noise increases the condition numbers at some frequencies, especially at higher frequencies, and also results in erratic behaviour at some frequencies. On the other hand it tends to reduce the condition number at lower

frequency. This is clear from Figures 2.30 and 2.31, which show the difference in condition numbers with and without additional noise. The added noise corresponds, as before, to high noise.

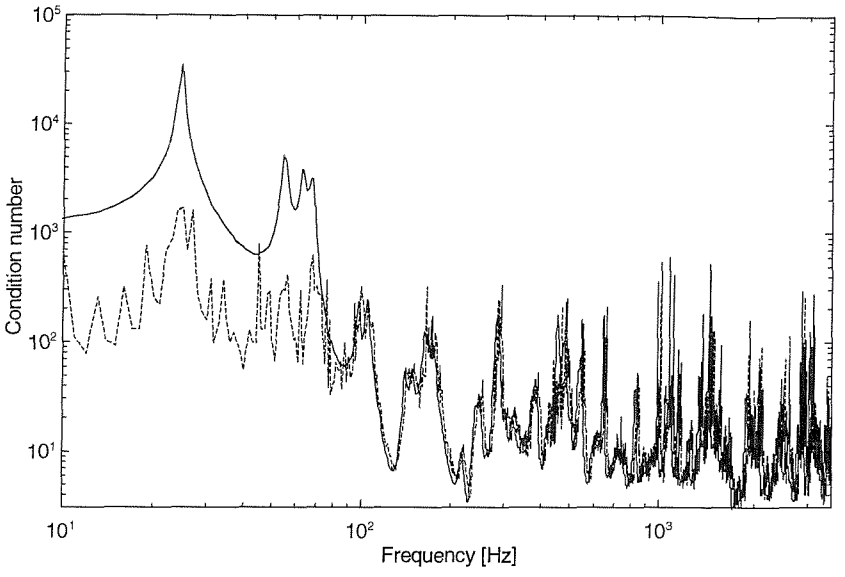

Figure 2.30. Influence of measurement noise on condition numbers for the case of 4 forces and 4 responses — — — — with high noise, ———— without noise.

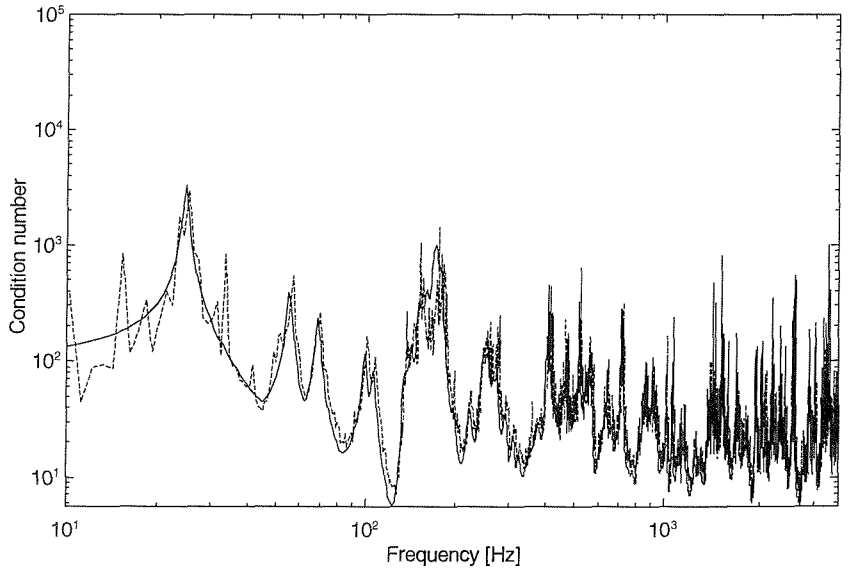

Figure 2.31. Influence of measurement noise on condition numbers for the case of 6 forces and 6 responses — — — — with high noise, ———— without noise.

The singular values associated with the accelerance matrices and their variation across the frequency range for the two cases with m=4, n=4, and m=6, n=4 are shown in Figures 2.32 and 2.33. Generally, all singular values increase in amplitude as the

frequency increases (corresponding to the behaviour of the accelerances) and the difference between the largest and smallest singular values reduces. With over-determination, the random variation in the smaller singular values appears to reduce considerably.

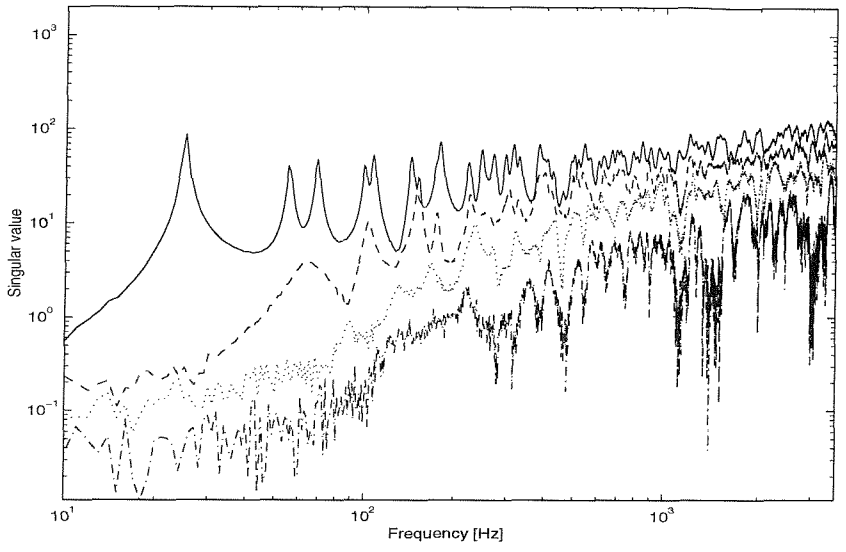

Figure 2.32. Singular values of accelerance matrix for the case of 4 forces and 4 responses.

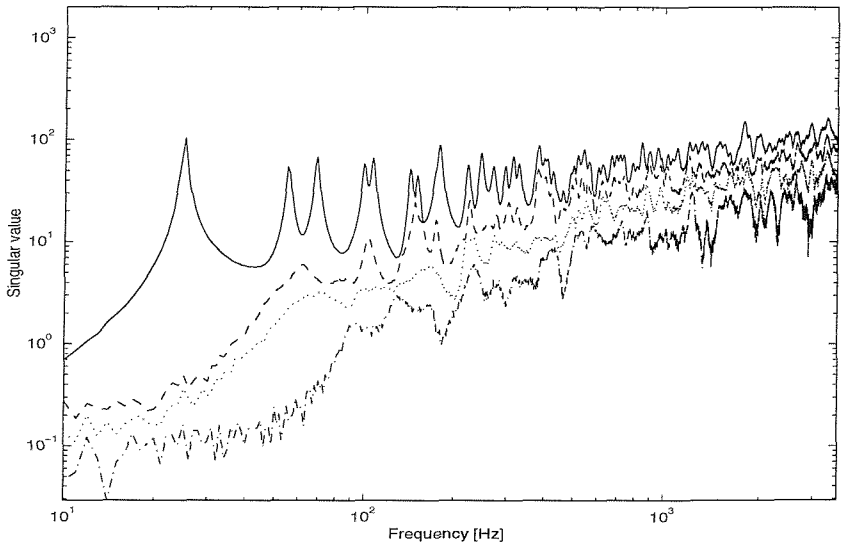

Figure 2.33. Singular values of accelerance matrix for the case of 4 forces and 6 responses.

The forces obtained using a 5 × 4 over-determined system by a least squares solution are shown in Figure 2.34. Above 100Hz the results are better than from the

square matrix case (Figure 2.8), especially for the smaller forces. The forces determined still have large errors in the low frequency region, although these errors are reduced compared with the square matrix case. This is due to the fact that only a small number of modes contribute significantly to the operational responses in the low frequency region; this number can be smaller than the number of forces to be identified [24]. Figure 2.35 shows reconstructed forces for the case of the 6×4 over-determined system. The errors are found to reduce further, particularly between 50 and 100 Hz compared with the 5×4 case (Figure 2.34) although there is little improvement below 50 Hz.

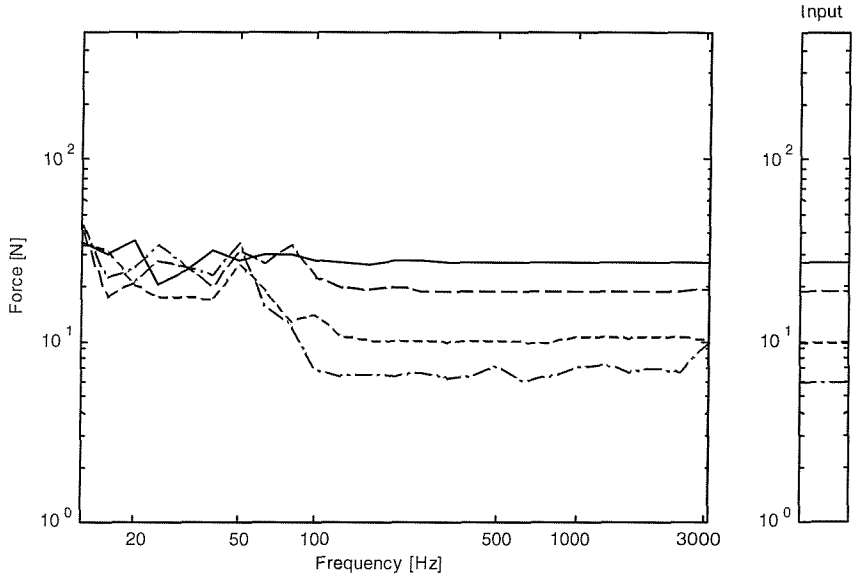

Figure 2.34. Reconstructed forces in 1/3 octave bands for 4 forces and 5 responses.
———— force 1, — — — — force 2, – – – – – – force 3, —·—·—· force 4.

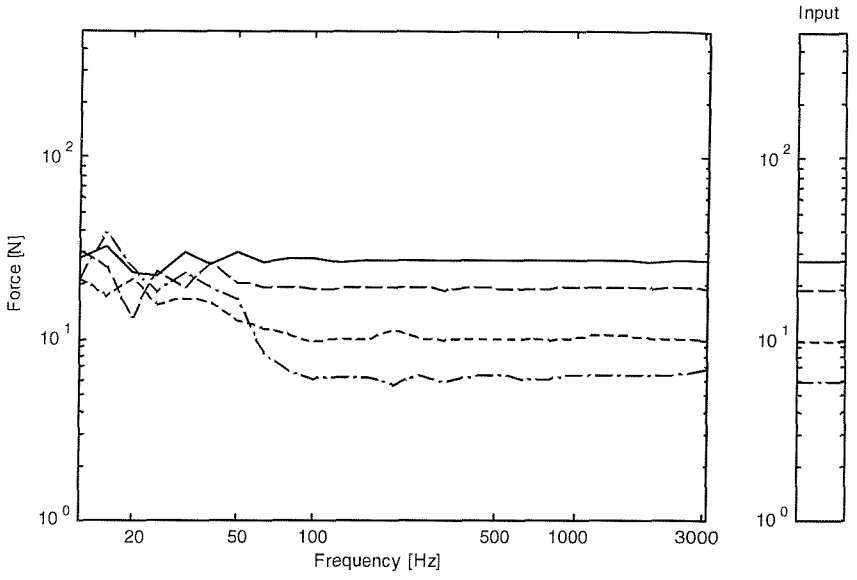

Figure 2.35. Reconstructed forces in 1/3 octave bands for 4 forces and 6 responses.
———— force 1, — — — — force 2, – – – – – – force 3, —·—·—· force 4.

Figure 2.36 shows the reconstructed response at the 'receiver' position for 4×4, 5×4 and 6×4 cases. Even though considerable errors still exist in reconstructed forces at low frequencies, the responses predicted are remarkably accurate with over-determination. In fact, it is difficult to distinguish between the actual and reconstructed responses for the case of the 6×4 over-determined system. Hence, although over-determination may give only limited improvement in force determination in the low modal density region, it has been shown to result in superior response reconstruction in this region. This is due to the fact that, although the forces cannot be distinguished in this region, as they all act on the same small number of modes, many possible combinations allow the combined effect to be reconstructed correctly.

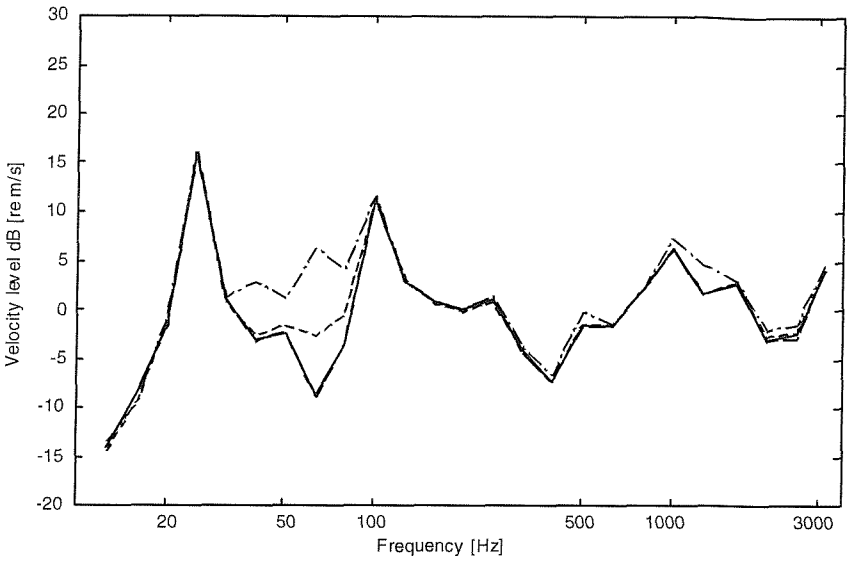

Figure 2.36. 1/3 octave band velocity response. — — —Actual response, — · — · — · reconstructed response using 4×4 matrix, – – – – – – reconstructed response using 5×4 matrix, ———— reconstructed response using 6×4 matrix.

2.8 DIFFERENT AVERAGING STRATEGY

In all the published studies on inverse force determination, for example [6-8, 11-15], only the mean values of the responses and accelerances are used to determine the forces. In this section, a different averaging technique is considered which does not assume the process to be Gaussian and hence allows some generalisation.

2.8.1 Method

The process used for force reconstruction and response prediction at the receiver location, in the proposed technique, is shown in Figure 2.37. To distinguish it from a process considered later, it is referred to as the 'single accelerance-based averaging' since only the mean value of accelerance is used (as above). It differs from the above technique, in the following way.

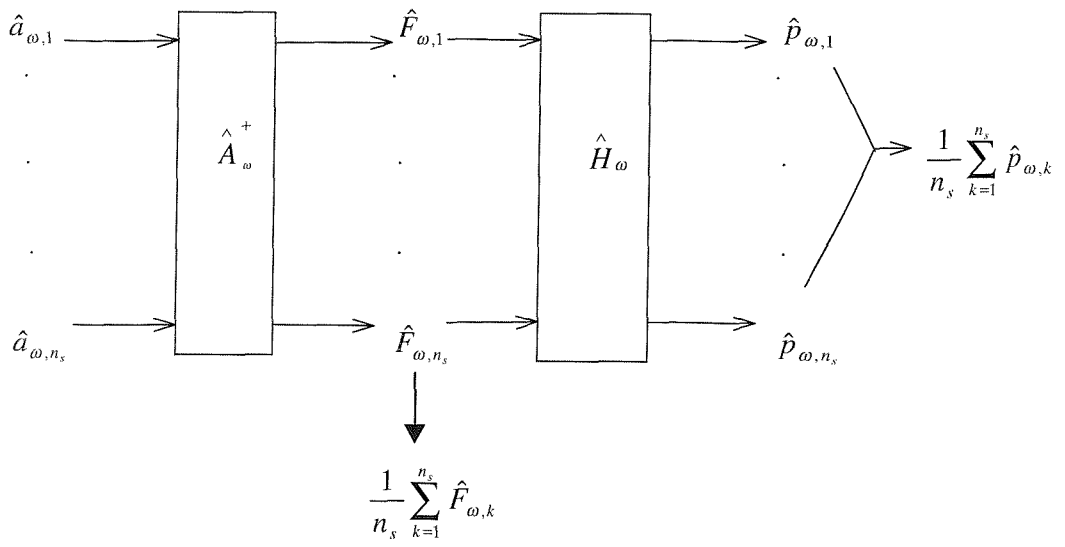

Figure 2.37. Flow chart showing single accelerance based averaging.

A series of experiments is performed to measure the operational accelerations $\hat{a}$ at m locations. The accelerances $\hat{A}_{ij}$ from each forcing location j to each operational response location i are also measured. The accelerances are estimated by averaging over n_{av} samples and this same average accelerance is used in the reconstruction of forces throughout. The operational acceleration data $\hat{a}$ is rearranged for each frequency to form a vector of length m. Each of the n_s measurement samples of this operational acceleration $\hat{a}_{\omega,k}$ is used to calculate a force vector $\hat{F}_{\omega,k}$ and the receiver response $\hat{p}_{\omega,k}$ at each frequency. Finally, averaging is performed by taking the vector sum of these estimations to form the mean of the responses. Confidence intervals can also be obtained from these sets of results.

The process described here differs from the more usual methods of application of TPA in the way that all samples of operational responses are used in the estimation of a series of reconstructed forces, while the usual methods [6-8, 11-15] consider only the mean operational response.

2.8.2 Reconstructed forces

For the averaging method proposed, the reconstructed forces for the case m=4, n=4 are shown in Figure 2.38. The reconstruction error is found to be large at lower frequencies, below 200 Hz as in Figure 2.8. There is a considerable effect of the higher

condition number on these estimations at lower and middle frequencies, but it improves considerably at higher frequencies. The force reconstruction does not differ from existing methods (Figure 2.8) since the noise added in the simulations is Gaussian as well. However, when applied to a real system this method would result in more reliable estimations.

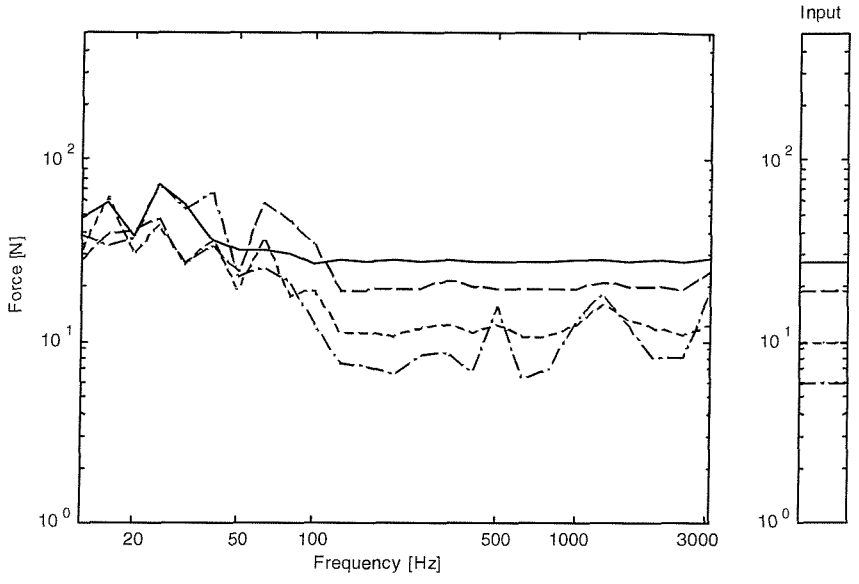

Figure 2.38. Reconstructed rms forces in 1/3 octave bands for 4 forces and 4 responses using modified averaging technique. ————force 1, — — — —force 2, – – – – – – force 3, — · — · — · force 4.

2.8.3 Velocity response at the receiver location

The response at the receiver location is shown in Figure 2.39. Also shown is a 68% confidence interval around the reconstructed spectrum. This range corresponds to the averaging performed over the operational response samples as shown in the flow chart (Figure 2.37). The reconstructed response at the receiver location obtained by this averaging technique is observed to be the same as that reconstructed with the usual method (Figure 2.10) for the case considered. Although the reconstructed response differs from the actual response, the predicted confidence interval mostly encloses the actual response.

The proposed averaging generalises the force reconstruction using experimental data. This procedure does not presume that the process generating errors is Gaussian. It

also leads to an estimation of confidence intervals that is more straight forward than the method of Monte Carlo simulation used by Janssens et al [11].

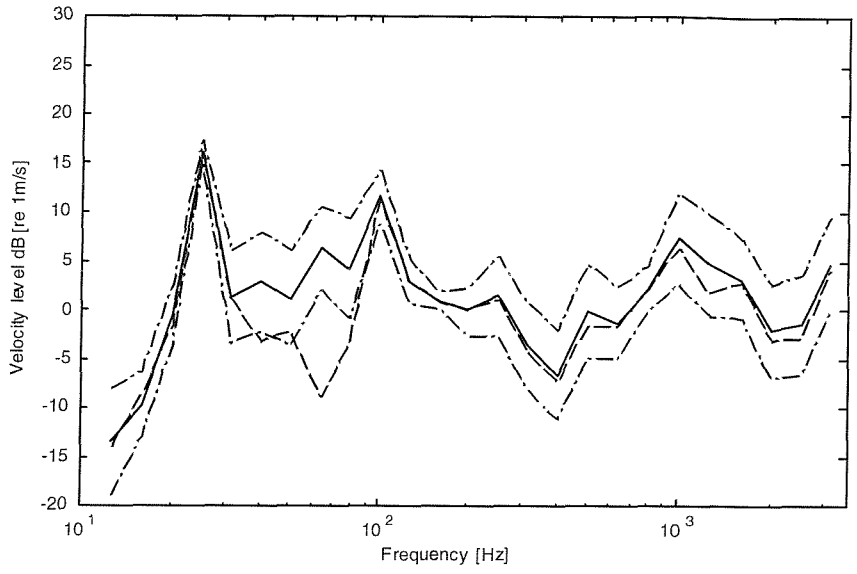

Figure 2.39. 1/3 octave velocity response at receiver location due to 4 forces reconstructed from 4 responses — — — —actual response, ———— reconstructed response, —·—· —68% confidence interval.

2.9 TESTS FOR ROBUSTNESS OF TECHNIQUES STUDIED TO NOISE LEVELS AND CONDITION NUMBERS

All the simulations in the previous sections were based on one set of data for forces and noise levels in the measurements. In this section the robustness of the pseudo-inverse is assessed by varying the amplitude of the added noise. In the previous sections the noise levels used correspond to high noise in the accelerances and a moderate noise in the operational responses. In Section 2.4.2 three noise levels for the accelerance and operational responses were presented. These noise levels can be used to construct 9 combinations, resulting in 9 experiments with different added noise levels. These 9 combinations are expected to cover the whole set of possible error levels in the measurements. The sensitivity of the pseudo-inverse in error amplification needs to be investigated in terms of the accelerance error, the response error and, indirectly, the condition number.

The average of the condition numbers across the frequency range for the 9 combinations are shown in the Table 2.4 for the case of m=4 and n=4. As expected from the discussion in Section 2.7, the average condition number is large for cases with low

levels of accelerance error. The response error has no effect on the condition number. The corresponding average condition numbers for the m=5, n=4 case are shown in Table 2.5. Significant reduction is seen in the average condition number compared with the square matrix case.

Table 2.4. The average condition number associated with the accelerance matrix due to addition of different levels of noises for the case of m=4 and n=4.

		Noise levels in operational responses		
		Low	medium	High
Noise levels in FRF's	Low	**91.1**	**91.1**	**91.1**
	medium	**40.8**	**40.8**	**40.8**
	High	**24.3**	**24.3**	**24.3**

Table 2.5. The average condition number associated with the accelerance matrix due to addition of different levels of noises for the case of m=5 and n=4.

		Noise levels in operational responses		
		Low	medium	High
Noise levels in FRF's	Low	**46.1**	**46.1**	**46.1**
	medium	**18.6**	**18.6**	**18.6**
	High	**12.4**	**12.4**	**12.4**

In Table 2.3 the noise added to generate 'measured' FRF's and operational responses was quantified by the average signal to noise ratios. The forces reconstructed using the 'measured' data contain errors which vary with frequency. To arrive at a single value to indicate the force reconstruction error across the frequency range, the root mean square error across the 1/3 octave bands error is evaluated. Since more than one force is reconstructed, to assess the sensitivity of the pseudo-inverse, the average of these root mean square errors is compared. The average error estimate is given below.

$$\varepsilon_{force} = \frac{1}{n}\sum_{j=1}^{n}\left[\frac{1}{N}\sum_{b=1}^{N}\left(\left|L_{\hat{F},j} - L_{F,j}\right|_b^2\right)\right]^{1/2} \tag{2.22}$$

where ε_{force} is the average force error in dB, N is the number of 1/3 octave bands b in the frequency range considered (here 25), $L_{\hat{F},j}$ is the reconstructed j^{th} force in 1/3 octave bands in dB and $L_{F,j}$ is the actual force in 1/3 octave bands in dB. While such a single

number indicator of the performance is attractive, it should be remembered that it involves averaging results at low and high modal overlap where the performance may differ considerably.

The average errors (equation (2.22)) in force determination for the square accelerance matrix are shown in Table 2.6. The equivalent results for the reconstructed receiver response are given in Table 2.7. The inverse force determination is observed to be very sensitive to the noise level in the responses when the condition numbers are large. Condition numbers can be large when noise in the accelerances is small (see Figure 2.30). The reconstructed responses generally contain smaller errors than the individual forces. However, the trends are the same, with the best performance for low noise in both FRF's and responses and the worst performance for high noise in the responses and low noise in the FRF's.

The forces determined for the case with moderate noise in the responses and low noise in the accelerances are shown in Figure 2.40. The forces contain very large errors at low frequencies where the condition numbers are high. At high frequencies, however, the forces are estimated reliably. The reconstructed response at the receiver location for this case is shown in Figure 2.41. Only near the anti-resonances do the force errors appear to result in large response errors.

Table 2.6. The average force errors in dB for different noise levels in operational responses and accelerances for the case of m=4 and n=4.

		Noise levels in operational responses		
		Low	**Medium**	**High**
Noise levels in FRF's	**Low**	**3.3**	**17.3**	**23.2**
	Medium	**5.3**	**12.9**	**20.3**
	High	**6.8**	**8.2**	**13.6**

Table 2.7. The average reconstructed response errors in dB for different noise levels in operational responses and accelerances for the case of m=4 and n=4.

		Noise levels in operational responses		
		Low	**Medium**	**High**
Noise levels in FRF's	**Low**	**0.8**	**8.7**	**13.3**
	Medium	**2.4**	**8.6**	**14.2**
	High	**2.9**	**3.0**	**8.0**

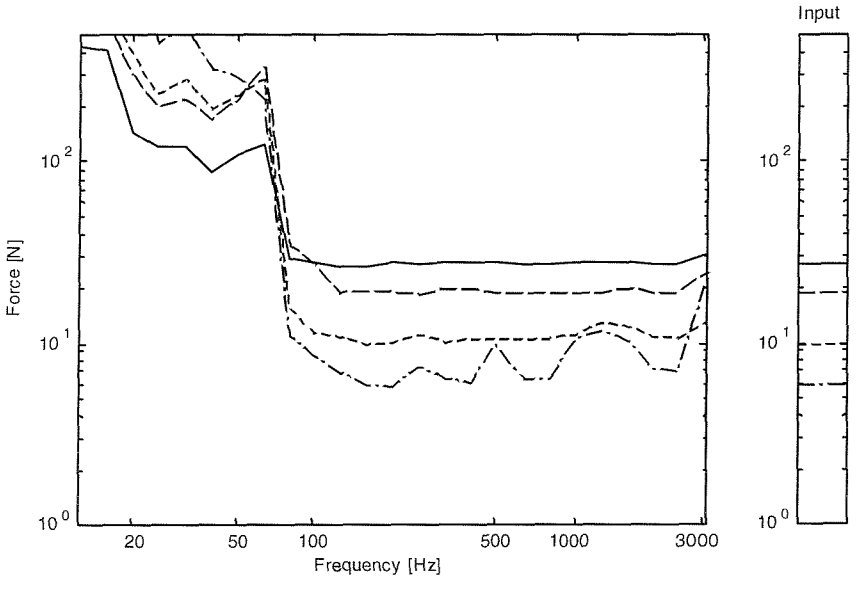

Figure 2.40. Reconstructed rms forces in 1/3 octave bands for 4 forces and 4 responses where responses contain moderate noise and accelerances contain low noise. ——— force 1, — — — — force 2, – – – – – – force 3, — · — · — · force 4.

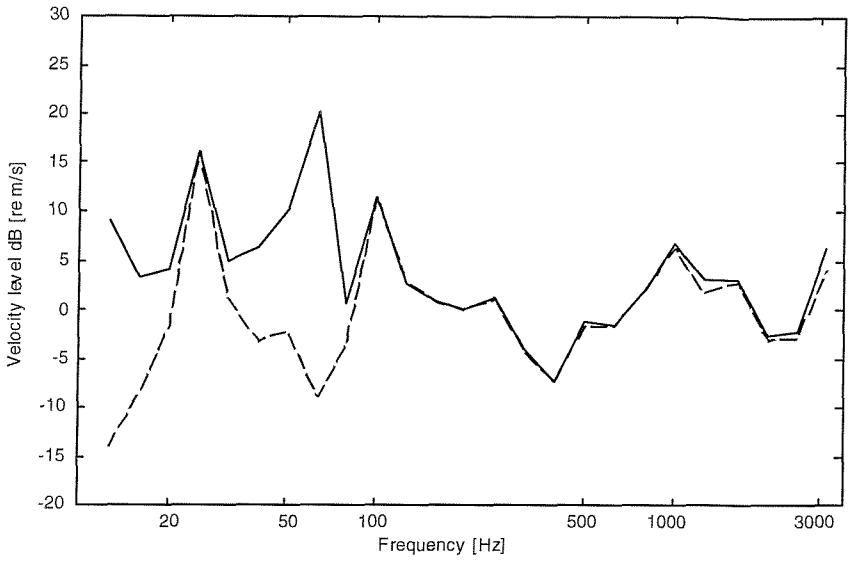

Figure 2.41. 1/3 octave velocity response at receiver location due to 4 forces reconstructed from 4 responses where responses contain moderate noise and accelerances contain small noise. — — — — actual response, ———— reconstructed response.

For the system with over-determination the corresponding error results are shown in Tables 2.8 and 2.9. Over-determination seems to reduce the error in force and velocities for all levels of noise in FRF and response measurements, although the improvement is smaller for low noise levels in FRF.

Table 2.8. The average force errors in dB for different noise levels in operational responses and accelerances for the case of m=5 and n=4.

		Noise levels in operational responses		
		Low	**Medium**	**High**
Noise levels in FRF's	**Low**	**2.2**	**13.1**	**19.9**
	Medium	**3.4**	**7.1**	**12.8**
	High	**3.2**	**4.2**	**8.3**

Table 2.9. The average reconstructed response errors in dB for different noise levels in operational responses and accelerances for the case of m=5 and n=4.

		Noise levels in operational responses		
		Low	**Medium**	**High**
Noise levels in FRF's	**Low**	**0.2**	**4.4**	**10.6**
	Medium	**0.7**	**2.9**	**6.4**
	High	**1.4**	**1.5**	**4.7**

In general, inverse force determination appears to be very sensitive to the variation of condition number and response errors.

2.10 CONCLUSIONS

In the inverse force determination, as the accelerance matrix may be ill-conditioned at many of the frequencies, erratic force predictions may occur at these frequencies due to the presence of small errors in the measurement of operational responses $\hat{a}$ and accelerances $\hat{A}$. Over-determination can produce some improvement in the high frequency region, where the modal density is high, provided that all paths of vibration transmission are included. It also improves condition number at low frequency. For high noise levels in the operational responses it has been seen to be essential to reduce the condition number of the matrix. In the present case this was achieved by introducing larger noise levels in the FRF's or by over-determination. Assuming that some errors in the measurements are inevitable, a means of improving the condition of the matrix is required without much compromise in the estimation of source strengths. This can be achieved by discarding singular values which are very small [7,11-12]. The potential of this technique is explored in the next chapter.

CHAPTER 3
DISCARDING SINGULAR VALUES TO IMPROVE FORCE DETERMINATION

3.1 INTRODUCTION

As has been seen, the forces determined indirectly by the inverse method often contain amplified measurement errors. The amplitude of these errors depends on the condition number of the accelerance matrix and the noise in the measurement of the responses and accelerances. In the previous chapter, over-determining the system was shown to reduce the error amplification. The over-determination helps to reduce the condition number of the system in the high frequency region where a large number of modes contribute to the response. It also helps to minimise the propagation of response errors by its use of a least squares solution. However, over-determination did not significantly improve force determination in the low frequency region where the number of forces determined can be more than the number of modes contributing significantly to the response. The effective condition number in the low frequency region can, however, be reduced by discarding insignificant singular values of the accelerance matrix [7] and hence the error amplification can be reduced. This technique has been used in the literature [7-8, 11-13] with success. However, an important aspect for its successful application is the criterion used for rejecting singular values. This method is considered further in this chapter.

3.2 SINGULAR VALUE REJECTION

Any matrix can be decomposed into two square unitary matrices U and V and a rectangular matrix S containing a diagonal matrix of singular values. Applying this to the accelerance matrix gives

$$\{\hat{a}\} = U\begin{bmatrix} diag(s_1,.....,s_n) \\ [0]_{m-n\times n} \end{bmatrix} V^H \{\hat{F}\} \tag{3.1}$$

The Moore-Penrose pseudo-inverse solution of $\hat{A}$, equation (2.22) allows this to be written as

$$\{\hat{F}\}=\left(VS^{T}U^{H}USV^{H}\right)^{-1}VS^{T}U^{H}\{\hat{a}\}$$

$$=V\left(S^{T}S\right)^{-1}S^{T}U^{H}\{\hat{a}\}$$

$$\{\hat{F}\}=V\left[diag\left(\frac{1}{s_1},.....,\frac{1}{s_n}\right)\middle|\ [0]_{n\times m-n}\right]U^{H}\{\hat{a}\} \tag{3.2}$$

In the direct equation, (3.1), the significance of the contribution from each singular value can be assessed. The ratio of the largest singular value to the smallest can be taken as a measure of the significance of the contribution from the smallest singular value. If this ratio is large, the contribution from the smallest singular value is negligible. The ratio mentioned above is also a definition of the condition number of the matrix (see Section 2.2.2). If the condition number is large, it should be possible to discard smaller singular values without introducing significant bias into the solution.

Similar considerations apply to the inverse solution, equation (3.2). However, it may be noted that, in the inverse solution, the contributions come from the reciprocal of the singular values. This means that larger contributions come from smaller singular values. It seems as if the inversion would be dominated by smaller singular values. However, this is not necessarily the case. The reciprocal of the singular value is pre- and post-multiplied by the right and left unitary vectors *V* and *U*. For the smaller singular values, the elements of these vectors tend to have more sign changes (more oscillation). This leads to a product, which is a matrix, the elements of which have large magnitude but frequent sign changes. This means that their contribution to the solution tends to be averaged out.

If the FRF measurements contain no error, the singular values also do not contain any error. However, any errors in the measured operational responses are amplified due to the large elements in the product matrix which will no longer cancel.

On the other hand if the accelerance matrix contains errors, then the smaller singular values are most affected. Sometimes the error contribution may be greater than the magnitude of the smaller singular values. This results in incorrect estimates of the

smaller singular values which ultimately affects the inverse (reciprocal of singular values). Hence, the total effect would be that the inverse would be inaccurate and result in force estimates which contain large errors.

From the above discussion, and the fact that, in the ideal situation (no errors in the measurements), smaller singular values result in a smaller contribution in the inverse due to the oscillatory nature of the unitary vectors, they can usually be discarded when condition numbers are large without introducing significant bias into the solution. The discarded singular values ($1/s_i$) are replaced by 0 in the inverse, equation (3.2).

The problem here is how to determine the 'smallness' of a singular value. A threshold value is required for the rejection of singular values. If the threshold level selected is wrong one of two extremes can happen. If the threshold level is very low the singular values corrupted by measurement error may not be rejected, leading to no improvement in the inverse. On the other hand, if the threshold is large, more singular values may be rejected than necessary resulting in the introduction of large bias errors. For example, differences between the reconstructed response and the actual response at the receiver location are shown in Figure 3.1. Different lines in the figure correspond to inversion where zero, one, two or three singular values are rejected from a 4×4 matrix across the whole frequency range.

It can be seen that, for each singular value rejected, the predicted response is usually reduced. At high frequencies it appears that the best results are achieved using 3 or 4 singular values; rejecting more than one leads to under-prediction. At other frequencies better results are achieved by rejecting more singular values. Up to 30 Hz it appears that rejecting even three singular values does not introduce any bias. This shows that the right level of threshold needs to be established at each frequency so as to reduce error amplification whilst avoiding the introduction of excessive bias.

In [7,12] the norm of the FRF error matrix or the operational response error vector was adopted with varying degrees of success. The formulations leading to these thresholds, and simulations carried out to assess their effectiveness, are described below.

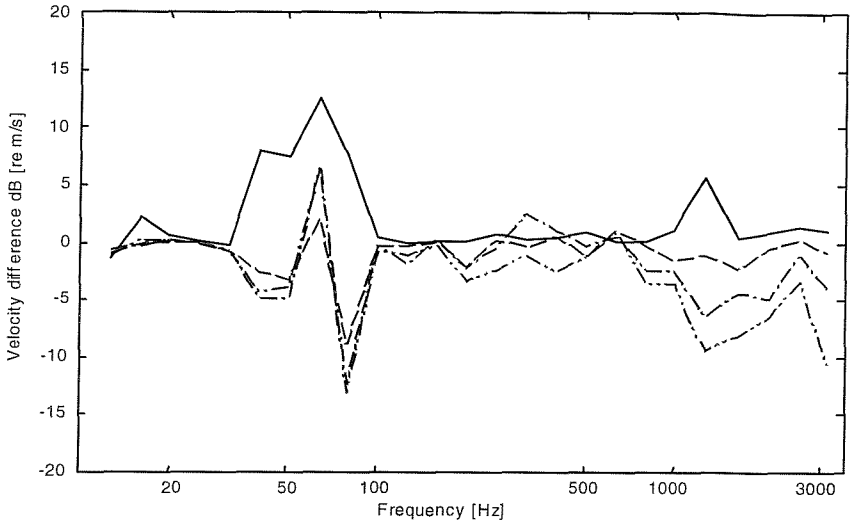

Figure 3.1. The difference in the reconstructed velocity and the actual response in dB at the receiver location due to 4 forces reconstructed from 4 responses. ———— *no singular value rejected,* — — — — *one singular value rejected,* —·—·— *two singular values rejected and* —··—··—*three singular values rejected.*

3.3 THRESHOLD BASED ON ACCELERANCE ERROR

The error in an FRF estimate can be taken as a basis for establishing the singular value rejection threshold. An estimate of the error for each element of the FRF matrix can be constructed following [70] as

$$E_{ij} = \alpha \left[\frac{1-\gamma^2_{\omega,ij}}{2n_{av}\gamma^2_{\omega,ij}} \right]^{1/2} \left| \hat{A}_{\omega,ij} \right| \tag{3.3}$$

where E_{ij} defines an error bound for $\hat{A}_{\omega,ij}$. Here, γ^2 is the coherence and n_{av} is the number of averages used in determining $\hat{A}$. If α is 1, for instance, E_{ij} represents one standard deviation of $\hat{A}_{ij}$. The 2-norm of the error matrix $\|E\|_2$ (see Appendix A) can be used as a threshold to reject the singular values, as suggested in [7]. If all the singular values are less than the error norm then the largest singular value may be replaced by the error norm itself.

3.3.1 Reconstructed forces

Numerical simulations have been carried out to represent 'measurements' as in Chapter 2. The noise levels used correspond to high noise in the FRF's and moderate noise in the operational responses as in Sections 2.5 and 2.7. Figure 3.2 shows the number of singular values used in the inversion for a square matrix case and Figure 3.3 gives the corresponding estimated forces. The value of α is taken as 3 in equation (3.3) for these calculations as in [7, 10]. The forces are estimated more reliably in the low frequency region compared with the method where all singular values are used (compare Figures 3.3 and 2.8). Between 40 and 100 Hz forces are under-estimated and in the high frequency region, the larger forces are under-estimated indicating that more singular values are being rejected than is essential. More singular values are rejected in the low frequency region than in the high frequency region, which is because at high frequencies condition numbers are generally lower (see Figures 2.28). The effect of rejecting singular values is also evident in the force determination below 40 Hz where the forces estimated are almost all equal. Here only one singular value is retained.

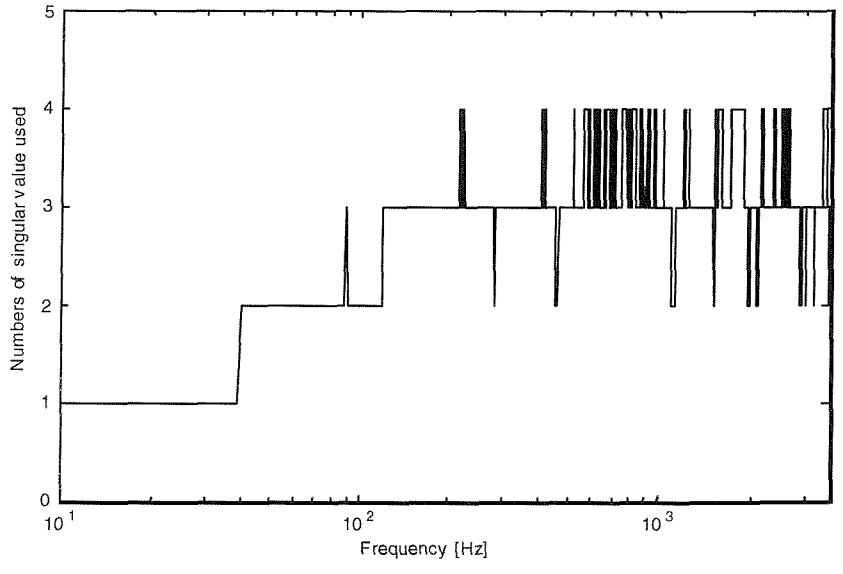

Figure 3.2. Number of singular values used in force reconstruction for 4 forces and 4 responses for high FRF error and α=3.

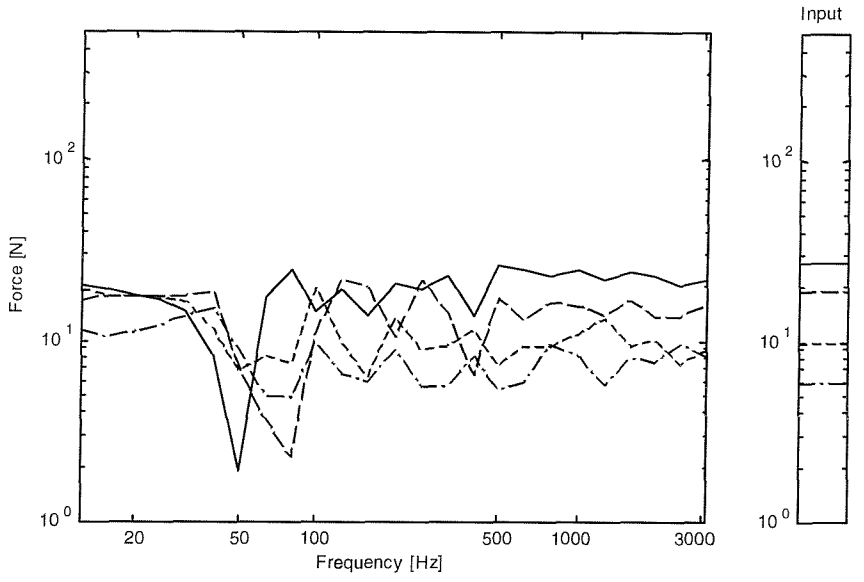

Figure 3.3. Reconstructed rms forces for 4 forces and 4 responses with singular value rejection ————— force 1, — — — force 2, - - - - - - force 3, — - — - — force 4.

In Figure 3.4 the singular values are compared with the error norm. It can be seen that the singular values are widely spaced at low frequencies and come much closer together at high frequencies. The error norm is observed to exceed all but the first singular value in the low frequency region, leading to the retention of only one singular value, see Figure 3.2.

With over-determination, considerably fewer singular values are rejected at high frequency (Figure 3.5) than for the square matrix (Figure 3.2). There is consequently an improvement in the reconstruction of the forces in the high frequency region (Figure 3.6). In the over-determined system the forces obtained, particularly the larger forces, are found to be inferior at high frequencies with singular value rejection to when all singular values are used (compare Figures 3.6 and 2.34). This is because over-determination has already improved the condition of the matrix at high frequency leading to better force reconstruction. When singular values are rejected some information is lost, resulting in an under-estimation of the forces.

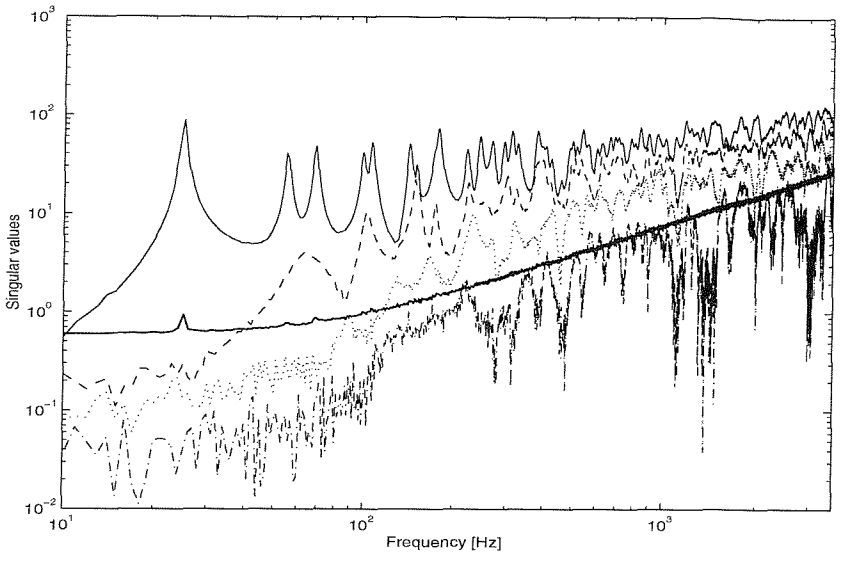

Figure 3.4. Variation of four singular values of 4x4 matrix and associated error norm for one of the 'measurements' for high noise level in FRF and α=3. ——— *error norm.*

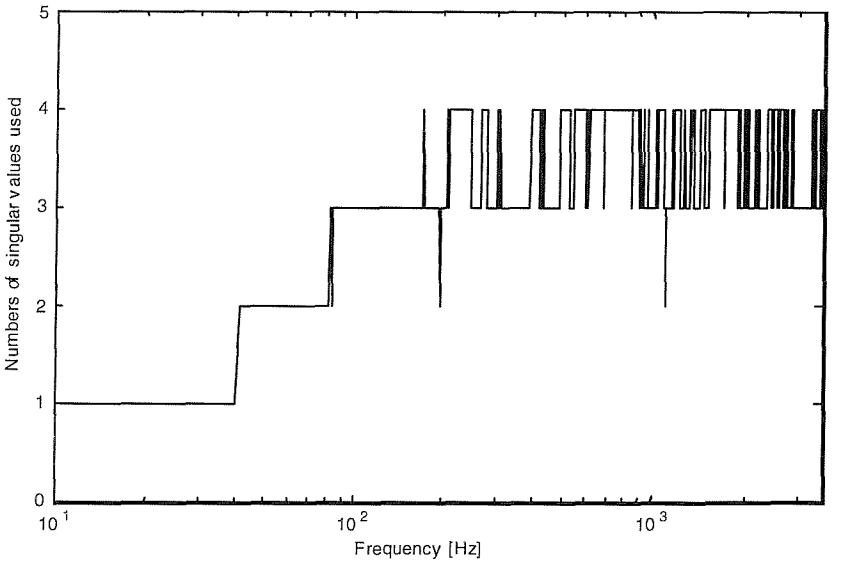

Figure 3.5. Number of singular values used in force reconstruction for 4 forces and 5 responses for high noise level in FRF and α=3.

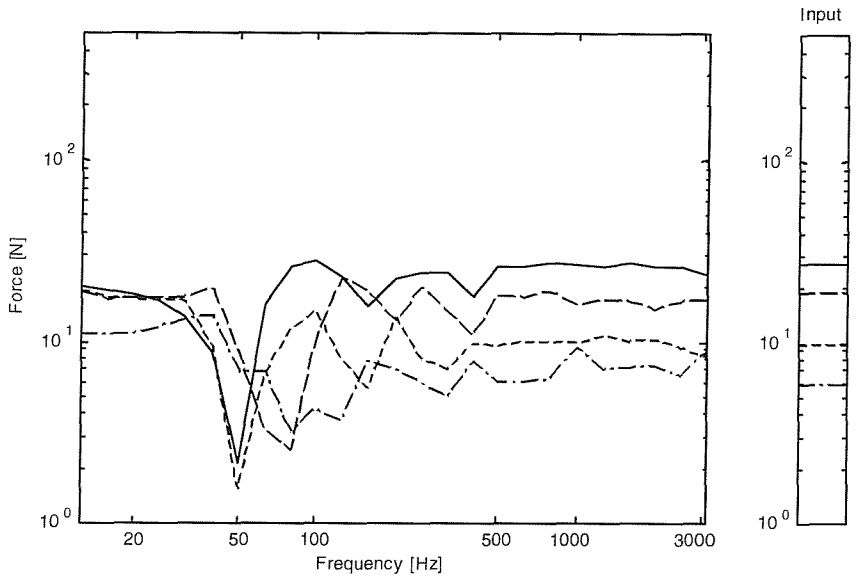

Figure 3.6. Reconstructed rms forces for 4 forces and 5 responses with singular value rejection. ————force 1, — — —force 2, - - - - - - force 3, — - — - — force 4.

3.1.2 Velocity response at the receiver location

As the accuracy of force reconstruction affects the final prediction of response at the receiver location, the response reconstruction is considerably improved when singular values are rejected. Figure 3.7 shows the reconstructed response at the receiver location for the square matrix case. Considerable improvement is observed compared with the case where all singular values are used. When the system is over-determined, the estimations improve somewhat at high frequency, as seen from Figure 3.8, but at low frequency the results are if anything slightly worse than without singular value rejection.

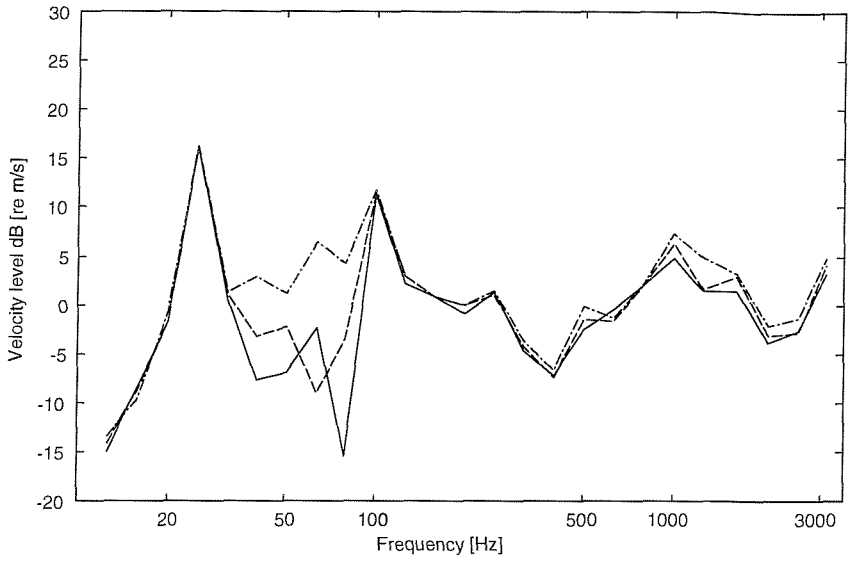

Figure 3.7. 1/3 octave velocity response at receiver location due to 4 forces reconstructed from 4 responses — — — — actual response, ———— reconstructed response obtained using singular value rejection and — - — - — reconstructed response obtained using all singular values.

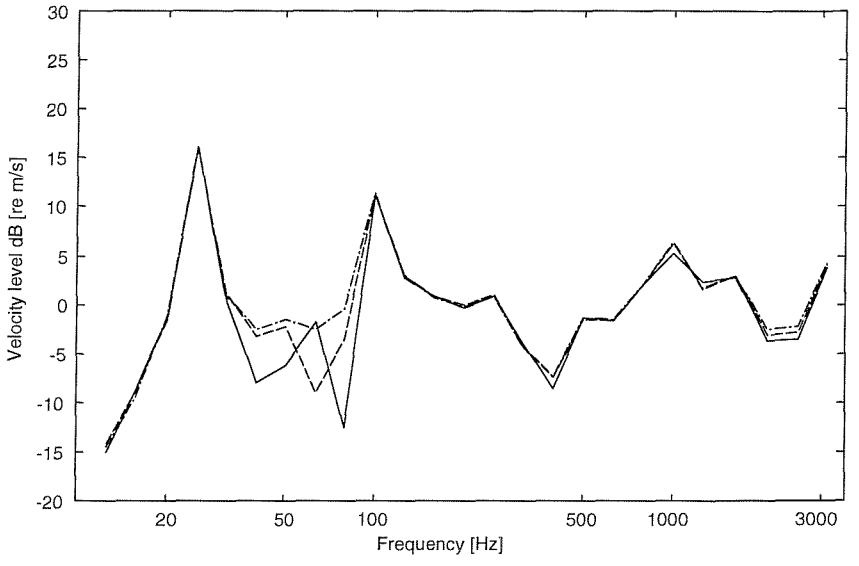

Figure 3.8. 1/3 octave velocity response at receiver location due to 4 forces reconstructed from 5 responses — — — — actual response, ———— reconstructed response obtained using singular value rejection and — - — - — reconstructed response obtained using all singular values.

3.1.3 Different bandwidth for rejection of singular values

In the simulations so far the threshold value is estimated using equation (3.3) taking $\alpha = 3$. This corresponds to a range of 3 standard deviations. It appears to result in loss of information leading to an under-estimation of forces and responses. If a different bandwidth is used, the results could be significantly different. In this section a 68% confidence interval bandwidth i.e. $\alpha = 1$ is used in establishing the threshold for rejecting singular values. The numbers of singular values retained for this case are shown in Figure 3.9. Considerably less singular values are rejected compared with the case of $\alpha = 3$ (compare with Figure 3.2). The force reconstruction is improved considerably as well as shown in Figure 3.10 (compare with Figure 3.3) with the larger forces no longer being under-predicted at high frequency. This improvement is due to the loss of less information from rejecting singular values. Although the differences are smaller, these conclusions are further confirmed by Figure 3.11 which shows the receiver location response (compare with Figure 3.7).

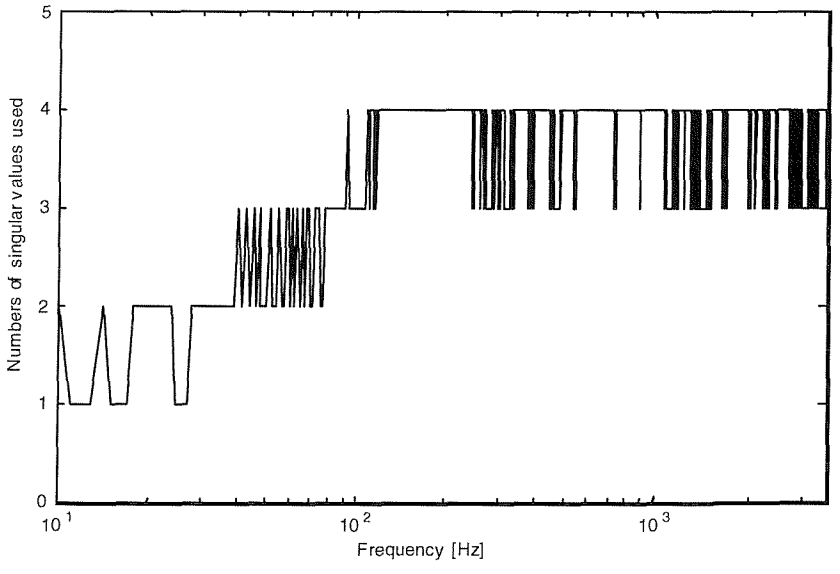

Figure 3.9. Number of singular values used at each frequency for 4 forces and 4 responses with $\alpha = 1$.

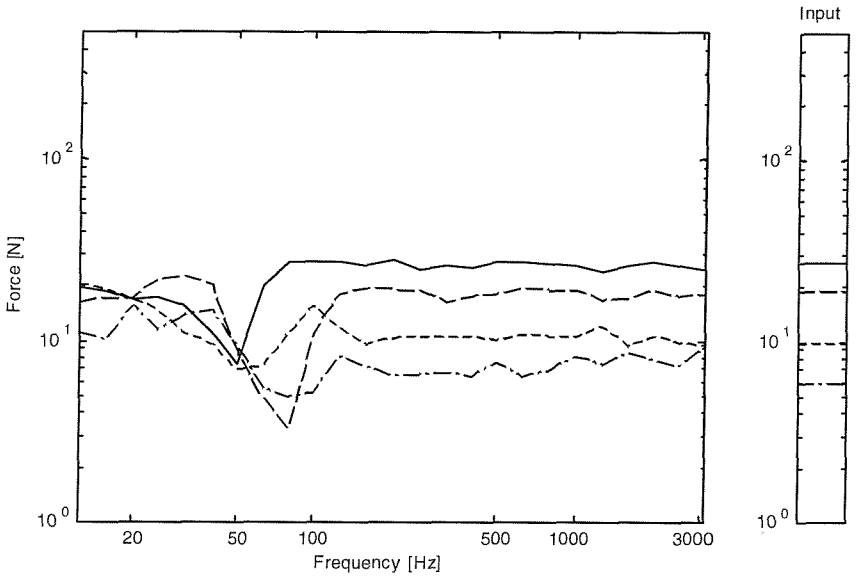

Figure 3.10. Reconstructed rms forces for 4 forces and 4 responses obtained by singular value rejection based on accelerance error with $\alpha = 1$. ———— *force 1,* — — — *force 2,* - - - - - - *force 3,* — - — - — *force 4.*

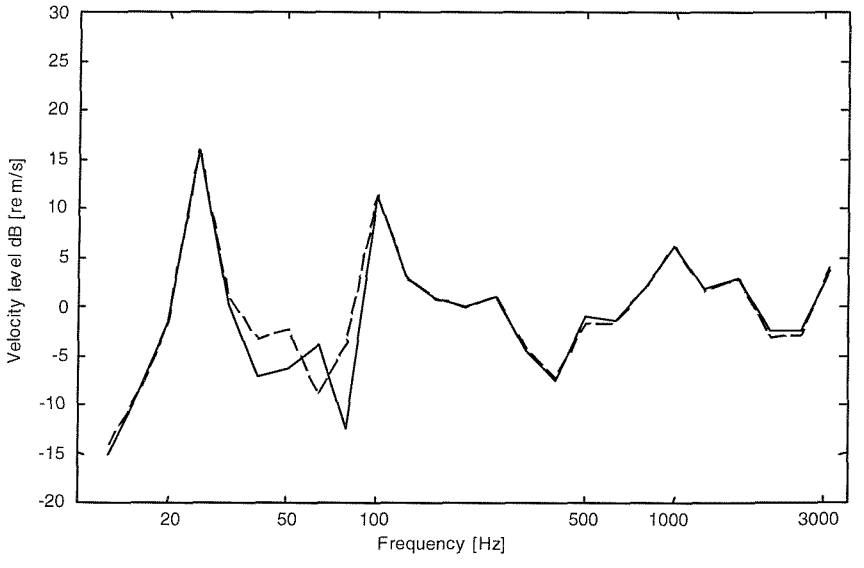

Figure 3.11. 1/3 octave band velocity response at the receiver location reconstructed using 4 forces and 4 responses obtained by singular value rejection based on accelerance error with $\alpha = 1$. — — — — *actual response,* ———— *reconstructed response.*

3.1.4 Cumulative sum of singular values

In the above criterion, each singular value is compared with the threshold and rejected if it falls below it. When more than one singular value is rejected this may introduce more bias than required. When the condition numbers are moderately high and the error in the accelerance measurement is large, the threshold criterion described may discard some useful information.

Each singular value of the accelerance matrix contributes partially in forming the matrix. Write $\left[A_{ij}\right]_k = U_{ik} s_k V_{kj}^H$ for j, k=1.....n and i=1.....m. Then $[A] = \sum_k [A]_k$. When a singular value is rejected, the corresponding information is removed from the whole accelerance matrix. Ideally the total contribution from the singular values that are rejected should be less than the threshold. If singular values are compared separately with the threshold (as in earlier sections) this need not be the case. At some frequencies the total contribution from the rejected singular values may exceed the threshold. To overcome this and generalise the comparison of singular values with the threshold, instead of comparing individual singular values with the error threshold, the cumulative sum of the last (n-r) singular values is compared, with r taking the values n-1, n-2, ...,1.

Figure 3.12 shows the force reconstructed using accelerance matrix inversion where the cumulative sum of singular values is compared with the error threshold, again using $\alpha = 1$. When the cumulative sum of singular values is used, some improvement is observed in force reconstruction below 100 Hz, particularly for the largest force (compare with Figure 3.10). This improvement is due to the retention of more singular values as shown in Figure 3.13 than in the case where singular values are treated separately (compare with Figure 3.9). The corresponding reconstructed velocity response at the receiver location is given in Figure 3.14. No significant improvement is observed over the case where singular values are compared separately (compare with Figure 3.11). In general, the use of the cumulative sum in comparing with the error threshold should reject singular values more optimally than comparing singular values individually, although the effect is modest.

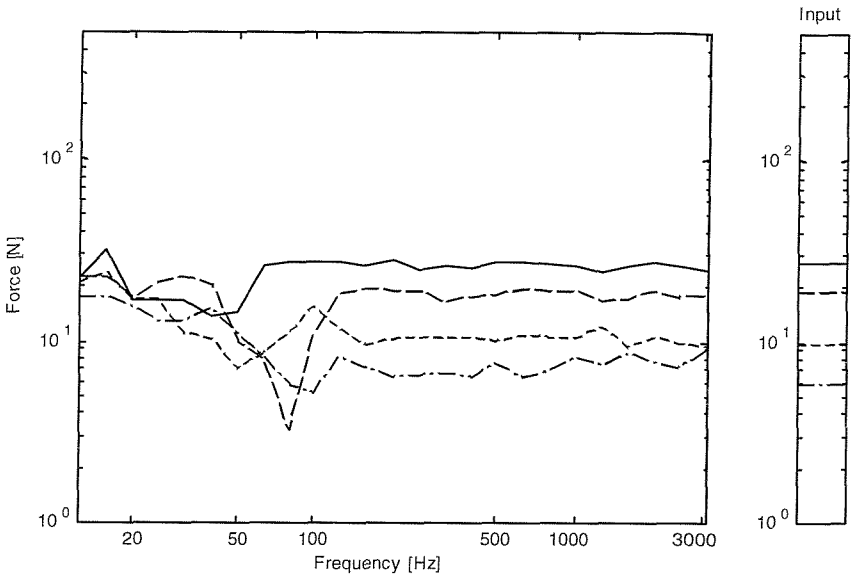

Figure 3.12. Reconstructed rms forces in 1/3 octave bands for 4 forces and 4 responses obtained by singular value rejection using cumulative sum to compare with the accelerance error when $\alpha = 1$. ————*force 1,* — — —*force 2,* - - - - - - *force 3,* — - — - — *force 4.*

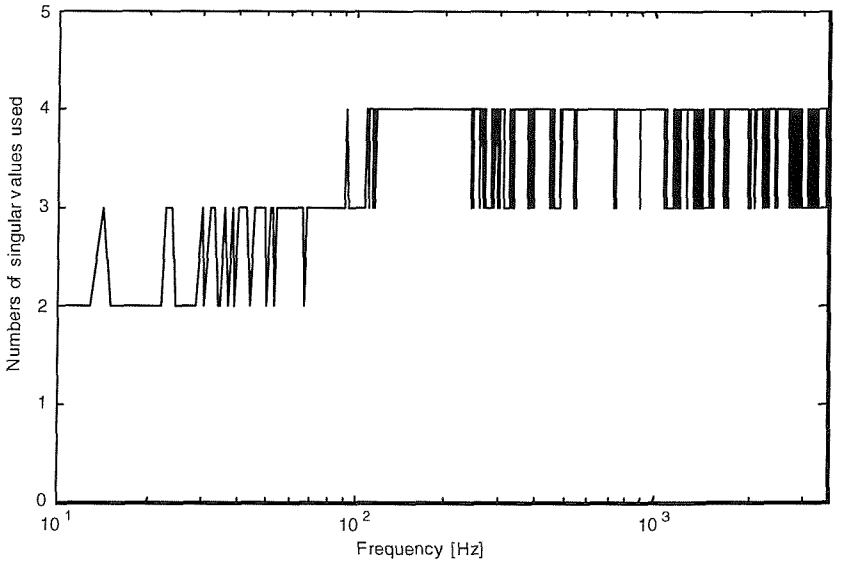

Figure 3.13. Number of singular values used at each frequency for 4 forces and 4 responses obtained using cumulative sum to compare with the accelerance error when $\alpha = 1$.

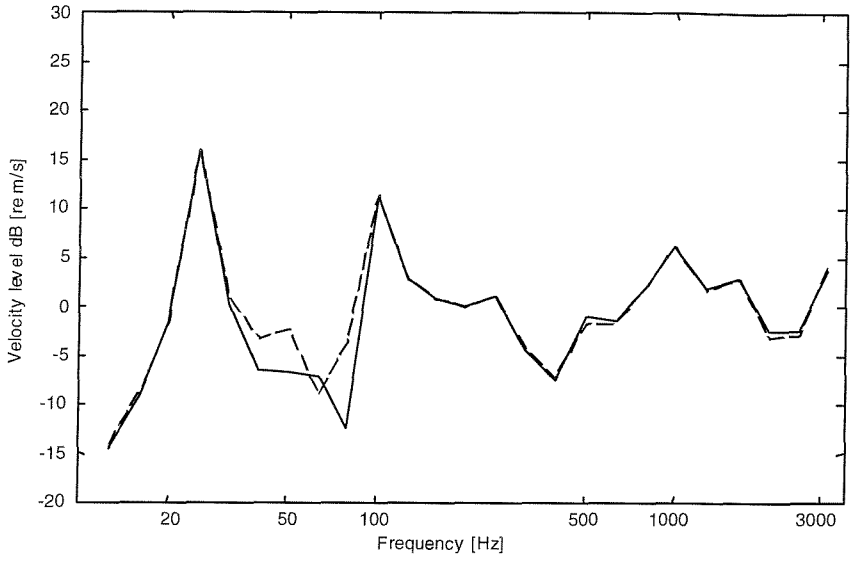

Figure 3.14. 1/3 octave band velocity response at the receiver location reconstructed using 4 forces and 4 responses obtained by singular value rejection using cumulative sum to compare with the accelerance error when $\alpha = 1$. — — — — *actual response,* ———— *reconstructed response.*

3.1.5 Robustness of singular value rejection based on FRF error

In Chapter 2 the methods studied were shown to be very sensitive to the noise level in the 'measurements'. It is interesting to know how the method based on singular value rejection fares when the noise level in the response and accelerance measurements is varied. Nine combinations of the noise level in the accelerances and the responses have been investigated, as in Chapter 2. Tables 3.1 and 3.2 show overall results for force determination and response reconstruction. The method of rejecting singular values based on the accelerance error fails to reduce significantly the error amplification where noise in the responses is large and noise in the FRF's is small. However, the results are still better than those based on the full rank inverse (see Tables 2.6-2.7). The present results improve on those of full rank inversion in all cases except low noise in FRF's and responses. The improvements are most marked for moderate noise in the FRF's. The results here correspond to $\alpha = 1$ and the cumulative sum of singular values.

Table 3.1. Average 1/3 octave band errors in forces determined for square matrix 4×4 using singular value rejection based on accelerance error with $\alpha = 1$ and cumulative sum of singular values is compared.

		Noise levels in operational responses		
		Low	**Medium**	**High**
Noise levels in FRF's	**Low**	**3.8**	**9.9**	**17.0**
	Medium	**1.7**	**2.8**	**7.9**
	High	**3.1**	**3.2**	**5.5**

Table 3.2. Average 1/3 octave band errors in reconstructed velocity response at the receiver location for square matrix 4×4 using singular value rejection based on accelerance error with $\alpha = 1$ and cumulative sum of singular values is compared.

		Noise levels in operational response		
		Low	**Medium**	**High**
Noise levels in FRF's	**Low**	**1.1**	**5.3**	**10.2**
	Medium	**0.4**	**0.8**	**5.1**
	High	**2.3**	**2.4**	**2.6**

Tables 3.3 and 3.4 show overall results for force determination and response reconstruction for an over-determined system (5×4 matrix). Similar improvements are observed over pseudo-inversion as in square matrix case (see Tables 2.8 and 2.9).

Table 3.3. Average 1/3 octave band errors in forces determined for matrix 5×4 using singular value rejection based on accelerance error with α = 1 and cumulative sum of singular values is compared.

		Noise levels in operational response		
		Low	**Medium**	**High**
Noise levels in FRF's	**Low**	**0.4**	**7.6**	**12.5**
	Medium	**1.5**	**2.0**	**5.7**
	High	**2.7**	**2.7**	**3.7**

Table 3.4. Average 1/3 octave band errors in reconstructed velocity response at the receiver location for matrix 5×4 using singular value rejection based on accelerance error with α = 1 and cumulative sum of singular values is compared.

		Noise levels in operational responses		
		Low	**Medium**	**High**
Noise levels in FRF's	**Low**	**0.1**	**3.7**	**7.5**
	Medium	**0.8**	**0.8**	**3.7**
	High	**1.7**	**1.8**	**2.0**

The estimated forces and reconstructed response for the over-determined system are given in Figures 3.15 and 3.16 respectively for one case where this method fails. These results correspond to moderate noise in the responses and low noise in the FRF's. The errors in the reconstructed forces are very large at low frequency where the condition numbers of the accelerance matrix are large. The reconstructed velocity response at the receiver location also contains large errors in the low frequency region, particularly at the anti-resonance frequency (63 Hz). However, in both the cases the results are very good above 100 Hz.

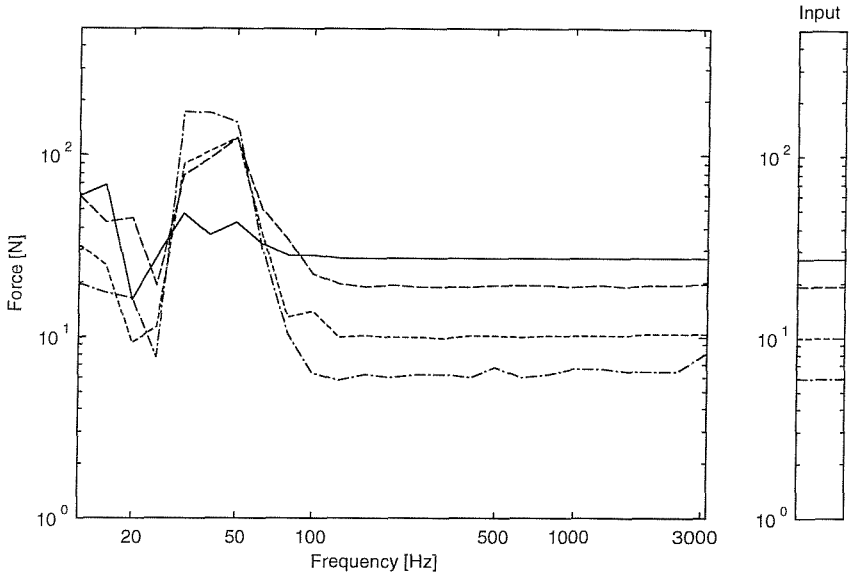

Figure 3.15. Reconstructed rms forces in 1/3 octave bands for 4 forces and 5 responses obtained by singular value rejection based on accelerance error with $\alpha = 1$ for the case of moderate noise in the responses and low noise in the FRF's.————force 1, — — —force 2, - - - - - -force 3, — - — - — force 4.

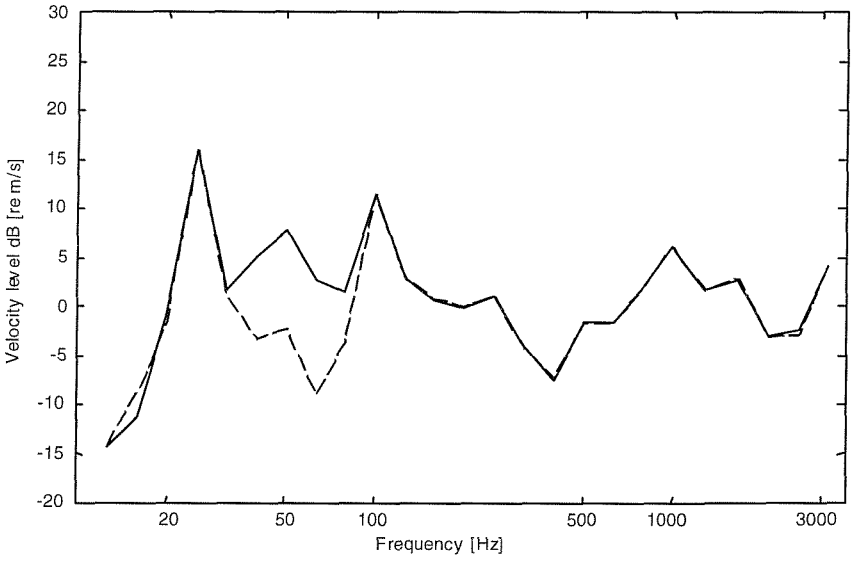

Figure 3.16. 1/3 octave band velocity response at the receiver location reconstructed using 4 forces and 5 responses obtained by singular value rejection based on accelerance error with $\alpha = 1$ for the case of moderate noise in the responses and low noise in the FRF's.

3.2 THRESHOLD BASED ON RESPONSE ERROR

When the threshold is selected on the basis of the accelerance error, as discussed above, it is assumed that the main source of error is the FRF matrix. However, the operational responses also form a source of error, and since they are often measured in a noisier environment, this may be dominant. Therefore the second criterion explored for threshold estimation for the singular values is based on the contribution of individual singular values to the operational response [12].

3.2.1 Derivation

The following analysis is based on that given by Janssens et al [12]. The operational responses can be written as a sum of contributions from each of the singular values. According to this criterion, smaller singular values are rejected if they contribute less to the responses than the error in the measurement of operational responses. The errors in the operational responses can be estimated based on the averaging process, where variations in auto spectra for each sample can be used to obtain the standard deviation, or by using approximate formulae as given by [70]. If estimated from the latter, the random error in the operational response measurements (frequency spectrum) can be based on the expression for the standard deviation for a Gaussian signal

$$\sigma = \frac{\left|\hat{S}_{xx}\right|}{\sqrt{n_s}} \tag{3.4}$$

where n_s is the number of samples taken for averaging and S_{xx} is the power spectral density (PSD) of x.

The response errors based on equation (3.4), are dependent on the number of averages used in estimating the auto spectrum. In this case, as 25 samples are used to estimate the responses, the response error is expected to be 20% of the response itself. This is true whatever the actual level of noise in the responses. This process of estimating response errors may result in larger errors than that corresponding to uncertainty present in the process. Hence it is observed to result in considerable under-estimation [77]. This necessitates the use of estimates based on the actual process, which in this case can be constructed by using the averaging. For this purpose, the 68%

percent confidence limit on the square root of the auto spectra can be taken as a standard deviation of the process while averaging. Based on this standard deviation, it is possible to estimate the actual confidence limit on the mean response following [68]. The expression for this is

$$\sigma = 1.68\frac{\sigma_p}{\sqrt{n_s}} \tag{3.5}$$

where σ_p is the standard deviation of the underlying process for which forces are determined. The standard deviation based on equation (3.5) has been used in the remainder of this thesis for rejecting singular values based on response errors.

From the accelerance matrix, if the forces are known, the acceleration can be calculated as

$$\{a\} = [A]\{F\} \tag{3.6a}$$

Due to the errors in the measurement, the measured acceleration can be represented as

$$\{\hat{a}\} = \{a + a_e\} \tag{3.6b}$$

The contribution from each singular value to the operational responses can be derived as follows. Using singular value decomposition, the accelerance matrix can be decomposed as

$$\hat{A} = USV^H$$

This can also be written as

$$[\hat{A}] = [A]_1 + [A]_2 + ... + [A]_n$$

where

$$\left[A_{ij}\right]_k = U_{ik} s_k V_{kj}^H \qquad \text{for } j,k=1.....n \text{ and } i=1.....m \tag{3.7}$$

The contribution from each singular value to the response is given by

$$\{a_k\} = [A]_k \{F\} \qquad \text{for } k=1.....n \tag{3.8}$$

The equation (3.8) cannot be evaluated since the forces are not known. However this difficulty can be overcome by normalisation. The contribution from the largest singular value can be taken as a first approximation to the acceleration response. Therefore

$$\{a_f\} \approx [A]_1 \{F\}$$

where a_f is a first approximation to the acceleration response. Taking the norm of the above equation

$$\|\{a_f\}\| \approx \|[A]_1 \{F\}\| \leq \|[A]_1\| \|\{F\}\| \tag{3.9}$$

Taking the norm of (3.8)

$$\|\{a_k\}\| = \|[A]_k \{F\}\| \leq \|[A_k]\| \|\{F\}\| \quad \text{for } k=1.....n \tag{3.10}$$

Taking the ratio of (3.9) and (3.10), although they are both inequalities, gives the qualitative relation

$$\frac{\|\{a_k\}\|}{\|\{a_f\}\|} \sim \frac{\|[A]_k\|}{\|[A]_1\|} \tag{3.11}$$

From (3.7) the 2-norm is given by $\|[A]_k\| = s_k$. Thus the the above relation, can be written as

$$\frac{\|\{a_k\}\|}{\|\{a_f\}\|} \sim \frac{s_k}{s_1} \tag{3.12}$$

This suggests that singular values should be rejected when

$$\frac{\|\{a_e\}\|}{\|\{\hat{a}\}\|} \geq \frac{\|\{a_k\}\|}{\|\{a_f\}\|} \quad \text{or} \quad \geq \frac{s_k}{s_1}$$

which can also be written as

$$s_k \leq \frac{\|\{\sigma\}\|_2}{\|\{\hat{a}\}\|_2} s_1 \tag{3.13}$$

where $\{\sigma\}$is the vector of response errors and $\{\hat{a}\}$ is the vector of measured responses.

3.2.2 Cumulative sum of singular values

In the study of Janssens [12], as in equation (3.13), individual singular values were compared to the norm of the error matrix. This may reject more information than necessary. In Section 3.3.4 a cumulative sum was tried out with good effect. Hence it is desirable to investigate the effect of comparing individual singular values or the cumulative sum of the last (*n*-*r*) singular values with the threshold while rejecting the singular values. The formulation for this latter criterion is discussed below.

Let the partial contribution from the last (n-r) singular values to the accelerations be given by

$$\{a_{partial}\} = [A_{r+1} ..... + A_n]\{F\} \tag{3.14}$$

Taking the norm of the above equation

$$\|\{a_{partial}\}\| = \|[A_{r+1} ..... + A_n]\{F\}\| \le (\|A_{r+1}\| + ... + \|A_n\|)\|\{F\}\| \tag{3.15}$$

Taking the ratio of relations (3.9) and (3.15) gives the qualitative relation

$$\frac{\|\{a_{partial}\}\|}{\|\{a_f\}\|} \sim \frac{(\|A_{r+1}\| ... + \|A_{n_e}\|)\|\{F\}\|}{\|[A_1]\|\|\{F\}\|} \tag{3.16}$$

In the above relation, if the norms are 2-norms, this can be written as

$$\frac{\|\{a_{partial}\}\|}{\|\{a_f\}\|} \sim \frac{s_{r+1} ... + s_n}{s_1}$$

This suggests that the contribution from the last (n-r) singular values can be neglected when

$$\frac{\|\{a_e\}\|}{\|\{\hat{a}\}\|} \ge \frac{\|\{a_{partial}\}\|}{\|\{a_f\}\|} \text{ or } \ge \frac{s_{r+1} ... + s_n}{s_1}$$

which can also be written as

$$s_1 \frac{\|\{\sigma\}\|_2}{\|\{\hat{a}\}\|_2} \ge s_{r+1} ... + s_n \tag{3.17}$$

If, instead of the 2-norm, the Frobenius norm is used then there is no necessity to consider the cumulative effect of singular values. This is because the Frobenius norm of a matrix is given by

$\|[A]\|_F = \sqrt{s_1^2 + ... + s_n^2}$ which considers all singular values.

3.2.3 Force and response reconstruction

Calculations have been performed for high noise levels (low S/N ratio) in the accelerances and moderate noise levels in the responses as before. Figure 3.17 shows the number of singular values included and Figure 3.18 shows the forces. The response error used to estimate the threshold for rejecting singular values is based on equation (3.5). The forces are under-estimated when singular values are rejected based on this threshold more than when based on the norm of accelerance error matrix, $\|E\|_2$ (compare Figures 3.18 and 3.10). In fact, more singular values are rejected with the threshold based on response error as shown in Figure 3.17 (compare with Figure 3.9). Due to the under-estimation of forces, the response at the receiver location is also under-estimated at some frequencies especially above 1 kHz (Figure 3.19).

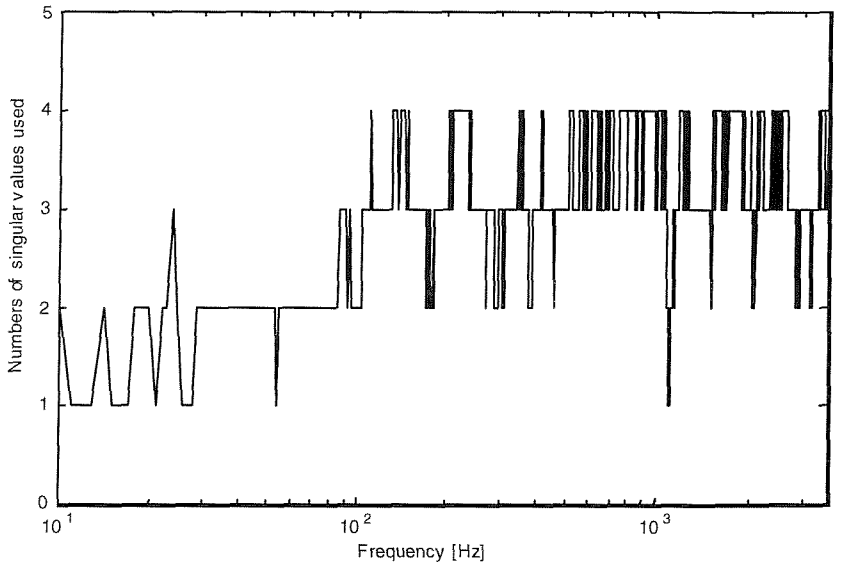

Figure 3.17. Number of singular values used at each frequency for 4 forces and 4 responses with threshold based on response errors.

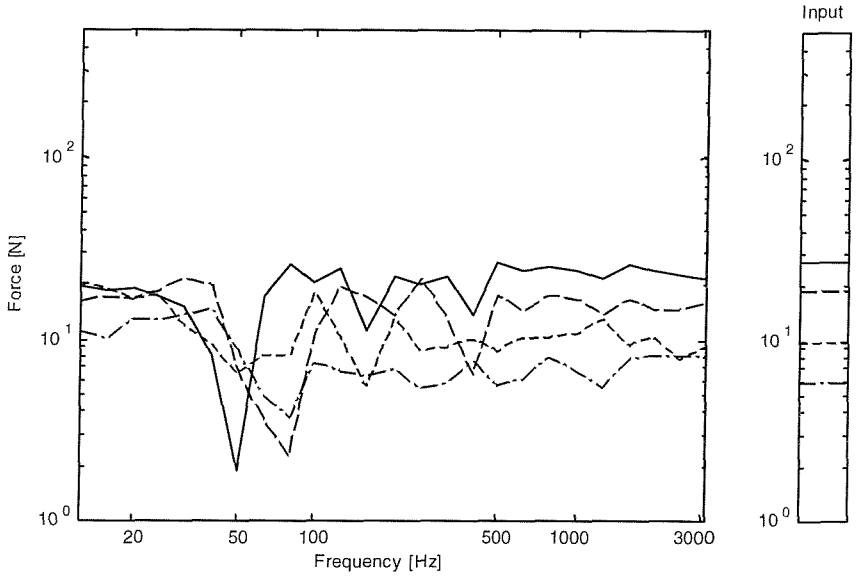

Figure 3.18. Reconstructed rms forces in 1/3 octave bands for 4 forces and 4 responses obtained by singular value rejection based on response error. ————— force 1, — — — force 2, - - - - - - force 3, — - — - — force 4.

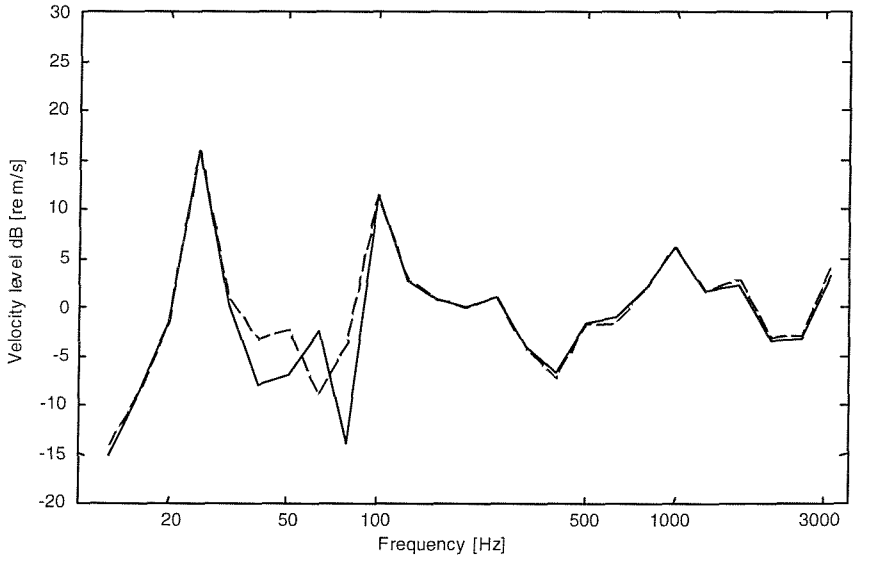

Figure 3.19. 1/3 octave band velocity response at the receiver location reconstructed using 4 forces and 4 responses obtained by singular value rejection based on response error. — — — — actual response, ————— reconstructed response.

Similar improvements as in Section 3.3.4 are observed when the cumulative sum of the last (n-r) singular values is compared with the threshold based on equation (3.5) to reject the singular values. For this case, the singular values included, forces and reconstructed response are shown in Figure 3.20-3.22 respectively. Here more singular values are used at many frequencies than for the separate comparison of singular values (compare Figure 3.20 and 3.17). The improvement in force reconstruction is not very clear from Figure 3.21, although some differences are seen in the frequency region below 200 Hz compared with Figure 3.18. Similarly the response reconstructed is not very different from that in Figure 3.19. In general, however, the concept of the cumulative sum of singular values can result in some improvements.

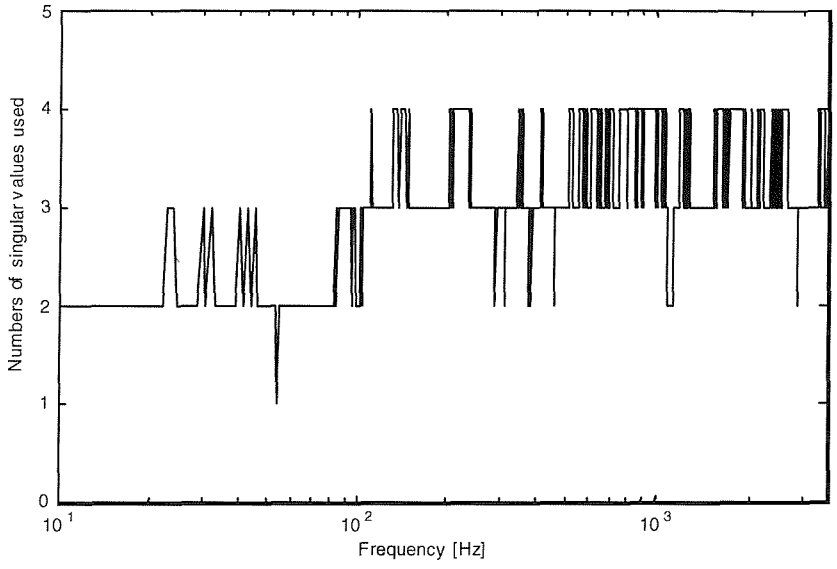

Figure 3.20. Number of Singular values used at each frequency for 4 sources and 4 responses with threshold based on response errors using cumulative sum comparison.

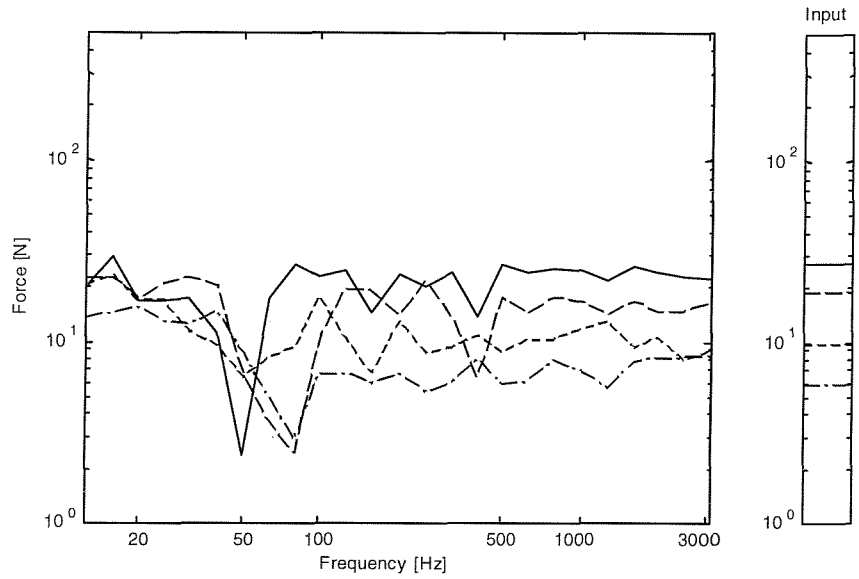

Figure 3.21. Reconstructed rms forces in 1/3 octave bands for 4 forces and 4 responses obtained by singular value rejection based on response error using cumulative sum comparison. ————force 1, — — —force 2, — - — - —force 3, - - - - - - force 4.

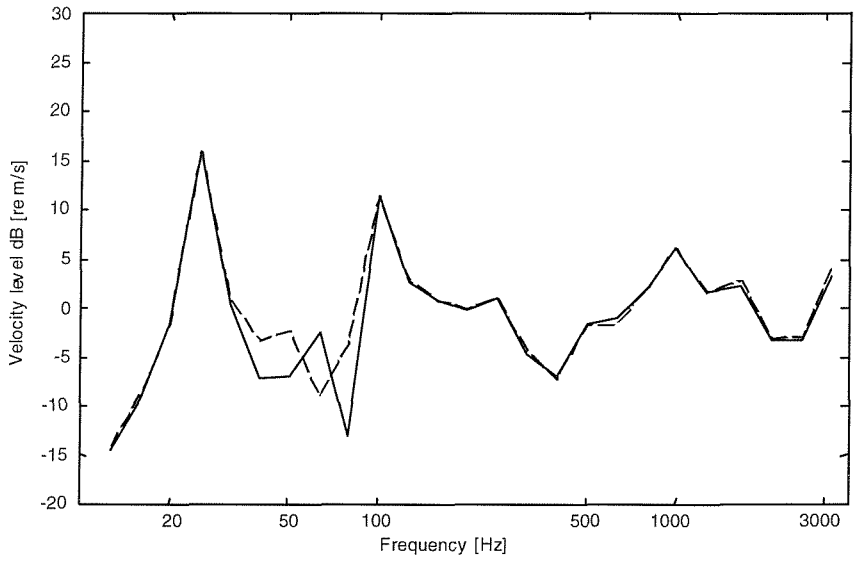

Figure 3.22. 1/3 octave band velocity response at the receiver location reconstructed using 4 forces and 4 responses obtained by singular value rejection based on response error using cumulative sum comparison. — — — —actual response, ———— reconstructed response.

3.2.4 Robustness of singular value rejection based on response error

Nine combinations of the noise level in accelerances and in responses have been investigated here, as in Section 3.3.5. Tables 3.5 and 3.6 show overall results for force determination and response reconstruction for the square matrix case. The threshold based on response error (equation (3.5)) appears to reduce error amplification in situations where noise in the responses is large. It appears to perform less well where the noise in the accelerances is large compared with the noise in the responses. However, the results are much better than those based on the full rank inverse or the threshold based on the accelerance error (compare with Tables 3.1-3.2 and 2.6-2.7).

Tables 3.7 and 3.8 show overall results for force determination and response reconstruction for the 5×4 over-determined system. Similar improvements are observed over the pseudo-inverse as in square matrix case (see Tables 2.8 and 2.9). No improvement is observed for the case where responses have low noise. For a high noise in the responses, the error in the receiver response is greater than for the square matrix case (see Table 3.6). This appears to be due to rejection of singular values at high frequency where condition numbers are small for over-determined system.

Table 3.5. Average 1/3 octave band errors in forces determined for square matrix 4×4 using singular value rejection based on response error and cumulative sum of singular values is compared.

		Noise levels in operational responses		
		Low	**Medium**	**High**
Noise levels in FRF's	**Low**	**0.9**	**4.3**	**5.7**
	Medium	**3.5**	**4.3**	**5.7**
	High	**6.7**	**4.3**	**5.7**

Table 3.6. Average 1/3 octave band errors in reconstructed velocity response at the receiver location for square matrix 4×4 using singular value rejection based on response error and cumulative sum of singular values is compared.

		Noise levels in operational responses		
		Low	Medium	High
Noise levels in FRF's	Low	0.5	2.2	3.7
	Medium	0.5	2.8	3.7
	High	2.8	2.7	3.7

Table 3.7. Average 1/3 octave band errors in forces determined for 5×4 matrix using singular value rejection based on response error and cumulative sum of singular values is compared.

		Noise levels in operational responses		
		Low	Medium	High
Noise levels in FRF's	Low	0.6	3.5	5.5
	Medium	3.3	3.5	5.5
	High	3.2	3.3	5.5

Table 3.8. Average 1/3 octave band errors in reconstructed velocity response at the receiver location for 5×4 matrix using singular value rejection based on response error and cumulative sum of singular values is compared.

		Noise levels in operational responses		
		Low	Medium	High
Noise levels in FRF's	Low	0.2	2.5	4.2
	Medium	0.2	2.5	4.2
	High	1.4	2.4	4.0

The results of force reconstruction and receiver velocity for the over-determined system for the case corresponding to high noise in the FRF's and low noise in the responses are shown in Figures 3.23 and 3.24 respectively. This case has been chosen

since the threshold here is based on response error and the case considered has FRF errors that are larger than the response errors. The forces reconstructed contain moderately large errors below 100 Hz. The reconstructed velocity response at the receiver location is reliable, although some differences occur in the anti-resonance region.

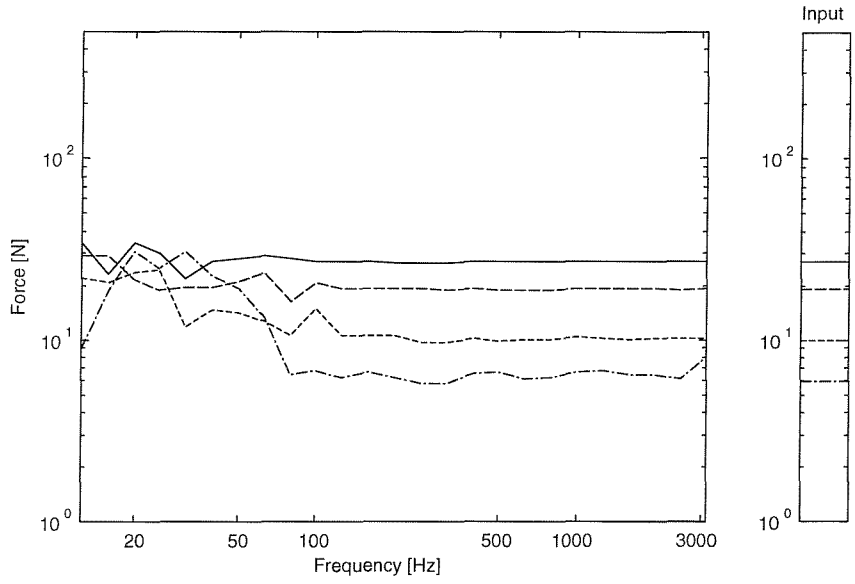

Figure 3.23. Reconstructed rms forces in 1/3 octave bands for 4 forces and 5 responses obtained by singular value rejection based on response error for the case of high noise in the FRF's and low noise in the responses. ————— force 1, — — — force 2, - - - - - - force 3, — - — - — force 4.

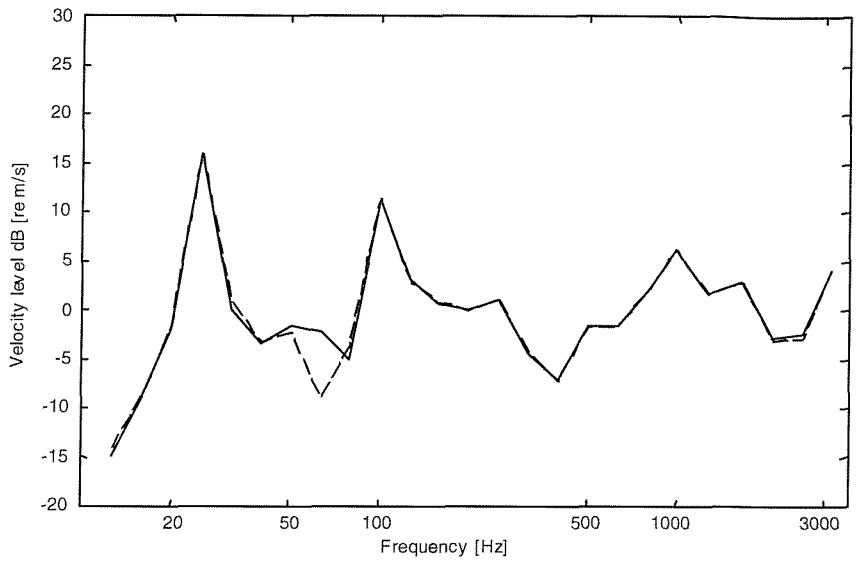

Figure 3.24. 1/3 octave band velocity response at the receiver location reconstructed using 4 forces and 5 responses obtained by singular value rejection based on response error for the case of high noise in the FRF's and low noise in the responses.

— — — —actual response, ———— reconstructed response.

3.3 Summary

The threshold for rejecting singular values based on response errors estimated using the expression for random errors (equation (3.4)) was observed to result in considerable under-estimation [77]. The error calculation suggested based on the actual process improves the force reconstruction by retaining uncorrupted singular values. In general, either a threshold based on response errors or accelerance errors gives reliable results when the norm is based on a band of ± one standard deviation error, although this depends on the amplitude of corrupting noise used. The thresholds mentioned are not universal and lead to failure in certain cases. The threshold based on response error has been found to be more robust than that based on accelerance error. However, errors still occur in forces for both cases. Hence it is essential to explore other potential techniques. Ideally both FRF errors and response errors should be accounted for. One such method is proposed in the next chapter. This technique is based on accelerance error behaviour.

CHAPTER 4

PERTURBED ACCELERANCE MATRIX METHOD

4.1 INTRODUCTION

It has been observed in Chapter 2 that the reconstructed forces, obtained by inversion of the accelerance matrix $\hat{A}$, contain large errors at frequencies with high condition numbers, due to the presence of small errors in the measurement of the accelerances and operational responses. Hence the prediction of the response at the receiver location is also poor at these frequencies. Different techniques were used to overcome these difficulties in Chapters 2 and 3. The improvements achieved depend on the different levels of noise in the measurements and on the condition numbers. It is therefore helpful to investigate other potential techniques to overcome force reconstruction errors.

A new technique is proposed in this chapter which exploits the randomness of errors present in the measured frequency response functions. Supposing the errors in the measured FRF's are random, a given measurement $\hat{A}$, lies within a region around the actual accelerance A as shown schematically in Figure 4.1(a). Suppose that a new set of measurements of the accelerances is made for each sample of $\hat{a}$ used to estimate the forces $\hat{F}$. This would allow the effect of random errors in $\hat{A}$ to be averaged out and allow the mean of the reconstructed forces to become more accurate, provided that a large number of samples are taken. This technique will be called the *resampled accelerance method.*

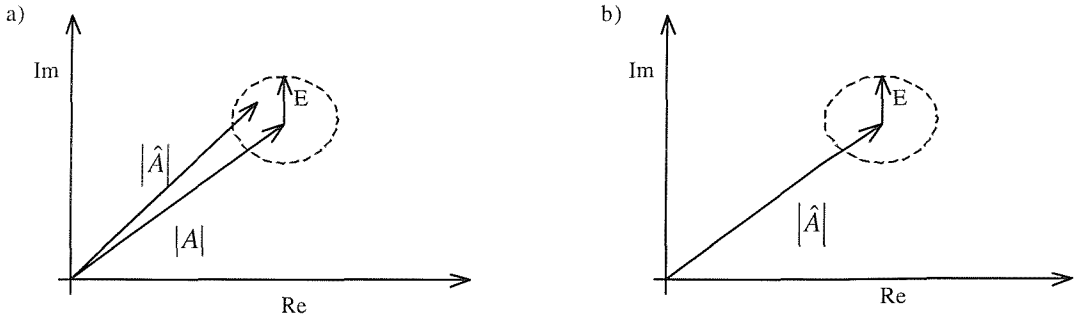

Figure 4.1. (a) Phasor representation of accelerance along with the error. (b) Estimate of error region based on measured accelerance.

The flow chart given in Figure 2.37 can then be modified to represent this process, as shown in Figure 4.2 below. Compared with Figure 2.37 it can be seen that $\hat{A}^{+}_{\omega,k}$ is different for each of the n_s responses $\hat{a}_{\omega,k}$.

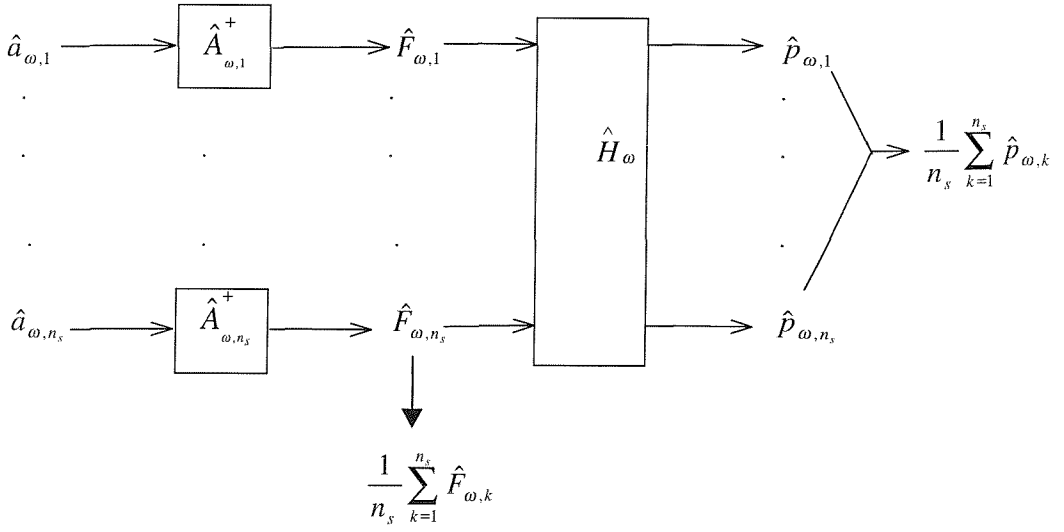

Figure 4.2. Representation of process for resampled accelerance.

The total number of samples required for estimating the accelerances for these calculations is ($n_{av}n_s$). Investigations have shown that the force and response reconstruction by using this method seems to result in good estimates [77] and the predictions based on this strategy have been shown to be reliable. The bias error is reduced considerably by the use of the accelerance resampling method. That is, the mean of the predictions is closer to the exact results. The effect of random errors due to noise in the accelerance measurement is cancelled out in the averaging strategy proposed. However, a major disadvantage with this strategy is that the number of measurements required is enormous. For practical implementation a variation is proposed and tested here.

4.2 PERTURBATION OF ACCELERANCE MATRIX

It is possible to simulate the effect of resampling by perturbing the measured accelerance matrix $\hat{A}$ with random noise before pseudo-inversion. The magnitude of the perturbation is based on the coherence at the frequency of calculation, along with the magnitude of the accelerance at that frequency. The expression for the standard deviation

of the FRF error given in equation (3.3) with α =1 can be used for this purpose. The expression for the modified accelerance matrix is

$$\hat{A}_{\omega k} = \hat{A}_{\omega} + A_{pert} \tag{4.1}$$

where $A_{pert} = N_{nd} E\, e^{j2\pi N_{nu}}$ is a perturbation matrix, N_{nd} is a random number with variance 1 and zero mean (normally distributed) and N_{nu} is a random number between 0 and 1 (uniformly distributed). This error has been represented in the phasor diagram shown in Figure 4.1(b). The zone within the circle indicates schematically the possible values that the accelerance can take. Since the estimated accelerance $\hat{A}$ is expected to be biased, the actual envelope in Figure 4.1(a) will differ slightly from that shown in Figure 4.1(b). The perturbation will only take care of random errors, which should still give reasonable results since bias errors are not magnified significantly [32]. The flow chart for this strategy is shown in Figure 4.3 below.

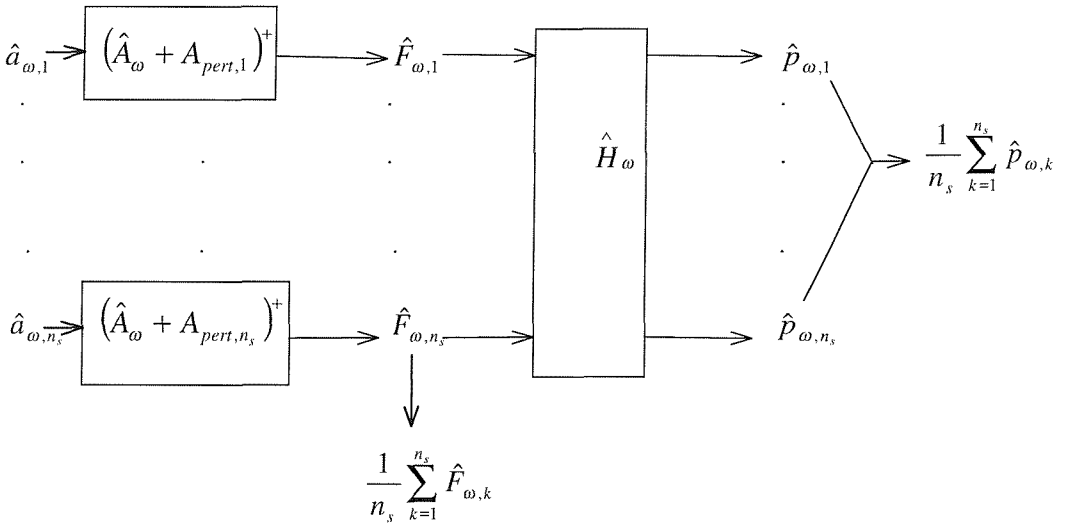

Figure 4.3. Representation of process for perturbation of accelerance matrix.

The reconstructed forces and velocity response obtained using this technique are shown in Figures 4.4 and 4.5 respectively for the case of a 4×4 accelerance matrix where the noise level in accelerances is large and the noise level in responses is moderate. The forces reconstructed by the accelerance perturbation technique are found to be slightly over-estimated below 100 Hz. In the high frequency region the force reconstruction improves. The force reconstruction errors are large compared with those from singular value rejection based on accelerance error (Figure 3.10) but they are smaller than those

from full rank matrix inverse (Figure 2.8). The reconstructed response at the receiver location is shown in Figure 4.6. This is more reliable than the result based on full rank matrix inverse (see Figure 2.10), and is as reliable as that obtained using singular value rejection based on the accelerance error (see Figure 3.11).

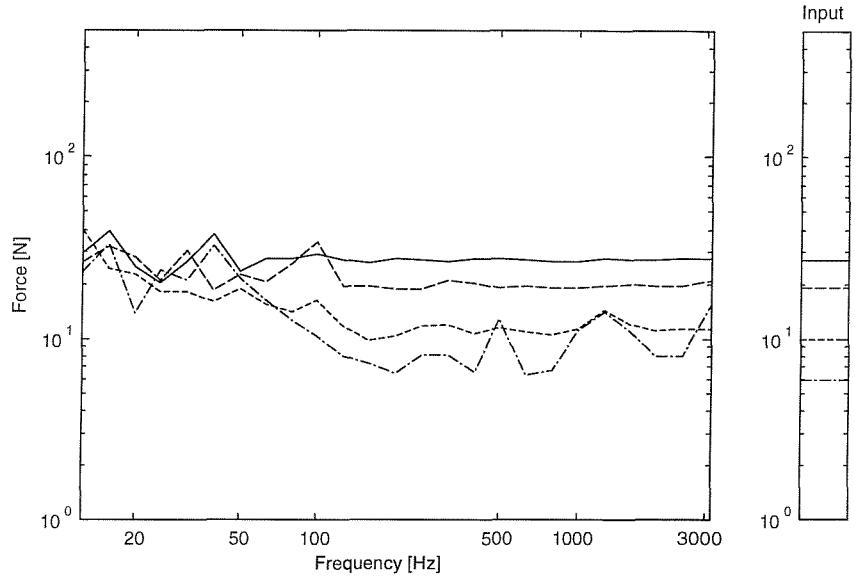

Figure 4.5. Reconstructed rms forces in 1/3 octave bands for 4 sources and 4 responses by perturbation technique. ———— force 1, — — — force 2, - - - - - - force 3, — - — - — force 4.

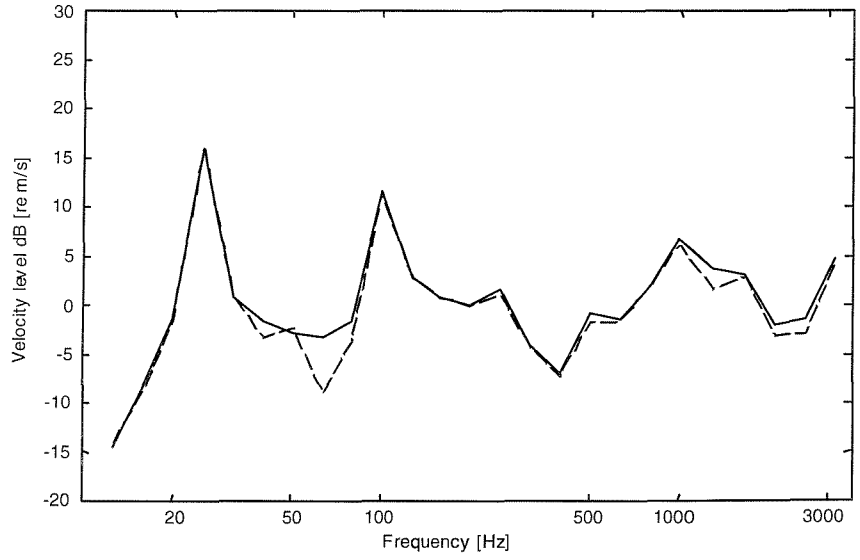

Figure 4.6. 1/3 octave velocity response at receiver location due to 4 forces reconstructed from 4 responses by perturbation technique. — — — — actual response, ———— reconstructed response.

4.3 ROBUSTNESS OF ACCELERANCE PERTURBATION TECHNIQUE

In Chapters 2 and 3 the methods studied were shown to be very sensitive to the noise level in the 'measurements'. The method based on accelerance perturbation also needs to be investigated for its sensitivity to the level of noise in the accelerances and responses. Numerical simulations have been carried out for all nine combinations of the noise levels in accelerances and responses as in Chapter 2. Tables 4.1 and 4.2 show the overall results for force determination and response reconstruction. The accelerance perturbation method appears to be very sensitive to the noise level in the responses. However, it effectively reduces accelerance error amplification when noise in the responses is small (see the first columns in Tables 4.1 and 4.2). The results are better than those from full rank matrix inverse in every case and are comparable to those from singular value rejection based on accelerance error when noise in the responses is small (see Tables 2.6-2.7 and 3.1-3.2).

Table 4.1. Average 1/3 octave band errors in forces determined for square matrix 4×4 using accelerance perturbation technique.

		Noise levels in operational responses		
		Low	**Medium**	**High**
Noise levels in FRF's	**Low**	**2.0**	**15.6**	**22.5**
	Medium	**3.4**	**7.3**	**13.7**
	High	**3.6**	**4.2**	**8.4**

Table 4.2. Average 1/3 octave band errors in reconstructed velocity response at the receiver location for square matrix 4×4 using accelerance perturbation technique.

		Noise levels in operational responses		
		High	**Medium**	**Low**
Noise levels in FRF's	**High**	**0.4**	**6.7**	**13.2**
	Medium	**2.0**	**3.1**	**7.6**
	Low	**1.0**	**1.4**	**4.9**

The results of force reconstruction and velocity for a square accelerance matrix at the receiver location for the case with moderate noise in the responses and low noise in the accelerances are shown in Figures 4.7 and 4.8 respectively. This is one of the worst

cases in Tables 4.1 and 4.2. The force reconstruction errors are very large in the low frequency region where the condition numbers of the accelerance matrix are large. The reconstructed velocity response at the receiver location also contains large errors in the low frequency region, particularly in the anti-resonance region.

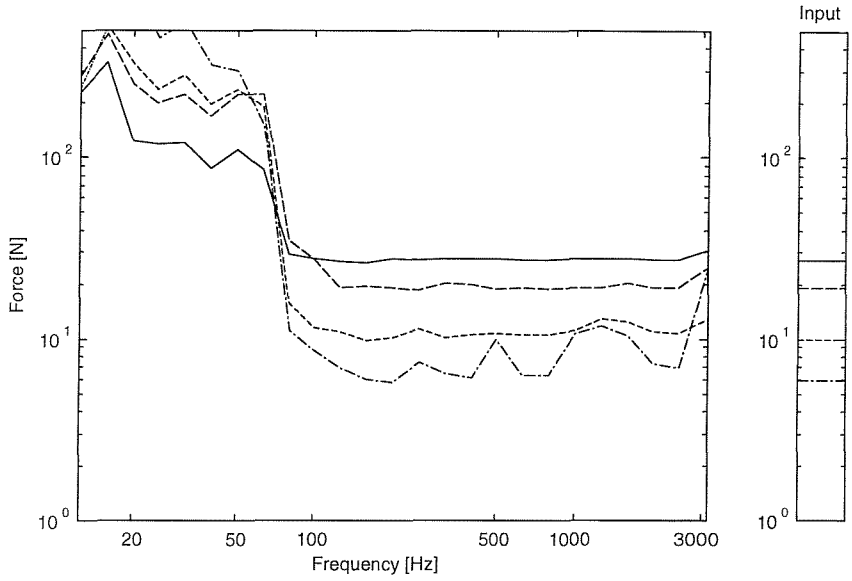

Figure 4.7. Reconstructed rms forces in 1/3 octave bands for 4 sources and 4 responses by perturbation technique for the case of moderate noise in responses and small noise in accelerances. ————force 1, — — —force 2, - - - - - force 3, — - — - — force 4.

4.4 REJECTION OF PERTURBED SINGULAR VALUES

In Chapter 3, where singular value rejection has been studied, it was observed that the threshold for the rejection of singular values based on either the accelerance error or the response error is not universally applicable. The success of these two thresholds depends on the respective noise levels in the accelerances and responses. It is possible to exploit the perturbation technique in order to take account of both kinds of errors.

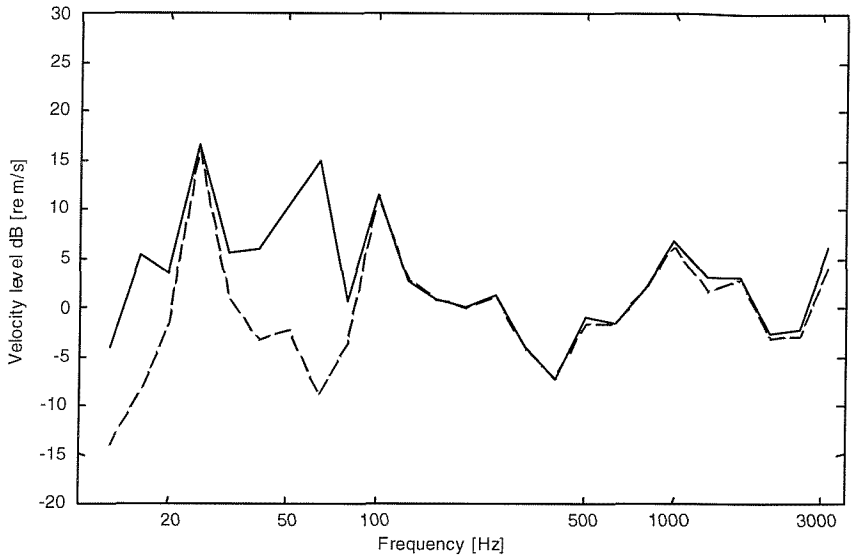

Figure 4.8. 1/3 octave velocity response at receiver location due to 4 forces reconstructed from 4 responses by perturbation technique for the case of moderate noise in responses and small noise in accelerances. — — — —actual response, ———— reconstructed response.

One observation, which helps in arriving at an effective threshold, is the extent to which the perturbation technique and threshold based on accelerance errors are similar. They do not result in similar error reduction. As no information is lost in the perturbation technique, the results will not be as biased as in singular value rejection provided the response error is small. The restriction of small response error is to reduce the amplification of response errors. This can also be achieved by rejecting singular values based on the response error. The net effect would then be to perturb the accelerance matrix to allow for FRF errors and reject the perturbed singular values if they are smaller than the response error norm.

This combined approach allows the error magnification due to FRF errors to be reduced by perturbation while singular value rejection minimises the error magnification due to response errors. In the presence of large response error, the singular value rejection will reduce the error amplification. In this case, perturbation may not have any

effect since perturbation mostly affects the smaller singular values which are then rejected. On the other hand if the response error is smaller than the FRF error, singular values may not be rejected and, since perturbation of the accelerance matrix combined with small response error works robustly, the results will still be reliable. Hence this approach corresponds to an effective threshold which should produce reliable results whatever the error level in responses and FRF's. This method is referred to here as *perturbed singular value rejection.*

Two cases in which singular value rejection methods failed have been investigated here. Figure 4.9 shows reconstructed forces obtained by perturbed singular value rejection for the case where noise in the responses is moderate and noise in the accelerances is small. For this case, singular value rejection based on accelerance error (see Figure 3.15, NB this corresponds to over-determined case 5×4) and accelerance perturbation (see Figure 4.7) both fail at low frequency. Compared with these methods the force reconstruction obtained using perturbed singular value rejection is marginally better.

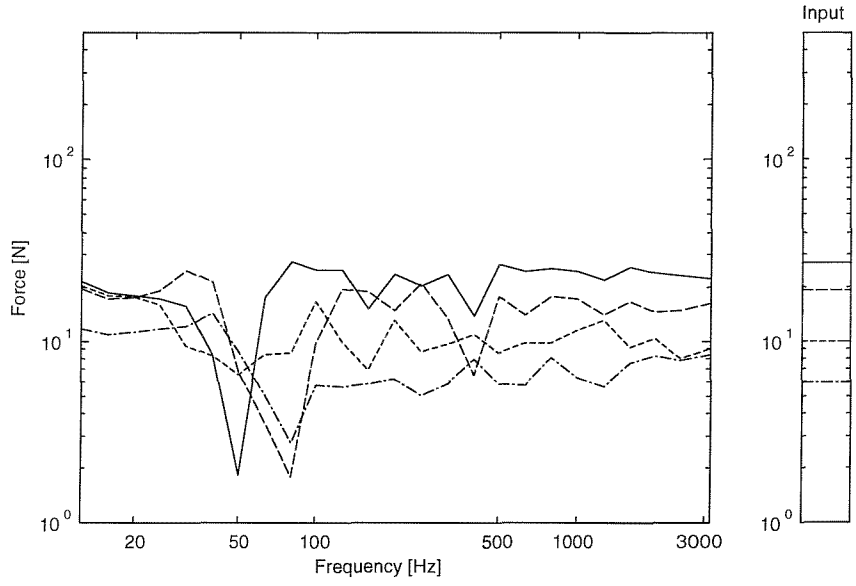

Figure 4.9. Reconstructed rms forces in 1/3 octave bands for 4 sources and 4 responses by perturbed singular value rejection for the case of moderate noise in responses and small noise in accelerances. ————force 1, — — —force 2, - - - - - force 3, — - — - — force 4.

The reconstructed response at the receiver location obtained using perturbed singular value rejection is shown in Figure 4.10. Compared with singular value rejection

based on the accelerance error (see Figure 3.16) and accelerance perturbation (see Figure 4.8), the reconstruction errors are small in the present case.

Figure 4.11 shows the forces reconstructed using perturbed singular value rejection for the case where noise in the responses is small and noise in the accelerances is large. In this case singular value rejection based on response error fails (see Figure 3.23). The reconstructed forces have errors similar to singular value rejection based on response error. The corresponding reconstructed response is shown in Figure 4.12. This is also similar to singular value rejection based on response error (see Figure 3.24) even though the latter is based on a 5×4 matrix.

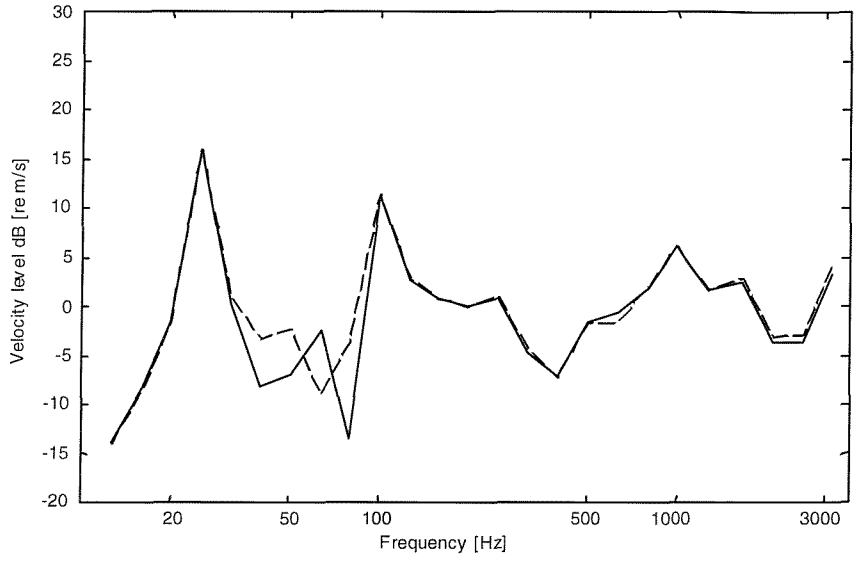

Figure 4.10. 1/3 octave velocity response at receiver location due to 4 forces reconstructed from 4 responses by perturbed singular value rejection for the case of moderate noise in responses and small noise in accelerances. — — — — actual response, ———— reconstructed response.

From these calculations, the perturbed singular value rejection method appears to be robust for all variations. This is confirmed by Tables 4.3 and 4.4 where overall force reconstruction errors and reconstructed response errors are given for nine combinations presented in Chapter 2. Improvement over singular value rejection is confirmed by comparing these results with Tables 3.1-3.2 and 3.5-3.6. While some situations are marginally worse than previously (eg moderate noise in FRF's with low/moderate noise in responses compared with Tables 3.1 and 3.2) the present method gives results that are robust for a wide variety of error combinations.

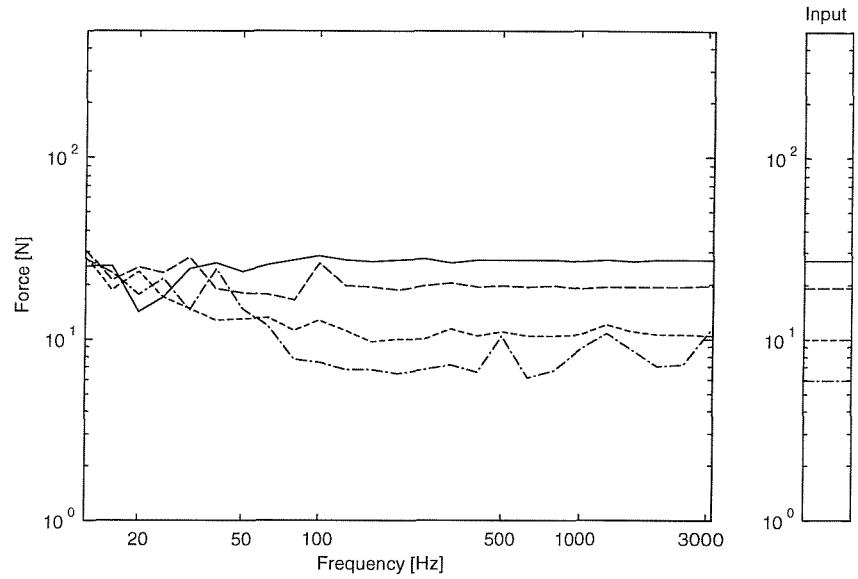

Figure 4.11. Reconstructed rms forces in 1/3 octave bands for 4 sources and 4 responses by perturbed singular value rejection for the case of small noise in responses and large noise in accelerances. ————force 1, — — —force 2, - - - - - -force 3, — - — - — force 4.

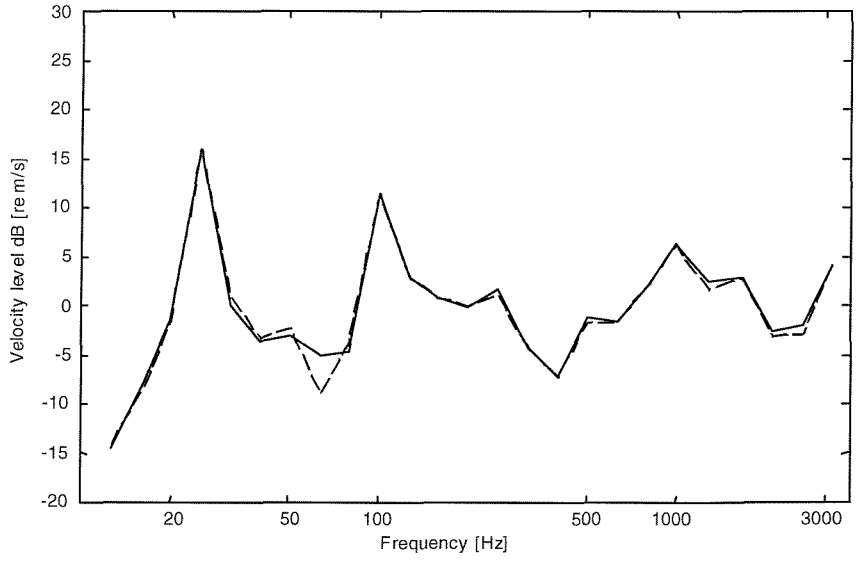

Figure 4.12. 1/3 octave velocity response at receiver location due to 4 forces reconstructed from 4 responses perturbed singular value rejection for the case of small noise in responses and large noise in accelerances. — — — —actual response, ———— reconstructed response.

Tables 4.5 and 4.6 show overall results for force determination and response reconstruction for an over-determined system of 5×4 matrix. Similar improvements are observed over singular value rejection (see Tables 3.3-3.4 and 3.7-3.8).

Table 4.3. Average 1/3 octave band errors in forces determined for square matrix 4×4 using perturbed singular value rejection.

		Noise levels in operational responses		
		Low	**Medium**	**High**
Noise levels in FRF's	**Low**	**0.9**	**4.2**	**5.4**
	Medium	**2.5**	**4.2**	**5.4**
	High	**3.2**	**4.2**	**5.2**

Table 4.4. Average 1/3 octave band errors in reconstructed velocity response at the receiver location for square matrix 4×4 using perturbed singular value rejection.

		Noise levels in operational responses		
		Low	**Medium**	**High**
Noise levels in FRF's	**Low**	**0.5**	**2.8**	**3.5**
	Medium	**0.4**	**2.8**	**3.5**
	High	**0.9**	**2.7**	**3.5**

Table 4.5. Average 1/3 octave band errors in forces determined for matrix 5×4 using perturbed singular value rejection.

		Noise levels in operational responses		
		Low	**Medium**	**High**
Noise levels in FRF's	**Low**	**0.5**	**3.2**	**4.8**
	Medium	**1.7**	**3.1**	**4.8**
	High	**2.2**	**3.3**	**4.8**

Table 4.6. Average 1/3 octave band errors in reconstructed velocity response at the receiver location for matrix 5×4 using perturbed singular value rejection.

		Noise levels in operational responses		
		Low	Medium	High
Noise levels in FRF's	Low	0.2	2.4	2.8
	Medium	0.2	2.4	2.8
	High	0.9	2.2	2.8

4.5 SUMMARY

The method of perturbing the accelerance matrix reduces the error amplification considerably. However, this method is sensitive to variations in noise level in the responses. A robust method has been proposed in this chapter which is called perturbed singular value rejection. This enables error amplification reduction for any level of noise in the responses and FRF's.

Although this method works well, it might still result in loss of information due to the singular value rejection. As discussed in Section 1.2.3 some methods have been used in digital image processing, and more recently in nearfield acoustical holography, where singular values are weighted rather than rejected outright. This might help reduce the loss of information compared with singular value rejection. The effectiveness of iterative inversion and Tikhonov regularization is therefore investigated in the next two chapters.

CHAPTER 5
TIKHONOV REGULARIZATION

5.1 INTRODUCTION

For a long time in the field of digital image processing and more recently in relation to Nearfield Acoustic Holography (NAH), other techniques have been employed to improve source reconstruction [35-42]. These include iterative inversion techniques and Tikhonov regularization. In these techniques, instead of minimising a cost function based on ordinary least square errors, a function which incorporates some bias is introduced. This new function is minimised to identify the source. In both techniques, applying them to inverse force determination, the error in the force reconstruction is divided into a bias error and the random error. In the ordinary least squares solution only the random error is minimised and no bias error is introduced. However, there can be a large magnification of the random errors at frequencies where the accelerance matrix is ill-conditioned. By introducing a bias error which increases with the value of, for example, a regularization parameter, it is observed that there exists a point (value of regularization parameter or number of iterations) where the bias error and the random error cross over. For larger values the bias error dominates, for smaller values the random error dominates. Near the cross-over point the overall cost function is minimised. The introduction of a bias error limits the magnification of random errors in the accelerance and the operational responses. This comes, however, at the cost of a small bias error in the force reconstruction.

In this chapter and the next one, these two techniques are used in a numerical simulation of a TPA application in which the test object is a rectangular simply supported flat plate as in previous chapters. Four simultaneous coherent forces are considered and five responses are used to reconstruct them. Five responses are used as the number must be at least one greater than the number of forces, as will be seen, but the level of over-determination is kept small to give greater discrimination between methods.

In this chapter Tikhonov regularization is explored. The steps leading to the formulation of this method are explained below [39-41].

5.2 TIKHONOV REGULARIZATION

Although the observed operational responses $\hat{a}$ differ from the true responses, this error is unknown. For purposes of matrix inversion, a fitting error can be identified given by

$$\tilde{e} = \hat{a} - \hat{A}\hat{F} \tag{5.1}$$

where $\hat{F}$ are the fitted forces and $\hat{A}$ is the measured FRF matrix. $\tilde{e}$ includes the effects of errors in $\hat{A}$ or in the completeness of the model and may be influenced by errors in $\hat{a}$.

A least squares solution (e.g. the Moore-Penrose pseudo-inverse) aims to determine $\hat{F}$ such that the fitting errors $\tilde{e}$ are minimised i.e.

$$\min(\tilde{e}^H \tilde{e}) \quad \text{or} \quad \min \sum_{i=1}^{m} \tilde{e}_i^{\,2} \tag{5.2}$$

Instead of the ordinary least squares solution, Tikhonov suggested [78] minimising a cost function given by

$$J = (\tilde{e}^H \tilde{e}) + \lambda(\hat{F}^H \hat{F}) \tag{5.3}$$

where λ is a regularization parameter. This cost function introduces a bias into the solution which can be adjusted (by varying the value of λ) to limit the magnification of measurement errors due to ill-conditioning. Therefore, expanding J from (5.1) [79]

$$\begin{aligned} J &= (\hat{a} - \hat{A}\hat{F})^H (\hat{a} - \hat{A}\hat{F}) + \lambda(\hat{F}^H \hat{F}) \\ &= \hat{a}^H \hat{a} - \hat{a}^H \hat{A}\hat{F} - \hat{F}^H \hat{A}^H \hat{a} + \hat{F}^H \hat{A}^H \hat{A}\hat{F} + \hat{F}^H \lambda \hat{F} \\ &= \hat{F}^H (\hat{A}^H \hat{A} + I\lambda)\hat{F} - \hat{a}^H \hat{A}\hat{F} - \hat{F}^H (\hat{a}^H \hat{A})^H + \hat{a}^H \hat{a} \end{aligned}$$

or

$$J = \hat{F}^H B \hat{F} - b^H \hat{F} - \hat{F}^H b + c \tag{5.4}$$

where $B = \hat{A}^H \hat{A} + I\lambda$, $b = \hat{A}^H \hat{a}$ and $c = \hat{a}^H \hat{a}$. The optimal solution which reduces the force reconstruction errors can be derived by minimising the cost function (5.4) for a given value of λ. For this cost function to be minimum, the first derivative of J with respect to the force vector must be zero. As the terms in the cost function contain complex variables it is necessary that it be separated into real and imaginary parts [79]. Therefore using $B = B_R + iB_I$, $\hat{F} = F_R + iF_I$ and $b = b_R + ib_I$ the first term in (5.4) can be expanded as (noting that B is a Hermitian matrix),

$$\hat{F}^H B\hat{F} = (F_R^T - iF_I^T)(B_R + iB_I)(F_R + iF_I)$$

$$= F_R^T B_R F_R + iF_R^T B_I F_R - iF_I^T B_R F_R + F_I^T B_I F_R + iF_R^T B_R F_I - F_R^T B_I F_I + F_I^T B_R F_I + iF_I^T B_I F_I \quad (5.5)$$

The above equation can be simplified as follows :

a. Since the imaginary part of B is skew symmetric, $F_R^T B_I F_R = 0$ and $F_I^T B_I F_I = 0$. This eliminates the 2nd and 8th terms.

b. Since $(F_R^T B_R F_I)^T = F_I^T B_R F_R$ and $F_I^T B_R F_R$ is a real scalar, $F_R^T B_R F_I = F_I^T B_R F_R$. This eliminates the 3rd and 5th terms.

c. Since $(F_R^T B_I F_I)^T = -F_I^T B_I F_R$ and $F_I^T B_I F_R$ is a real scalar, $F_R^T B_I F_I = -F_I^T B_I F_R$. So the 4th and 6th terms are equal.

Therefore (5.4) can be written as

$$J = F_R^T B_R F_R + F_I^T B_R F_I - 2F_R^T B_I F_I - b^H \hat{F} - \hat{F}^H b + c \quad (5.6)$$

The fourth and fifth terms in equation (5.6) can be expanded to give,

$$-b^H \hat{F} - \hat{F}^H b = -(b_R^T F_R + ib_R^T F_I - b_I^T F_R + b_I^T F_I + F_R^T b_R + iF_R^T b_I + iF_I^T b_R + F_I^T b_I) \quad (5.7)$$

Since all the terms represent scalar real numbers this reduces to

$$-b^H \hat{F} - \hat{F}^H b = -(2b_R^T F_R + 2b_I^T F_I) \quad (5.8)$$

Therefore equation (5.6) can be written as

$$J = F_R^T B_R F_R + F_I^T B_R F_I - 2F_R^T B_I F_I - (2b_R^T F_R + 2b_I^T F_I) + c \quad (5.9)$$

Now the cost function can be differentiated with respect to each of the real and imaginary components.

$$\frac{\partial J}{\partial F_R} = \left(\frac{\partial J}{\partial F_{1R}}, \frac{\partial J}{\partial F_{2R}}, \ldots\ldots \frac{\partial J}{\partial F_{nR}} \right)^T \quad (5.10)$$

$$\frac{\partial J}{\partial F_I} = \left(\frac{\partial J}{\partial F_{1I}}, \frac{\partial J}{\partial F_{2I}}, \ldots\ldots \frac{\partial J}{\partial F_{nI}} \right)^T$$

Following the derivation in [79], use can be made of various properties of such derivatives, two of which are

$$\frac{\partial(\phi^T \alpha)}{\partial \alpha} = \phi \quad \text{and} \quad \frac{\partial(\alpha^T X \alpha)}{\partial \alpha} = (X + X^T)\alpha \quad (5.11)$$

where ϕ is a vector and X is a matrix both of which are independent of α.

In the second relation, if X is symmetric then

$$\frac{\partial(\alpha^T X\alpha)}{\partial\alpha} = 2X\alpha \tag{5.12}$$

Using the above two properties, the derivatives can be written as

$$\frac{\partial J}{\partial F_R} = 2B_R F_R - 2B_I F_I - 2b_R \tag{5.13}$$

$$\frac{\partial J}{\partial F_I} = 2B_R F_I + 2B_I F_R - 2b_I \tag{5.14}$$

Using the concept of a complex gradient g,

$$g = \frac{\partial J}{\partial F_R} + i\frac{\partial J}{\partial F_I} \tag{5.15}$$

$$g = 2B_R F_R - 2B_I F_I - 2b_R + i2B_R F_I + i2B_I F_R - i2b_I \tag{5.16}$$

For a minimum value of J, g has to be equal to zero. Therefore

$$2(B_R F_R + iB_R F_I + iB_I F_R - B_I F_I) - 2(b_R + ib_I) = 0 \tag{5.17}$$

The first term in the above equation is simply $B\hat{F}$, so therefore

$$B\hat{F} - b = 0 \tag{5.18}$$

and hence the optimal solution which minimises the error amplification in force reconstruction is given by

$$\hat{F} = B^{-1}b \tag{5.19}$$

By expanding B the solution can also be written as

$$\hat{F} = \left(\hat{A}^H\hat{A} + I\lambda\right)^{-1}\hat{A}^H\hat{a} \tag{5.20}$$

To obtain insight into this solution and in order to compare it with pseudo-inversion, equation (5.20) can be represented in terms of the singular value decomposition of the accelerance matrix, $\hat{A} = USV^H$

$$\hat{F} = \left((USV^H)^H USV^H + I\lambda\right)^{-1}(USV^H)^H\hat{a} \tag{5.21}$$

Since U and V are unitary matrices this gives

$$\hat{F} = \left(VS^H SV^H + VI\lambda V^H\right)^{-1} VS^H U^H\hat{a}$$

$$= \left(V(S^H S + I\lambda)V^H\right)^{-1} VS^H U^H\hat{a}$$

$$\hat{F} = V(S^H S + I\lambda)^{-1} S^H U^H\hat{a} \tag{5.22}$$

This can be compared with the pseudo-inversion equation (3.2) in which $\hat{F} = VS^{-1}U^H \hat{a}$. In (5.22) the term $(S^H S + I\lambda)^{-1} S^H$ is a diagonal matrix having elements $\frac{s_k}{(s_k^2 + \lambda)}$, which replaces S^{-1} the terms of which are s_k^{-1}.

The effect of variation of the regularization parameter on the inverted accelerance matrix is shown in Figure 5.1. The effect of singular value rejection is shown in Figure 5.1b where singular values that are smaller than 0.01 are rejected. The effect of variation of the regularization parameter λ on the reciprocal of singular value is shown in Figures 5.1c-e. Introduction of λ in equation (5.22) leads to weighting of the singular values rather than rejection of them. The weighting is seen to affect the smaller singular values which are more prone to corruption by measurement noise. If λ is too small information about most of the singular values is retained (see Figure 5.1c). If it is too large the weighting 'rejects' too many singular values.

5.3 SELECTION OF REGULARIZATION PARAMETER

As can be seen from the above relation, the regularization parameter λ effectively modifies the singular values in the inverse. In doing this it introduces a bias error into the solution. When the condition number of the accelerance matrix is high, the effect of smaller singular values which are prone to errors can be nullified by choosing an appropriate regularization value λ. When associated with a high condition number, the effect of adding the optimal regularization parameter to larger singular values results in minimal bias. However, it is essential to choose a proper regularization value so that it results in minimum magnification of measurement errors while also introducing negligible bias in the solution. To do this, it is necessary to know the errors in the measurement or to use mathematical methods which approximate them. One of the mathematical concepts to choose regularization parameters when errors in the measurement are not known is explained below.

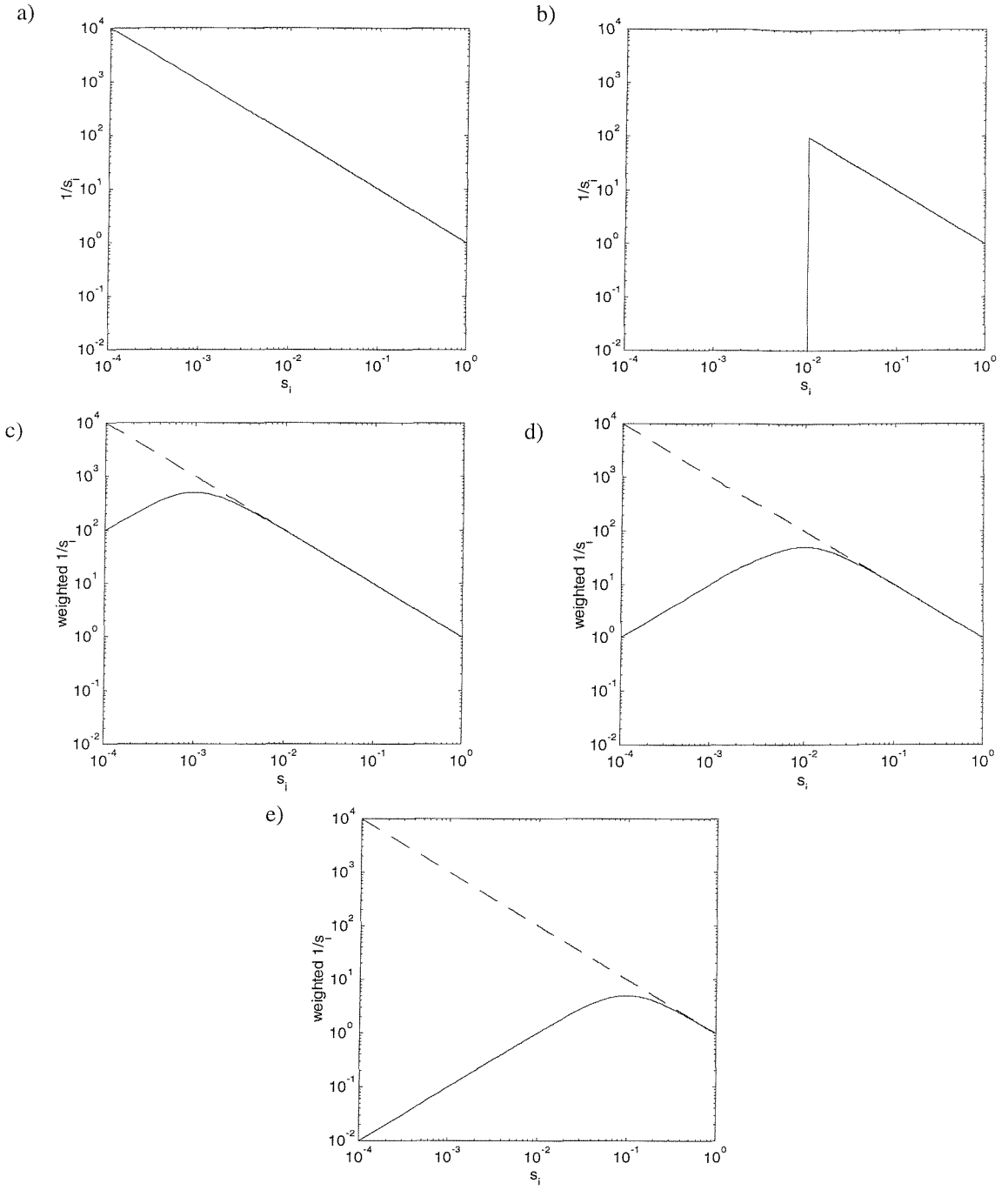

Figure 5.1. (a) Reciprocal of singular value as in pseudo-inverse (b) Truncated reciprocal of singular value as in singular value rejection (c) Weighted reciprocal of singular value for $\lambda=10^{-6}$ (d) Weighted reciprocal of singular value for $\lambda=10^{-4}$ (e) Weighted reciprocal of singular value for $\lambda=0.01$.

5.3.1 Ordinary cross validation

The method of ordinary cross validation (OCV) was suggested by Allen [45]. In this method, out of m responses only m-1 are used initially in the force determination. The forces so determined are then used in reconstructing the remaining response. This can be done for different values of regularization parameter. The closeness of reconstruction of this response indicates the effectiveness of the chosen regularization parameter. This method is also referred to as the PRESS method ('Prediction sum of squares' of deviations). The procedure followed is given below.

a. The number of responses m measured is ensured to be at least one more than the number of forces n. Starting with a zero value of λ, the forces are determined based on m-1 responses using (5.20). Using these forces, the remaining response is reconstructed. Writing $\hat{F}_k$ for the reconstructed force obtained with the k^{th} response $\hat{a}_k$ left out, the square of the deviation is $\left(\hat{a}_k - \hat{A}_k \hat{F}_k\right)^2$, where $\hat{A}_k$ is a row vector of FRF's containing the transfer functions from the n force locations to the k^{th} response location.

b. This procedure of leaving out one response and calculating the sum of squares of deviations is repeated for each of the response elements in turn. Based on the above deviations, the averaged square deviation Δ is calculated for that value of λ (initially λ =0) as

$$\Delta(\lambda) = \frac{1}{m}\sum_{k=1}^{m}\left(\hat{a}_k - \hat{A}_k \hat{F}_k\right)^2 \tag{5.23}$$

c. The above steps are repeated for different values of λ (NB value is increased using a fixed interval). The value of λ which gives smallest Δ is the optimum value of regularization parameter for that frequency. An example of variation of Δ with respect to regularization parameter is shown in Figure 5.2. A definite minimum is observed in the deviation for a particular value of λ.

d. This value of λ is used in the inversion of the full $m \times n$ matrix to obtain the forces.

Other procedures also exist like generalised cross validation [43-44, 46] to select regularization parameter but are not considered here.

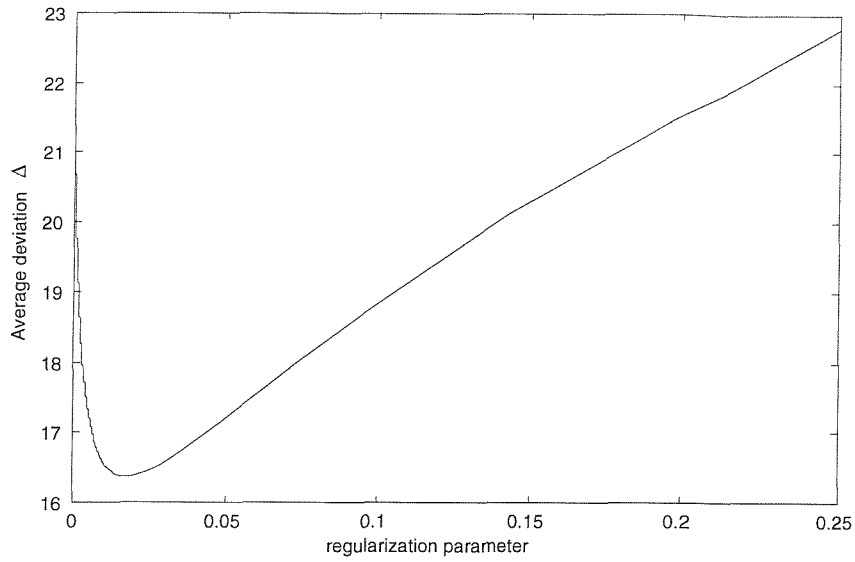

Figure 5.2. Variation of average cross validation deviation with different values of regularization parameter at 40 Hz for the example considered later.

5.3.1.1 *Force reconstruction*

In all the simulations the same flat plate is used as previously with four forces and five responses. The over-determined system is used here to allow the application of ordinary cross validation to select the regularization parameter while keeping the over-determination as small as possible to ensure maximum discrimination between methods. The case considered here corresponds to moderate noise in the responses and high noise in the FRF's (see Table 2.3).

The force reconstruction using ordinary cross validation to select the regularization parameter is shown in 1/3 octave form in Figure 5.3. Some improvement is observed below 100 Hz when compared with singular rejection based on accelerance error norm (see Figure 5.4). The variation of the square root of the regularization parameter chosen with frequency is shown in Figure 5.5. Also shown in the figure are the singular values. When this variation is compared with the error norm of Figure 3.4, it is seen that the square root of the regularization parameter is smaller than the error norm at most of the frequencies.

The forces reconstructed using Tikhonov regularization with OCV are also observed to be more reliable than those obtained using singular value rejection based on response errors or perturbed singular value rejection (see Figures 5.6 and 5.7).

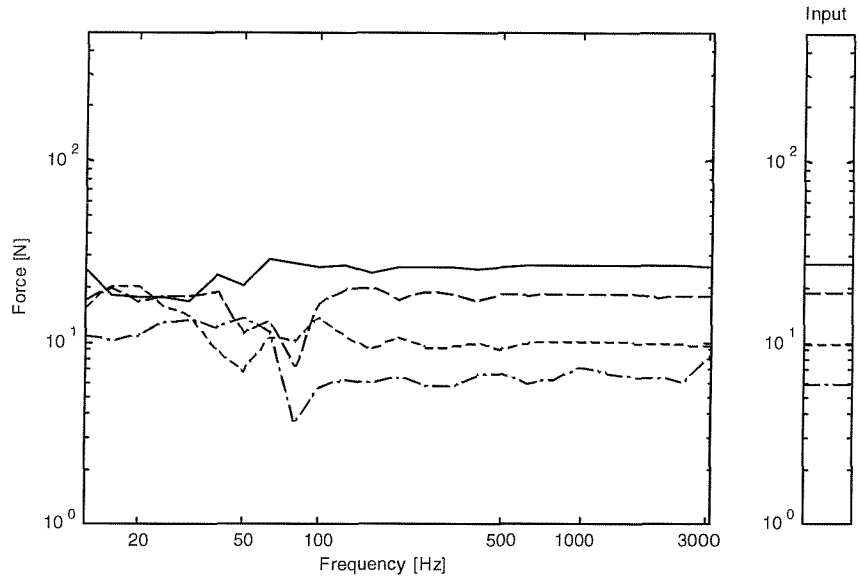

Figure 5.3. Reconstructed rms forces in 1/3 octave bands by Tikhonov regularization with ordinary cross validation for 4 forces and 5 responses. ——— force 1, — — — force 2, – – – – – force 3, — · — · —force 4.

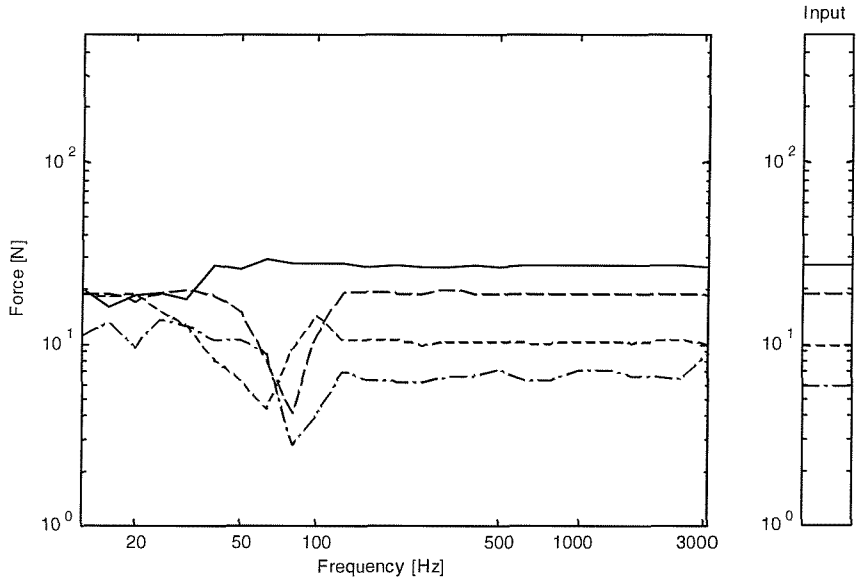

Figure 5.4. Reconstructed rms forces in 1/3 octave bands by singular value rejection based on +/- one standard deviation in accelerance for 4 forces and 5 responses.

——— force 1, — — — force 2, – – – – – force 3, — · — · — force 4.

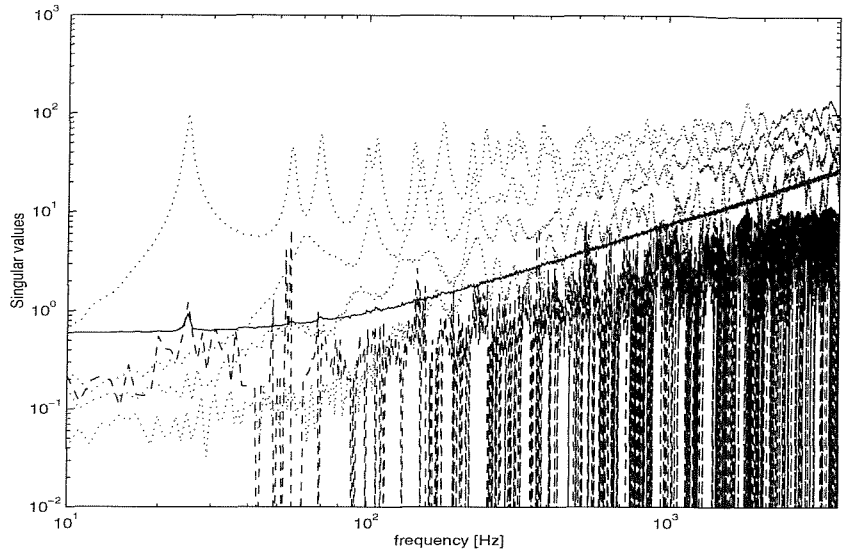

Figure 5.5. Variation of square root of the regularization parameter selected by OCV and the threshold based on accelerance error to reject singular values. ——— threshold based on accelerance error and — — — regularization parameter selected by OCV and · · · · · · · · singular values.

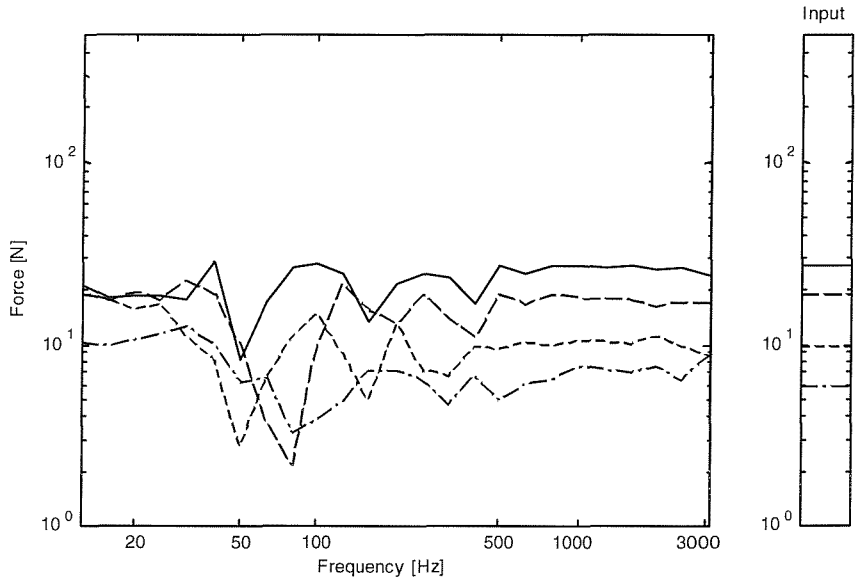

Figure 5.6. Reconstructed rms forces in 1/3 octave bands by singular value rejection based on +/- one standard deviation in response for 4 forces and 5 responses. ——— force 1, — — — force 2, – – – – – force 3, — · — · — force 4.

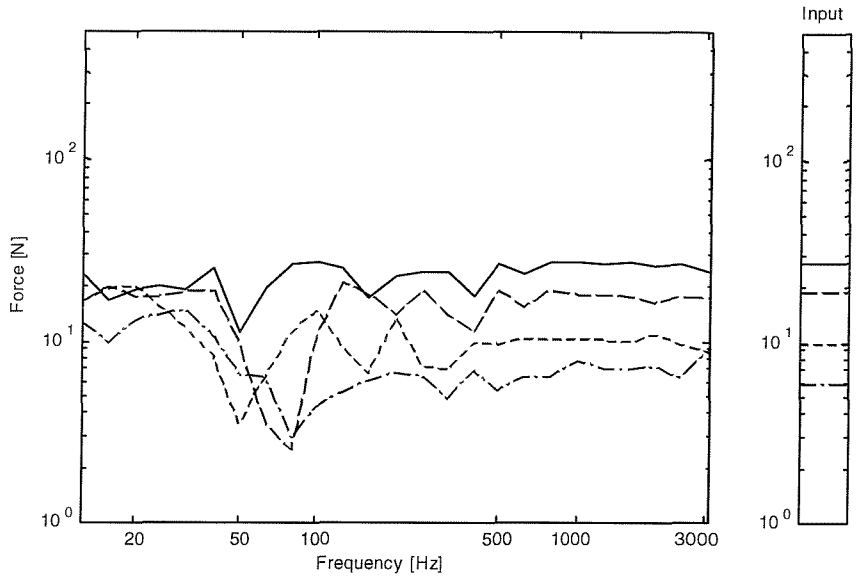

Figure 5.7. Reconstructed rms forces in 1/3 octave bands by perturbed singular value rejection for 4 forces and 5 responses. ——— force 1, — — — force 2, – – – – – force 3, — · — · —force 4.

5.3.1.2 *Velocity at the receiver location*

The reconstructed velocity response at the receiver location is shown in Figure 5.8. In narrow band form it appears to be similar for both Tikhonov regularization and singular value rejection based on accelerance error (see Figure 5.9). However, the response reconstructed is more reliable than that for singular value rejection based on response error or perturbed singular value rejection (see Figures 5.10-11).

Figure 5.12 shows the velocity response at the receiver location in 1/3 octave band form. Between 30 and 100 Hz some deviations from the actual response are observed.

For the simulation considered, Tikhonov regularization with ordinary cross validation performs similarly in force reconstruction as singular value rejection based on accelerance error. The performance of singular value rejection, as observed earlier, is dependent on the noise level present in the responses and accelerances. Hence this does not represent a universal comparison.

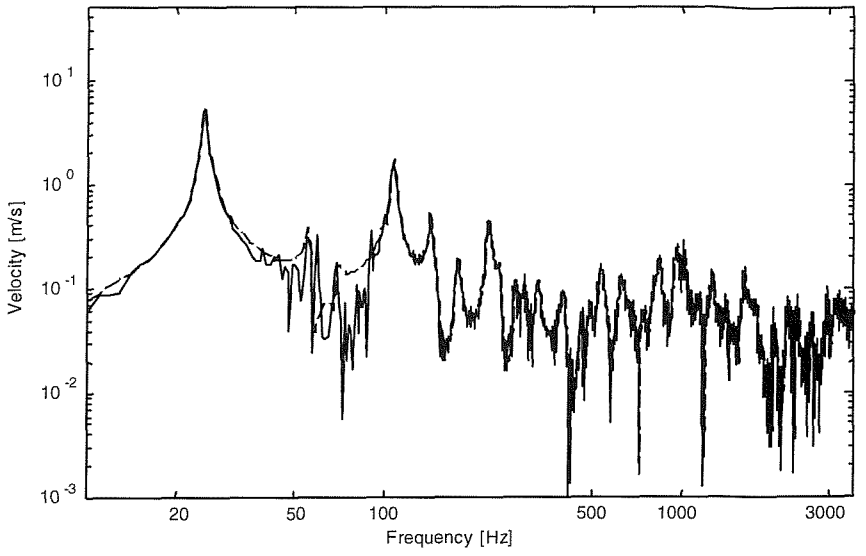

Figure 5.8. Velocity response at the receiver location obtained by Tikhonov regularization with ordinary cross validation. — — — actual response, ——— reconstructed response.

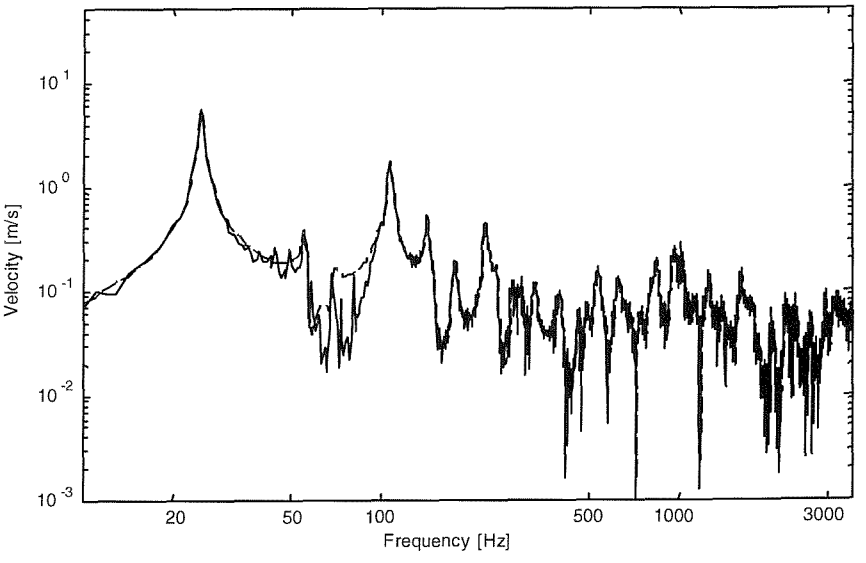

Figure 5.9. Velocity response at the receiver location by singular value rejection based on accelerance error. — — — — actual response, ——— reconstructed response.

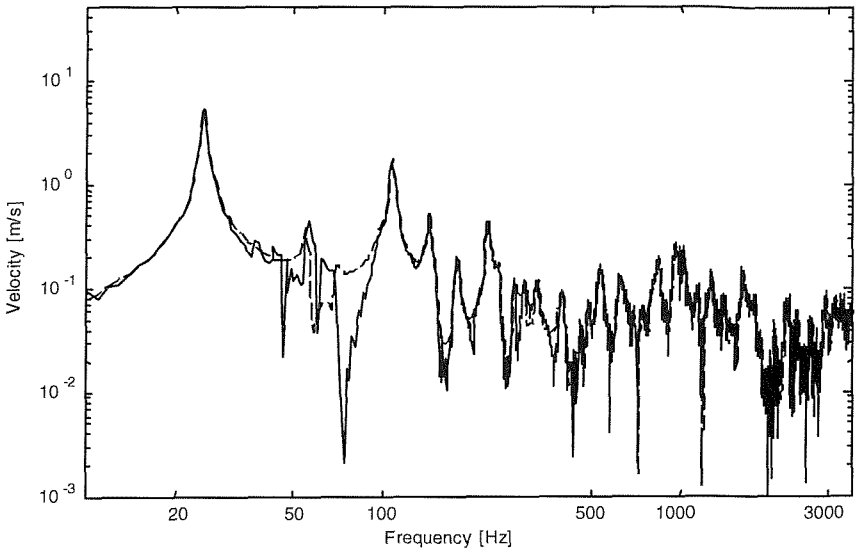

Figure 5.10. Velocity response at the receiver location by singular value rejection based on response error. — — — — actual response, ———— reconstructed response.

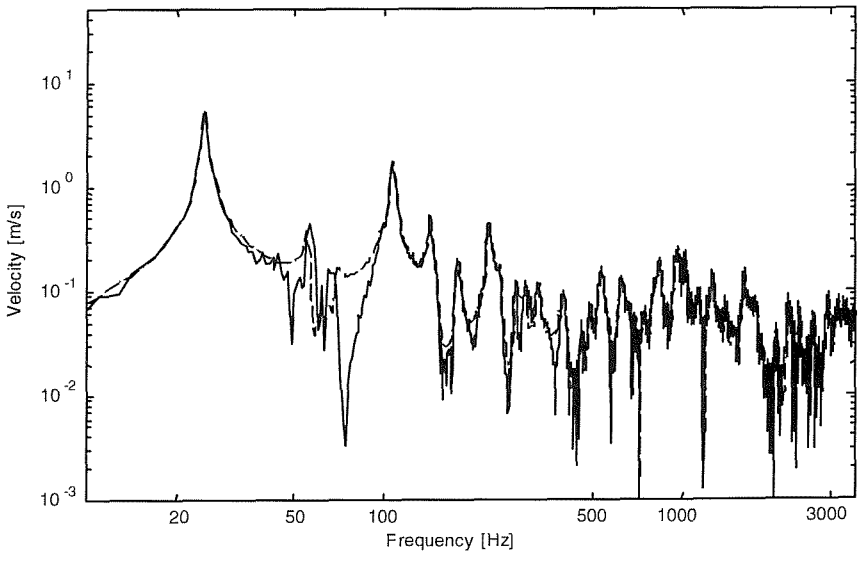

Figure 5.11. Velocity response at the receiver location by perturbed singular value rejection. — — — — actual response, ———— reconstructed response.

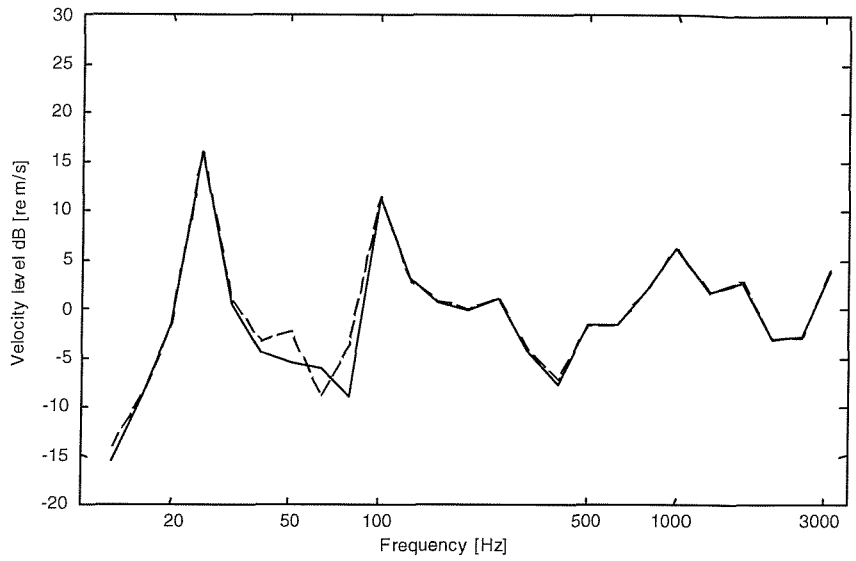

Figure 5.12. 1/3 octave velocity response at the receiver location obtained by Tikhonov regularization with ordinary cross validation. — — — actual, ——— reconstructed.

5.3.2 Effect of variation of regularization parameter on force determination

To illustrate the effect of varying the regularization parameter λ on the reconstructed forces, results for 51 Hz are shown in Figure 5.13. Force 1 is estimated reliably when λ=0 but the other forces are observed to be over-estimated (Figure 5.13a). As λ is increased, the errors in the smaller forces reduce (Figure 5.13b-c). The variation in λ here affects smaller forces more than the larger ones. The value of λ corresponding to Figure 5.13c appears to be very close to the optimal value. For larger values of λ, the larger forces are under-estimated. As the regularization parameter becomes very large, the forces become almost equal and cannot be distinguished from each other (Figure 5.13f). The regularization parameter selected by ordinary cross validation appears very close to the optimal value since most of the forces are reliably estimated (Figure 5.13d). This value lies between the ones corresponding to Figures 5.13c and 5.13e.

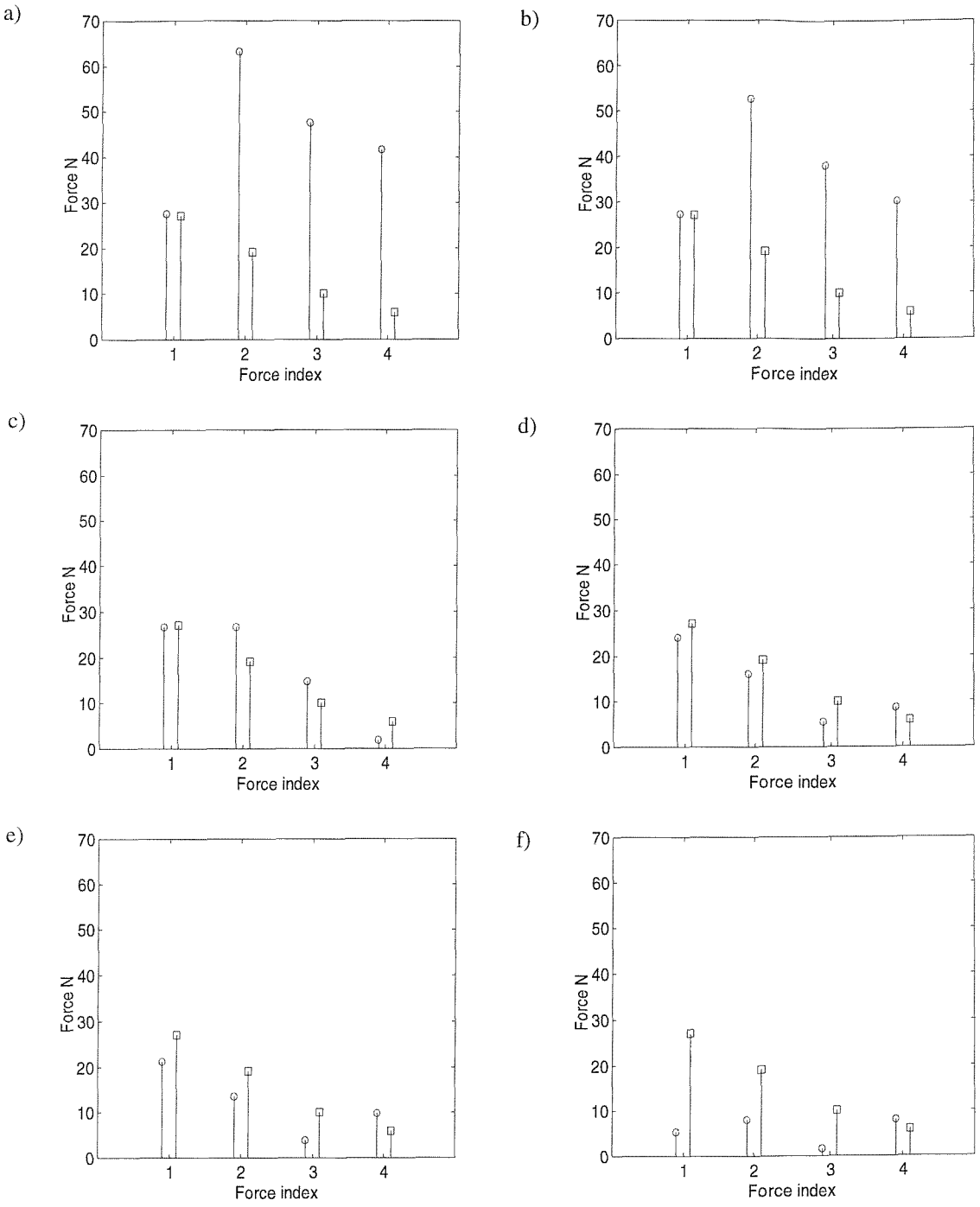

Figure 5.13. Effect of variation of regularization parameter on force reconstructed at 51 Hz for the case of Figure 5.3. (a) λ=0 (b) λ=0.001 (c) λ=0.01 (d) λ=0.0496 as selected by OCV (e) λ=0.1 (f) λ=1. O reconstructed force and □ actual force.

5.3.3 Robustness of OCV for different noise levels

The selection of the regularization parameter by ordinary cross validation depends mainly on the accuracy of the response measurements. It takes account of FRF measurement errors indirectly when estimating the validation error. It is desirable to know whether this is sufficient to ensure robustness in selecting the regularization parameter for different levels of noise in responses and FRF's. It is clear that the noise levels in the responses will always be considered, and amplification of them is reduced by selecting a proper regularization parameter value. If, however, the noise in responses is considerably smaller than the noise in FRF's the performance of OCV might be affected. It is this performance which will be studied in this section.

Table 5.1 shows the average errors in the forces determined using ordinary cross validation for different noise levels present in the responses and FRF's. The method appears not to work very well when the condition numbers are very high (high S/N ratio for FRF's) in combination with large noise in responses (small S/N ratio). Nevertheless these results are still better than those for pseudo-inversion in every case (compare with Table 2.8). The method is also better than singular value rejection based on the accelerance error (see Table 3.3). The singular value rejection based on the response error (see Table 3.7) appears to work better than Tikhonov regularization for combinations where the FRF's contain low noise (high S/N ratio) and noise in responses is large (small S/N ratio). For the combination of large noise in FRF's (small S/N ratio) and large noise in responses (small S/N ratio), OCV seems to work reasonably well.

The average errors in reconstructed responses are shown in Table 5.2. As expected, the error levels are smaller than those in the forces. These results are better than those from pseudo-inversion and singular value rejection based on the accelerance error (see Tables 2.9 and 3.4). Overall, the responses from OCV are equally good or better than those from singular value rejection based on response error (see Table 3.8).

The results corresponding to the case of small noise in FRF's and moderate noise in responses are shown in Figures 5.14 and 5.15. This is one of the case where OCV appears not to perform well (see Tables 5.1 and 5.2). Figures show the forces and the reconstructed response respectively. The forces contain large errors at low frequencies where the condition numbers are very high. Although the assumed operational response errors are large when considered over the whole frequency range, the relative errors near resonances are small (Figure 2.5). This has the result that the regularization parameter is

decreased in the region of high condition number. Hence, OCV is expected to fare poorly at low frequencies where the condition numbers are high and the response errors are relatively small.

Table 5.1. Average errors in dB calculated in 1/3 octave bands in forces determined using ordinary cross validation to select regularization parameter.

		Noise levels in operational responses		
		Low	**Medium**	**High**
Noise levels in FRF's	**Low**	**1.5**	**5.6**	**11.8**
	Medium	**1.9**	**3.8**	**6.2**
	High	**2.2**	**2.4**	**3.8**

Table 5.2. Average errors in dB calculated in 1/3 octave bands in reconstructed response based on forces determined using ordinary cross validation to select regularization parameter.

		Noise levels in operational responses		
		Low	**Medium**	**High**
Noise levels in FRF's	**Low**	**0.2**	**1.4**	**5.5**
	Medium	**0.7**	**1.3**	**4.0**
	High	**1.3**	**1.5**	**1.6**

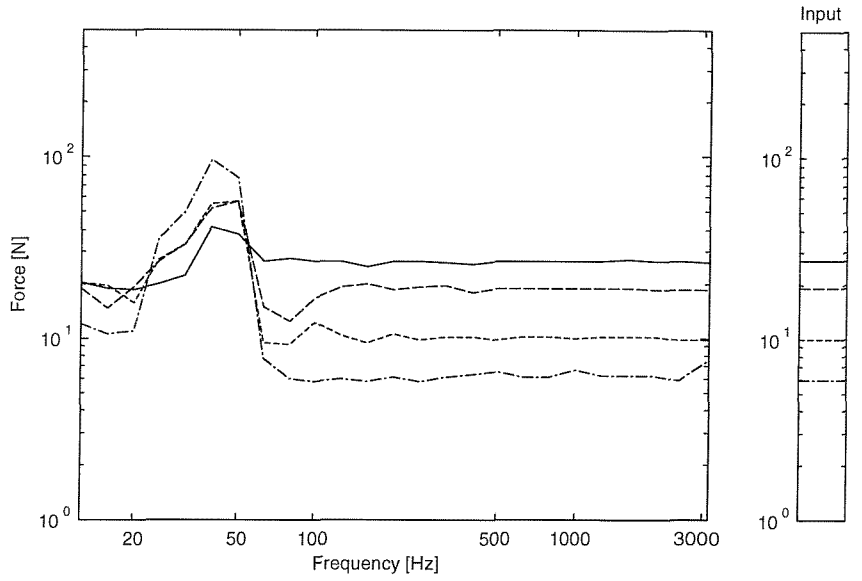

Figure 5.14. Reconstructed rms forces in 1/3 octave bands obtained by Tikhonov regularization with ordinary cross validation for 4 forces and 5 responses. Noise in responses is moderate and noise in FRF's is small. ——— force 1, — — — force 2, – – – – – force 3, — · — · —force 4.

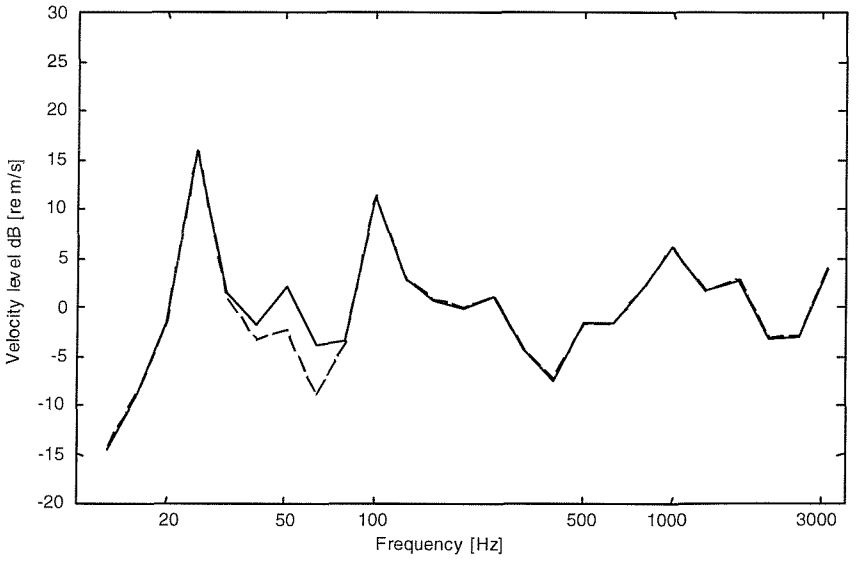

Figure 5.15. 1/3 octave velocity response at the receiver location obtained by Tikhonov regularization with ordinary cross validation. Noise in responses is moderate and noise in FRF's is small. — — — actual response, ———reconstructed response.

5.4 IMPROVING THE PERFORMANCE OF ORDINARY CROSS VALIDATION

5.4.1 Dependence of OCV performance on condition number and response error

In ordinary cross validation, as discussed earlier, the regularization parameter that minimizes the sum of square errors in the reconstructed responses is chosen as an optimum value for the frequency concerned. The components of the summation in equation (5.23) involve m combinations of accelerance matrices of size $(m-1)\times n$. This means that m different condition numbers are involved and that m different error amplifications are included, depending on the response errors present.

As will be shown the regularization parameter selected depends both on the response errors and the condition numbers. As shown below the over-determined $m\times n$ system is expected to have a condition number that is close to the smallest of the condition numbers of the $(m-1)\times n$ submatrices considered by the OCV. However, the regularization parameter selected need not be based on the smallest condition number within the set considered in the OCV. This might result in the selection of a larger than optimal regularization parameter by OCV. It is worth noting that this kind of a problem may not arise in acoustic inverse problems, such as Nearfield Acoustic Holography, where the size of the transfer function matrix is very large and significantly over-determined. The leaving out of one response in such cases is not expected to result in significant variation in condition numbers. It is interesting to know how the variation of the condition numbers within OCV combinations affects the regularization parameter selection. Some numerical simulations are carried out on the simply supported rectangular steel plate to analyse the variations in condition number and the effect on the selection of the regularization parameter.

The simulations performed here consist of several sizes of accelerance matrix. For the case of a 4×3 accelerance matrix, the condition number, κ is shown against frequency in Figure 5.16. The frequency range is restricted to the region below 500 Hz where modal behaviour is strongest. These results correspond to moderate noise levels in the FRF's (moderate S/N ratio) and moderate noise levels in the responses (moderate S/N ratio). The band within which the condition numbers κ_s vary for different sub-matrices of the accelerance matrix is also shown in the figure. The condition

numbers κ of the complete accelerance matrix are very close to minimum of the condition numbers κ_s of the sub-matrices used in the OCV. This implies that the regularization parameter selected in OCV, which is based on all values of κ_s, would not be the same as that based on κ (as the condition numbers of the sub-matrices will always tend to be greater than or equal to the condition number of the complete accelerance matrix).

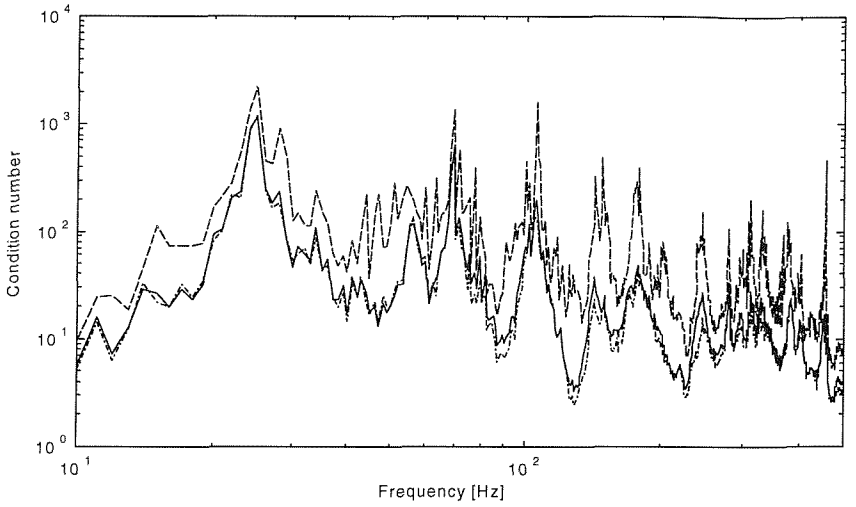

Figure 5.16. Condition number variation for accelerance matrix size 4x3. ——— condition number of accelerance matrix, — — — maximum condition number in OCV and —·—· — minimum condition number in OCV.

The regularization parameter selected by OCV for the above case is shown in Figure 5.17. The regularization parameter selected can be seen to be large when the condition numbers κ_s are large. Ideally, the regularization parameter should correspond to the condition number of the full matrix κ. Moreover it was observed in Chapter 2 that the condition numbers play a more important role than the response errors in determining the amplified errors. This means that the use of OCV probably results in a regularization parameter that is too large, whereas if the regularization parameter were to correspond to the minimum κ_s then it would probably be closer to an optimum value. This is especially important where the difference in sub-matrix condition numbers is large. The regularization parameter would then ensure that the errors propagate without too much amplification. For the case considered in this thesis of a structural dynamics inverse problem where there is usually not a large degree of over-determination, the

spread in values of κ_s will mean that the over-estimate of the regularization parameter by OCV will be significant. With a slight modification to OCV it is possible to take more account of the minimum value of κ_s.

Further examples will be considered below, after the introduction of a modified form of cross validation.

5.5 SELECTIVE CROSS VALIDATION

5.5.1 Formulation

Instead of minimising the sum of validation errors to select the regularization parameter (equation (5.23)), the minimum validation error is used:

$$\Delta(\lambda) = \min_k \left| \hat{a}_k - \hat{A}_k \hat{F}_k \right|^2 \tag{5.24}$$

The method proposed is called *Selective Cross Validation* (SCV). The minimum validation error may correspond to the minimum value of κ_s, but it also takes account of the response errors. The regularization parameter selected using this method for the case considered above is also shown in Figure 5.17. This change would force the process to select the combination which results in minimum magnification of errors. Since the bound on response error amplification is $\kappa_s \varepsilon$ [64] (where ε is the response error), the change in process tends to select the minimum condition number more often than OCV. When Figures 5.16 and 5.17 are compared this new regularization parameter can be seen to correspond more closely in shape to the condition number κ.

The errors in force determination and the receiver response are shown in Table 5.3. For this case, SCV and OCV are observed to estimate different forces more reliably. SCV does not appear to have a significant advantage over OCV as the condition numbers from the whole and sub-matrix do not differ much (see Figure 5.16). The overall receiver response error was, however, found to be slightly better.

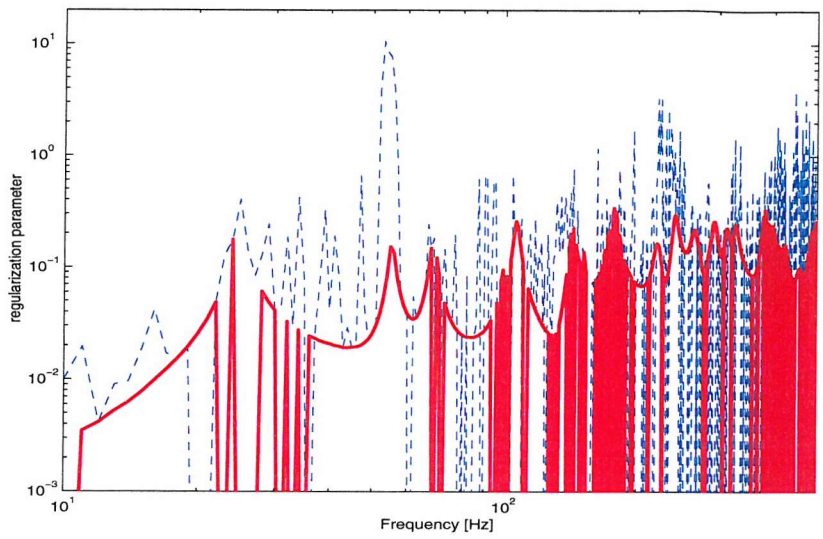

Figure 5.17. Regularization parameter for accelerance matrix size 4x3. — — —OCV, ——— SCV.

Table 5.3. Root mean square errors in dB for the case of 4x3 accelerance matrix.

	Force errors			*Receiver response error*
Method	*Force 1*	*Force 2*	*Force 3*	
OCV	2.3	1.3	2.8	2.4
SCV	1.5	2.6	3.6	2.1

Simulations were also carried out for different degrees of over-determination and greater numbers of forces. Figures 5.18-5.20 show the condition number variation for different degrees of over-determination. The variations of both parameters are observed to be consistent in all the cases. In all the cases the condition number of the whole matrix corresponds closely to the minimum condition number of the sub-matrices. The performance of SCV is seen to depend on the width of band within which condition numbers lie. The errors in the forces and reconstructed responses for the corresponding cases are shown in Tables 5.4-5.6. Some forces are better estimated by OCV. The larger value of regularization parameter selected by OCV appears to suit the high condition numbers at resonances in the low frequency region. This situation is addressed later in the chapter. Apart from this, SCV gives consistent improvements over OCV.

When the number of forces is increased to 7, the condition numbers are as shown in Figure 5.21. The condition numbers vary consistently as expected. The errors in the forces and responses for this case are shown in Tables 5.7. Since the condition numbers of whole matrix and sub-matrix differ significantly, consistent improvements are observed in the reconstructed forces. Note that the Force 7 contains the largest errors since it is the smallest (0.1 N).

The above simulations have demonstrated the consistent performance of SCV when the band within which sub-matrix condition numbers lie is wide.

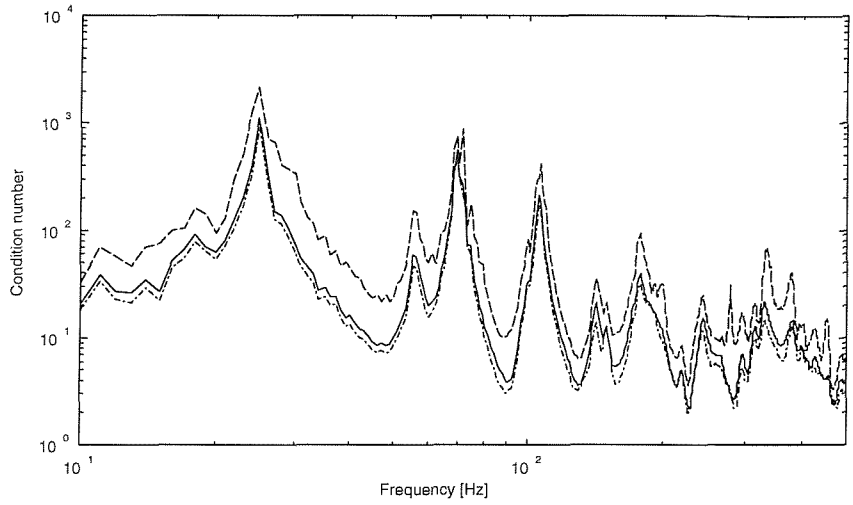

Figure 5.18. Condition number variation for accelerance matrix size 5x3. ——— condition number of accelerance matrix, — — — maximum condition number in OCV and —·—· — minimum condition number in OCV.

Table 5.4. Root mean square errors in dB for the case of 5x3 accelerance matrix size.

	Force errors			*Receiver response error*
Method	*Force 1*	*Force 2*	*Force 3*	
OCV	1.3	2.3	3.5	1.3
SCV	1.3	1.6	3.8	1.4

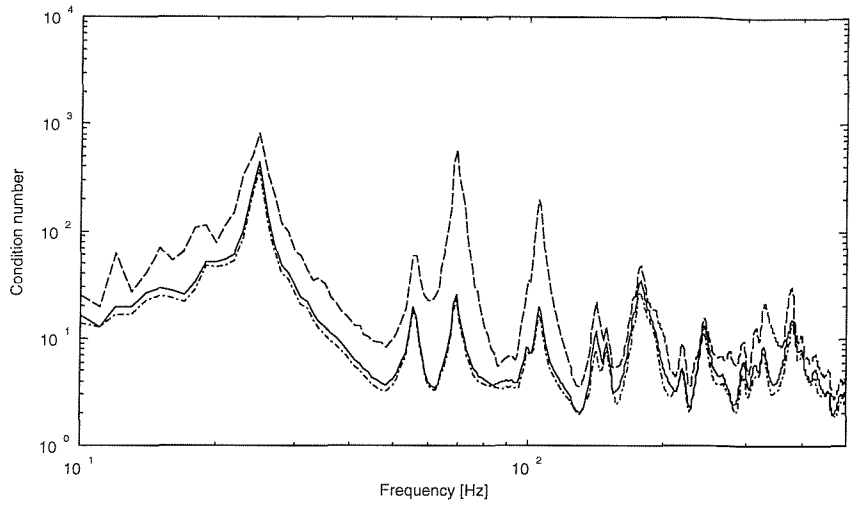

Figure 5.19. Condition number variation for accelerance matrix size 6x3. ——— condition number of accelerance matrix, — — —maximum condition number in OCV and —·—· — minimum condition number in OCV.

Table 5.5. Root mean square errors in dB for the case of 6x3 accelerance matrix size.

	Force errors			*Receiver response error*
Method	*Force 1*	*Force 2*	*Force 3*	
OCV	1.2	1.3	2.7	1.2
SCV	0.7	0.5	2.3	1.3

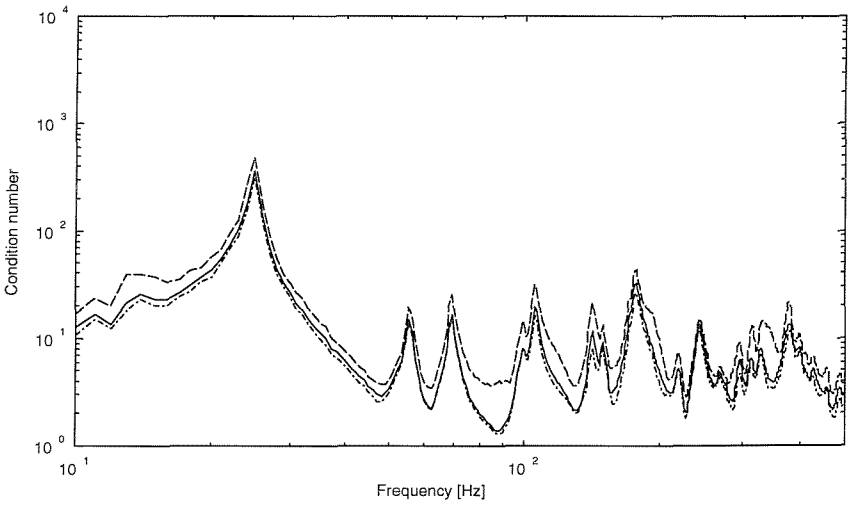

Figure 5.20. Condition number variation for accelerance matrix size 7x3. ——— condition number of accelerance matrix, — — —maximum condition number in OCV and —·—· — minimum condition number in OCV.

Table 5.6. Root mean square errors in dB for the case of 7x3 accelerance matrix size.

	Force errors			*Receiver response error*
Method	*Force 1*	*Force 2*	*Force 3*	
OCV	0.8	1.8	2.3	1.2
SCV	0.6	1.2	2.3	1.2

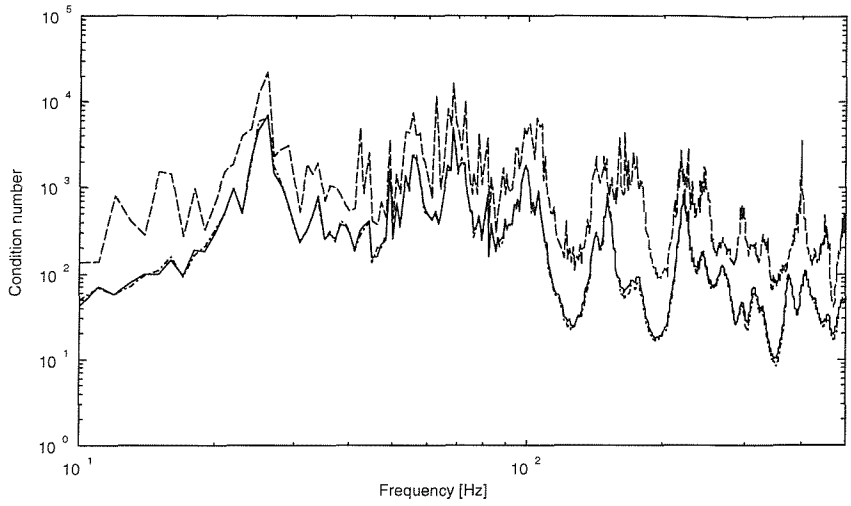

Figure 5.21. Condition number variation for accelerance matrix size 8x7. ——— condition number of accelerance matrix, — — — maximum condition number in OCV and —·—· — minimum condition number in OCV.

Table 5.7. Root mean square errors in dB for the case of 8x7 accelerance matrix size.

	Force errors							*Receiver response error*
Method	*Force 1*	*Force 2*	*Force 3*	*Force 4*	*Force 5*	*Force 6*	*Force 7*	
OCV	2.3	2.7	6.1	12.4	3.2	4.6	31.1	0.3
SCV	1.3	1.9	4.8	11.5	2.0	4.0	32.5	0.2

Reconstructed forces obtained using selective cross validation to choose the regularization parameter for the case considered in Section 5.3.2 are shown in Figure 5.22. The larger forces are observed to be slightly better reconstructed by selective cross validation than was the case with ordinary cross validation (see Figure 5.3). Some differences are observed at low frequency between these results for selective cross validation and those for ordinary cross validation. However, it is difficult to determine which one performs better in this region. The velocity at the receiver location in 1/3

octave bands is shown in Figure 5.23. This is very similar to the one reconstructed using ordinary cross validation (Figure 5.12) except between 50 to 100 Hz, where SCV appears to perform better, and higher frequencies where OCV appears to perform better. A small over-estimation is observed for the response reconstructed using selective cross validation at high frequency.

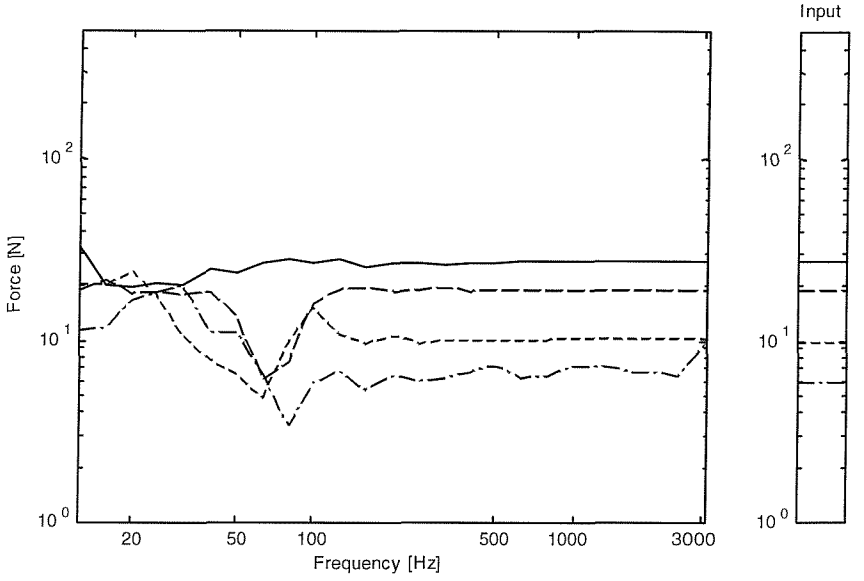

Figure 5.22. Reconstructed rms forces in 1/3 octave bands obtained by Tikhonov regularization with selective cross validation for 4 forces and 5 responses. ——— force 1, — — — force 2, – – – – – force 3, —·—· —force 4.

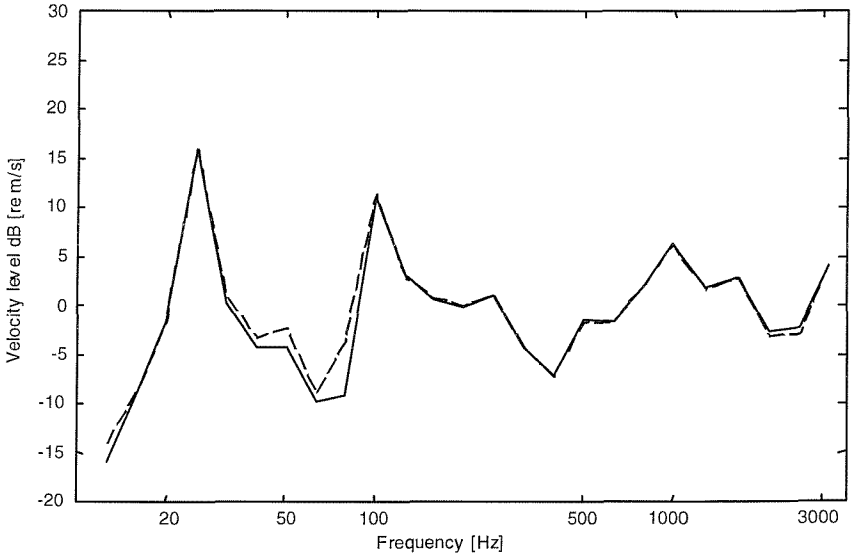

Figure 5.23. 1/3 octave velocity response at the receiver location obtained by Tikhonov regularization with selective cross validation. — — — actual, ——— reconstructed.

5.5.2 Robustness of SCV for different noise levels

Average errors in forces and responses reconstructed using selective cross validation for all nine combinations of noise level in FRF's and responses are shown in Tables 5.8 and 5.9. Some variation is observed in the performance compared with that of ordinary cross validation (see Tables 5.1 and 5.2). These two methods appear to perform with varying levels of reliability for different noise levels in the 'measurements'. This may be due to variation in the width of the band of sub-matrix condition numbers in these cases. Selective cross validation seems to be more sensitive to high condition numbers (high S/N ratios on FRF's) than ordinary cross validation. However, response reconstruction appears to be consistent and comparable with ordinary cross validation.

The forces determined for the case where noise in FRF's is small and noise in responses is moderate are shown in Figure 5.24. The sensitivity of SCV to high condition numbers at low frequency is confirmed by the forces estimated. Maximum errors occur at different frequencies for SCV and OCV (see Figure 5.14). Figure 5.25 shows the reconstructed response at the receiver location. Although force errors are large at low frequency, the reconstructed response contains smaller errors which are comparable to those from OCV. In general, both OCV and SCV are observed to be sensitive to the presence of high condition numbers at low frequencies.

Table 5.8. Average errors in dB calculated in 1/3 octave bands in forces determined using selective cross validation to select regularization parameter.

		Noise levels in operational responses		
		Low	**Medium**	**High**
Noise levels in FRF's	**Low**	**2.5**	**10**	**11.3**
	Medium	**2.5**	**2.8**	**7.1**
	High	**2.5**	**2.7**	**5.4**

Table 5.9. Average errors in dB calculated in 1/3 octave bands in reconstructed response based on forces determined using selective cross validation to select regularization parameter.

		Noise levels in operational responses		
		Low	**Medium**	**High**
Noise levels in FRF's	**Low**	**1.5**	**1.9**	**5.0**
	Medium	**1.5**	**0.9**	**2.3**
	High	**1.4**	**1.3**	**1.8**

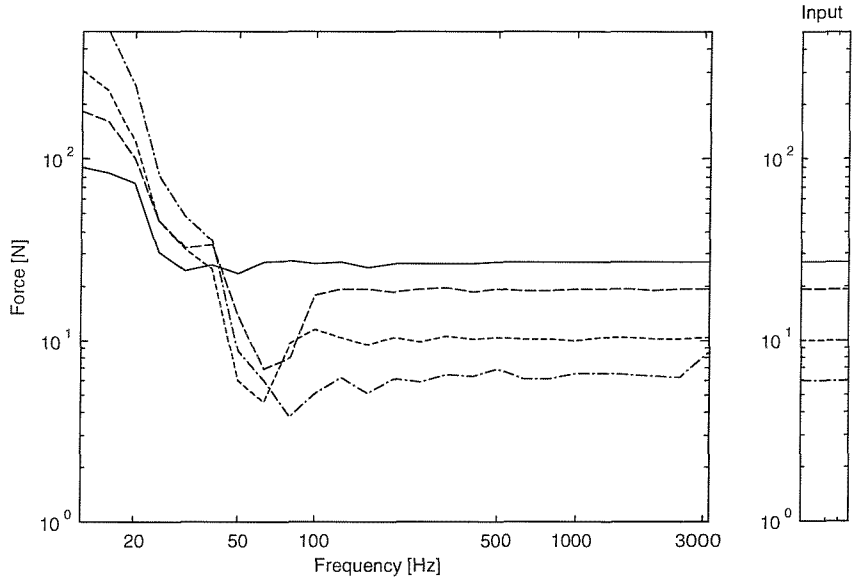

Figure 5.24. 1/3 octave band reconstructed forces obtained by Tikhonov regularization with selective cross validation for 4 forces and 5 responses. Noise in responses is moderate and noise in FRF's is small.——— force 1, — — — force 2, – – – – – force 3, — · — · — force 4.

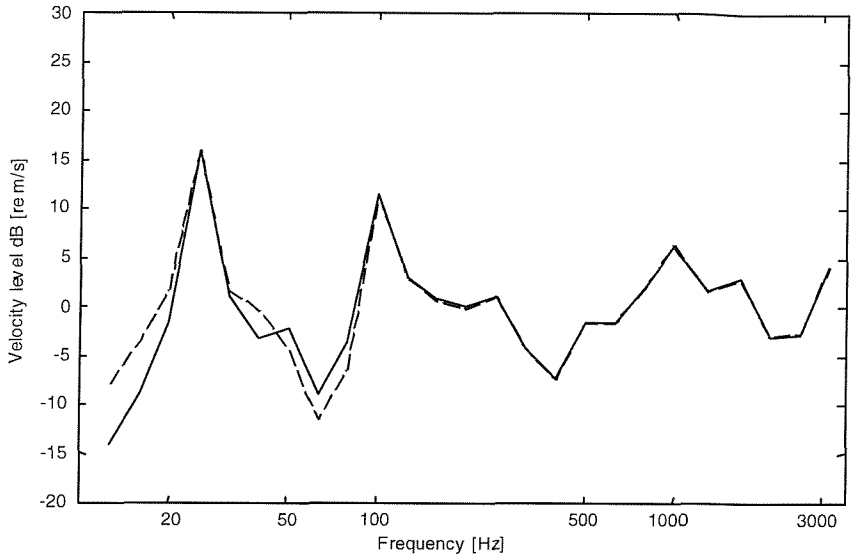

Figure 5.25. 1/3 octave velocity response at the receiver location obtained by Tikhonov regularization with selective cross validation. Noise in responses is moderate and noise in FRF's is small. ———— actual response, — — — reconstructed response.

5.6 NON-ZERO REGULARIZATION PARAMETER CONCEPT

In Figures 5.14 and 5.24, the cases with high condition numbers at resonances and low noise in the responses were seen to result in the selection of small values of regularization parameter by OCV and SCV. Although it may not affect the reconstructed receiver location response, the individual forces are expected to have large errors. It is suggested that the enforcement of a non-zero starting regularization parameter value might improve the force identification in the frequencies where modal behaviour is very strong. This should help to reduce error amplification in the frequency region where modal behaviour is very strong but it may result in biased estimates at higher frequencies where the modal density is large and the condition numbers are lower. If the enforced non-zero starting value of regularization parameter is optimal it is expected that the improvement at low frequency would more than compensate the small bias introduced at high frequency. It is necessary to know how to determine a suitable minimum value of regularization parameter.

In this section different levels of assumed errors (bias) that correspond to different signal to noise ratios in 'measured' operational responses are initially used to evaluate the effect of the minimum value of regularization parameter to arrive at an optimal one. To check the validity of these different levels, they are used with cases with

different combinations of condition numbers and different noise levels in both the FRF's and responses. The four combinations which are the corners of the Tables 2.3 and 2.5, considered earlier, have been used. The formulation leading to this concept is explained below.

The reconstructed response using the full rank pseudo-inverse is given by

$$\breve{a} = \hat{A}\, V S^{-1} U^{H} \hat{a} \tag{5.26}$$

The reconstructed response from Tikhonov regularization is given by

$$\tilde{a} = \hat{A}\, V \left(S^{H} S + I\lambda\right)^{-1} S^{H} U^{H} \hat{a} \tag{5.27}$$

An objective estimate of the bias error introduced by regularization can be written as

$$\varepsilon_b = \frac{\|\breve{a}\|_2 - \|\tilde{a}\|_2}{\|\breve{a}\|_2} \tag{5.28}$$

Three levels of ε_b that result in operational response being 1%, 3% and 10% different (biased) from the actual responses have been used to establish an optimal value. The errors in forces and responses determined are shown in Table 5.10 for four combinations of noise as indicated above. For the first two cases all levels for ε_b are found to perform reasonably well with a zero level for ε_b seen to give the best results. However, this level results in the largest errors for the last two cases in Table 5.10. The third case is observed to result in especially large amplification. For these last two cases a 1% level works reasonably well, although for the third case a 3% level yields better results. Overall, 1% level seems to work reasonably well for all cases. However, since for OCV and SCV, the forces and reconstructed responses contain the largest errors in the case where noise in the responses is large and noise in the FRF's is small (see Tables 5.1-5.2 and 5.8-5.9), as a compromise the 3% level for ε_b seems to be a reasonable choice. In the remainder of this chapter, this value has been used to estimate the minimum value of regularization parameter.

Table 5.10. Average errors in dB calculated in 1/3 octave bands in forces determined using selective cross validation to select regularization parameter.

Operational response difference from actual response	Noise level in operational responses / FRF's							
	Low/Low		Low/High		High/Low		High/High	
	F_e	R_e	F_e	R_e	F_e	R_e	F_e	R_e
0%	2.5	1.5	2.5	1.4	11.3	5.0	5.4	1.8
1%	3.7	2.1	3.5	2.1	4.9	1.9	3.5	1.3
3%	4.2	2.6	4.1	2.6	3.8	2.3	3.8	1.9
10%	5.2	3.0	5.1	3.0	4.4	2.9	4.4	2.9

where F_e is the force error and R_e the response error. Smallest errors are underlined.

The above method can be refined slightly. All the operational responses estimated from measured data, with finite signal to noise ratio, always contain some measurement error. Over and above this, some percentage of response has been now assumed as the difference between the actual response and the 'measured' response that is enforced on it. The bias introduced into the solution could therefore be more than is needed. It is necessary to check the measurement error in the responses so that the proper level of bias can be introduced. The reconstruction of the responses that are used to determine the forces gives some measure of the measurement errors in responses. The reconstruction error is given by

$$\varepsilon_{reconst} = \frac{\|\hat{a}\|_2 - \|\breve{a}\|_2}{\|\hat{a}\|_2} \tag{5.29}$$

The difference increases as the measurement errors increase. If the reconstruction error $\varepsilon_{reconst}$ is less than the assumed bias (ε_b=3%), the actual assumed bias is taken as $\varepsilon_b' = \varepsilon_b - \varepsilon_{reconst}$ and this is used to select the minimum value of regularization parameter. If $\varepsilon_{reconst} \geq \varepsilon_b$ no minimum regularization parameter is enforced.

The concept developed here to select the regularization parameter is called *biased selective cross validation* (BSCV), the bias refering to the enforcement of a minimum regularization parameter. If it is used along with ordinary cross validation it is called *biased ordinary cross validation* (BOCV).

The forces reconstructed using BSCV are shown in Figure 5.26 for the case of large noise in responses and small noise in FRF's. Forces are estimated reliably even for this case where large error amplification was observed in OCV and SCV (see Tables

5.1-5.2 and 5.8-5.9). The response at the receiver location obtained using biased selective cross validation is shown in Figure 5.27.

Average errors in the forces and responses reconstructed using biased selective cross validation for all nine combinations of noise levels in FRF's and responses are shown in Tables 5.11 and 5.12. Generally the method appears to be robust in situations of different noise levels in FRF's and responses. However this comes at a penalty of worse results for situations where there is low measurement noise in the operational responses where OCV and SCV gave even better results.

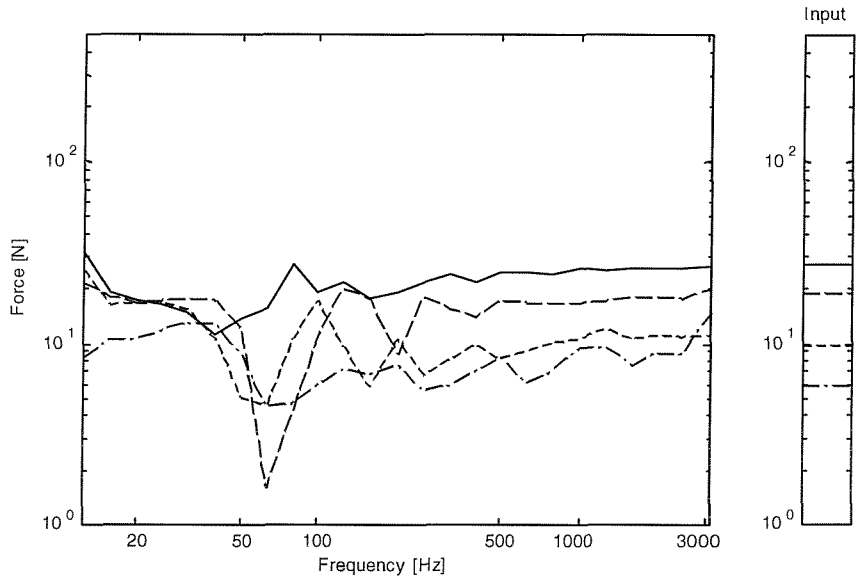

Figure 5.26. Reconstructed forces in 1/3 octave bands obtained by Tikhonov regularization for 4 forces and 5 responses using biased selective cross validation. Noise in responses is large and noise in FRF's is small.——— force 1, — — — force 2, – – – – – force 3, —·—· —force 4.

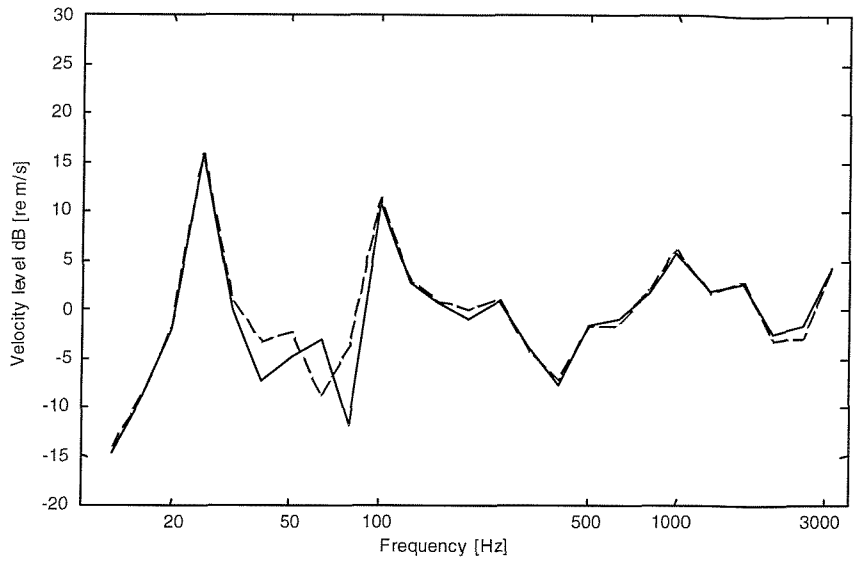

Figure 5.27. 1/3 octave velocity response at the receiver location obtained by Tikhonov regularization with biased selective cross validation. Noise in responses is large and noise in FRF's is small. — — — actual response, ———— reconstructed response.

Table 5.11. Average errors in dB calculated in 1/3 octave bands in forces determined using biased selective cross validation to select regularization parameter.

		Noise levels in operational responses		
		Low	**Medium**	**High**
Noise levels in FRF's	**Low**	**4.2**	**4.1**	**4.1**
	Medium	**4.2**	**4.1**	**4.1**
	High	**3.8**	**4.1**	**3.8**

Table 5.12. Average errors in dB calculated in 1/3 octave bands in reconstructed response based on forces determined using biased selective cross validation to select regularization parameter.

		Noise levels in operational responses		
		Low	**Medium**	**High**
Noise levels in FRF's	**Low**	**2.6**	**2.7**	**2.6**
	Medium	**2.6**	**2.7**	**2.5**
	High	**2.3**	**2.7**	**1.9**

5.7 CONCLUSIONS

Extending the investigation of regularization techniques in improving force determination, Tikhonov regularization has been explored. Simulations have been carried out to represent experiments. Ordinary cross validation has been studied and improved versions referred to as selective cross validation (SCV) and biased SCV have been developed for selecting the regularization parameter. The following conclusions are drawn based on these simulations,

1. The weighting of singular values as performed by Tikhonov regularization gives better results than singular value rejection as it offers a greater degree of control.
2. Ordinary cross validation is sensitive to noise levels in the operational responses (small S/N ratio) and FRF's (high S/N ratio).
3. Selective cross validation, which attaches more importance to condition numbers in selecting the regularization parameter, is also sensitive to the noise level in the responses and FRF's.
4. Biased OCV or SCV are much more robust to changes in noise levels in the responses and FRF's, but they are not always better.

CHAPTER 6

ITERATIVE INVERSION

6.1 INTRODUCTION

Two types of regularization have already been studied in Chapter 3 and Chapter 5: viz. singular value rejection and Tikhonov regularization. Iterative inversion is an alternative means of achieving regularization. The solution in iterative inversion is based on the principle that when an infinite number of iterations is used in a proper formulation, the solution tends to the usual mean square solution. As before it is concerned with weighting singular values rather than eliminating them.

6.2 FORMULATION FOR ITERATIVE INVERSION

In the iteration process errors in the force determination can be classified into two groups: bias error and variance around the mean. The bias error in the forces tends to zero as the number of iterations is increased, while the random error goes on increasing. By seeking a compromise in the bias error it is possible to limit the variance. In fact, there is an optimum number of iterations where the total error is minimum. At this iteration number, the combined error reaches a minimum. This property of iterative inversion can be effectively utilized to reduce the combined error.

Iterative inversion [35] can be applied to force identification as follows (details of the derivation are given in Appendix E). The k+1$^{\text{th}}$ estimate of the forces is given in terms of the k^{th} estimate by

$$\hat{F}_{k+1} = \hat{F}_k + \beta \hat{A}^H \left(\hat{a} - \hat{A}\hat{F}_k\right) \tag{6.1a}$$

This can be rearranged to give $\hat{F}_{k+1} = \beta \hat{A}^H \hat{a} + \left(I - \beta \hat{A}^H \hat{A}\right)\hat{F}_k$ where I is the unit matrix. The first approximation for the force vector is taken as $\hat{F}_0 = \beta \hat{A}^H \hat{a}$. The k^{th} estimate of the forces can also be written, using geometric series as

$$\hat{F}_k = \beta\left(I - \left(I - \beta \hat{A}^H \hat{A}\right)\right)^{-1}\left(I - \left(I - \beta \hat{A}^H \hat{A}\right)^{k+1}\right)\hat{A}^H \hat{a} \tag{6.1b}$$

where β is the convergence factor. The solution converges for an infinite number of iterations only when

$$\left(I-\beta\hat{A}^H\hat{A}\right)^{k+1}\rightarrow[0]\quad\text{as}\quad k\rightarrow\infty \tag{6.2}$$

In the limiting case (when k tends to infinity) the solution tends to the Moore-Penrose pseudo-inverse (equation (2.13),

$$\begin{aligned}\hat{F}_\infty &= \beta\left(\beta\hat{A}^H\hat{A}\right)^{-1}\hat{A}^H\hat{a} \\ &= \left(\hat{A}^H\hat{A}\right)^{-1}\hat{A}^H\hat{a}\end{aligned} \tag{6.3}$$

which minimizes the mean square error $\left|\hat{A}\hat{F}_\infty-\hat{a}\right|^2$.

Alternatively using singular value decomposition of the matrix $\hat{A}=USV^H$ equation (6.1) can be written as

$$\hat{F}_k = V[diag(\psi_1,.....\psi_n)|\,[0]_{n\times m-n}]U^H\hat{a} \tag{6.4}$$

where $\psi_i=\dfrac{1-\left(1-\beta s_i^2\right)^{k+1}}{s_i}$ for i=1,2,.....n. (6.5)

Comparing this with equation (3.2) reveals that iterative inversion can be seen as an alternative means of regularizing the inverse of $\hat{A}$, replacing s_i^{-1} by $\psi_i(k)$.

6.3 BASIS FOR NUMBER OF ITERATIONS

To find the optimum number of iterations in order to minimize the combined error it is necessary to formulate expressions for the bias error and the variance. The expressions can be derived following [36], the details of which are given in Appendix E. The overall mean square error of the estimation is given by

$$\varepsilon_k^2 = E\left[(\tilde{a}-a)^H(\tilde{a}-a)\right] \tag{6.6}$$

where $a=AF$ is the exact operational response, $\tilde{a}=\hat{A}\hat{F}$ is the reconstructed response and E signifies the expected value. If it can be assumed that the same variance σ^2 exists for all the measurement points, after extensive manipulation the above equation is simplified to give (see Appendix E)

$$\varepsilon_k^2 = \sigma^2\left(2\sum_{i=1}^{n}\phi_i-n\right)+\hat{b}^H\hat{b} \tag{6.7}$$

where $\phi_i=1-\left(1-\beta s_i^2\right)^{k+1}$. The first term on the right hand side of equation (6.7) represents variance and the second the bias in the iterative solution. The bias introduced into the solution is given by

$$\hat{b}^H \hat{b} = \hat{a}^H U(diag(\phi_1,..\phi_n,0_{n+1}..0_m)-I)^H (diag(\phi_1,..\phi_n,0_{n+1}..0_m)-I)U^H \hat{a} \tag{6.8}$$

Equation (6.7) is used in arriving at a compromise between the bias error and the variance. The cross-over occurs when the following condition is satisfied:

$$\sigma^2\left(2\sum_{i=1}^{n}\phi_i\right) = \hat{a}^H U(diag(\phi_1,..\phi_n,0_{n+1}..0_m)-I)^H (diag(\phi_1,..\phi_n,0_{n+1}..0_m)-I)U^H \hat{a} \tag{6.9}$$

After cross-over the magnification of random errors starts to dominate. The iteration number k which results in the above condition is the optimum iteration number which gives a compromise between bias error and the magnified random errors. This iteration number can be used in (6.4) to obtain the reconstructed forces with minimum error.

6.4 CONVERGENCE PARAMETER β

The convergence parameter β determines how fast the solution will converge to the Moore-Penrose pseudo inverse. The larger the value of convergence parameter, the faster is the convergence. As already mentioned, however for convergence to occur the condition $\left(I-\beta\hat{A}^H\hat{A}\right)^{k+1} \rightarrow [0]$ as $k \rightarrow \infty$ has to be satisfied. This expression determines the upper limit for the convergence parameter. Using singular value decomposition, this convergence criterion can also be written as $\left(1-\beta s_i^2\right)<1$ for i=1,2,.....n. Therefore $\beta < \frac{1}{s_i^2}$.

If only one convergence parameter value β is used for all singular values, as indicated in the above, the part of the solution contributed by the larger singular values converges faster than the smaller ones. The difference increases as the condition number increases. Since, in the case of a large condition number, smaller singular values are prone to modification by measurement errors, the slower convergence can be effectively utilised in restricting the iteration to reduce the error propagation. To accommodate the above criterion, the convergence parameter can be written as $\beta = \frac{c}{s_1^2}$ where c is a constant less than one.

To improve the resolution i.e. to ensure that a sufficient number of iterations occur, it is necessary that the convergence parameter constant c has different values for different condition numbers. This is because, at smaller condition numbers, if a large constant is used the cut-off iteration occurs at a very low iteration number. This is found

to reduce the resolution. Hence the constant c can be varied based on the condition number. The following exponential expression has been devised for use in the simulations in this study

$$c = 1 - 0.99e^{-\gamma\kappa} \tag{6.10}$$

where κ is a condition number of the accelerance matrix and γ is a constant that controls the exponential decay; in this study it is taken to be 0.1. This expression is represented graphically in Figure 6.1.

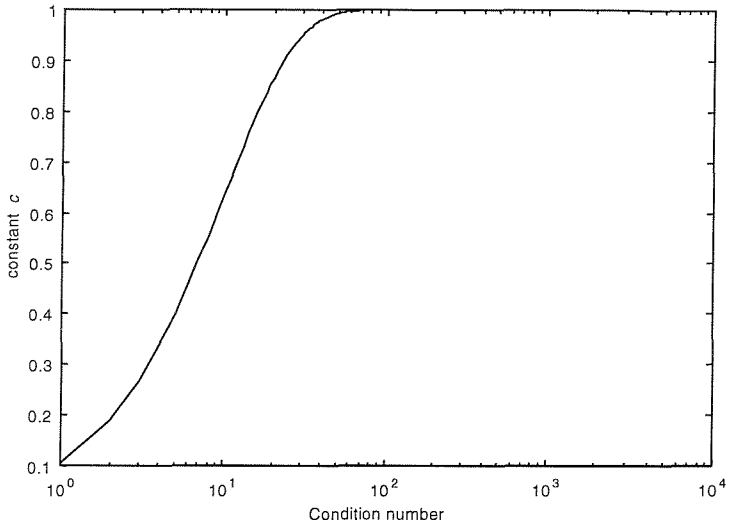

Figure 6.1. Variation of 'c' for $\gamma = 0.1$.

6.5 NOISE IN THE OPERATIONAL RESPONSES

The standard deviation in the operational response is required to determine the optimum iteration number. It can be obtained either directly using equation (3.5) or indirectly as in equation (3.4). There is a difficulty in choosing the cut-off iteration number in this way when the standard deviation is larger than or considerable in magnitude compared to the response itself. This can occur at antiresonance for example. In this situation, based on the error expression it is observed that the cut-off criterion is satisfied already at the first iteration. This results in an under-estimation of the forces concerned. Another problem is faced at resonance where the standard deviation is very small compared with the operational response which might lead to a larger number of iterations being required for error equalization (bias and variance). A large number of iterations means larger amplification of measurement errors. Hence the force reconstruction would be incorrect in both cases.

To overcome these problems it is proposed to use a fixed percentage of the operational response as the assumed standard deviation, for example 10% or 20% etc. of the response. This introduces a small bias in the response predicted at the receiver location. This strategy results in another problem, however, that of finding the fraction of operational response to be used as the assumed standard deviation. In this study a form of cross validation is proposed in which the reconstructed forces are used to recreate operational responses other than the ones used for force reconstruction and these are compared with the measured values. In this there are two variants. In the first case, one of the responses is used as a basis for the validation and the standard deviation resulting in minimum reconstruction error for this response is chosen as the optimal value. In the second case a concept similar to 'selective cross validation' as applied in Tikhonov regularization is used. These two variants are referred to here as *single response cross validation* (SRCV) and *multi-response cross validation* (MRCV) respectively. Here, the fraction of response assumed as the standard deviation is varied in some range (5 to 50%) in small steps (5% step) and the fraction which results in the minimum validation error at each frequency is used for force reconstruction at those frequencies. The expression for the validation error for SRCV concept is given by

$$VE = \frac{|\tilde{a}_{valid} - \hat{a}_{valid}|}{|\hat{a}_{valid}|} \tag{6.11}$$

The expression for the validation error in MRCV concept is given by

$$VE = \min_{r} \frac{|\tilde{a}_{valid} - \hat{a}_{valid}|_r}{|\hat{a}_{valid}|_r} \tag{6.12}$$

where $\tilde{a}_{valid}$ is a validating reconstructed operational response and $\hat{a}_{valid}$ is a measured operational response.

An alternative approach is also considered. In the derivation of the total reconstruction error, it was assumed that the standard deviation in the measurement of operational responses is same for all the responses. To generalize further, it is possible to incorporate individual standard deviations in the measurement of operational responses (see Appendix E) as below

$$\varepsilon_k^2 = E\left[trace\left\{\delta_k(\hat{a}-AF)(\hat{a}-AF)^H \delta_k{}^H\right\}\right] + E\left[trace\left\{(\delta_k - I)(\hat{a}-AF)(\hat{a}-AF)^H(\delta_k - I)^H\right\}\right] - \hat{b}^H\hat{b} \tag{6.13}$$

where $\delta_k = Udiag(\phi_1,.....\phi_n,0_{n+1},...0_m)U^H$.

The above equation can be simplified as

$$\varepsilon_k^2 = trace(\delta_k diag(\sigma)\delta_k{}^H) + trace\{(\delta_k - I)diag(\sigma)(\delta_k - I)^H\} - \hat{b}^H\hat{b} \tag{6.14}$$

6.6 FORCE RECONSTRUCTION

In all the simulations the same flat plate is used as previously, with four sources and five responses. In the case considered here responses contain moderate noise and FRF's contain large noise. In SRCV and MRCV to arrive at an assumed standard deviation, a 4×4 FRF matrix is used for force reconstruction and either the last response is used for single response cross validation or all responses are used for multi-response cross validation, one at a time. The standard deviation which results in the minimum validation error (*VE*) at each frequency is then used to find the optimal iteration number which is used in the reconstruction of forces using the 5×4 FRF matrix.

The variation of bias error and variance with respect to the number of iterations for one of the frequencies is shown in Figure 6.2. The iteration number where these two errors coincide is taken as the cut-off iteration number. Figure 6.3 shows the cut-off iteration numbers for each of the frequencies determined using the single response cross validation method.

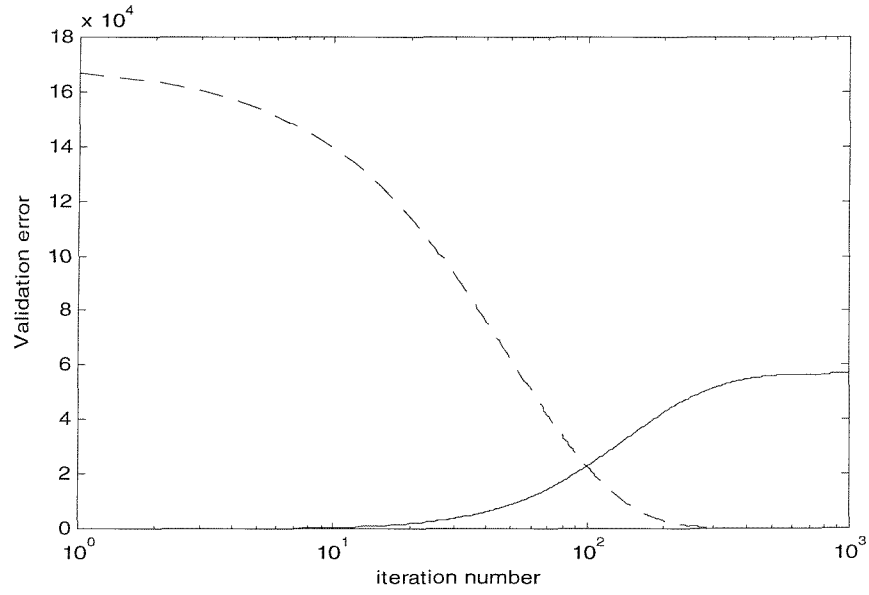

Figure 6.2. The bias error and variance as function of iterations at 29 Hz. _ _ _ _ bias, _____variance.

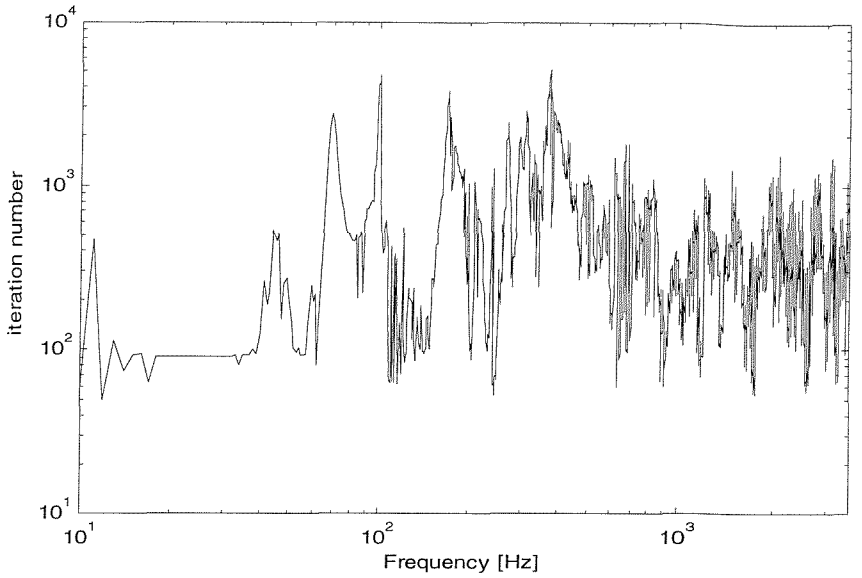

Figure 6.3. Number of iterations for cut-off where total error is minimum.

Figures 6.4–6.7 show the force reconstruction in 1/3 octave band representation for the four variants in implementation of iterative inversion. When the standard deviation of the operational responses is assumed to be the same for all channels, the forces are observed to be under-estimated significantly (Figure 6.4). If the standard deviation for each response is used no improvement is observed over the above case and the forces are still under-estimated (Figure 6.5). The force reconstruction improves considerably above 100 Hz with the use of the single response cross validation concept as shown in Figure 6.6. The forces are still under-estimated at some frequencies. The use of the multi-response cross validation concept does not improve the force reconstruction compared with single response cross validation. The forces reconstructed appear to be similar in both these cases. All four variants in the implementation of iterative inversion appear to be inferior to Tikhonov regularization with OCV or SCV (compare with Figures 5.3 and 5.22).

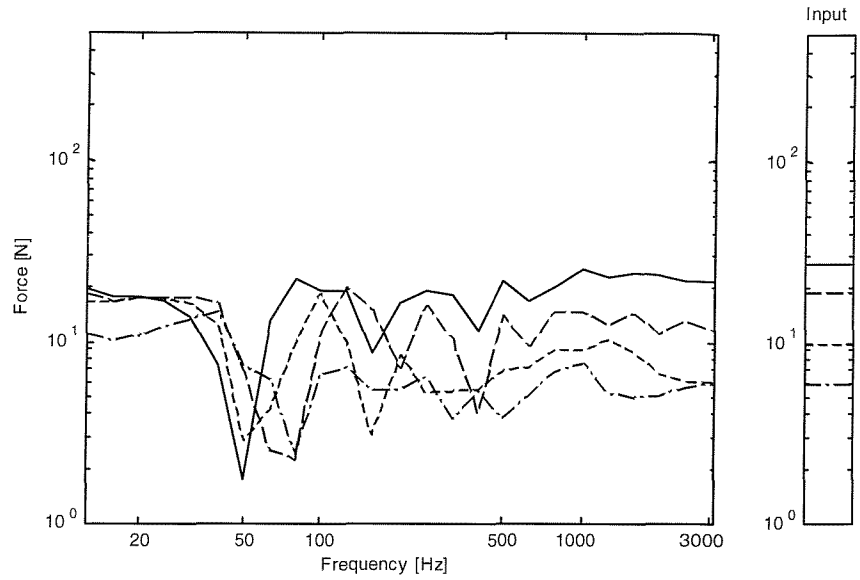

Figure 6.4. Reconstructed rms forces in 1/3 octave bands representation for iterative inversion with common standard deviation in the responses. ————force 1, — — — force 2, - - - - - - force 3, —·—·— force 4.

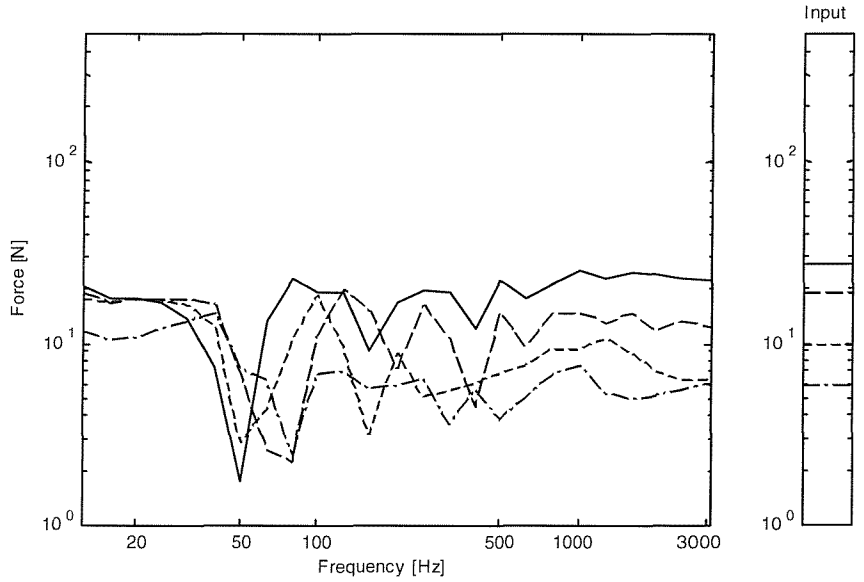

Figure 6.5. Reconstructed rms forces in 1/3 octave bands representation for iterative inversion with individual standard deviation for 4 sources and 5 responses. ———— force 1, — — —force 2, - - - - - - force 3, —·—·— force 4.

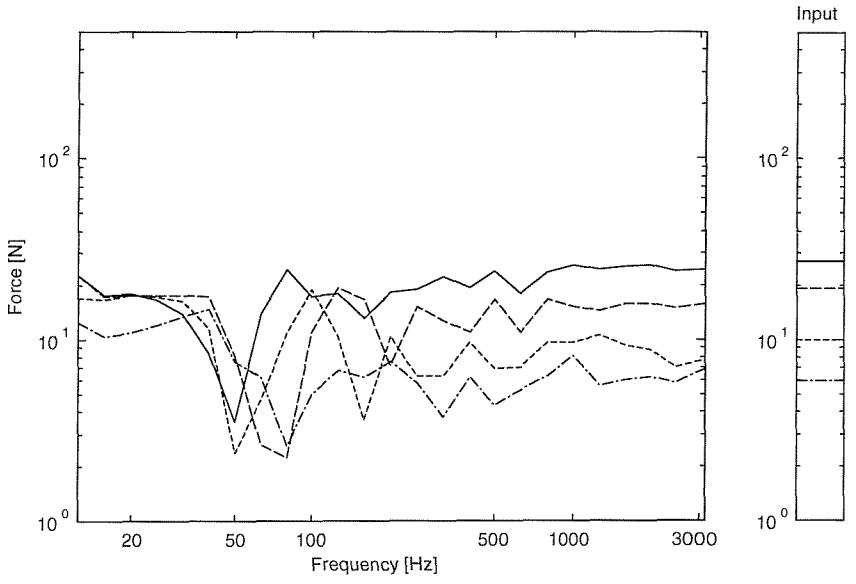

Figure 6.6. Reconstructed rms forces in 1/3 octave bands representation for iterative inversion with SRCV. ————force 1, — — —force 2, - - - - - - force 3, —·—·— force 4.

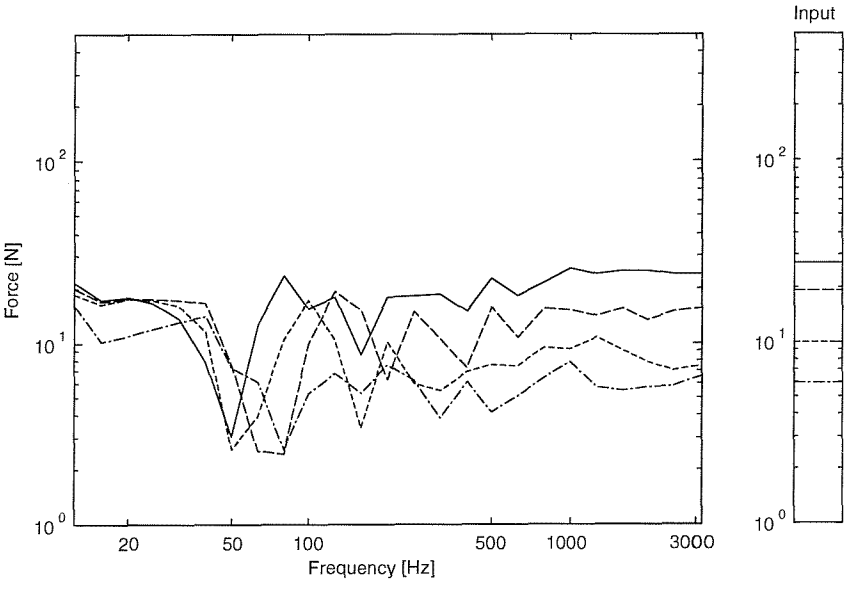

Figure 6.7. Reconstructed rms forces in 1/3 octave bands representation for iterative inversion with MRCV. ————force 1, — — —force 2, - - - - - - force 3, —·—·— force 4.

6.7 VELOCITY AT THE RECEIVER LOCATION

The errors in force estimation translate into errors in the reconstructed response. However, at low frequency where mostly one mode is dominant, the errors may not add up but rather may cancel out and result in a good overall response estimation. This can be seen from the velocity response shown in Figures 6.8-6.11. All four options based on iteration appear to result in slight under-estimation at high frequencies in general. This is more evident when the velocity responses are represented in 1/3 octave bands as shown in Figures 6.12-6.15. However, SRCV and MRCV appear to reduce the difference between reconstructed response and the true response at high frequencies compared with the first two methods.

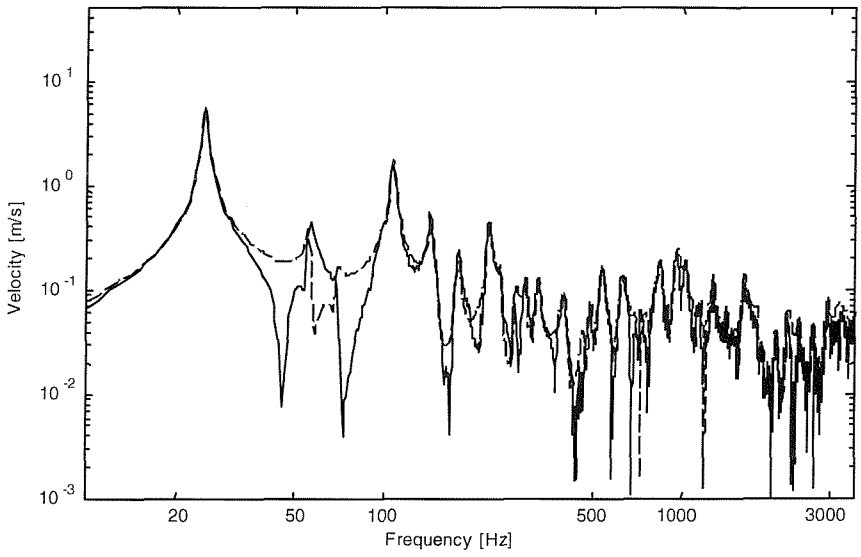

Figure 6.8. Velocity response at the receiver location by iterative inversion with common standard deviation in response. — — — — actual response, ———— reconstructed response.

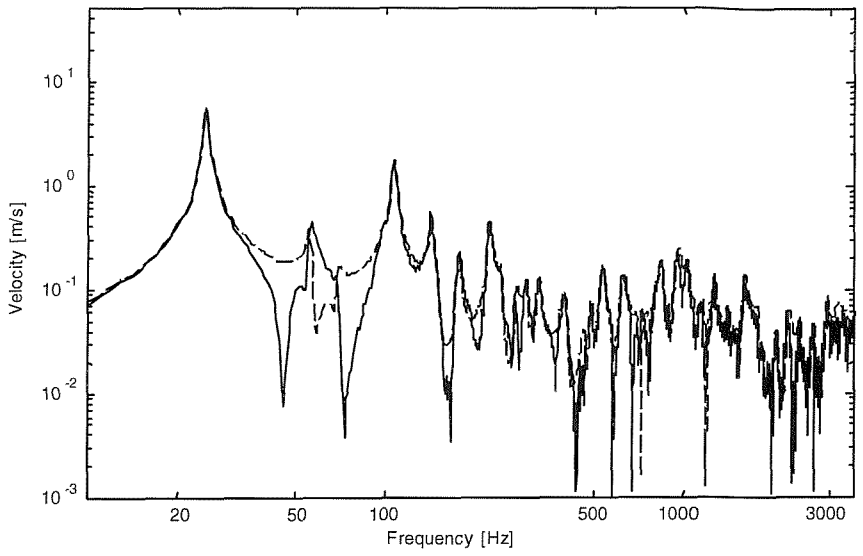

Figure 6.9. Velocity response at the receiver location by iterative inversion with individual standard deviation in responses. — — — — actual response, ——— reconstructed response.

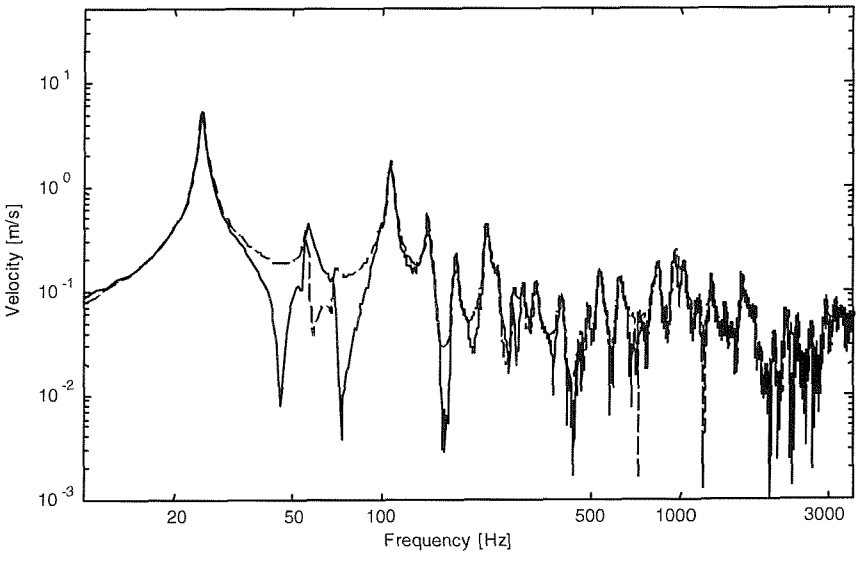

Figure 6.10. Velocity response at the receiver location by iterative inversion with SRCV. — — — — actual response, ——— reconstructed response.

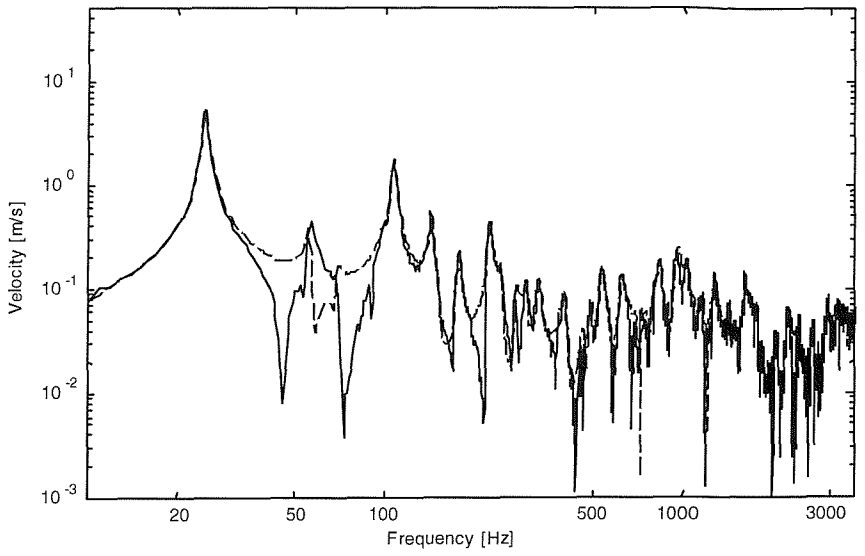

Figure 6.11. Velocity response at the receiver location by iterative inversion with MRCV. — — — — *actual response,* ———— *reconstructed response.*

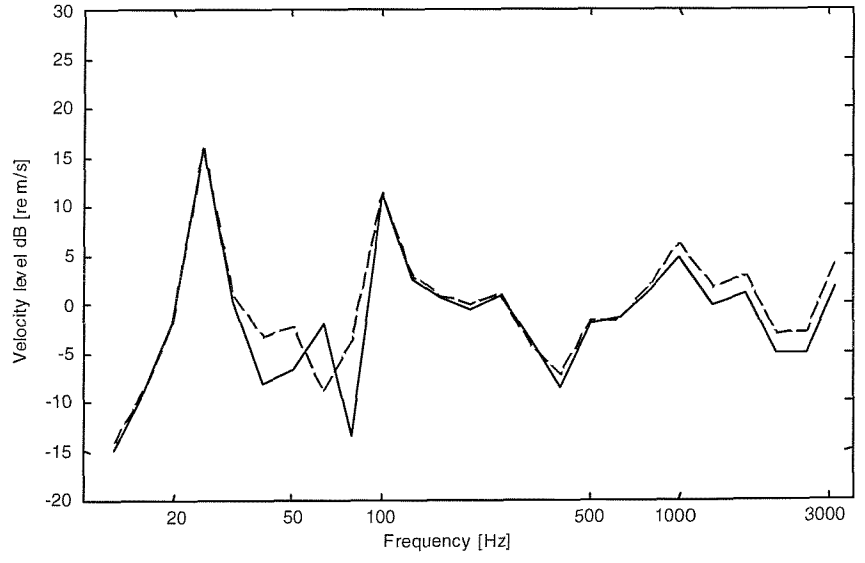

Figure 6.12. 1/3 octave band velocity response at the receiver location by iterative inversion with common standard deviation in response. — — — — *actual response,* ———— *reconstructed response.*

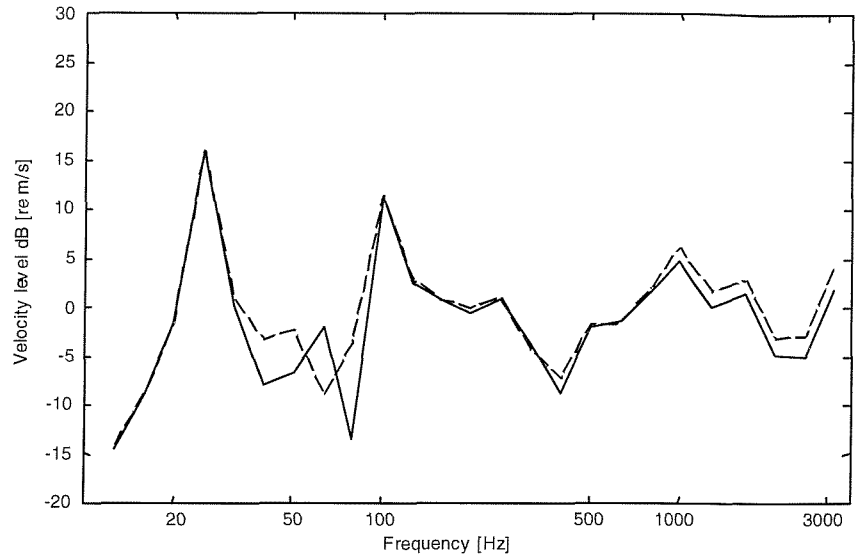

Figure 6.13. 1/3 octave band velocity response at the receiver location by iterative inversion with individual standard deviation in responses. — — — — actual response, ———— reconstructed response.

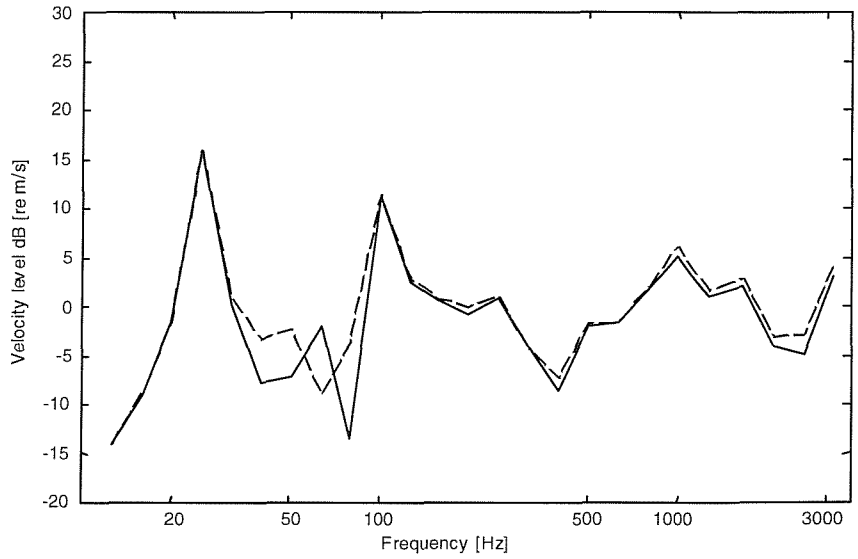

Figure 6.14. 1/3 octave band velocity response at the receiver location by iterative inversion with SRCV. — — — — actual response, ———— reconstructed response.

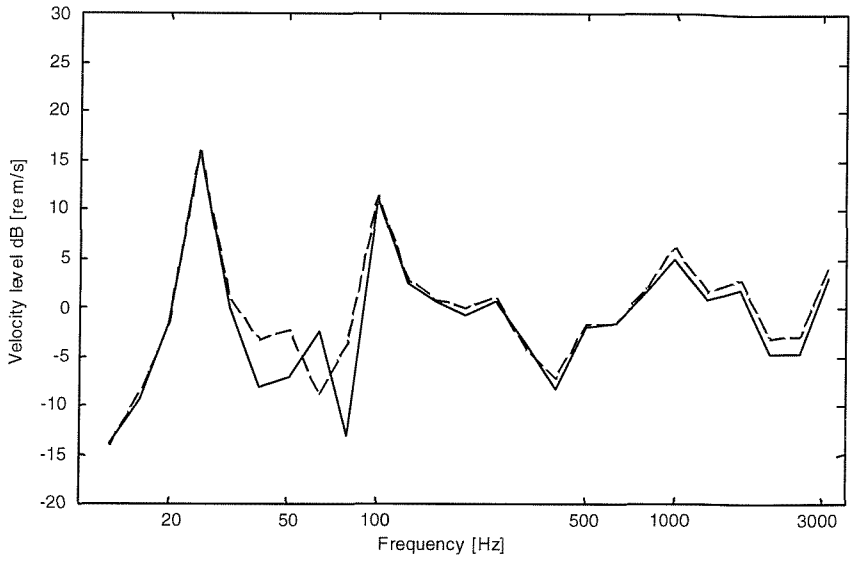

Figure 6.15. 1/3 octave band velocity response at the receiver location by iterative inversion with MRCV. — — — — actual response, ———— reconstructed response.

6.8 ROBUSTNESS OF ITERATIVE METHOD TO DIFFERENT NOISE LEVELS

Out of the nine combinations of different noise levels in responses and accelerances only the four extreme cases (corners in Table 2.3) have been used here to test the robustness of iterative inversion with single response cross validation. The average errors in reconstructed forces and responses are shown in Tables 6.1 and 6.2. The level of error is similar in each case. Iterative inversion with single response cross validation therefore appears to be more robust than most of the methods considered in Chapters 2-4 except singular value rejection based on response error and the perturbed singular value rejection. However, the level of error obtained is higher than singular value rejection based on response error for low response noise (see Tables 3.7-3.8). The performance when compared with Tikhonov regularization with BSCV, appears to be inferior (Tables 5.11 and 5.12).

Table 6.1. Average errors in dB calculated in 1/3 octave bands in forces determined using determined iterative inverse with SRCV.

		Noise levels in operational responses	
		Low	High
Noise levels in FRF's	Low	4.7	4.6
	High	4.7	4.6

Table 6.2. Average errors in dB calculated in 1/3 octave bands in reconstructed response based on forces determined using iterative inverse with SRCV.

		Noise levels in operational responses	
		Low	High
Noise levels in FRF's	Low	2.7	1.9
	High	2.7	2.8

6.9 SUMMARY

In this chapter iterative inversion is investigated for force reconstruction using numerical simulations on a simply supported flat plate. Estimates of the bias error and variance are used to arrive at an optimum number of iterations. Using an example of a 5×4 FRF matrix it has been shown that iterative inversion based on cross validation methods gives reliable results. The results have been confirmed for different error levels in Tables 6.1 and 6.2. The following conclusions are drawn based on these simulations.

1. The iterative inversion based on a common standard deviation under-estimates the forces near antiresonances.
2. Even when the individual measured response standard deviations are used, the force reconstruction is similar.

3. Results with single response cross validation or multi-response cross validation also appear to be the same for the case considered.
4. The single response cross validation or multi-response cross validation are found to be robust to any level of noise in responses and accelerances.

The simulations for iterative inversion using multi-response cross validation range from 4 to 12 hours depending on the matrix condition number on a 450 MHz PC. This may be compared with 5 min for both pseudo-inversion and singular value rejection, 12 min for matrix perturbation and 23 min for Tikhonov regularization with BSCV. For this reason iterative inversion is not pursued further here.

CHAPTER 7
EXPERIMENTS ON HANGING PLATE

7.1 INTRODUCTION

In the preceding chapters various matrix regularization strategies have been investigated for improving inverse force determination and these have been tested using simulated 'measurement' data. The conclusions reached are dependent on the assumed noise model used in the numerical simulations. Ultimately the performance of the various techniques must also be confirmed by experimental validation. Experiments have therefore been carried out on a hanging rectangular flat steel plate for this purpose. The experimental set-up, measurements, data processing and the predictions based on the various techniques considered in this thesis are discussed in this chapter.

7.2 EXPERIMENTS ON PLATE

The experimental set-up used is shown in Figure 7.1. A rectangular plate (700×500×1.5 mm), made of steel, was hung from a frame using elastic cord. Additional damping was introduced by damping films glued to the back of the plate. Two electrodynamic shakers were used for excitation. These were fed with signals from the same signal generator and the amplitudes of the forces were varied by using the gain adjustment on the amplifier. The shakers were connected to the plate through force gauges, which were mounted on the plate in such a way that the mass loading is minimal.

Accelerometers and force gauges were mounted on cementing studs which were glued to the plate. This was done to ensure repeatability in the high frequency range by eliminating spatial deviations. The locations of the force gauges and accelerometers are shown in Figure 7.2. Three force positions are shown in the figure – F_1 and F_3 were driven by the two shakers while the force applied to F_2 was zero. This third force is thus included in the experiment but actually had zero amplitude in the operational response measurements. This was done to ensure that the problem is of sufficient size to provide realistic matrix condition numbers whilst remaining a practical measurement. Ten accelerometer positions were used, although not all of them were measured simultaneously. Four are omitted from Figure 7.2 as they have not been used in this chapter. Some positions are deliberately placed on lines of symmetry.

Figure 7.1. Experimental set-up for rectangular plate.

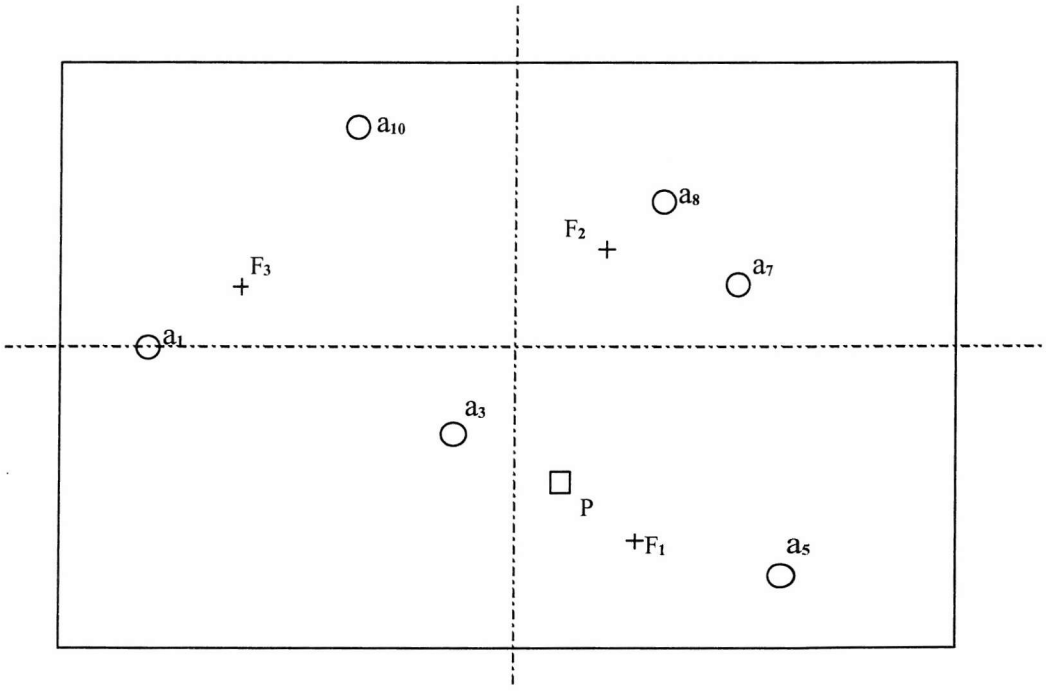

Figure 7.2. Locations of accelerometers (O), force gauges (+) and microphone (□) on rectangular plate. NB a_2, a_4, a_6 and a_9 are not used here (omitted from the figure).

The equipment used was as follows:

Accelerometers	Piezoelectric B&K type 4393 V (mass 2.4 g + 0.23 g for mounting stud)
Microphone	Condenser microphone B&K type 4191
Force gauges	PCB force gauges type 218C (mass 11.0 g + 1.48 g for mounting stud)
Charge amplifier	FLYDE type FE-128-CA 4 channel
Measuring amplifier	B&K type 2609
Preamplifier	B&K type 2669
Analyser	HP 3566A 8-channel data acquisition system

A frequency range of 30 to 1600 Hz is used in the analysis. Below 30 Hz the coherence was found to be very low and errors were large on FRF estimates. The high frequency limit corresponds to the frequency at which the modal overlap is large enough for individual modes to be indistiguishable. The frequency resolution was chosen as 1 Hz. Improvement in the coherence because of further refinement of the resolution was found to be small. If the resolution were insufficient, the coherence would be adversely affected by leakage. As the resolution is improved the length of window used in time domain increases, ensuring that the response within the window is caused primarily by excitation within the window.

7.3 MEASUREMENTS

All data were recorded as time histories at a sampling frequency of 4096 Hz using the in-built anti-aliasing filter of the analyser. Frequency analysis was performed using dedicated routines written in the Matlab environment.

7.3.1 Procedure

The measurements for transfer path analysis consist of two sets:

a. Operational response measurements

Operational responses were measured at locations 'a' on the plate when both shakers were in operation (this represents a situation where some machine is mounted on the plate). Two sets of measurements were made. Due to the availability of only 8

channels, 6 accelerations were measured along with the two forces in the first set. In a second set of measurements, one of the channels was used to measure the sound pressure near the rear surface of the plate (shown in Figure 7.3). Excitation was applied at force locations F_1 and F_3 and F_2 was zero. The two sets of measurements contained the following responses (the order is based on the channel number used for the respective locations)

I. $\mathbf{a_8}$, $\mathbf{a_{10}}$, $\mathbf{a_7}$, $\mathbf{a_1}$, $\mathbf{a_3}$, $\mathbf{a_5}$ and $\mathbf{F_1}$, $\mathbf{F_3}$

II. $\mathbf{p}$, $\mathbf{a_{10}}$, $\mathbf{a_7}$, $\mathbf{a_1}$, $\mathbf{a_3}$, $\mathbf{a_5}$ and $\mathbf{F_1}$, $\mathbf{F_3}$ - where **p** represents sound pressure.

NB: Positions $\mathbf{a_2}$, $\mathbf{a_4}$, $\mathbf{a_6}$,and $\mathbf{a_9}$ were not used.

a. Transfer function measurements

Frequency response functions from each of the three forcing locations F to response the locations a and p were measured, keeping one shaker operational and disconnecting the other shaker. All transducers were left screwed to the plate through cementing studs during these measurements.

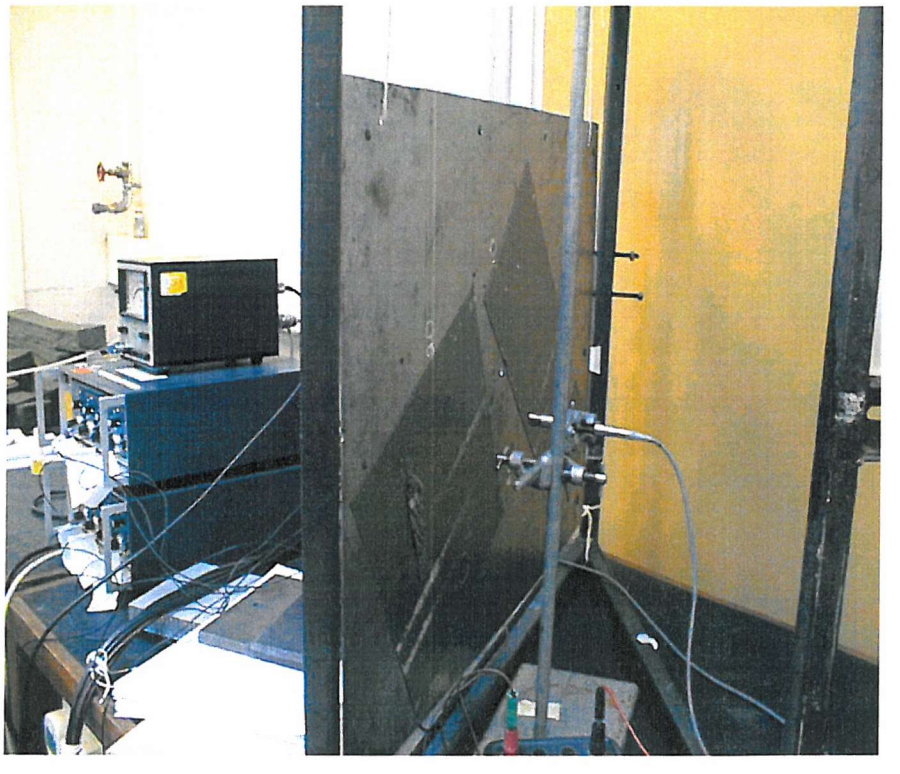

Figure 7.3. View showing microphone location.

7.1.1 Mass loading

An assessment is made of the mass loading effect of the accelerometers and force gauges. The frequency above which the mass of the accelerometer plays a significant

role is determined by equating the magnitude of the impedance of the mass with that of an infinite plate. The expression is derived as follows

$$m_{ad}\omega = 8\sqrt{\frac{E\rho h^4}{12(1-\nu^2)}} \tag{7.1}$$

where E is Young's modulus of the plate, ρ is the density, h is the thickness of the plate and ν is the Poisson's ratio, while m_{ad} is the added mass of the transducer. For $\nu = 0.3$, this reduces to

$$f_{crossover} = \frac{0.39h^2\sqrt{E\rho}}{m_{ad}} \tag{7.2}$$

For the structure under consideration, a 1.5mm thick steel plate, this frequency is 13300 Hz for the accelerometer mass of 2.63 g including the stud.

For the force gauge (mass 12.48 g) the cut off frequency is calculated as 2790 Hz. As the active mass is only 59% of this, the frequency increases to 4729 Hz. At 1600 Hz, error expected due to added mass is about 1.2 dB. Hence it is safe to consider that the frequency range 30 to 1600 Hz is not greatly influenced by mass loading.

7.3.3 Background noise

Noise levels in all the channels were measured when both shakers were switched off. Examples of frequency spectra for one force and one response channel along with noise levels are shown in Figures 7.4 and 7.5.

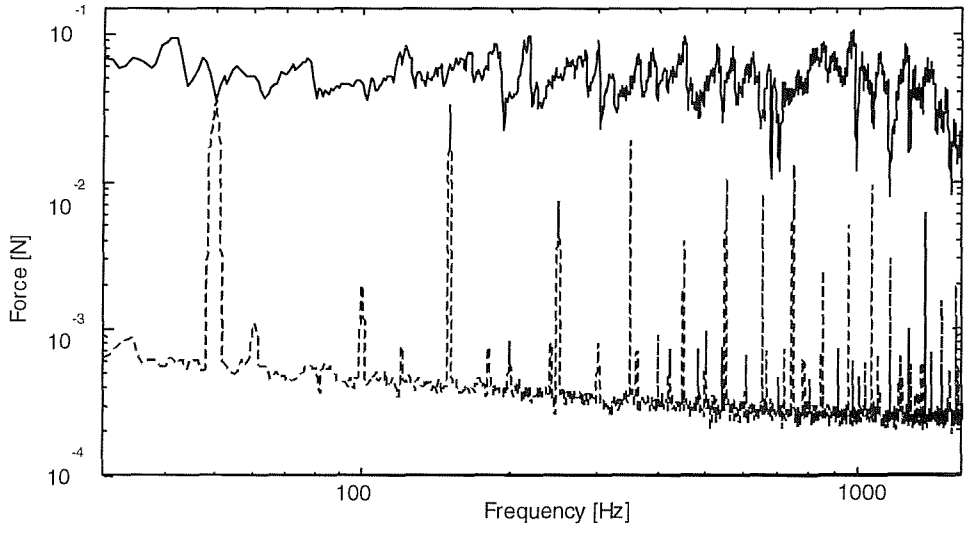

Figure 7.4. Force spectrum during operational measurements along with noise in channel (F_1). ———— measured force, – – – – – – noise.

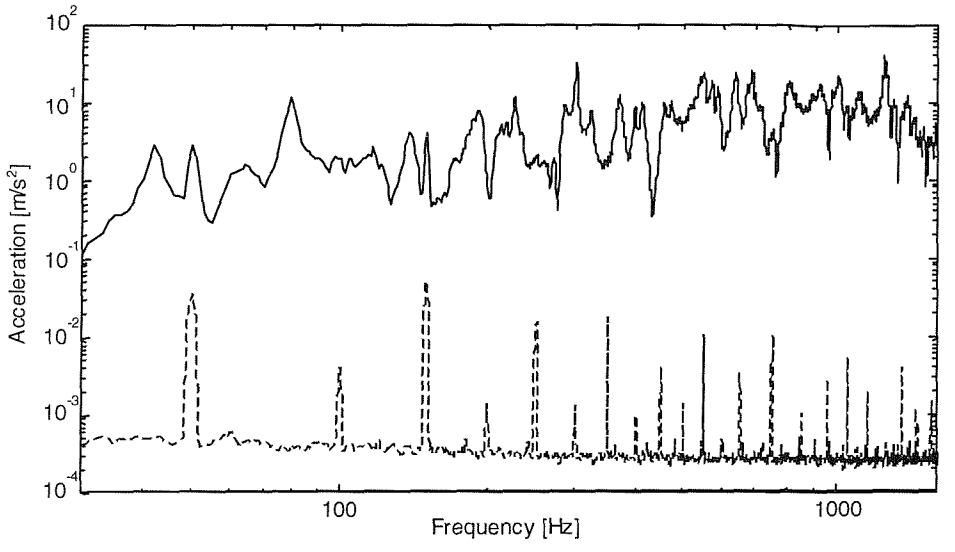

Figure 7.5. Example of acceleration spectrum during operational measurements along with noise in channel (a_1). ——————measured acceleration, – – – – – –noise.

The force measurement is found to be influenced by a significant amount of measurement noise (Figure 7.4) particularly at the mains related frequencies of 50, 150 and 350 Hz. This might create problems in comparing the reconstructed forces with the measured ones. However, the response signals are found to be well above the noise floor in most of the frequency range (Figure 7.5).

7.3.4 Analysis

All data were captured initially as time histories. The operational responses were estimated by taking the magnitude of the response as the square root of the auto spectrum and the phase from the cross spectrum between the response and a reference signal. One of the responses was taken as the reference signal (in this case response channel 6, which is position a_5). The expression for the response can thus be written as

$$a_i = \sqrt{S_{i,i}}\, e^{i\angle S_{i,n}} \tag{7.3}$$

where i is a response number and n is the reference response number. The magnitude of one of the responses calculated by this method is given in Figure 7.6. All the responses for the first set of measurements are shown in Figure 7.7 in one-third octave bands.

Based on the earlier study in Chapter 2, the H_1 estimator is used in calculating the frequency response functions between different forcing points and response points.

One of the frequency responses (accelerance) is given in Figure 7.8. From the figure, the first few modes are seen to have very high damping. The coherence is observed to be poor at low frequencies and at 50, 150 and 250 Hz. Above 300 Hz it is mostly good.

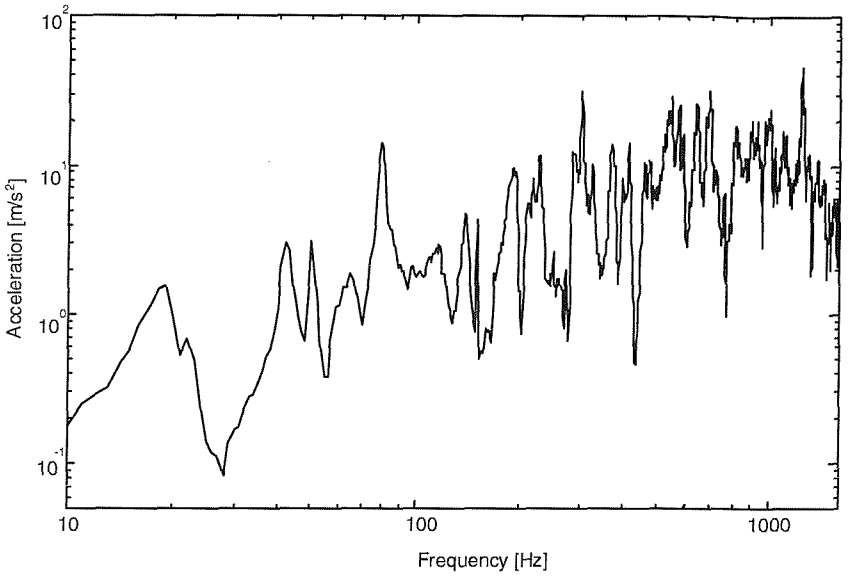

Figure 7.6. Operational acceleration spectrum at location a_8 for first set of measurements

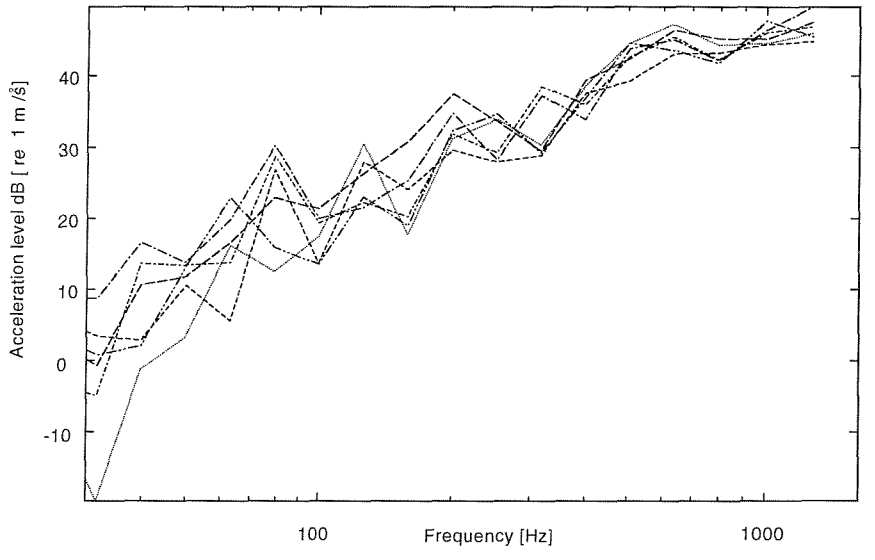

Figure 7.7. Measured acceleration responses in one-third octave bands - first set of measurements

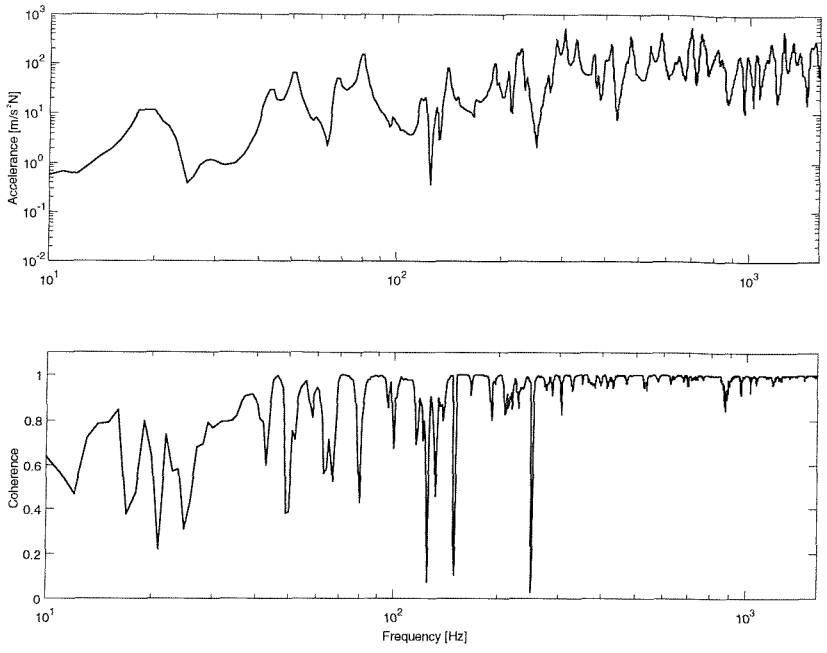

Figure 7.8. Magnitude of accelerance from force location 1 to response location 8 and associated coherence

Modal damping ratios have been calculated from the measured FRF's using the half power bandwidth for the first few modes and are shown in Figure 7.9. The modal damping ratio is found to decrease from 0.08 to around 0.01 as the frequency increases. These may be compared with the value of 0.015 (loss factor 0.03) used throughout in the simulations. At higher frequencies it was not possible to extract reliable damping values using this method.

7.3.5 Checking of data

The consistency of the measurements can be established by reconstructing the response in a direct way, which is possible here since the forces were also measured. Therefore the following expression is used in calculating the operational response, which is then compared with the measured response

$$a_i^r = \sum_{j=1}^{3} \hat{A}_{ij} F_j \tag{7.4}$$

where a_i^r is a directly reconstructed i^{th} response, $\hat{A}_{ij}$ is the measured accelerance and F_j is the measured force.

The directly reconstructed response and the measured response for location a_8 in the first set of measurements is given Figure 7.10. The direct reconstruction of the response agrees very well with the measured one although some minor differences can be seen, particularly in the high frequency region. The differences between directly reconstructed and measured responses at all locations are shown in Figure 7.11 in 1/3 octave form. The variations in direct reconstruction are found to average out when converted into 1/3 octave band representation, so that rms dB difference averaged over all bands and measurement locations is 1.2 dB. This is considered acceptable.

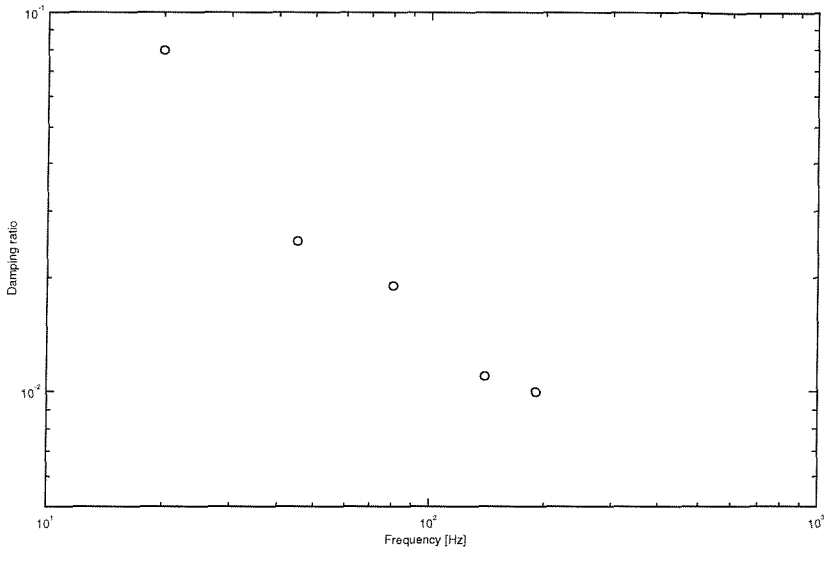

Figure 7.9. Measured modal damping ratio for first few modes.

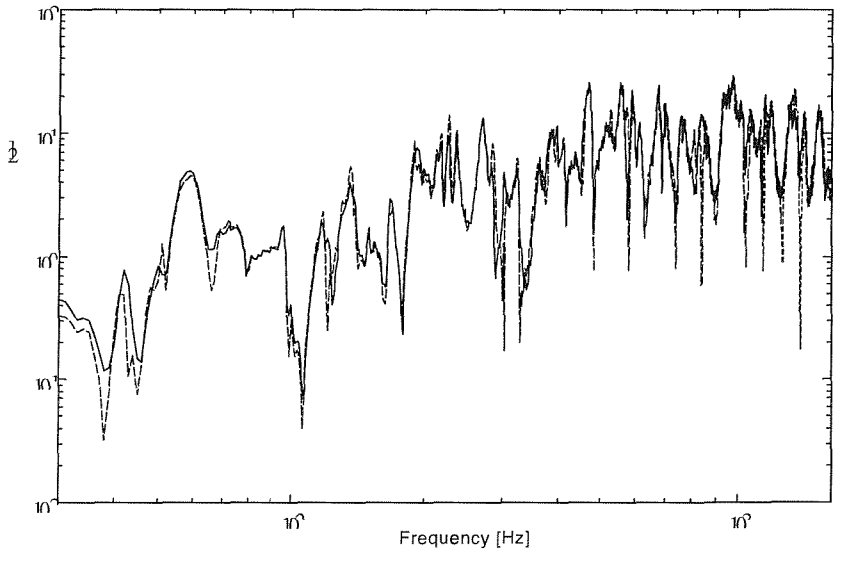

Figure 7.10. Acceleration response a_8 measured and directly reconstructed. ——— measured acceleration, – – – – – directly reconstructed.

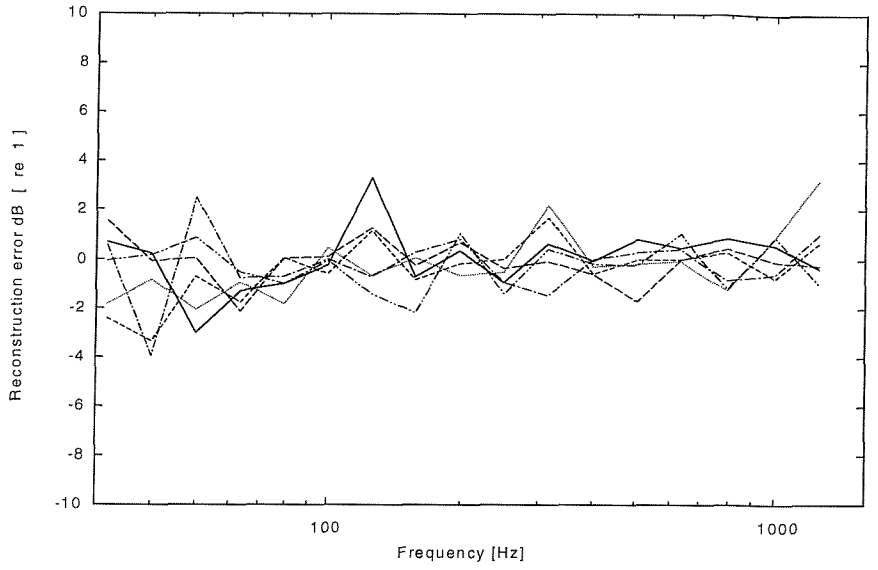

Figure 7.11. 1/3 octave acceleration response difference between measured and directly reconstructed.

The measured forces are shown in Figure 7.12a in 1/3 octave bands. One of the forces was deliberately always larger than the other one by an average of 3.5 dB. The coherence between these two forces is shown in Figure 7.12b. In most of the frequency region the forces are found to be reasonably well correlated ($\gamma^2 > 0.9$), although there are dips at some particular frequencies and the coherence falls somewhat at low frequencies.

7.4 EXPERIMENTAL VALIDATION OF INVERSE METHODS

7.4.1 Selection of combinations of positions

In order to validate the theoretical concepts developed in earlier chapters, one of the response points is chosen as the 'receiver' location and the others are used for force determination. Throughout this section, 4 responses are used to reconstruct 3 forces. In general it is found that the quality of the inversion obtained from the measured data presented here is much greater than in the numerical simulations. This is due to the fact that the noise in the measurement data is much lower than that assumed in the rather extreme noise model in the simulations. Also, the condition numbers encountered in the measured problem are small. The condition numbers for one of combinations, which is evaluated later, are shown in Figure 7.13.

a)

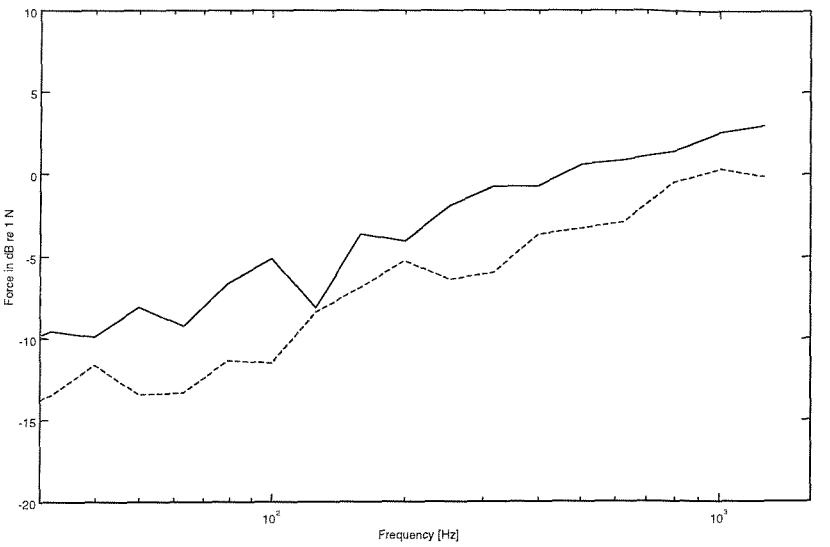

b)

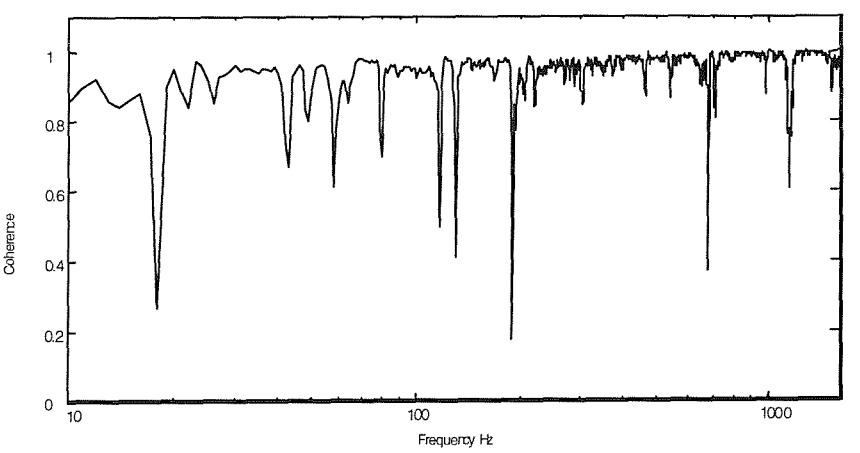

Figure 7.12. (a) 1/3 octave measured forces _____ F_3, _ _ _ _ _ _ F_1 (b) Coherence between force F_1 and force F_3.

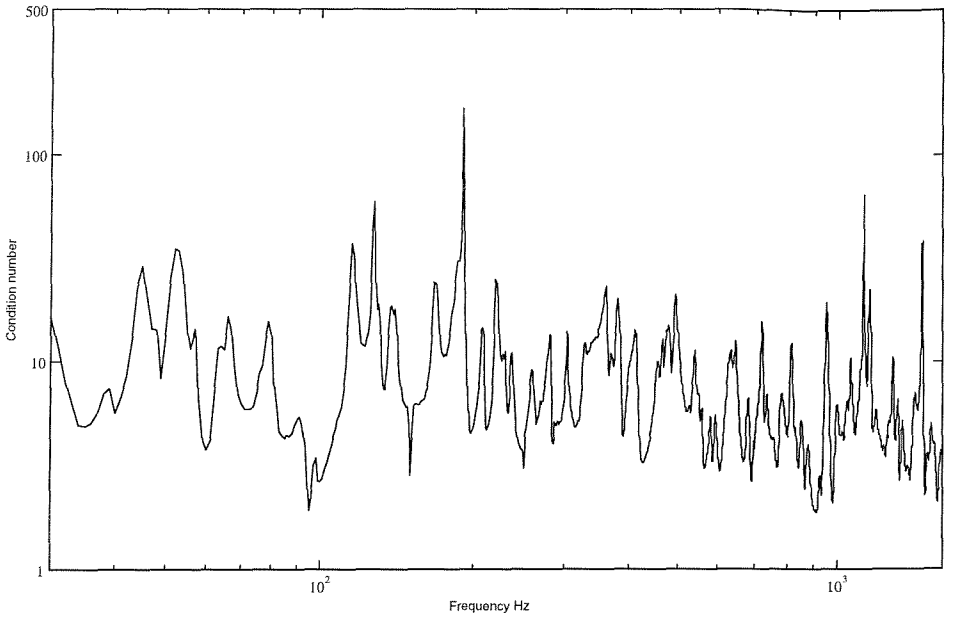

Figure 7.13. Condition numbers for the combination $a_7a_3a_5a_8$

There are many possible combinations of response points that could be used. In order to discriminate more readily between the various inversion methods, combinations that give a *poor* prediction using Moore-Penrose pseudo-inversion have been selected. To select the combinations of response points, the reconstruction errors were evaluated using the Moore-Penrose pseudo-inversion for all combinations.

The root mean square errors over all 1/3 octave bands for the first set of measurements are shown in Table 7.1 for 10 combinations of response points. The first column shows the 4 responses used for the force determination and the second column shows the response that is predicted. For example, in the first case the positions 8, 10, 7 and 1 are used for force determination and the response at location 3 is predicted. The error in the predicted response and the errors in the contributions from each of the forces are shown in the table. The contributions to the response are formed from the reconstructed forces and the corresponding accelerances. The errors in force contributions 1 and 3 are obtained by comparing the results with those calculated using the measured forces and the accelerances. The contribution from force 2 should be zero, so its predicted contribution is compared instead with the total response. This number should therefore be as *large* as possible for a good prediction, whereas the others should be as *small* as possible.

It is found in this table that, due to the 1/3 octave band conversions, the variations in narrow band results are found to be largely averaged out. The differences between the different combinations are consequently found to be minimal. It is interesting to note that when a_8 (close to F_2) is used for the receiver location, the 'error' in the force 2 contribution is very large (i.e. the contribution of F_2 is small compared to the total response) whereas when a_8 is used in the inversion the results for F_2 are less good and when a_8 is not used at all they are slightly worse again.

To give more emphasis to the errors found in narrow bands, two other representations are also investigated: 1/12 octave bands and bands with a constant 15 Hz bandwidth. Examples of the results for these are given in Tables 7.2 and 7.3.

Table 7.1. Average errors in contributions from each of the forces and the overall response in dB 1/3 octave bands (first set of measurements)

Responses in inversion	**Receiver location**	**Error in force 1 contribution**	**Error in force 2 contribution**	**Error in force 3 contribution**	**Overall error**
$a_8a_{10}a_7a_1$	a_3	1.5	22.9	1.5	***1.6***
$a_8a_{10}a_7a_3$	a_1	1.4	25.7	1.3	***1.9***
$a_8a_{10}a_1a_3$	a_7	1.4	22.2	1.2	***1.9***
$a_8a_7a_1a_3$	a_{10}	1.7	22.4	1.3	***1.6***
$a_{10}a_7a_1a_3$	a_8	1.6	80.2	1.5	***1.5***
$a_{10}a_7a_1a_3$	a_5	1.5	19.9	1.3	***1.2***
$a_{10}a_7a_1a_5$	a_3	1.6	20.6	1.4	***1.4***
$a_{10}a_7a_3a_5$	a_1	1.6	21.0	1.2	***1.7***
$a_{10}a_1a_3a_5$	a_7	1.5	20.6	1.3	***1.9***
$a_7a_1a_3a_5$	a_{10}	1.8	17.6	1.4	***1.5***

Table 7.2. Average errors in 1/12 octave representation in dB.

(first set of measurements)

Responses in inversion	Receiver location	Error in force 1 contribution	Error in force 2 contribution	Error in force 3 contribution	Overall error
$a_8a_{10}a_7a_1$	a_3	2.1	24.9	1.8	***2.2***
$a_8a_{10}a_7a_3$	a_1	2.2	26.9	1.5	***2.3***
$a_8a_{10}a_1a_3$	a_7	2.2	23.6	1.6	***2.6***
$a_8a_7a_1a_3$	a_{10}	2.5	25.2	1.6	***2.2***
$a_{10}a_7a_1a_3$	a_8	2.3	83.5	1.7	***1.8***
$a_{10}a_7a_1a_3$	a_5	1.5	25.8	2.0	***1.8***
$a_{10}a_7a_1a_5$	a_3	1.6	23.2	2.2	***2.2***
$a_{10}a_7a_3a_5$	a_1	1.6	24.7	2.0	***2.2***
$a_{10}a_1a_3a_5$	a_7	1.5	21.2	2.1	***2.3***
$a_7a_1a_3a_5$	a_{10}	1.8	23.4	2.1	***2.0***
$a_7a_3a_5a_8$	a_1	1.6	26.9	2.3	***2.0***

Table 7.3. Average errors in constant 15 Hz band representation in dB.

(first set of measurements)

Responses in inversion	Receiver location	Error in force 1 contribution	Error in force 2 contribution	Error in force 3 contribution	Overall
$a_8a_{10}a_7a_1$	a_3	2.4	22.3	2.0	***1.9***
$a_8a_{10}a_7a_3$	a_1	2.8	21.7	2.0	***2.8***
$a_8a_{10}a_1a_3$	a_7	2.8	23.3	1.8	***3.0***
$a_8a_7a_1a_3$	a_{10}	2.4	22.1	2.2	***2.3***
$a_{10}a_7a_1a_3$	a_8	2.5	78.0	1.9	***2.0***
$a_{10}a_7a_1a_3$	a_5	2.4	19.7	1.9	***2.4***
$a_{10}a_7a_1a_5$	a_3	2.2	21.7	1.8	***2.3***
$a_{10}a_7a_3a_5$	a_1	2.2	20.5	1.7	***2.6***
$a_{10}a_1a_3a_5$	a_7	2.2	21.0	1.7	***2.7***
$a_7a_1a_3a_5$	a_{10}	2.4	20.5	1.7	***2.2***
$a_7a_3a_5a_8$	a_1	2.9	22.0	2.0	***3.0***

The representations in 1/12 octave bands and constant bandwidth bands are found to show the errors more distinctly than those in 1/3 octave bands, although the results are still remarkably consistent. In the 1/12 octave band representation, as with 1/3 octave bands, the bandwidths are greater at higher frequencies. This means that the errors at each frequency are effectively weighted differently. Since this weighting matches the human perception of sound, when predicting the sound pressure at the receiver location, the 1/12 octave band representation has been implemented. However, when predicting the vibration response, or if only the force determination is of significance, then the errors are given equal weighting in each of the bands. This can be achieved by the constant bandwidth representation. Accordingly in this study both representations are followed in estimating the errors. Out of all the combinations from constant bandwidth representation, as the vibration response is to be predicted, one is selected from the first set of measurements (errors for all combinations are given in [80]) to investigate the techniques described in earlier chapters. The combination used is $a_7a_3a_5a_8$ with a_1 as receiver location. This combination has poor force determination, and high overall response error, as shown in Table 7.3.

To investigate the techniques in relation to the sound pressure prediction, the second set of measurements is used. The errors in predictions for all five combinations are shown in Table 7.4 (the sound pressure response is predicted in all cases). From the table, one combination is chosen for further investigation. This combination is $a_1a_3a_5a_{10}$ with a_p as receiver location. This has been chosen since force 2 is not well predicted in this case and overall response error is similar to cases 1 and 5, which have poor force estimations as well.

Table 7.4. Average errors in 1/12 octave band representation in dB.

(second set of measurements)

Responses in inversion	**Receiver location**	**Error in force 1 contribution**	**Error in force 2 contribution**	**Error in force 3 contribution**	**Overall**
$a_{10}a_7a_1a_3$	a_p	2.9	21.6	2.4	***3.1***
$a_7a_1a_3a_5$	a_p	2.3	20.6	2.1	***2.8***
$a_1a_3a_5a_{10}$	a_p	2.3	19.6	2.0	***3.0***
$a_3a_5a_{10}a_7$	a_p	2.3	20.6	2.1	***2.9***
$a_5a_{10}a_7a_1$	a_p	2.6	21.3	2.4	***3.2***

7.4.2 Techniques used for inversion

Of the combinations selected from the two sets of measurements, the forces are reconstructed and the 'receiver' responses predicted using the following techniques:

- Moore-Penrose pseudo-inversion (Chapter 2)
- Singular value rejection (Chapter 3) based on threshold selected by

  Error in accelerance measurement

  Error in response measurement
- Perturbation of accelerance matrix (Chapter 4)
- Tikhonov regularization with ordinary cross validation (Chapter 5)
- Tikhonov regularization with biased selective cross validation (Chapter 5)
- Iterative inversion based on single response cross validation approach (Chapter 6)

The method of perturbed singular value rejection has been not considered here. The reason for this will become clearer later in the chapter.

The problem to be solved is the inversion of a 4×3 matrix. In Tikhonov regularization and iterative inversion with single response cross validation, however, a 3×3 inversion is initially performed with the fourth position used for cross validation to find the amount of regularization. Then the 4×3 problem is solved.

7.4.3 Vibration response prediction

All seven techniques listed above have been used in force determination and response prediction for the combinations of response positions mentioned earlier. The results are tabulated in Table 7.5. From the table it can be seen that the iterative inversion method combined with single response cross validation results in better overall *response* predictions than all other techniques. Tikhonov regularization and the perturbation technique give predictions that are better than or the same as Moore-Penrose pseudo-inversion. The technique based on singular value rejection is found to give marginally worse predictions than Moore-Penrose pseudo-inversion.

In *force determination*, Tikhonov regularization, iterative inversion and the perturbation technique are found to be consistently better than any other techniques. To illustrate the results, the graphical results for the combination considered are also given for all seven cases. These are discussed below.

Table 7.5 Root mean square errors in dB over 15 Hz bands from all the techniques for predicting a_1 from a_7 a_3 a_5 and a_8

	Force errors			*Overall response error*	Response contribution errors		
Method	F 1	F 2	F 3		FC 1	FC 2	FC 3
Moore-Penrose	2.9	28.4	1.9	***3.0***	2.9	22.0	2.0
Sv rej (accelerance)	2.9	28.1	2.0	***3.0***	3.1	21.5	2.0
Sv rej (response)	3.0	24.5	3.7	***3.6***	3.3	17.3	3.8
Perturbation	2.8	25.5	1.5	***2.8***	2.9	20.2	1.6
Tikhonov -OCV	2.6	26.6	1.4	***2.6***	2.6	21.3	1.5
Tikhonov -BSCV	2.6	25.5	1.9	***2.4***	2.7	19.2	1.9
Iterative - SRCV	2.5	24.6	1.8	***2.3***	2.5	18.4	1.9

(F1, F3, FC1 and FC3 should be small, F2 and FC2 should be large for a good reconstruction)

Figure 7.14 shows force 1 as reconstructed by the seven different methods, along with the measured force. The result for Moore-Penrose pseudo-inversion contains considerable errors in most of the frequency range considered (Figure 7.14a). The result improves considerably in the low frequencies when the accelerance matrix is perturbed (Figure 7.14b). When singular values are rejected based on accelerance errors (Figure 7.14c), the result is very similar to pseudo-inversion. This is because the accelerance errors are small in the measurements so few singular values are rejected. The numbers of singular values used in the inversion for the threshold based on the accelerance error are shown in Figure 7.15a. On the other hand when singular values are rejected based on response errors, force 1 is under-estimated over most of the frequency range (Figure 7.14d). The numbers of singular values used in this case are shown in Figure 7.15b. More are rejected than using FRF errors to set the threshold. Some improvements are observed when either iterative inversion or Tikhonov regularization with OCV are used (Figures 7.14e-g). Tikhonov regularization is found to be marginally better in the low frequency region and iterative inversion in the high frequency region.

The corresponding results for force 2 and force 3 are shown in Figures 7.16 and 7.17. Since force 2 is actually zero, the calculated force itself is the error. From the graphical representation, it is very difficult to arrive at any conclusion for this force as all results are similar. Force 3 is the largest force applied to the structure, so consequently it is reconstructed much better than forces 1 and 2. The relative performance of the different methods remains the same as for force 1.

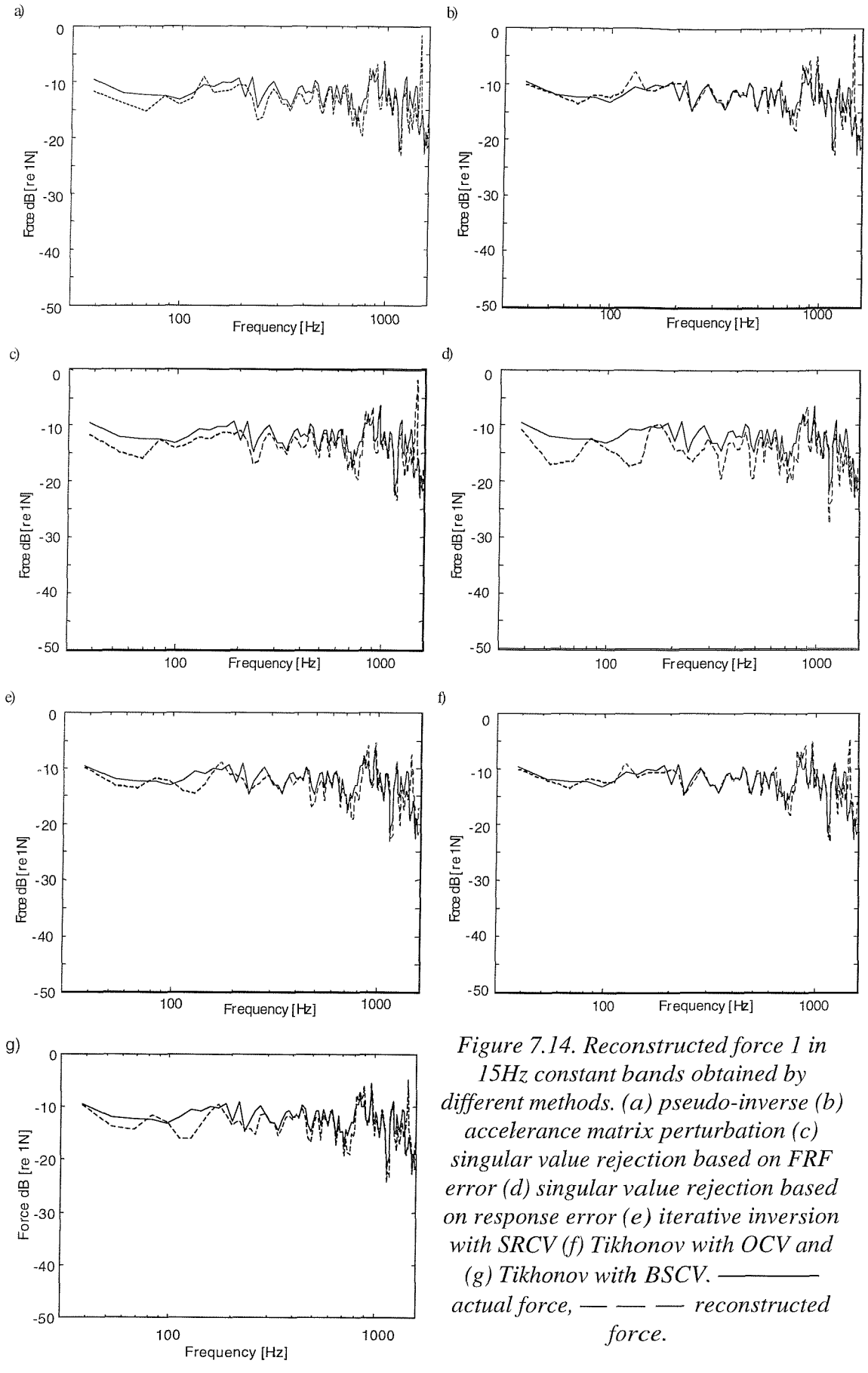

Figure 7.14. Reconstructed force 1 in 15Hz constant bands obtained by different methods. (a) pseudo-inverse (b) accelerance matrix perturbation (c) singular value rejection based on FRF error (d) singular value rejection based on response error (e) iterative inversion with SRCV (f) Tikhonov with OCV and (g) Tikhonov with BSCV. ——— actual force, — — — reconstructed force.

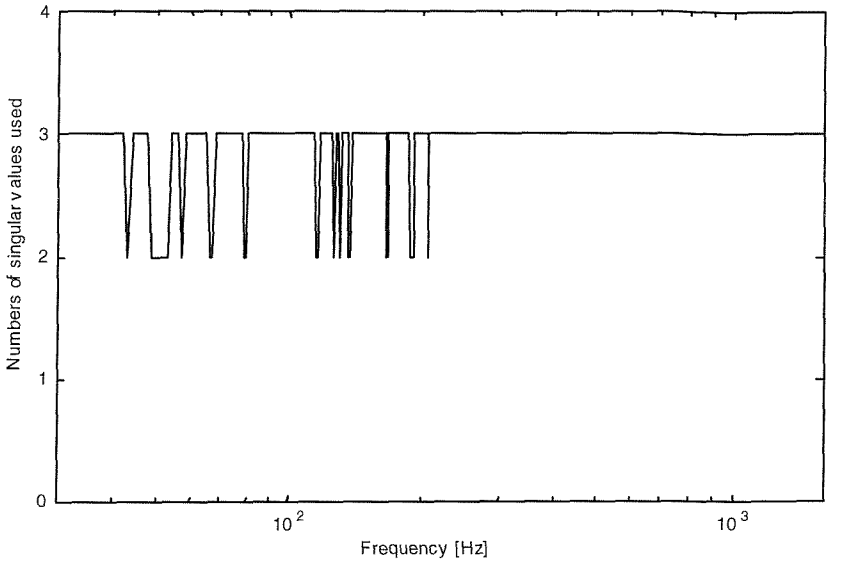

a. Using threshold based on FRF error.

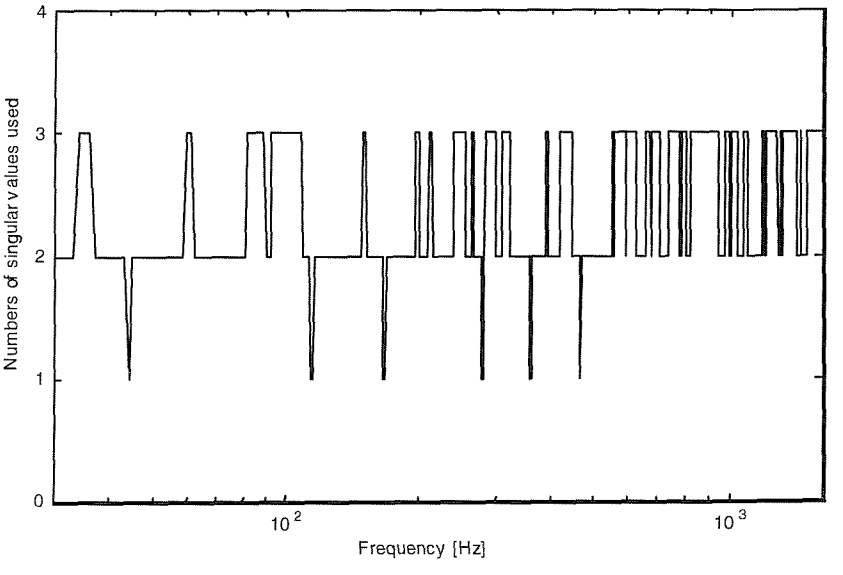

b. Using threshold based on response error.

Figure 7.15. Numbers of singular values used in the inversion.

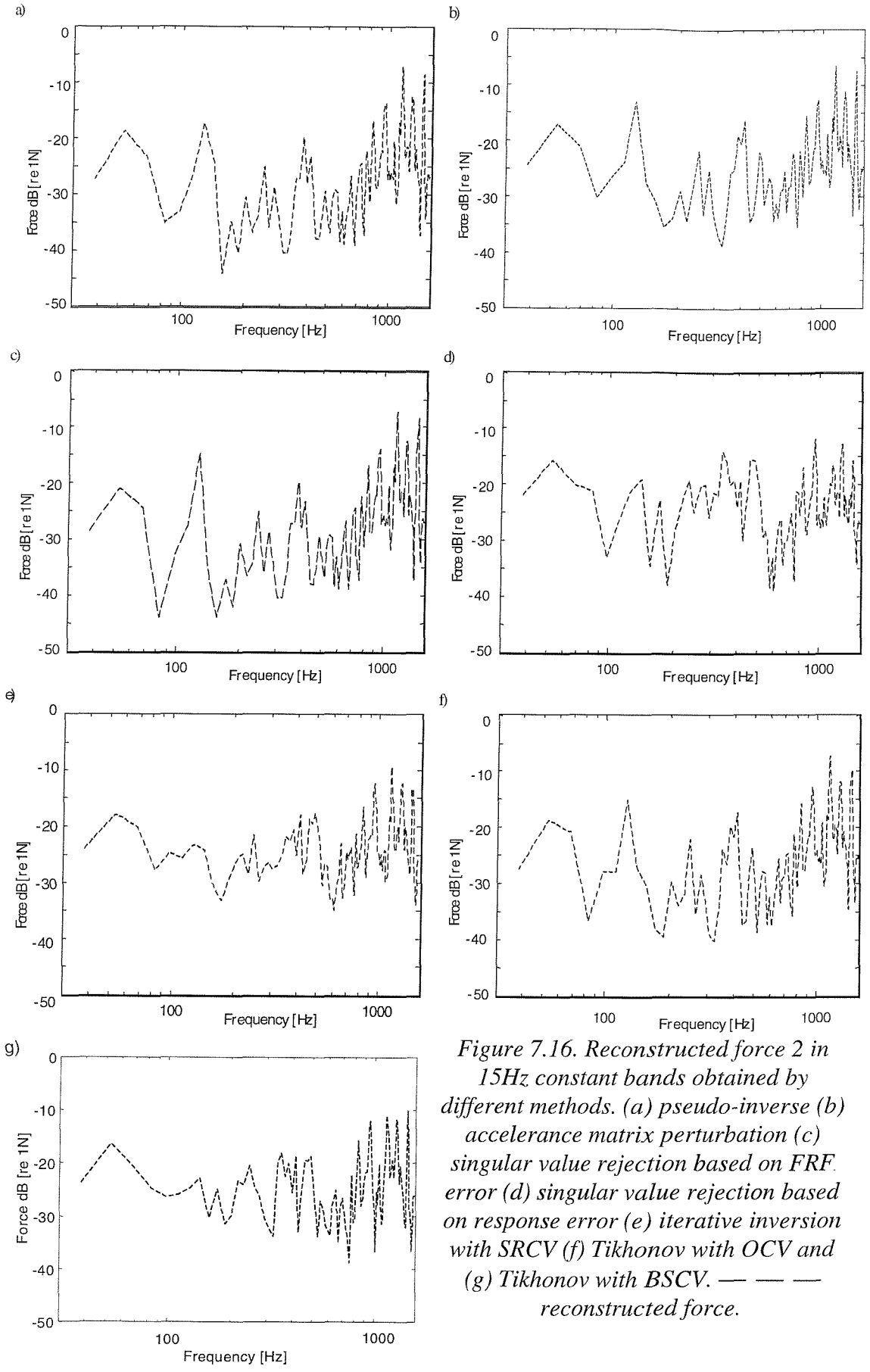

Figure 7.16. Reconstructed force 2 in 15Hz constant bands obtained by different methods. (a) pseudo-inverse (b) accelerance matrix perturbation (c) singular value rejection based on FRF error (d) singular value rejection based on response error (e) iterative inversion with SRCV (f) Tikhonov with OCV and (g) Tikhonov with BSCV. — — — reconstructed force.

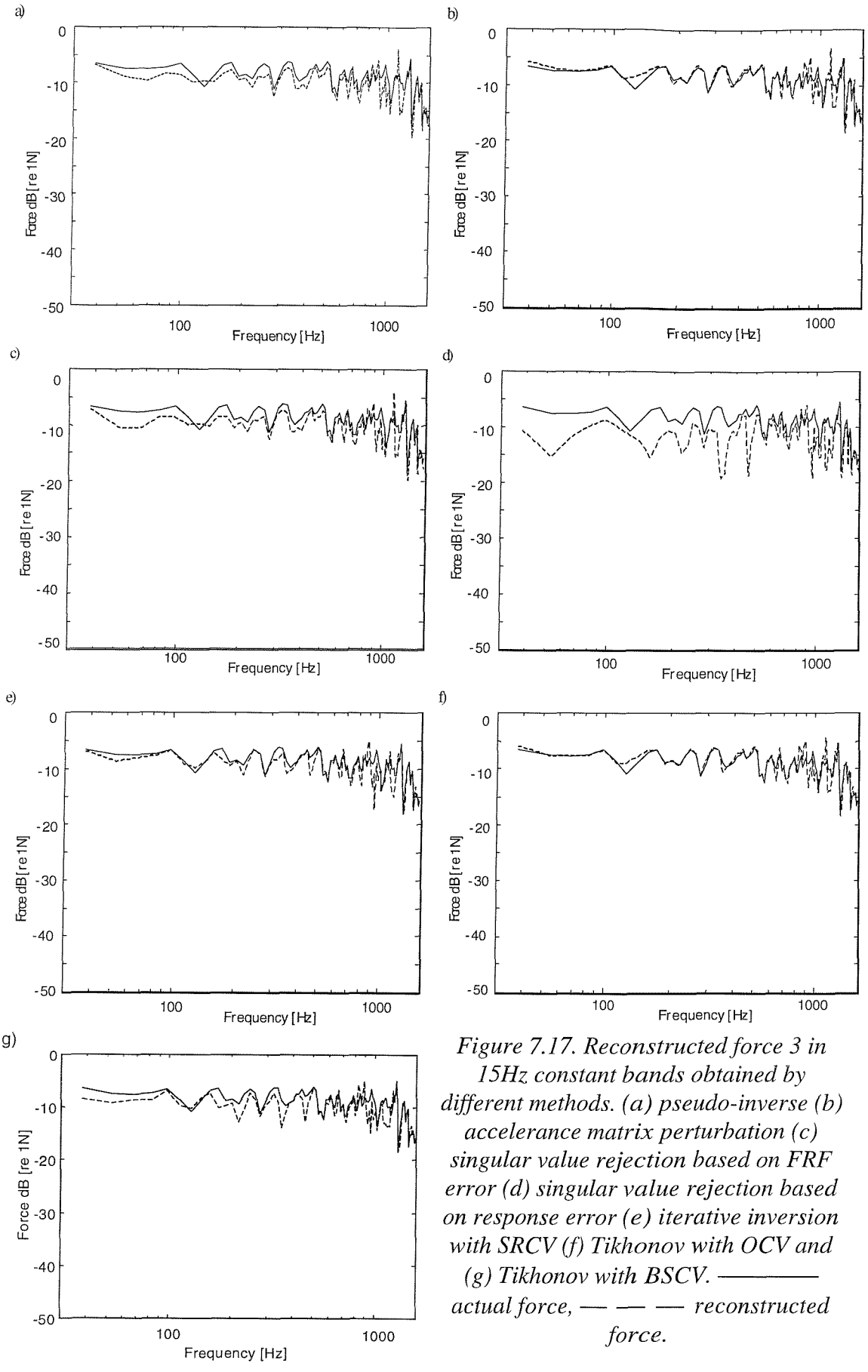

Figure 7.17. Reconstructed force 3 in 15Hz constant bands obtained by different methods. (a) pseudo-inverse (b) accelerance matrix perturbation (c) singular value rejection based on FRF error (d) singular value rejection based on response error (e) iterative inversion with SRCV (f) Tikhonov with OCV and (g) Tikhonov with BSCV. ———— actual force, — — — reconstructed force.

The overall velocity response predictions from different methods are shown in Figures 7.18-7.24. For the pseudo-inversion (Figure 7.18), the response is slightly under-predicted in the low frequency region and over-predicted in the high frequency region. The low frequency performance improves considerably when accelerance perturbation is used (Figure 7.19). When singular values are rejected based on the accelerance error (Figure 7.20) the velocity prediction does not differ much from that using the pseudo-inverse. This was expected since the force reconstructions did not differ due to the retention of most singular values (Figure 7.15). The velocity at the receiver location is under-estimated at most of the frequencies when singular values are rejected based on response error (Figure 7.21) and this under-estimation is greater than for pseudo-inversion particularly at low frequencies. However, most of the peaks are reasonably well estimated by this method. It seems to eliminate erratic behaviour in the high frequency region, suggesting a large influence of response errors in this region. Due to the improvements in force contributions for Tikhonov regularization and iterative inversion the overall response is predicted more reliably than with the earlier methods (Figures 7.22-24). Iterative inversion and Tikhonov regularization with BSCV give better results in the high frequency region compared to other methods.

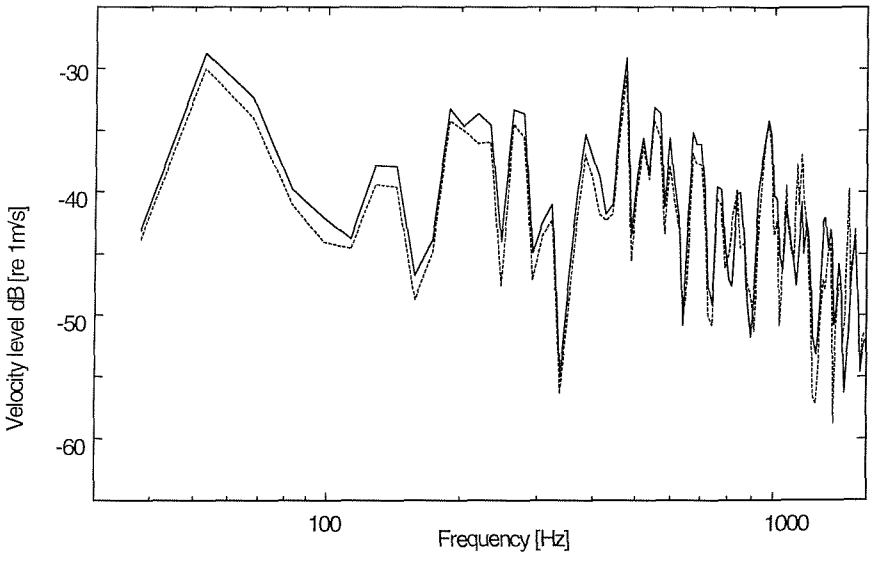

Figure 7.18. Reconstructed velocity response at the receiver location represented in 15Hz constant bands obtained using pseudo-inverse. ———— measured response, — — — reconstructed response.

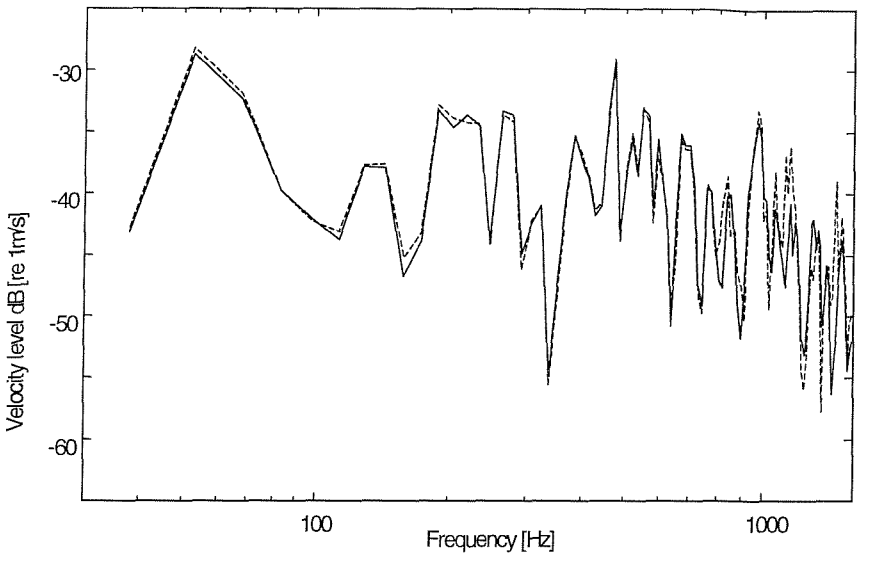

Figure 7.19. Reconstructed velocity response at the receiver location represented in 15Hz constant bands obtained using accelerance matrix perturbation. ———— measured response, — — — reconstructed response.

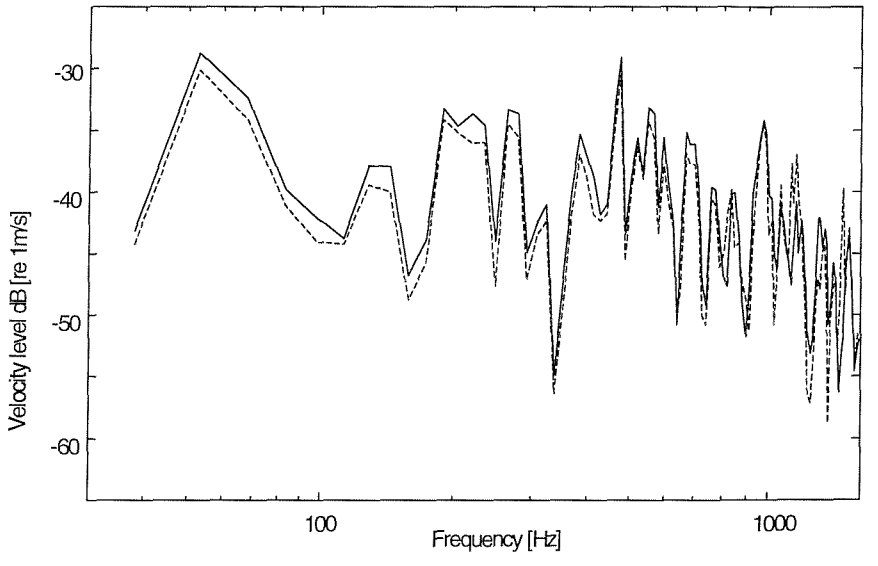

Figure 7.20. Reconstructed velocity response at the receiver location represented in 15Hz constant bands obtained using singular value rejection based on accelerance error. ————measured response, — — — reconstructed response.

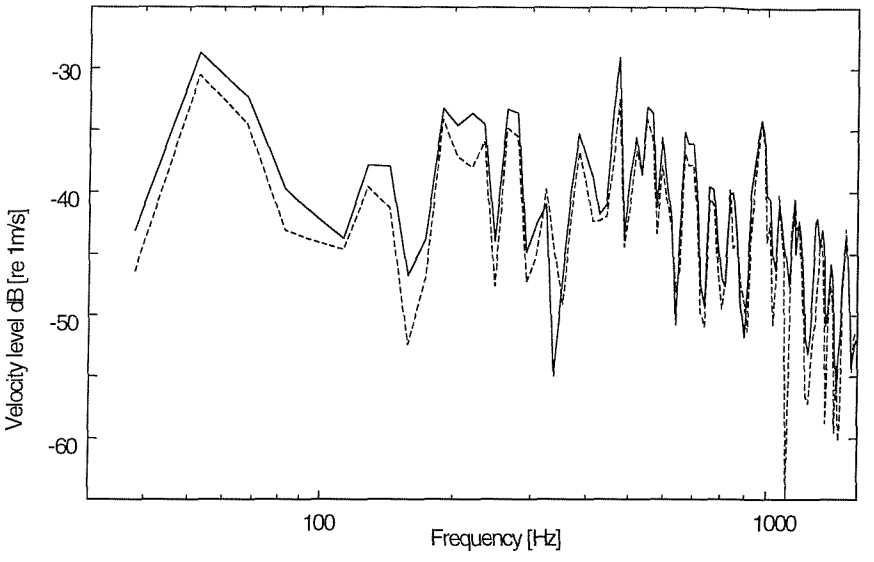

Figure 7.21. Reconstructed velocity response at the receiver location represented in 15Hz constant bands obtained using singular value rejection based on response error.

———— measured response, — — — reconstructed response.

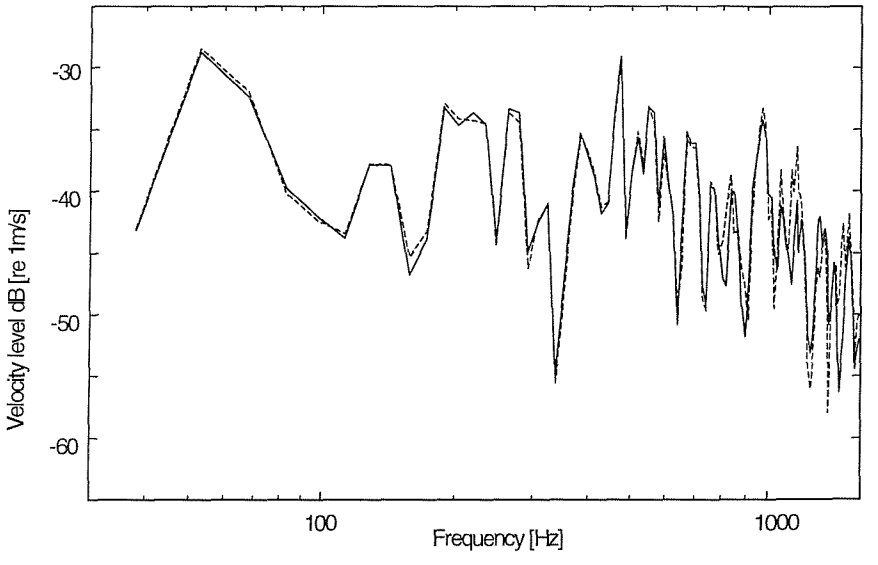

Figure 7.22. Reconstructed velocity response at the receiver location represented in 15Hz constant bands obtained using Tikhonov regularization along with OCV.

———— measured response, — — — reconstructed response.

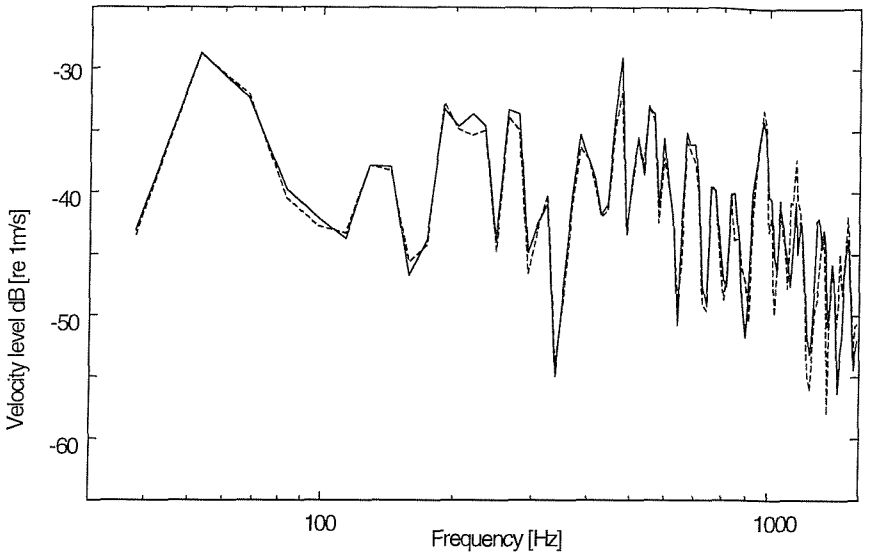

Figure 7.23. Reconstructed velocity response at the receiver location represented in 15Hz constant bands obtained using iterative inversion with single response cross validation. ———— measured response, — — — reconstructed response.

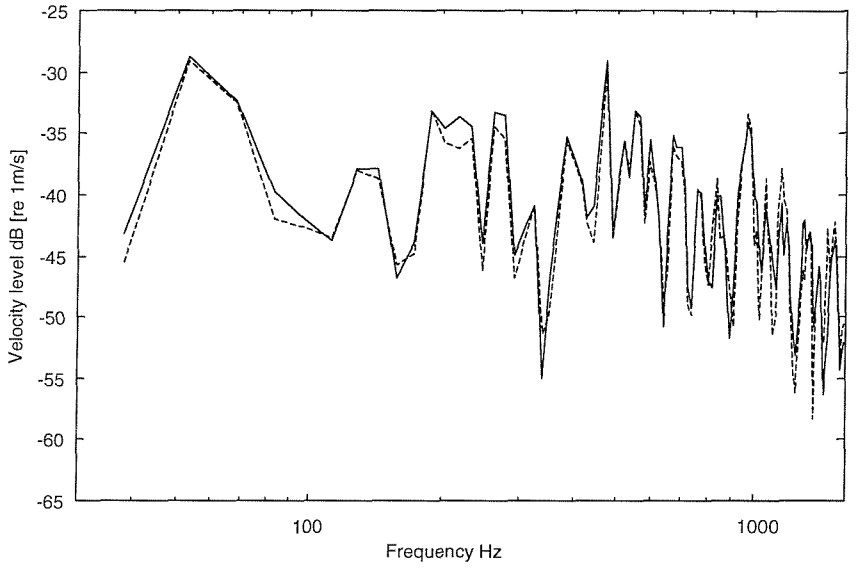

Figure 7.24. Reconstructed velocity response at the receiver location represented in 15Hz constant bands obtained using Tikhonov regularization along with BSCV. ———— measured response, — — — reconstructed response.

7.4.4 Sound pressure prediction

For the second set of measurements, the errors estimated for all the techniques used are shown in Table 7.6. Here 1/12 octave bands are used. As in the first set of measurements, iterative inversion is found to give the most consistent results in response

predictions. This is closely followed by Tikhonov regularization with OCV and accelerance matrix perturbation. However, the forces themselves are better predicted by Tikhonov regularization. Tikhonov regularization with BSCV appears to under-estimate forces at some frequencies. Since the measurement errors are very small, it is difficult to make thorough comparisons.

Graphical results (1/12 octave band sound pressure response) are given to demonstrate the effects of different methods in Figures 7.25-31. In all the cases at 150 Hz there is a sharp rise in the deviation. This is because the coherence is very low at this frequency (due to electrical noise) and the response is affected by noise as well (see Figures 7.5 and 7.8). Singular value rejection methods give the best result at this frequency, with iterative inversion the next best (Figure 7.27-28 and 7.29). Overall sound pressure prediction errors are smallest using iterative inversion with single response cross validation, Tikhonov regularization with ordinary cross validation and accelerance matrix perturbation.

Table 7.6. Root mean square errors in dB averaged over all 1/12 octave bands from all the techniques for predicting a_p from a_1 a_3 a_5 and a_{10}

	Force errors			***Overall response error***	**Response contribution errors**		
Method	F 1	F 2	F 3		FC 1	FC 2	FC 3
Moore-Penrose	2.3	29.1	2.0	***3.0***	2.3	19.6	2.0
Perturbation	1.6	27.0	1.2	***2.3***	1.7	19.1	1.3
Sv rej (accelerance)	2.8	28.9	2.3	***3.1***	2.9	19.3	2.7
Sv rej (response)	4.5	27.2	4.7	***3.8***	4.9	17.1	5.4
Tikhonov -OCV	1.7	28.3	1.0	***2.4***	1.8	20.1	1.2
Tikhonov -BSCV	3.2	28.0	2.4	***2.7***	3.6	19	2.8
Iterative - SRCV	1.8	27.7	1.8	***2.2***	1.9	19.6	2.0

(F1, F3, FC1 and FC3 should be small, F2 and FC2 should be large for a good reconstruction)

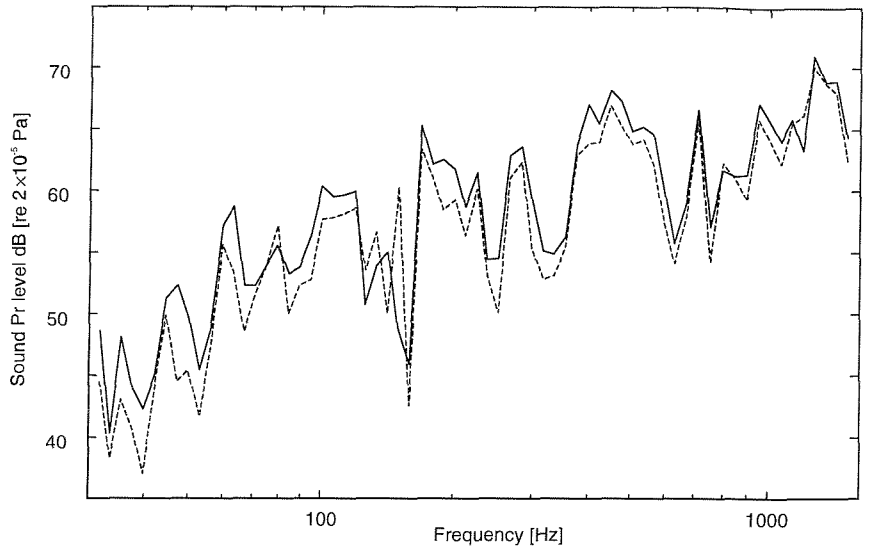

Figure 7.25. Overall sound pressure response in 1/12 octave bands obtained by Moore-Penrose pseudo inversion. ———— measured response, — — — reconstructed response.

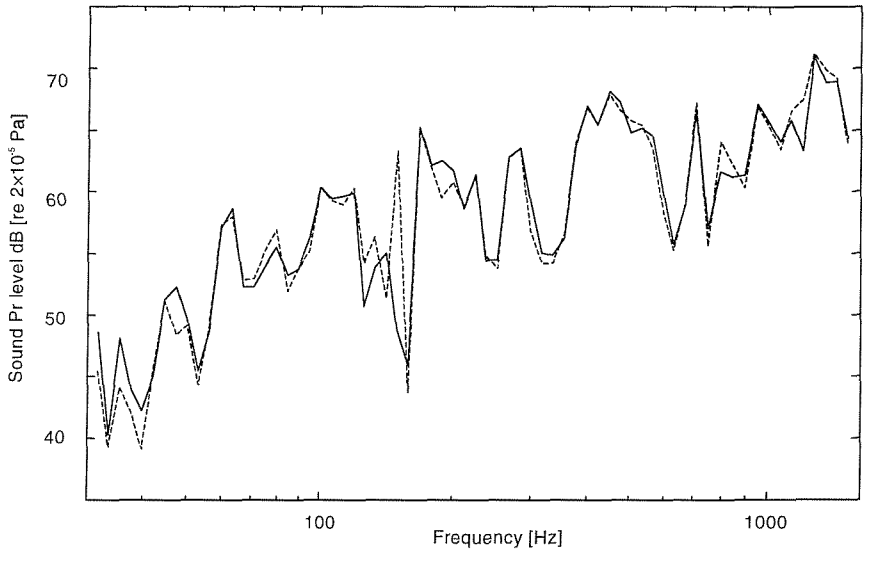

Figure 7.26. Overall sound pressure response in 1/12 octave bands obtained by accelerance matrix perturbation. ———— measured response, — — — reconstructed response.

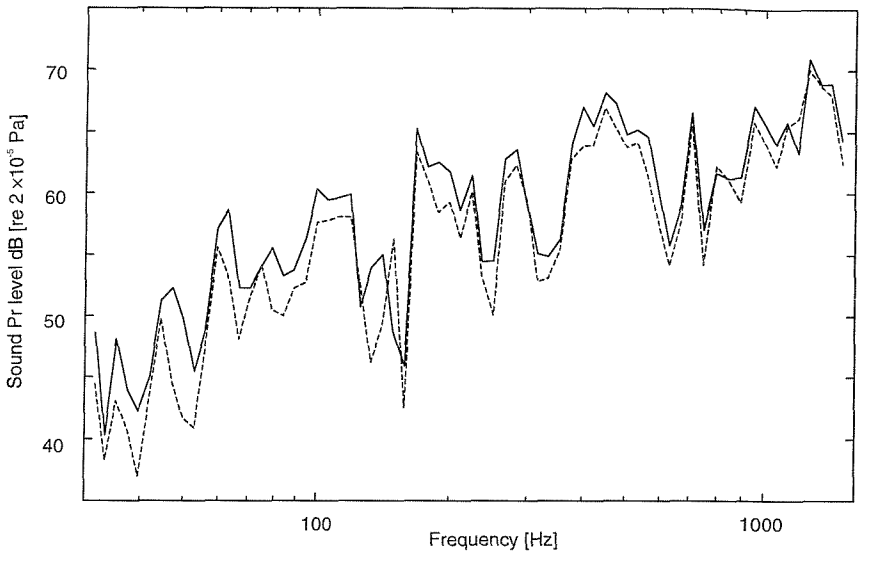

Figure 7.27. Overall sound pressure response in 1/12 octave bands obtained by singular value rejection based on error in accelerance. ———— measured response, — — — reconstructed response.

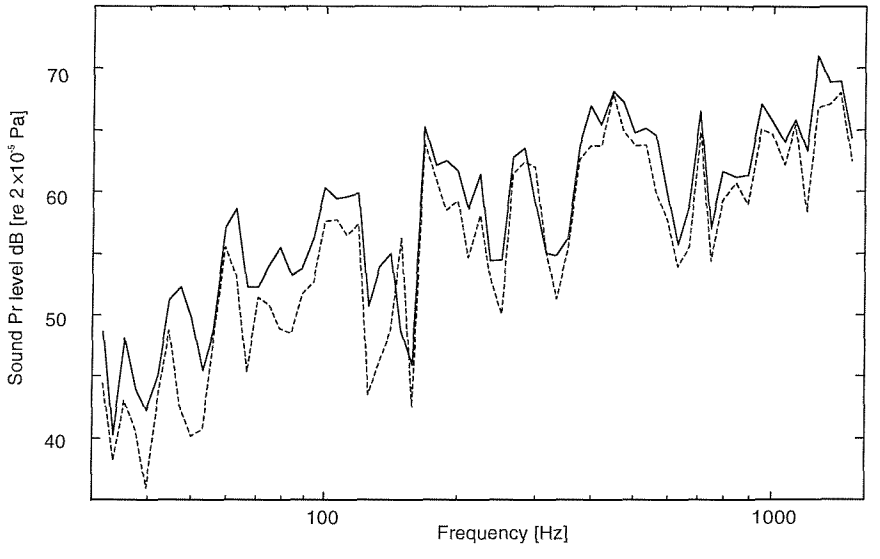

Figure 7.28. Overall sound pressure response in 1/12 octave bands obtained by singular value rejection based on error in responses. ———— measured response, — — — reconstructed response.

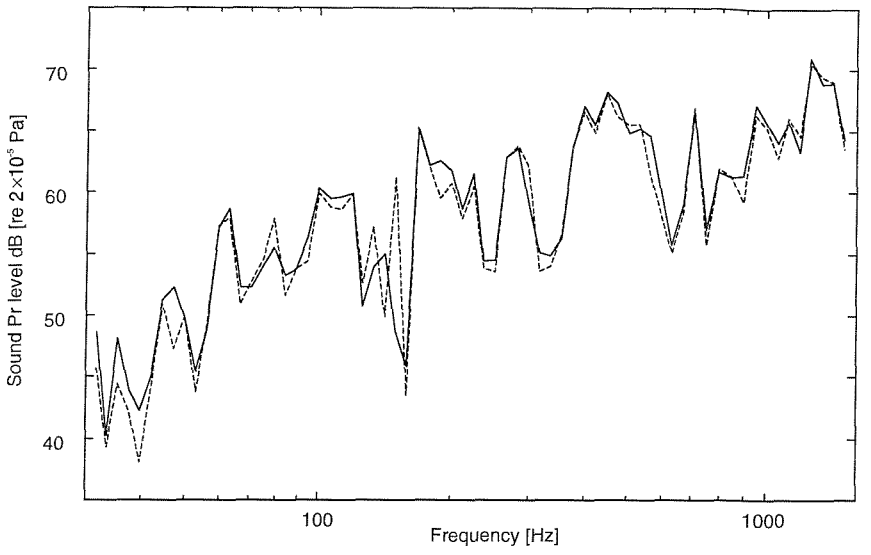

Figure 7.29. Overall sound pressure response in 1/12 octave bands obtained by iterative inversion with single response cross validation. ———— measured response, — — — reconstructed response.

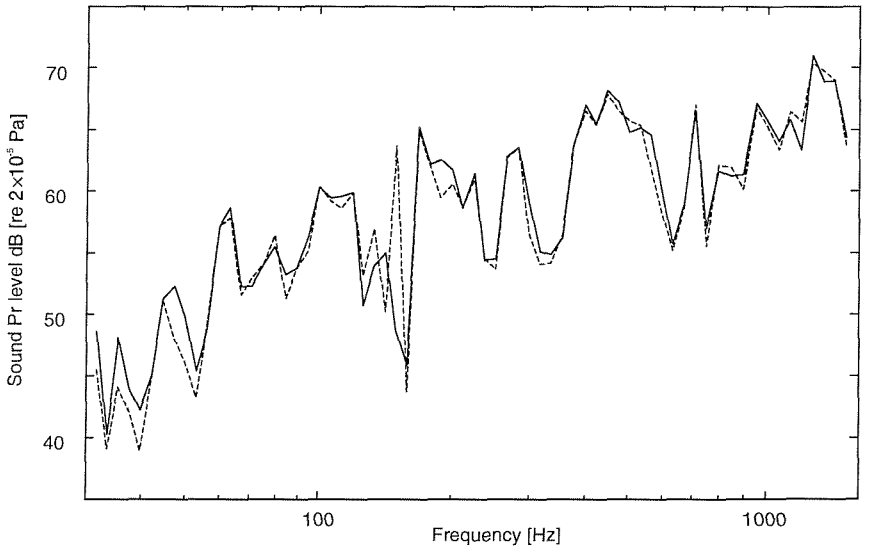

Figure 7.30. Overall sound pressure response in 1/12 octave bands obtained by Tikhonov regularization with OCV. ———— measured response, — — — reconstructed response.

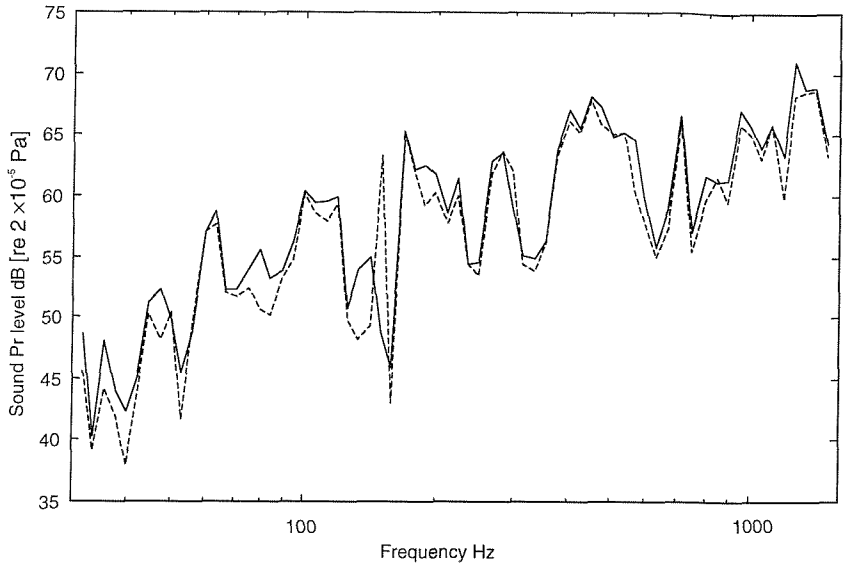

Figure 7.31. Overall sound pressure response in 1/12 octave bands obtained by Tikhonov regularization with BSCV. ———— measured response, — — — reconstructed response.

7.5 CONCLUSIONS

Experiments have been conducted on a hanging rectangular flat plate. Operational responses and FRF's were measured for three force positions, ten accelerometer positions and a microphone position. Operational forces were also measured to compare with the calculated forces. The validity of measurements has been checked by directly reconstructing the responses from the measured forces and accelerances and comparing with the measured responses. Based on the force determination and response predictions by all seven methods, the following conclusions can be drawn.

1. Singular value rejection based on the norm of the accelerance error matrix does not improve the predictions compared with the Moore-Penrose pseudo-inverse. This is due to good coherence in most of the frequency range, which means that the error matrix has small values. This is consistent with the earlier conclusion that, for an effective singular value rejection strategy, a threshold for singular value rejection should be based on both response and FRF errors.
2. The singular value rejection method based on the threshold established by the norm of the response error results in reliable prediction of peaks in the responses. However, at

antiresonances the responses are under-estimated to a large extent. It might be necessary to evolve a different analytical approach in establishing the threshold.

3. The perturbation technique was observed to result in much superior force prediction than singular value rejection. However, this method is not robust since perturbation only takes care of errors in FRF's, leaving errors in responses to be magnified.
4. Since most of the smaller singular values are rejected when the threshold is based on the response error, perturbed singular value rejection is not expected to result in any further improvement.
5. Tikhonov regularization with OCV for regularization parameter selection is found to calculate the forces better than all the other methods investigated. Tikhonov regularization with BSCV appears to improve the prediction at high frequency but to result in under-estimations at low frequency.
6. Iterative inversion combined with single response cross validation is found to give the best results of all the methods investigated. However, in arriving at the best fit response prediction, this method results in under-estimation of some forces at many frequencies. Hence the individual contributions might contain large errors.

CHAPTER 8

EXPERIMENTS ON BOX STRUCTURE

8.1 INTRODUCTION

The robustness of the techniques investigated in earlier chapters was validated experimentally in the last chapter on a hanging rectangular flat steel plate using artificial excitation. Since the noise in the measurements was small because of various precautions taken during the experiments, the results did not allow large differences to be seen between the methods. Indeed even the results for pseudo-inversion were quite reasonable. For this reason a further set of experiments has been performed on a built-up structure with a more realistic source which is reasonably stationary up to 500 Hz. The experiments and the performance of the different methods are discussed in this chapter.

8.2 EXPERIMENTAL SET-UP

The experimental set-up used is shown in Figure 8.1. Basically it consists of a box made of 1.5mm thick steel sheet (see Figure 8.2), which is open at one of the sides. This was originally constructed as part of a demonstration of noise control techniques (see [81]). It is constructed from a single sheet of steel with welded joints. Three sides are fitted with squeeze film dampers to introduce a realistic level of damping into the structure. These consist of thin steel plates bolted to the main structure. The whole structure sits on isolating pads attached to its base. On the top plate, local stiffness variations are introduced by a pair of stiffeners which are bolted to the structure.

The source consists of a tapping device driven by batteries. It was mounted on the structure through three isolators and force gauges via a triangular aluminium base plate. The isolators ensure that predominantly an axial force is transmitted since the stiffness of these in the lateral direction is very small. The force gauges were attached to the structure using cementing studs. The 'top' end of the force gauges faced the structure which reduces the mass loading effects. One of the force gauges (number 3) was mounted on top of a stiffener. The source has a fundamental operating frequency of about 15 Hz and it introduces a reasonable amount of energy in harmonics of this frequency up to quite high frequencies.

Accelerometers were also mounted on cementing studs which were glued to the plate, in order to ensure repeatability in the high frequency range by eliminating spatial deviations. Twenty locations were selected on the structure for response measurements. Ten of these were located near to the source on the top plate. The other ten were distributed on the sidewalls. These positions on the structure are shown in Figure 8.2.

Figure 8.1a. Experimental set-up for operational measurements for the box structure.

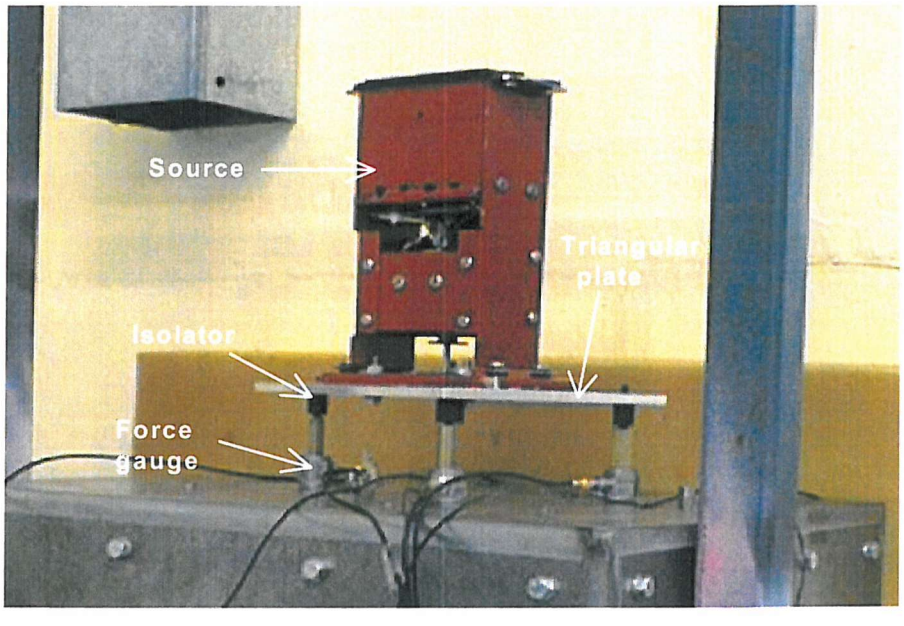

Figure 8.1b. Close-up view of the source.

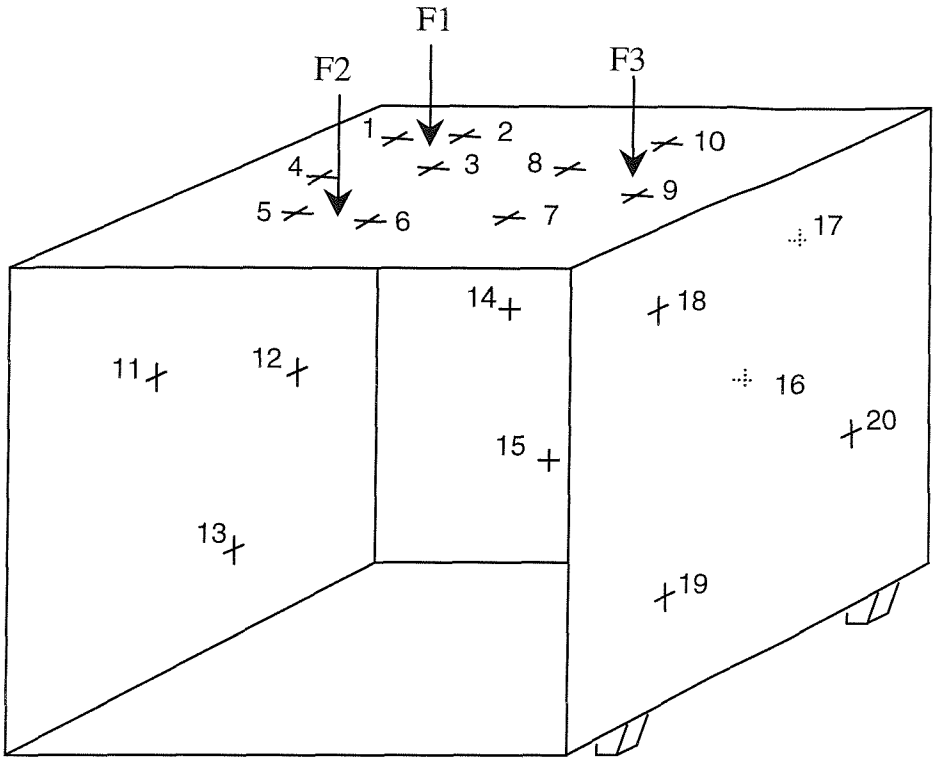

Figure 8.2. Box structure. + accelerometer positions. The front of the box is open.

Initial measurements were made of some frequency response functions from the 3 forcing locations to decide on the frequency range, frequency resolution and number of averages needed before proceeding with the complete measurements. The structure was excited by a shaker hanging from a frame. The frequency responses were determined using an average of 50 samples. At this number the random variation was found to be small.

The frequency resolution was chosen as 1 Hz. Coherence improvement because of further refinement of the resolution was found to be small. As in the previous chapter all measurements were recorded as time histories, in the present case using a sample frequency of 4096 Hz, and the processing was carried out in Matlab giving spectra up to 1600 Hz. A frequency range of 30 to 500 Hz is used in the analysis of inverse force determination. Below 30 Hz the coherence was found to be very low and errors were large in the FRF estimates. The high frequency limit corresponds to the frequency above which the source signal fluctuates considerably and also the mounting plate of the source influences the dynamics beyond this limit.

8.3 MEASUREMENTS

The measurements required for transfer path analysis were carried out in two stages as explained in the previous chapters. Initially transfer functions were measured from each forcing point to all the response locations. The H_1 estimator was used in calculating the frequency response functions. One of the measured accelerances is shown in Figure 8.3 along with the associated coherence. Clear modal behaviour can be seen below 300Hz. Coherence appears to be good above 50 Hz.

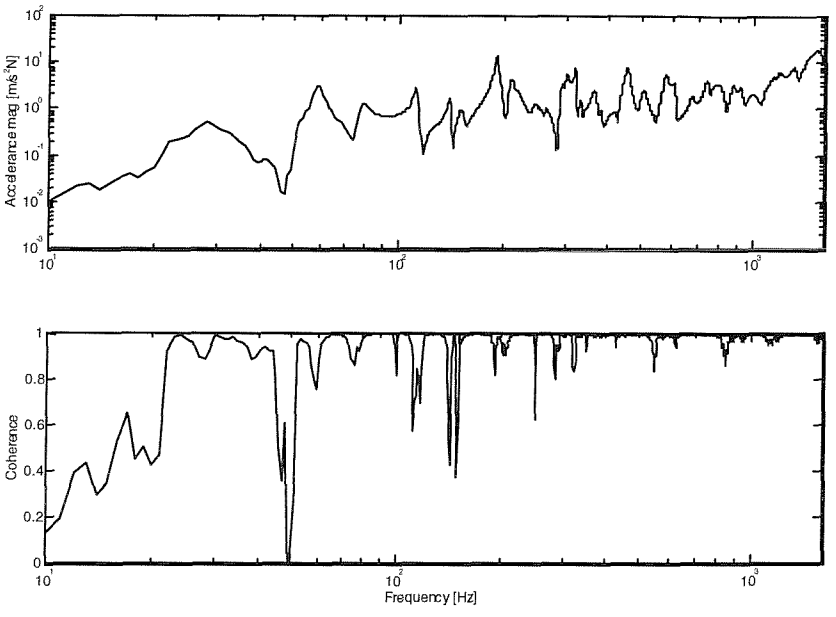

Figure 8.3. Magnitude of accelerance from force location 3 to response location 1 and associated coherence

Since 20 sensor locations were available but the number of measurement channels available was limited to 8, several subsets have been chosen. These are referred to as 'best' and 'worst' cases and were selected according to methods discussed later in Chapter 9. Due to fluctuations in the source, it was found to be essential to measure the forces simultaneously with the other responses. Therefore, of the 8 channels available, 3 were used to measure the forces, 4 for response (acceleration) positions and the final channel for a receiver position which was also an acceleration. The subset which is called the 'worst' locations was used to determine the forces. The locations used to measure operational responses for this case are 2, 5, 13 and 19. The location 8 is used as a receiver point where acceleration was measured.

The measurements are characterised by relatively low errors in the FRF's (as before in Chapter 7) but large fluctuations in the operational responses.

The magnitude of one of the responses is given in Figure 8.4. The fundamental frequency of 15Hz and its harmonics can be clearly seen up to about 300Hz. All the responses measured are shown in Figure 8.5 which are averaged over constant bands of 15Hz. This bandwidth has been used to avoid the large dynamic range of the narrow band results and to concentrate on the spectral peaks of the 15Hz harmonics.

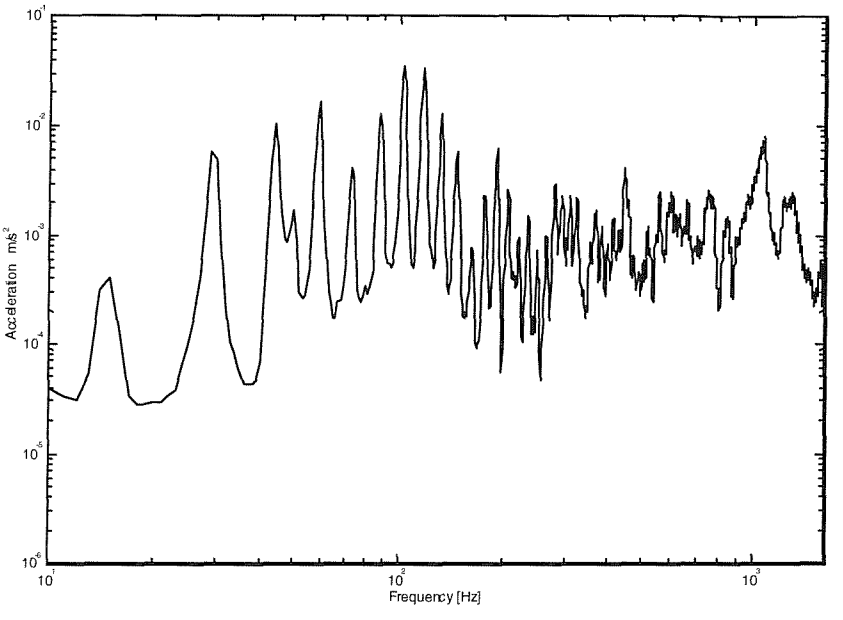

Figure 8.4. Example of acceleration spectrum during operational measurements

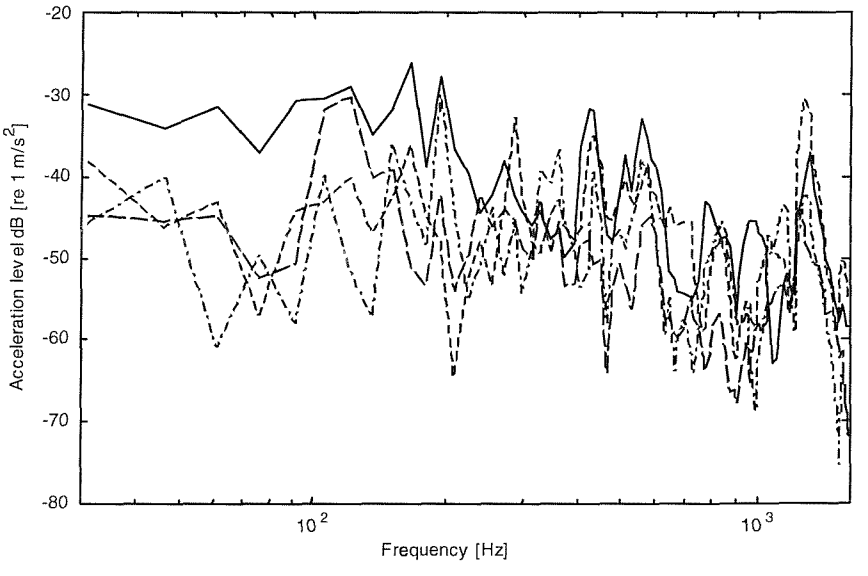

Figure 8.5. Measured acceleration responses of box structure in constant bands of 15 Hz.

The consistency of the measurements can be established by reconstructing the response in a direct way as in the previous chapter, which is possible here since the forces are also directly measured. This directly reconstructed response and the measured response for one of the locations are given in Figure 8.6. The direct reconstruction of the response agrees very well with the measured one below about 300 Hz. Considerable differences can be seen in the high frequency region where the source mounting plate influences the dynamics and results in forces not accounted for. The differences between directly reconstructed responses and the measured ones in 15Hz constant bands are shown in Figure 8.7. The mains noise effect is seen at frequencies which are multiples of 50 Hz. Apart from this, the responses appear to have been well measured in the frequency range between 60 and 500 Hz.

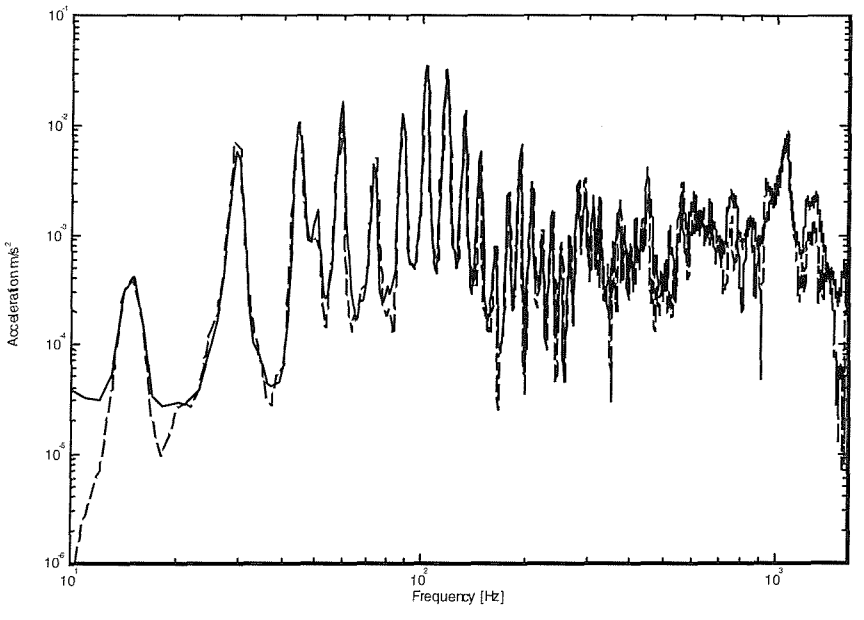

Figure 8.6. Example of acceleration response measured ———— and directly reconstructed — — — —.

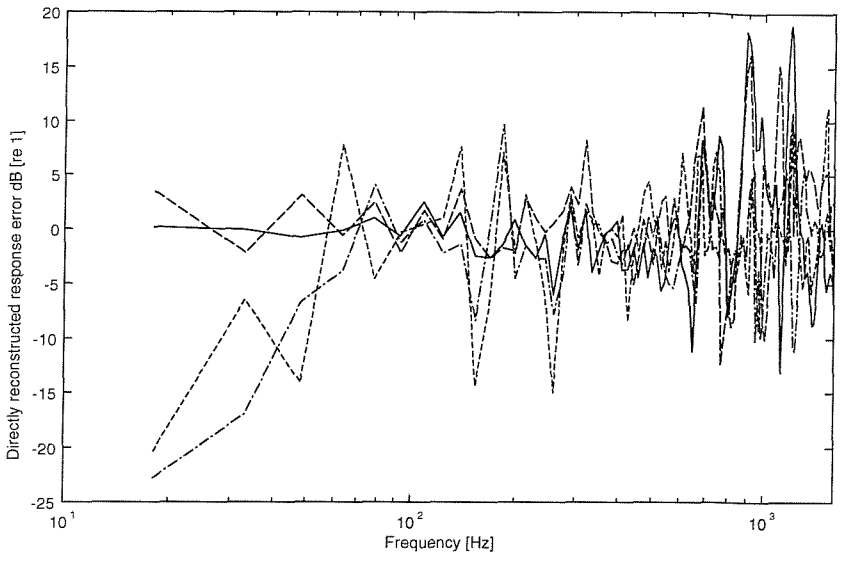

Figure 8.7. 15Hz constant band representation of errors in directly reconstructed response as compared to measured ones.

The measured operational forces averaged over bands of 15 Hz bandwidth are shown in Figure 8.8. The forces are mostly of similar amplitudes although force 1 is largest around 100 Hz. The coherence between these three forces is shown in Figure 8.9. It appears that the forces are partially coherent in the low frequency region and non-coherent at many frequencies. This implies that the approach followed until now cannot be used as it does not account for lack of coherence between different responses, since it is based on taking one of the responses as a reference. A full spectral matrix must be used in inverse force determination to take account of the inter-dependence of responses. The formulation used for this is given in Appendix C. Each of the regularization techniques can still be used in conjunction with this approach, although iterative inversion has not been implemented.

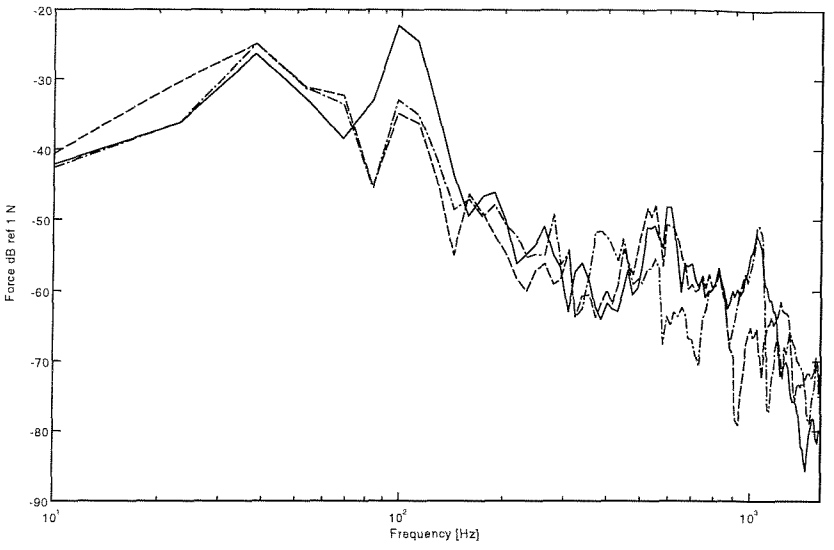

Figure 8.8. Force spectrum during operational measurements

——— F_1, — · — · — · F_2 and — — — — F_3

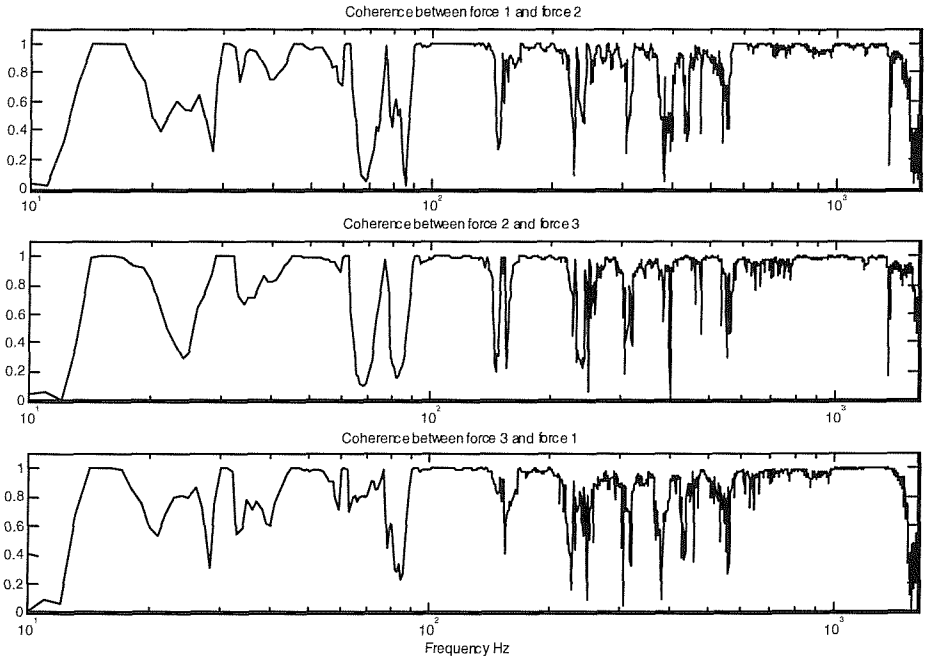

Figure 8.9. Coherence between force F_1 and F_2, F_2 and F_3, F_3 and F_1.

8.4 FORCE RECONSTRUCTION

The forces reconstructed by pseudo-inversion are shown in Figure 8.11. All the forces are over-estimated in most of the frequency range. The third force is reasonably well estimated in the frequency range 300 to 500Hz where it is largest.

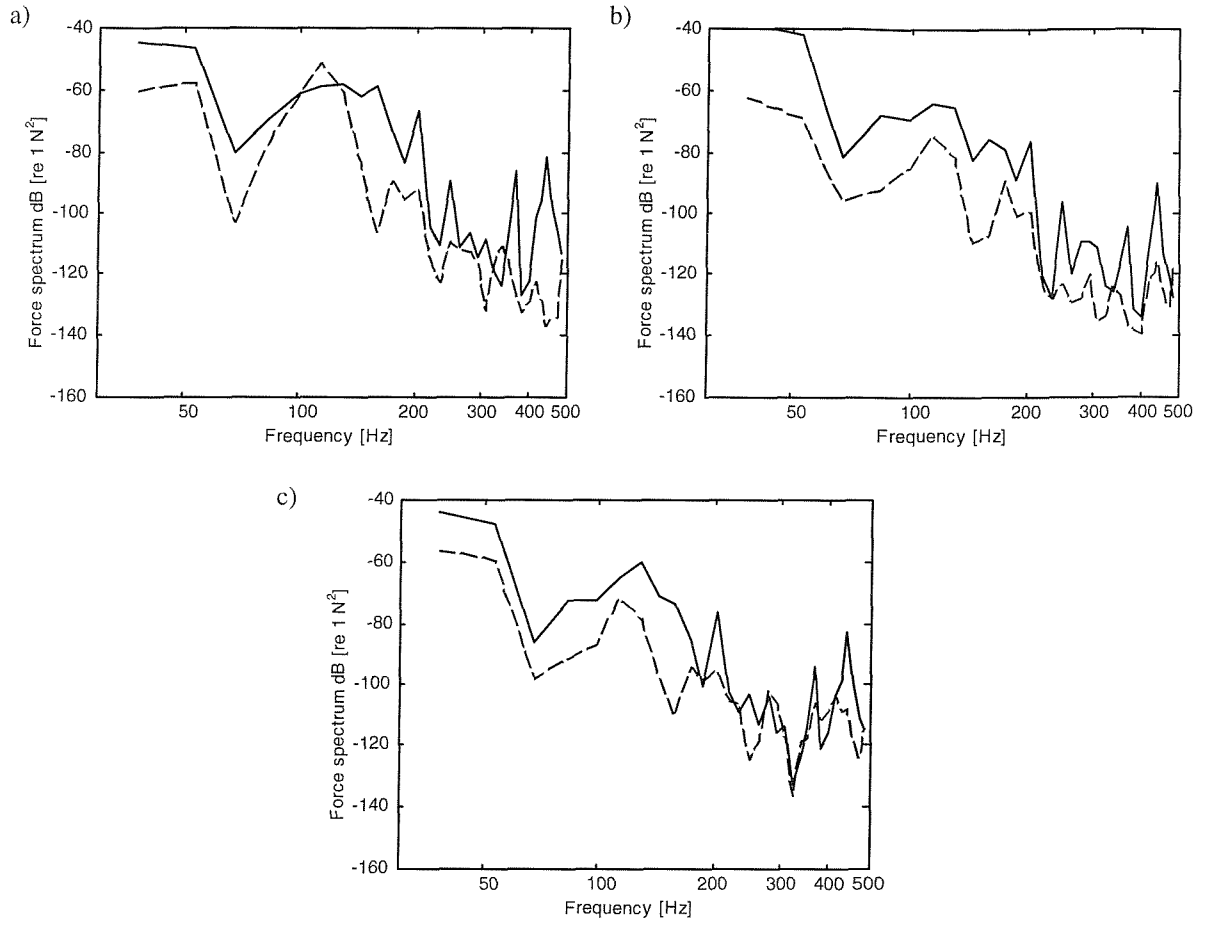

Figure 8.11. Forces reconstructed using pseudo-inverse represented in 15Hz constant frequency bands. (a) force 1, (b) force 2 and (c) force 3. — — — — measured force, ———— force determined.

Figure 8.12 shows the forces reconstructed by rejecting singular values based on the accelerance error. Marginal improvement is observed in the reconstructed forces at low frequencies compared with the pseudo-inversion. The reconstruction does not change much from that of pseudo-inversion in the high frequencies since hardly any singular values are rejected as the coherence associated with the FRF's is good in this region.

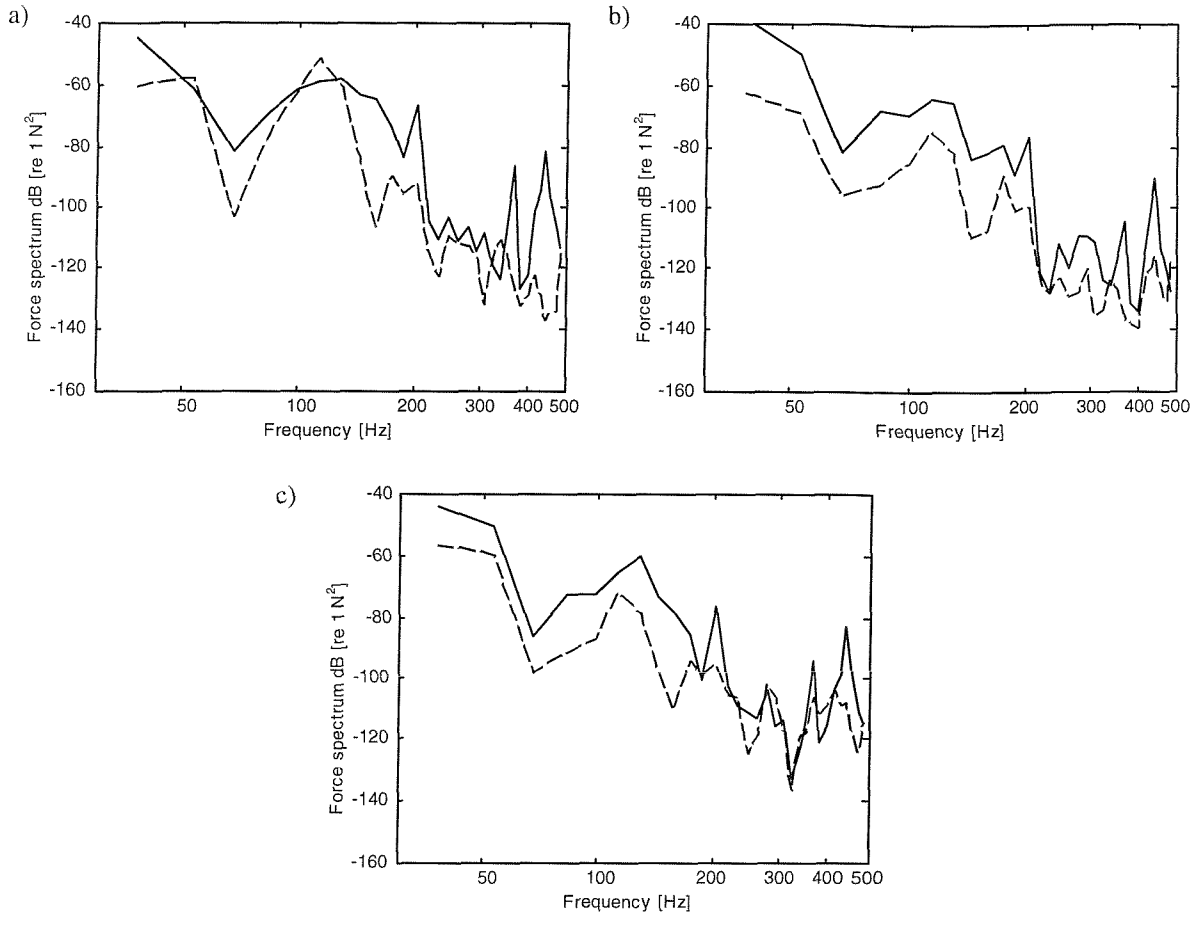

Figure 8.12. Forces reconstructed using singular value rejection based on accelerance error represented in 15Hz constant frequency bands. (a) force 1, (b) force 2 and (c) force 3. — — — — measured force, ————— force determined.

Figure 8.13 shows the reconstructed forces obtained by rejecting singular values based on the response error. All forces are well reconstructed at high frequency. In the low frequency region no improvement is found over the above methods. Response errors seem to be relatively large at high frequency, making this method more effective there.

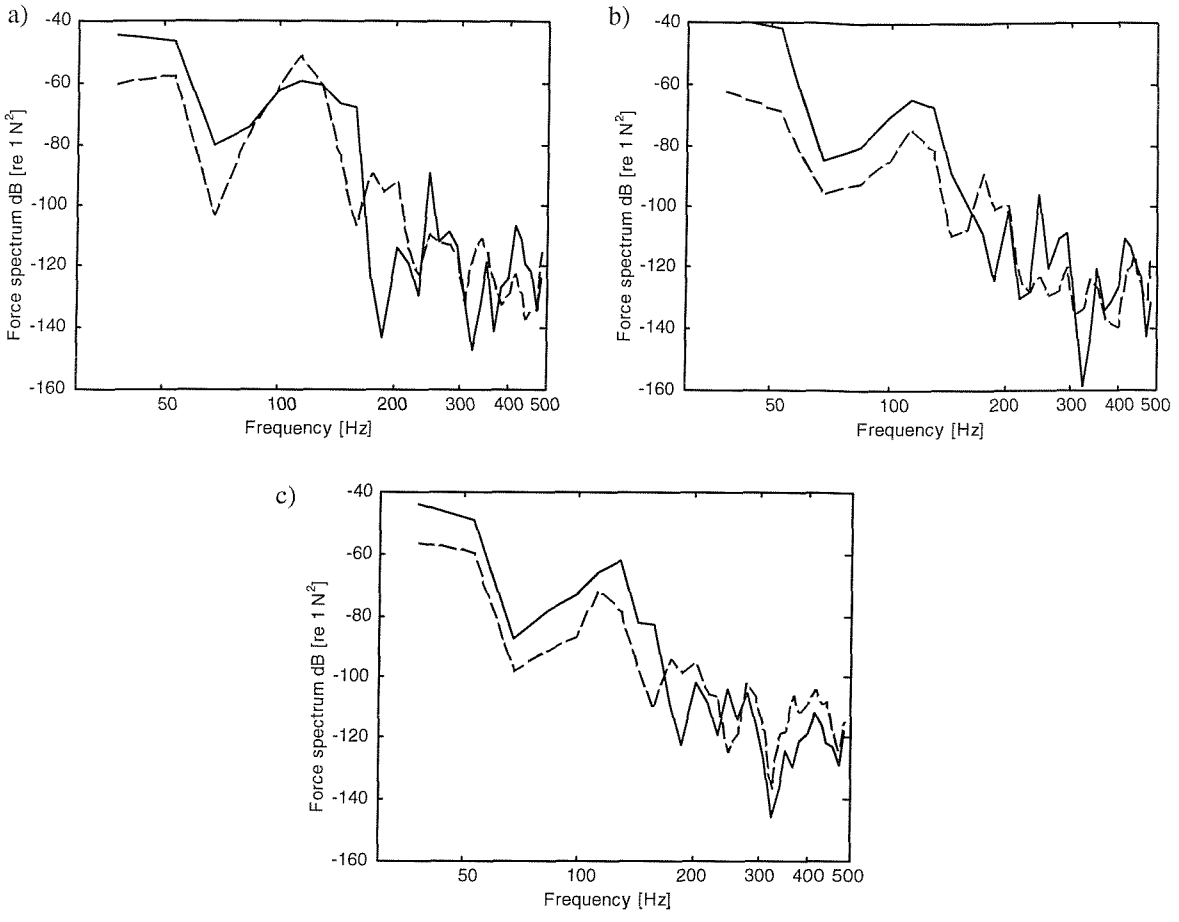

Figure 8.13. Forces reconstructed using singular value rejection based on response error represented in 15Hz constant frequency bands. (a) force 1, (b) force 2 and (c) force 3. — — — — measured force, ———— force determined.

The use of perturbed singular value rejection does not result in considerable improvements over singular value rejection based on response error (compare Figure 8.13 and 8.14). This shows the effects of large measurement errors in the operational responses. Since the errors in FRF's are small at high frequency (the coherence is good in most of the frequency range) the perturbation has little effect. However, marginal improvements are seen in the low frequency where coherence is less than one and response errors are small.

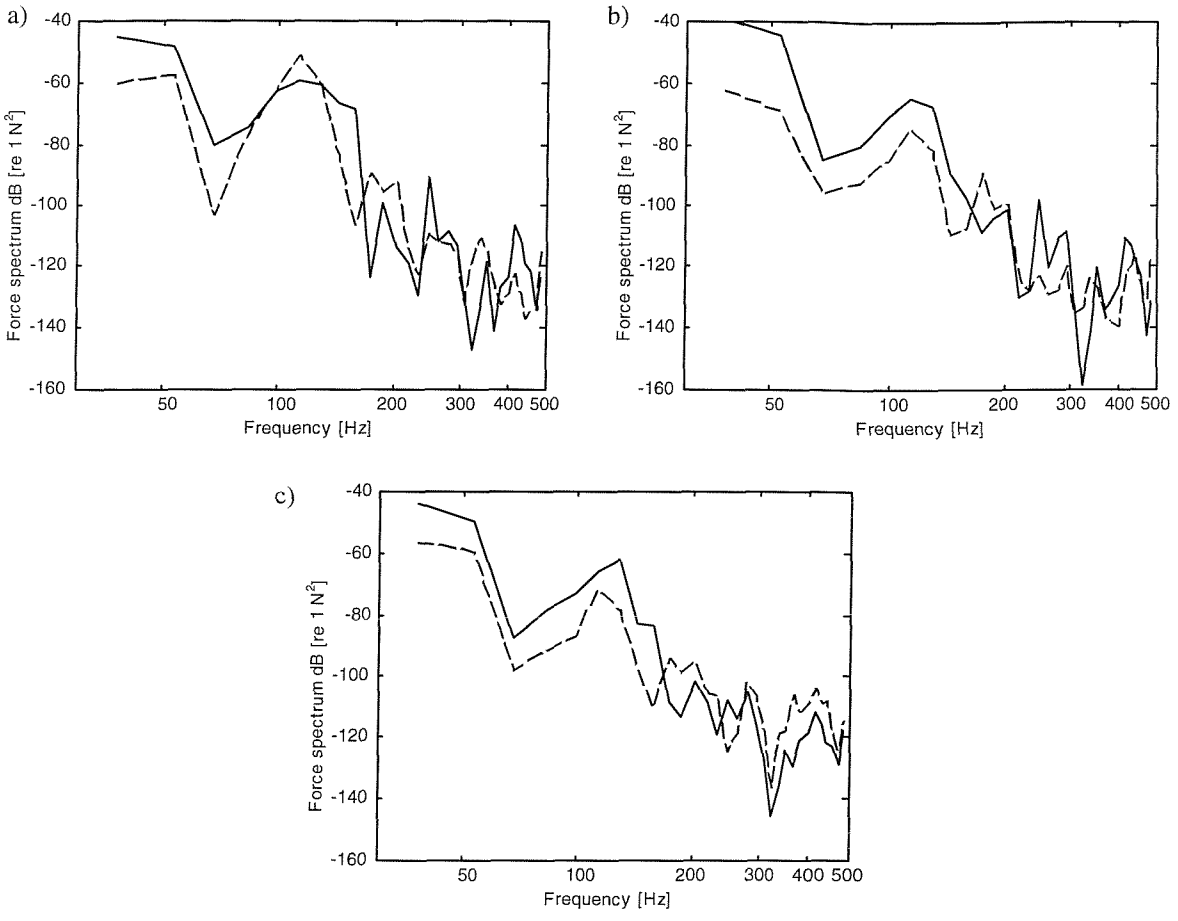

Figure 8.14. Forces reconstructed using perturbed singular value rejection based on response error. (a) force 1, (b) force 2 and (c) force 3. — — — — measured force, ———— force determined.

Figure 8.15 shows the reconstructed forces using Tikhonov regularization with OCV to select the regularization parameter. Forces 2 and 3 are quite well estimated while force 1 is under-estimated around the peak at 100 Hz.

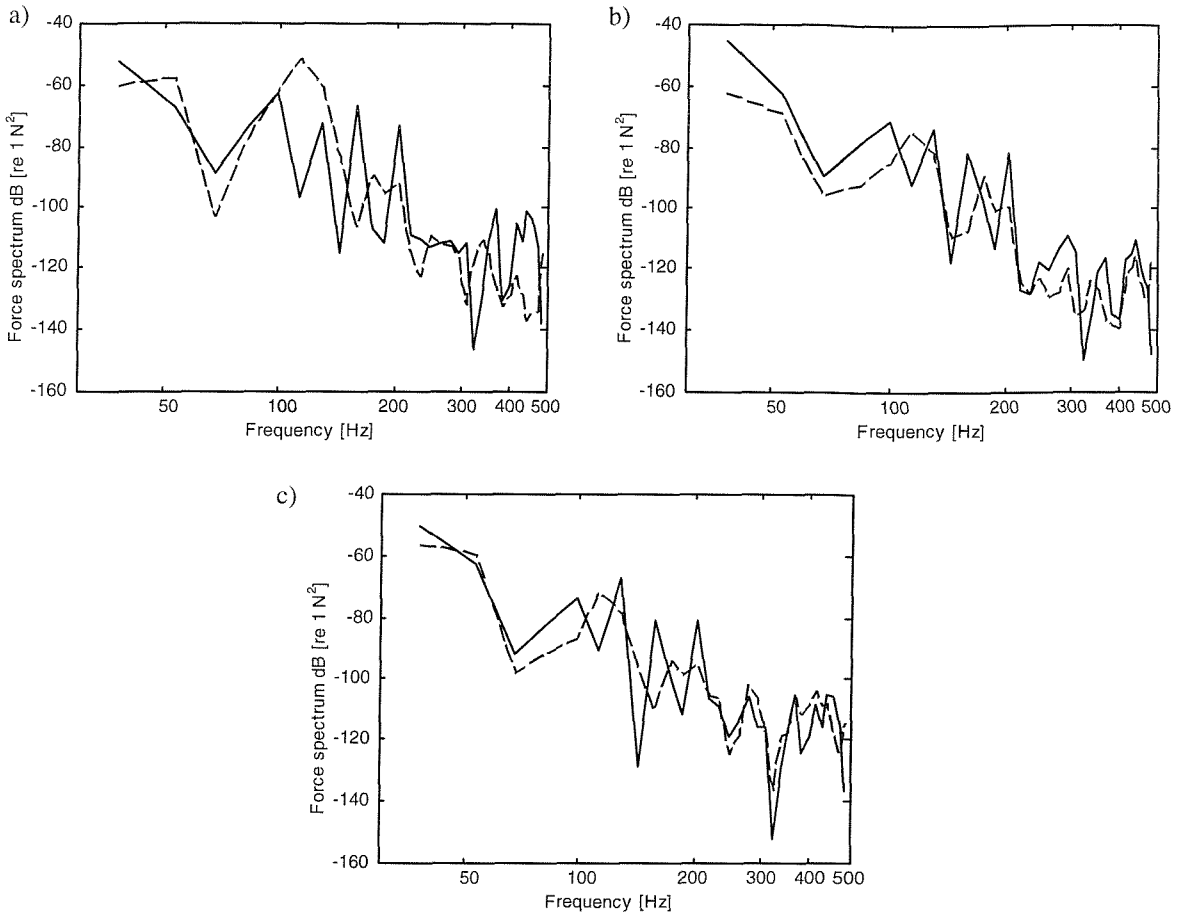

Figure 8.15. Forces reconstructed using Tikhonov regularization with ordinary cross validation to select regularization parameter. (a) force 1, (b) force 2 and (c) force 3.

— — — — measured force, ———— force determined.

Figure 8.16 shows forces reconstructed using selective cross validation to choose the regularization parameter. The forces are accurately estimated at low frequency, but some errors are found above 200 Hz. Overall the forces seem to be better reconstructed than using most of the methods considered so far.

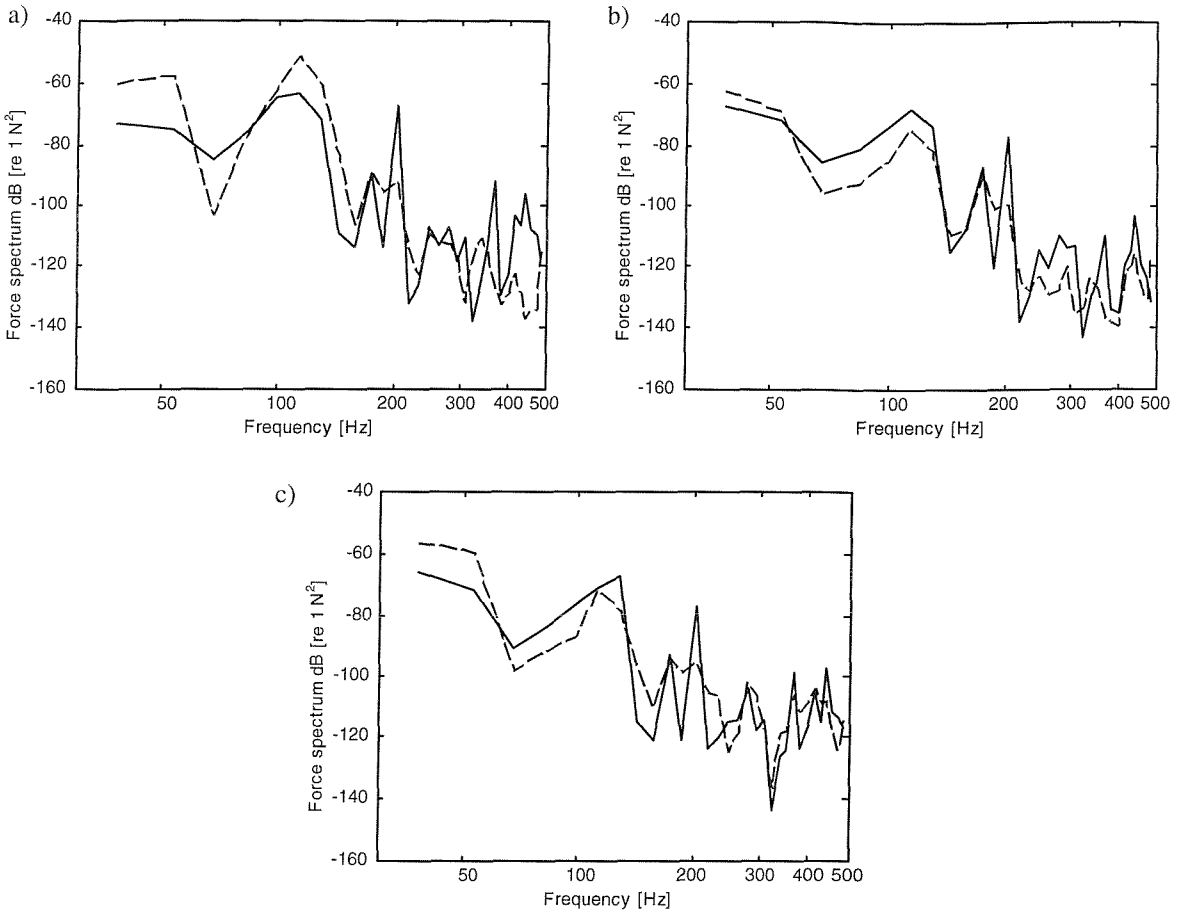

Figure 8.16. Forces reconstructed using Tikhonov regularization with selective cross validation to select regularization parameter. (a) force 1, (b) force 2 and (c) force 3.
— — — — measured force, ———— force determined.

Further improvements are seen in force reconstruction using biased selective cross validation as seen from Figure 8.17. It seems to improve force reconstruction at low frequencies.

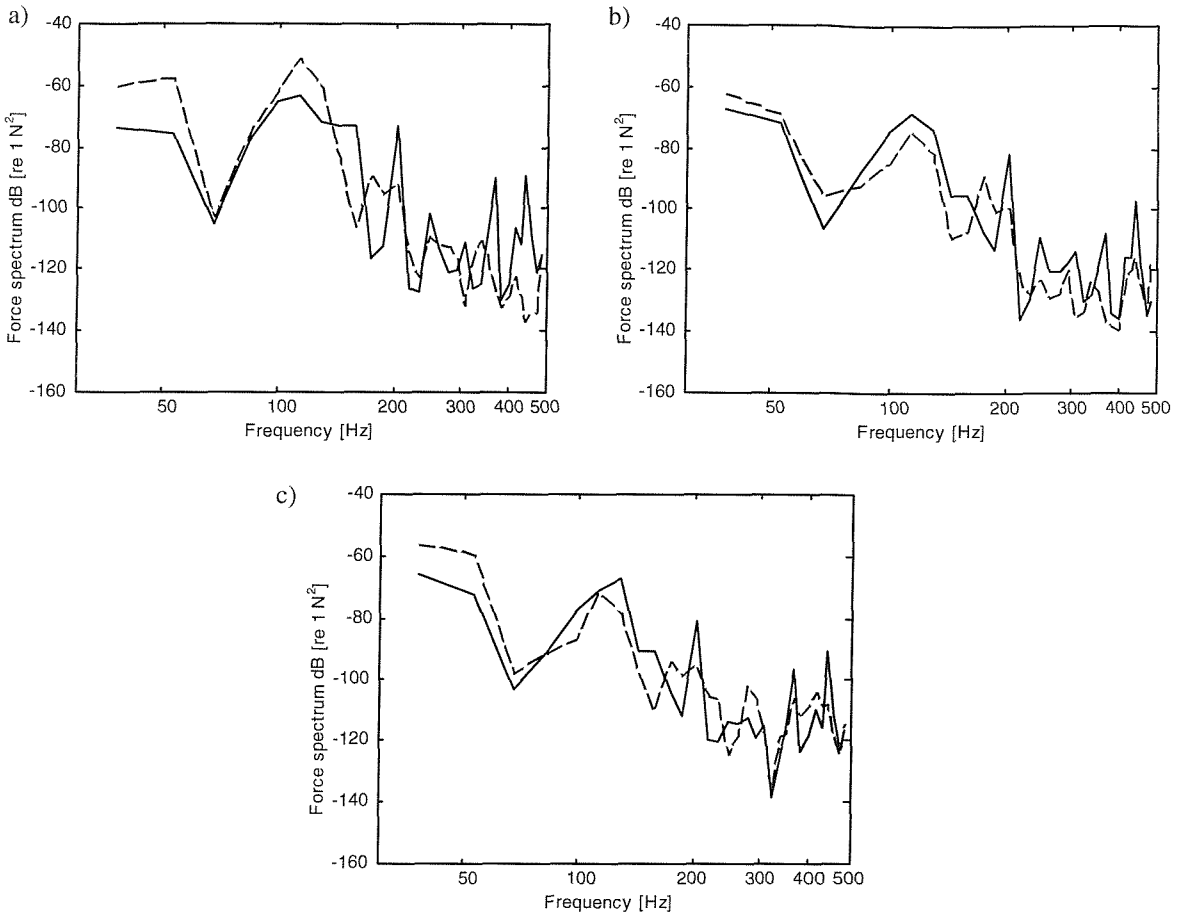

Figure 8.17. Forces reconstructed using Tikhonov regularization with biased selective cross validation to select regularization parameter. (a) force 1, (b) force 2 and (c) force 3. — — — — measured force, ———— force determined.

8.5 RESPONSE RECONSTRUCTION

The differences between the reconstructed responses and the corresponding measurements are shown in Figures 8.18 and 8.20 for all the methods. Pseudo-inversion, singular value rejection based on accerance error and accelerance perturbation result in over-estimation in most of the frequency range. However, singular value rejection based on accelerance error is much better than above methods at high frequencies. In the low frequency region singular value rejection based on response error appears to work better. Small improvements are observed when perturbed singular value rejection is used. Tikhonov regularization with ordinary cross validation appears to result in considerable under-estimation. Similar is the case of biased cross validation but to a lesser extent than

OCV. The responses reconstruction by biased selective cross validation appear to be the best of all in most of the frequency range.

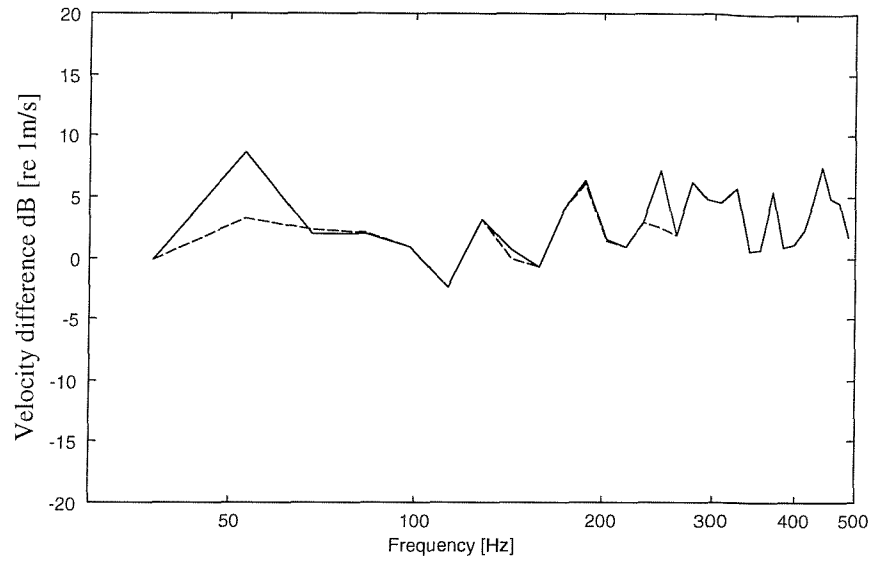

Figure 8.18. Difference between reconstructed velocity response using spectral matrix approach and measured response.———— pseudo-inverse and — — — — singular value rejection based on FRF error.

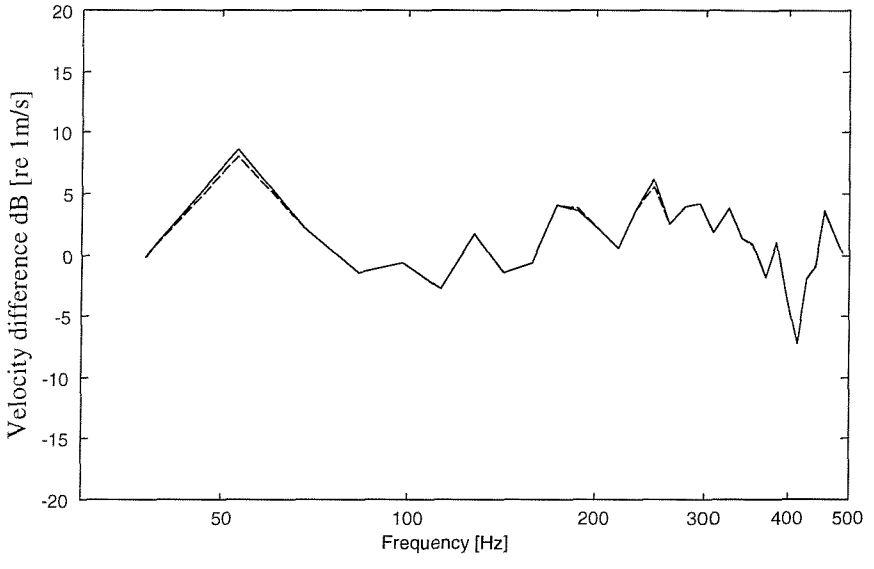

Figure 8.19. Difference between reconstructed velocity response using spectral matrix approach and measured response.———— singular value rejection based on response error and — — — — perturbed singular value rejection.

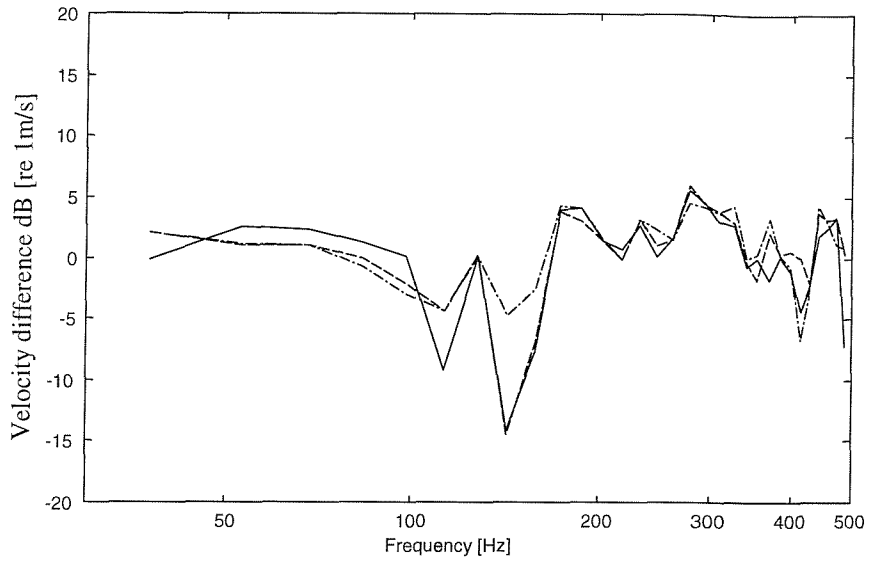

Figure 8.20. Difference between reconstructed velocity response using spectral matrix approach and measured response.———— ordinary cross validation, — — — — selective cross validation and —·—·—·— biased selective cross validation.

The results are also summarised in Table 8.1, which shows the root mean square errors in the forces determined and the reconstructed responses in dB averaged over all 15 Hz bands. The differences are quite large compared with the simulations or the experiments on the flat plate. The forces are relatively well reconstructed by Tikhonov regularization with biased SCV and perturbed singular value rejection. These methods also result in good response reconstruction. Apart from Tikhonov regularization with OCV, all methods appear to improve on the reconstructed response compared with the result from pseudo-inverse. The result for Tikhonov regularization with OCV is dominated by a large under-estimation at some frequencies which dominate the root mean square error estimation. Also note that large errors in the forces do not always correspond to large response errors.

Table 8.1. The summary of results in root mean square dB level errors for the experiment on the box.

Method	Force 1 error	Force 2 error	Force 3 error	Response error
Pseudo-inverse	21.7	17.8	13.9	4.0
SVR- frf error	20.9	16.5	13.0	3.5
SVR- resp error	17.9	14.6	12.9	3.2
PSVR	15.5	13.7	12.1	3.2
Tikhonov - OCV	20.0	13.0	12.3	4.3
Tikhonov - SCV	17.3	11.3	10.3	3.8
Tikhonov - BSCV	17.5	11.3	9.7	3.0

8.6 SUMMARY

Experiments were conducted on a box structure with a realistic source. The operational response data from this experiment are observed to contain larger measurement errors than in the experiment on a hanging plate (Chapter 7). The data are also observed to be contaminated by mains noise which affects measurements at 50, 150 and 250 Hz.

Using the experimental data, forces were determined using all methods discussed in earlier chapters, except iterative inversion. The force reconstruction was poor in most cases due to the use of a 'worst' set of response locations as discussed in the next chapter. This allows a better descrimination between the methods. Based on these estimations, Tikhonov regularization with biased SCV to select the regularization parameter and perturbed singular value rejection result in better performance than the other methods.

CHAPTER 9

METHODS TO SELECT GOOD MEASUREMENT LOCATIONS

9.1 INTRODUCTION

In earlier chapters different regularization techniques have been used to reduce the error amplification caused by matrix inversion. As mentioned in the introduction, an alternative approach might be to reduce the error amplification by an appropriate selection of the response locations used in the inversion. The reason for this is explained below.

As has been seen in Chapters 2-6, the error amplification in inverse force determination is influenced by two main factors viz., errors in the measurements and high condition numbers in the matrix of transfer functions to be inverted. The latter may be a consequence of strong modal behaviour of the structure. These two factors must occur simultaneously for error amplification in the forces. Thus the reduction of either measurement errors or condition numbers usually results in improved force determination. If the measurement errors in $\hat{a}$ and $\hat{A}$ are negligible then individual force estimates will be reliable provided that the number of modes contributing to the FRF's at a given frequency exceeds the number of forces to be identified. If the errors are significant and the condition numbers of the accelerance matrix are small then the errors simply propagate to the forces without much amplification [30-34]. On the other hand, high condition numbers of the accelerance matrix can result in small errors being magnified significantly. Thus the condition numbers play a major role in error amplification.

The condition numbers of accelerance matrices vary significantly over the frequency range because of modal behaviour of the structure under consideration. Again due to modal behaviour, condition numbers depend on the spatial location of the response measurements (the forces usually being fixed). This variation could be quite significant across the structure. Some combinations of measurement locations could be worse than others, resulting in large condition numbers at some frequencies. This characteristic presents an alternative possibility to reduce error magnfication in inverse methods. By selecting an appropriate set of response positions the condition number can be prevented from becoming too large. However, it is not necessarily obvious a priori

what is an optimal set of positions. It is interesting to note that over-determination can reduce condition numbers at high frequencies, but it is ineffecive at low frequencies (Figures 2.28-2.29). In over-determination some positions may also be redundant. It is therefore desirable to develop a method for the selection of a set of response locations that gives the best results in terms of force reconstruction.

In this chapter, different methods are explored to select response locations on the structure in order to reduce the condition number of the accelerance matrix. It is envisaged that FRF measurements would be made for a relatively large selection of positions. After application of the selection techniques, the operational responses would be measured only for the smaller optimum set of positions. Various methods which are employed in modal testing are explored first as discussed in Section 1.2.4. Then a new method, based on an 'amplification factor', is proposed to select measurement locations. The error amplification factor is closely related to the condition number of the accelerance matrix. Numerical simulations are performed to assess the effectiveness of the methods adapted from modal testing and the one based on the amplification factor. Experimental data from the box structure considered in Chapter 8 are then used to validate the method based on the amplification factor.

9.2 METHODS FROM MODAL TESTING

Several methods are employed in modal testing to extract the maximum modal information with the minimum number of measurement locations. These will be explored for their effectiveness in reducing the condition numbers in the present application. One of the methods, Gram-Smidt orthogonalization is explored in detail. A variation of this method is also evaluated. The following paragraphs give some insight into the methods currently employed in selecting locations and how many to use.

The methods described here were developed specifically for modal testing [50-54]. As discussed in Chapter 1, in modal testing the choice of forcing and acceleration measurement locations influences the quality of modal parameters extracted. Most of the procedures developed concentrate on using an FE model in selecting the sensor location, with the exception of two methods that use test data to select sensor locations. Since, in TPA, FE models are not usually available because of the complexity of structure, the methods solely dependent on FE are not discussed

further. However those methods which can be adapted for use with experimental data are discussed below.

9.2.1 Test reference identification procedure

The only method covered by the review of Avitabile [52] that uses experimental data to determine sensor locations is the test reference identification procedure. It is based on singular value decomposition of the accelerance matrix. Originally, this was applied to find the best forcing locations for excitation in modal testing. However, with some modification it could also be applied to select sensor locations. In this method, FRF's are initially measured at several locations for all forcing locations to be considered. Using these measurements, FRF matrices are constructed for each frequency. The singular values of this matrix for each frequency are then plotted. Visually, the number of modes depicted by this plot is counted (peaks indicate a resonance). Then one of the sensor locations is left out and the singular values are plotted again. If leaving out this sensor location does not reduce the number of modes identified, then that location is considered not to contain independent information and can be eliminated. This process is repeated for all the locations in order to reduce the number of locations to a set containing no redundancy while retaining the information about all the modes considered. A difficulty in implementing this method is that when the frequency range is wide, the graphical descrimination of singular values could be difficult. In TPA, where the frequency range may cover a region of high modal overlap, and where identification of modes is not the primary objective, this method cannot be applied effectively.

9.2.2 Method based on Gram-Schmidt orthogonalization

The Gram-Schmidt orthogonalization method [51], which is based on an FE model, can be adapted for use with experimental data. The adaptation involves generating the impulse response functions required from the experimental accelerances. Another significant difference is that only one force is used at a time in the modal analaysis application, while multiple forces have to be used in the inverse force determination case.

The basic principle of the method based on Gram-Schmidt orthogonalization is to ensure that the impulse response functions at sensor locations are as independent as

possible. To start with, a matrix of impulse responses is constructed. Each row of this matrix consists of an impulse response function, the elements of each row representing the impulse response value at different instants of time. The cross-correlation matrix is then constructed for each of these locations with a time delay of zero. This results in a square matrix of size equal to the number of responses. The summation of elements in each row indicates the degree of correlation for the position concerned. The position with the smallest correlation is identified as the best possible position. This position is then omitted and the impulse response matrix is again constructed after making the other impulse responses linearly independent with the one omitted using Gram-Schmidt orthogonalization (see Appendix B). The correlation matrix is again constructed for the remaining responses. The location with the minimum correlation is again identified. This location is the second best measurement location. This procedure is repeated until all positions are ranked.

The steps followed in implementing the Gram-Schmidt orthogonalization procedure using experimental data are listed below.

a. Assuming a unit force at each forcing location j, the impulse response $a_{ij}(t)$ is generated for each of the sensor locations i using the inverse Fourier transform of the measured frequency response functions. [+]

b. The overall 'impulse response' $a_i(t)$ at the i^{th} location is then taken to be the summation of all $a_{ij}(t)$ corresponding to the sensor location i from all forcing positions.

c. A response matrix a is formed with each row consisting of one combined impulse response $a_i(t)$. The elements of row i are the impulse response at the particular instant of time, t_k.

d. The correlation between each of the responses is then estimated as $r_{pq} = \dfrac{|a_p a_q^T|}{|a_p||a_q^T|}$

where $|.|$ is modulus.

e. A total correlation coefficient for each response i is then calculated as $c_i = \dfrac{1}{m}\sum_{p=1}^{m} r_{pi}$

for $i = 1,2,\ldots m$

f. The response location that results in the minimum correlation c_i is identified as the first optimum sensor location. This response is taken as a reference for the next step and it is left out of the response matrix.

g. The orthonormal row vector for the reference response is calculated as $u = \frac{a_{ref}}{\|a_{ref}\|_2}$ where $\|.\|_2$ is the 2 norm, which is same as modulus for a vector.

h. All other response vectors left in the response matrix are made independent with respect to the reference response by writing $a_{ui} = a_i - (a_i u^H)u$ for $i = 1,2,\ldots m\text{-}1$.

i. The correlation coefficient is formed again as in step (c) using the reduced vector a_{ui}. The steps c-h are repeated until all the responses are exhausted.

j. The responses taken as the reference in each step form the most suitable locations in descending order. Depending on how many responses are needed, the first few locations are selected for measuring the operational responses.

This method is explored further in the next few sections with the help of numerical simulations on a simply supported rectangular flat plate as in Chapter 2.

9.2.3 Simulation

Numerical simulations were carried out to represent 'measurements' on a simply supported rectangular steel plate of size 0.6m x 0.5m x 0.0015m. Material properties used in the simulation were the same as in Chapter 2. A series of 20 new locations were selected on the plate to represent the sensor positions (see Table 9.1) and 4 new force locations were selected at random. The frequency response functions were generated for these locations from the individual force positions. The noise levels used here correspond to moderate noise in the FRF's. Out of the 20 possible locations a few 'good' locations were selected using Gram-Schmidt orthogonalization.

Two sets of sensor locations were chosen to validate this method. In the first set, 4 locations were selected out of the first 10 from the table, and in the second case 4 were selected out of 20. In each case the 'worst' 4 were also identified. Using these sets of four locations, the forces were reconstructed and the response at the receiver location was predicted and compared with the 'exact' result.

[+] The impulse response function could be measured directly using impact exciation but in the present experiments shaker excitation using a random signal has been used.

The order of optimum locations determined by this method from the first 10 in Table 9.1 and the corresponding correlation coefficient at each stage are given below in Table 9.2. The selection is also shown in Figure 9.1. Positions with square marks are the 'optimum locations' while the crossed ones are the 'worst' locations. Forcing locations are shown by +.

Table 9.1. Non-dimensional force and response positions

Force positions			**Response positions**		
Position	x/a	y/b	Position	x/a	y/b
1	0.41	0.2	1	0.55	0.4
2	0.51	0.59	2	0.8	0.2
3	0.8	0.41	3	0.9	0.8
4	0.1	0.8	4	0.6	0.5
			5	0.2	0.3
			6	0.3	0.7
			7	0.5	0.9
			8	0.7	0.71
			9	0.61	0.31
			10	0.23	0.89
			11	0.1	0.6
			12	0.16	0.1
			13	0.17	0.8
			14	0.63	0.67
			15	0.87	0.37
			16	0.83	0.13
			17	0.91	0.19
			18	0.79	0.82
			19	0.89	0.93
R	0.15	0.45	20	0.53	0.17

Table 9.2. Ranking of 10 positions by Gram-Schmidt orthogonalization.

Ranking	*1*	*2*	*3*	*4*	*5*	*6*	*7*	*8*	*9*	*10*
Order of positions	8	6	9	3	2	1	4	7	5	10
Correlation coeff	0.32	0.36	0.35	0.48	0.37	0.60	0.51	0.68	0.99	1.0

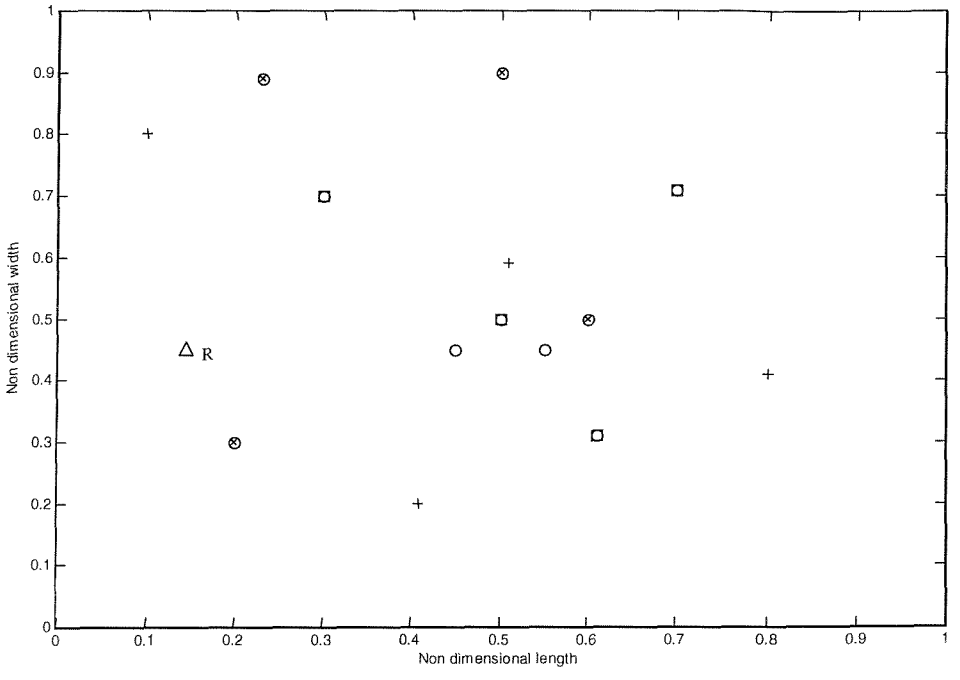

Figure 9.1. The 'best' and 'worst' locations selected from 10 potential locations using Gram-Schmidt orthogonalization. O *potential locations,* □ *best locations,* × *worst locations and* + *forcing locations.* Δ *receiver location.*

In the second case, for 20 locations, the order in which locations were selected is given in Table 9.3 and are shown in Figure 9.2. The first four positions are quite different from those in Figure 9.1 apart from position 3; even though positions 1 and 4 are also contained in the set of 10 they were not selected there, indeed position 4 was identified as one of the 'worst' positions there.

Table 9.3. Ranking of 20 positions by Gram-Schmidt orthogonalization.

Ranking	Order of positions	Correlation coeff	Ranking	Order of positions	Correlation coeff
1	11	0.31	*11*	12	0.72
2	4	0.31	*12*	10	0.55
3	1	0.35	*13*	13	0.54
4	3	0.38	*14*	2	0.52
5	8	0.41	*15*	20	0.56
6	17	0.46	*16*	14	0.74
7	18	0.38	*17*	19	0.62
8	6	0.47	*18*	7	0.70
9	9	0.45	*19*	15	0.97
10	5	0.59	*20*	16	1.0

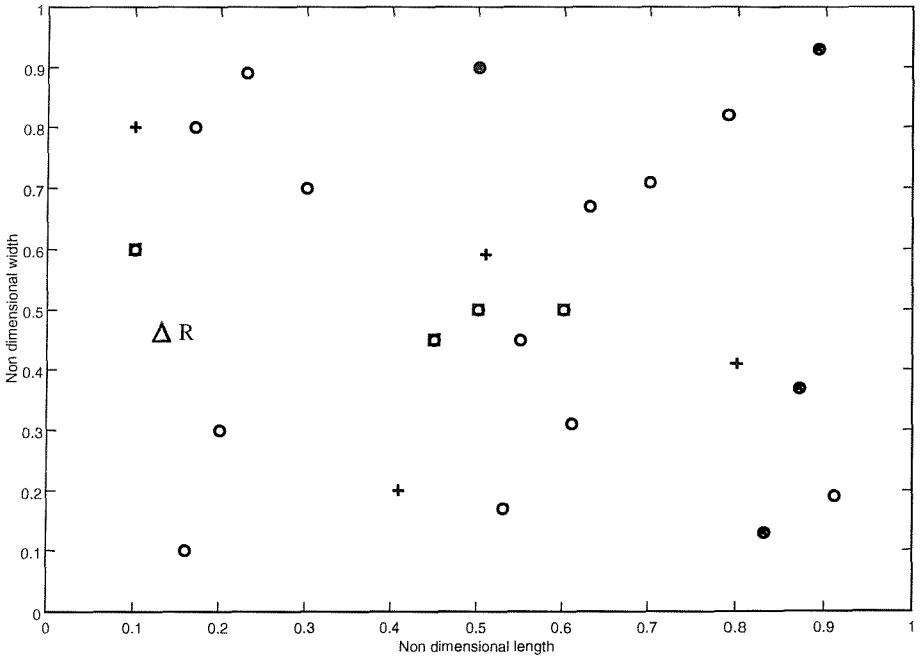

Figure 9.2. The 'best' and 'worst' locations selected from 20 potential locations using Gram-Schmidt orthogonalization. O *potential locations,* □ *best locations,* × *worst locations and* + *forcing locations.* Δ *receiver location.*

Numerical simulations were carried out on the plate to represent the next stage of experiments so that operational responses could be obtained at the locations selected (best and worst) from the second case, where out of a potential 20 locations, two sets of

four locations were selected as the 'best' and 'worst'. The forces used have amplitudes 50, 20, 10 and 1N respectively when converted to 1/3 octave form. The noise level used in the responses corresponds to high noise (low S/N ratio). By inverting the square accelerance matrix at each frequency the forces were determined. Note that no regularization is used here. The reconstructed forces obtained using the 'best' locations is shown in Figure 9.3. The results can be compared with input forces shown at the right hand side of the figure. These results are significantly better than those for the 'worst' locations, shown in Figure 9.4. However, the forces still contain some errors at low frequency.

The response at the receiver location reconstructed from these forces for the 'best' location case matches well with the actual response, as shown in Figure 9.5. When using the 'worst' locations, Figure 9.6, the errors are not as large as in the forces, but are still large compared to the 'best' location case.

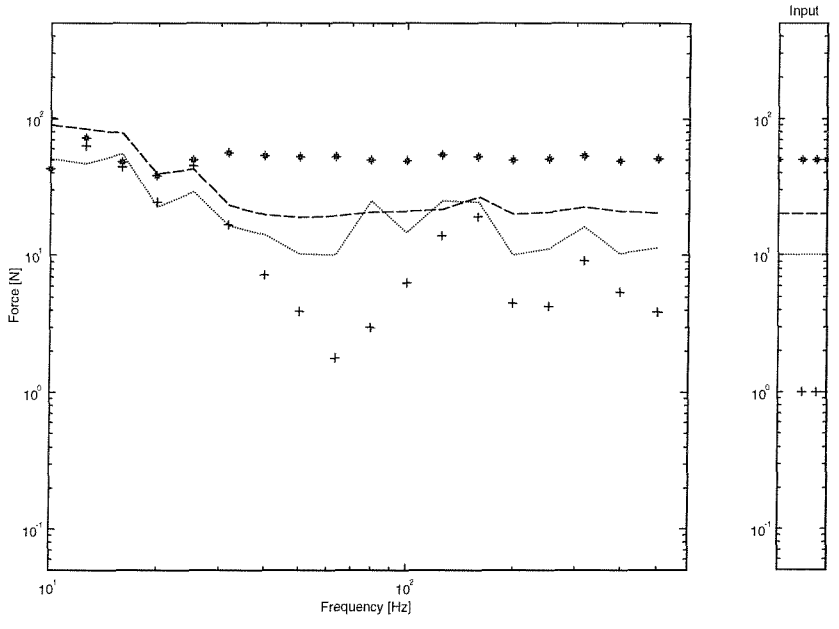

Figure 9.3. Reconstructed forces in 1/3 octave bands for 4 forces and 4 responses. Best locations from 20 according to Gram-Schmidt orthogonalization are used.

* * * * * *force 1,* — — — *force 2,* · · · · · · · · *force 3,* + + + + + *force 4.*

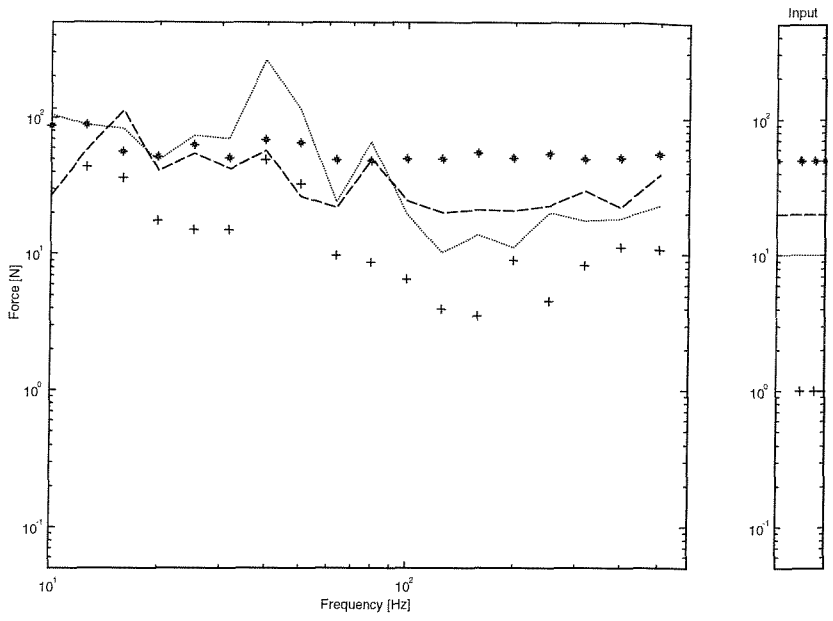

Figure 9.4. Reconstructed forces in 1/3 octave bands for 4 forces and 4 responses. Worst locations from 20 according to Gram-Schmidt orthogonalization are used.

* * * * * *force 1,* — — — *force 2,* · · · · · · · · · *force 3,* + + + + + *force 4.*

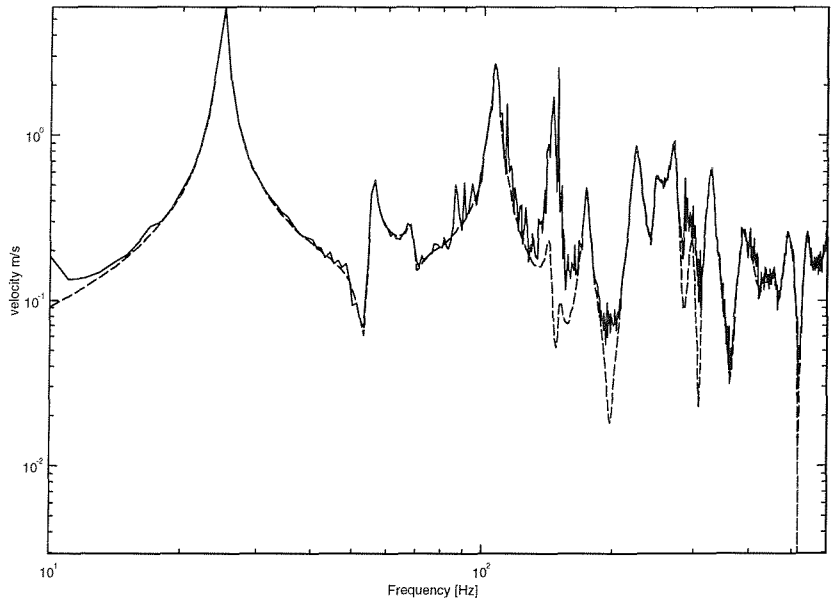

Figure 9.5. Receiver location response reconstructed using forces obtained from best locations from 20 as selected according to Gram-Schmidt orthogonalization.

———— *reconstructed,* — — — *actual.*

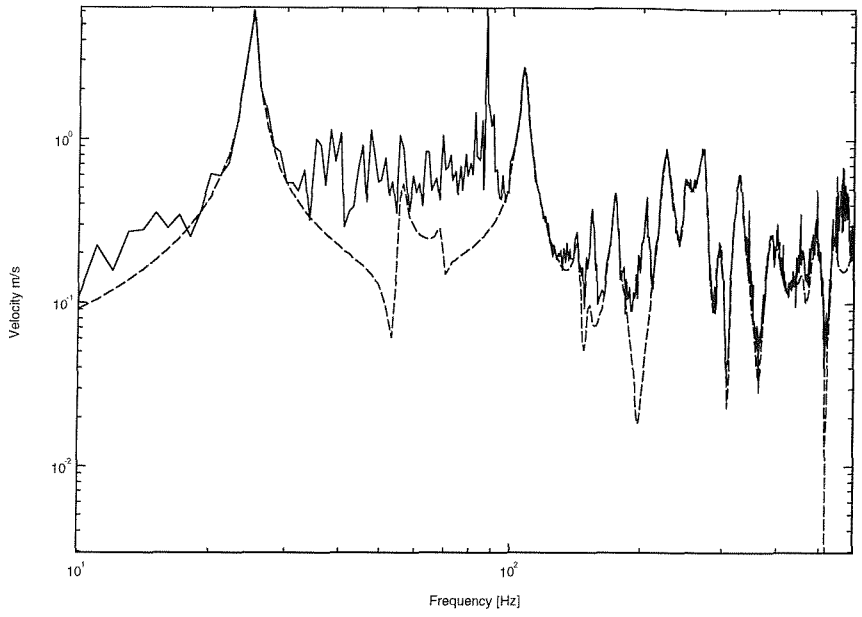

Figure 9.6. Receiver location response reconstructed using forces obtained from worst locations from 20 as selected according to Gram-Schmidt orthogonalization.
——————— reconstructed, — — — actual.

These observations are confimed by 1/3 octave band plots in Figure 9.7. Note, however, that the 'worst' locations give better results between 100 and 200 Hz than the 'best' locations.

Even though, in the example shown, the results are encouraging, further investigation has revealed that the selections are not always optimal and the performance varies from case to case. The optimality is not achieved, since once a response position is selected, it is never considered for any other combination. If instead of n locations, n-1 are used, the selection could be completely different. This effect becomes significant when a small number of locations is used.

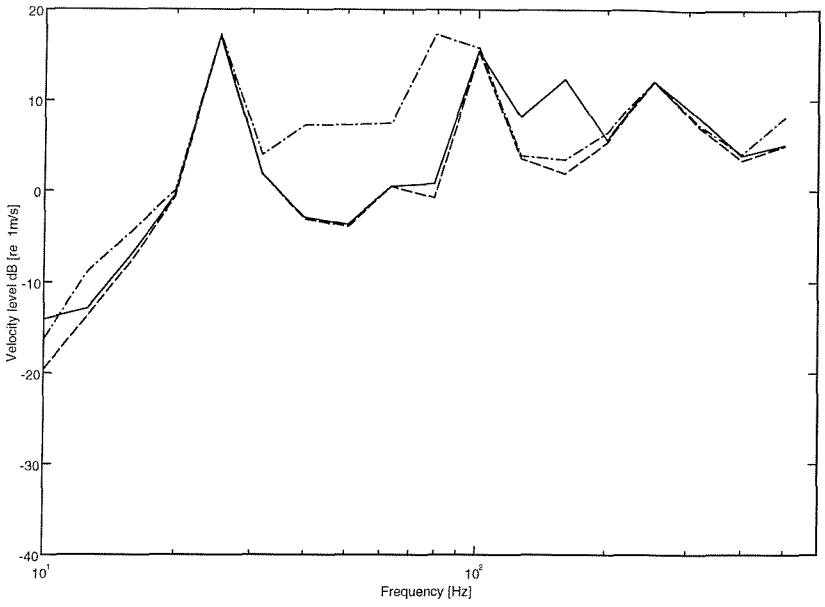

Figure 9.7. Receiver location response in 1/3 octave bands reconstructed using forces obtained from best and worst locations from 20 as selected by Gram-Schmidt orthogonalization. ———— reconstructed response from best locations, — · — · — · reconstructed response from worst locations, — — — — actual response.

The optimality of location selection can be gauged by the difference in condition numbers of the 'best' locations and the 'worst' locations. For the two cases considered here, Figures 9.8 and 9.9 show the condition numbers. In the case where locations were selected from ten available ones, the reduction in condition number seems to be small although significant reductions are seen for the selection from 20 locations. Hence this approach might give reasonable results if a large number of locations is available. These statements, however, are qualitative in nature. In order to overcome the above difficulties, an alternative approach is considered in which the average of the condition numbers across the frequency range is used to compare the selection of locations. In the next section this objective comparison is used in developing a new method to select the sensor locations which minimize the condition numbers across the range of frequency considered.

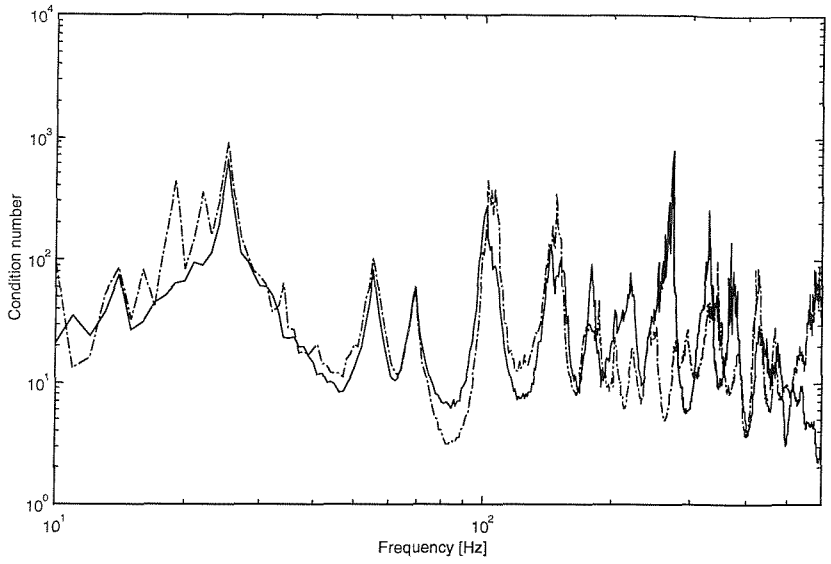

Figure 9.8. Condition numbers of best and worst locations out of available 10 locations as selected by Gram-Schmidt orthogonalization. ———— best locations, · — · — · — · worst locations.

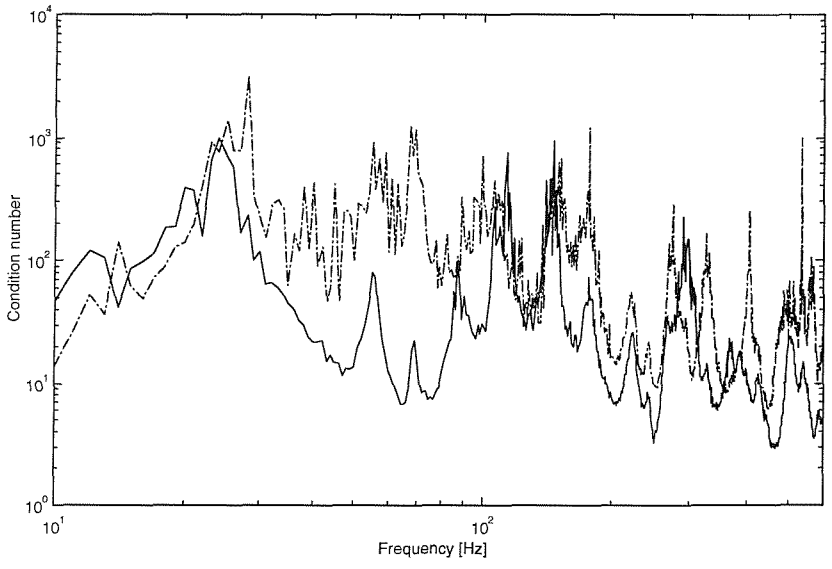

Figure 9.9. Condition numbers of best and worst locations out of available 20 locations as selected according to Gram-Schmidt orthogonalization. ———— best locations, · — · — · — · worst locations.

9.3 SENSOR SELECTION BASED ON AMPLIFICATION FACTOR

As proposed in the last section the average of the condition numbers across the frequency range of analysis may be used as a measure to select the sensor locations which can reduce the error amplification. The process, however, would involve the

estimation of condition numbers at each frequency for many different combinations of locations. When a large number of locations is available this task rapidly becomes impractical. For example, selecting four positions from 20 would require the testing of 38760 combinations, for each of which the condition number of a $4\times n$ matrix would have to be determined at each frequency. To overcome this, an approximate method is proposed which is explained in the following paragraphs.

In the approach proposed, the condition numbers are evaluated for FRF matrices based on just two response locations at a time taken from those available and all force locations. These condition numbers are combined and used as a measure of the condition of the matrix for a set (eg $4\times n$) of the locations. In order to combine them, the condition numbers for the pairs of locations are added for all combinations of the set of locations considered. Then comparing this quantity for all possible sets, the set giving the largest value is chosen as the 'best' combination of locations. Although it may not seem obvious, it will be shown in Section 9.4 below that this produces a measure that is reasonably well correlated with the average condition number of the actual matrix. The detailed procedure followed is as follows:

a. Select m_{all} locations that are candidates for measuring the operational response.
b. Construct $2\times n$ matrix of accelerances for one set of 2 response locations (i,j) at each frequency and calculate the condition number of this matrix (n is the number of force positions).
c. Average the condition numbers over the frequency range and write this as x_{ij} with i,j corresponding to the two response locations considered.
d. From these x_{ij}, construct the $m_{all} \times m_{all}$ matrix $[x]$, the diagonal elements of which are zero.
e. Decide the number of responses m to be used.
f. Determine all possible combinations of m responses taken from m_{all} i.e. $\frac{m_{all}!}{m!(m_{all}-m)!}$ combinations.
g. Select the first combination 1,2,.... m and find all possible pairs of responses within this combination eg 12,13,23 etc. For these sets of two take the average of

x_{ij} from step (d). This will be called the amplification factor X relating to the combination 1,2,3,...,m.

$$X = \left(\frac{n}{m}\right)\frac{n(n-1)}{m(m-1)}\sum_{i,j} x_{ij}$$

This factor in front of the summation has been introduced as it is found that X then corresponds more closely with the condition number of the $m \times n$ matrix.

h. Construct a vector of all amplification factors from (g) for all combinations identified in step (f).

i. The combination giving the minimum amplification factor is taken as the optimal combination of locations.

When this technique is applied to the sets of locations, as in Section 9.2, the selected positions are as follows. In the first case, out of 10 available response locations, the best and worst possible combinations of locations are shown in Figure 9.10. They are

Best combination : 1 5 8 10

Worst combination : 1 2 3 4

In the second case, out of 20 available response locations, the best and worst possible combinations of locations are shown in Figure 9.11. They are

Best combination : 5 13 15 18

Worst combination : 8 14 18 19

It will be noted immediately that these sets are totally different from those identified by Gram-Schmidt orthogonalization. It will also be noted that positions 1 and 18 are included in both best and worst combinations for the two cases.

The corresponding condition number plots of the 4×4 FRF matrices are given in Figures 9.12 and 9.13. These can be compared to Figures 9.8 and 9.9 in the previous section. The method proposed seems to work much better than the Gram–Schmidt orthogonalization for the application concerned, at least in terms of minimizing the condition numbers. It does not seem to depend on the number of locations available to select the optimal ones. The method also selects the worst cases more clearly than Gram–Schmidt orthogonalization.

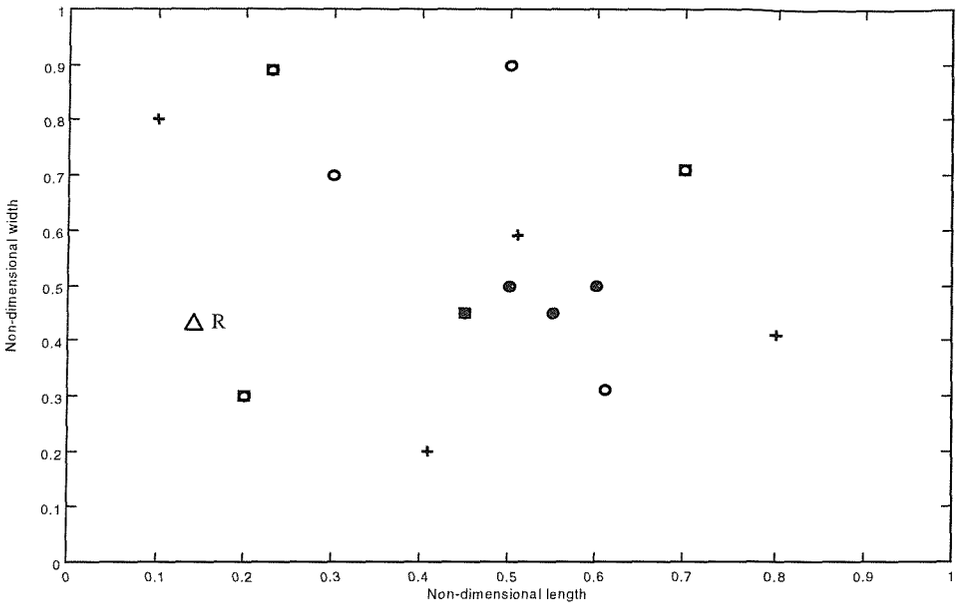

Figure 9.10. The best and worst location combinations from 10 potential locations using method based on amplification factor. O *potential locations,* □ *best locations,* × *worst locations and* + *forcing locations.* Δ *receiver location.*

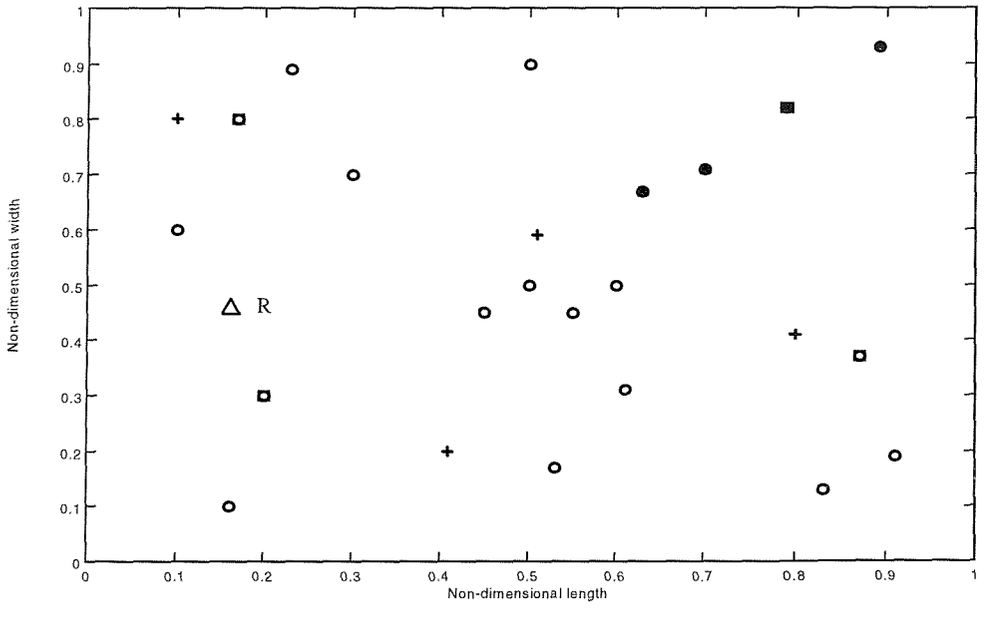

Figure 9.11. The best and worst location combinations from 20 potential locations using method based on amplification factor. O *potential locations,* □ *best locations,* × *worst locations and* + *forcing locations.* Δ *receiver location.*

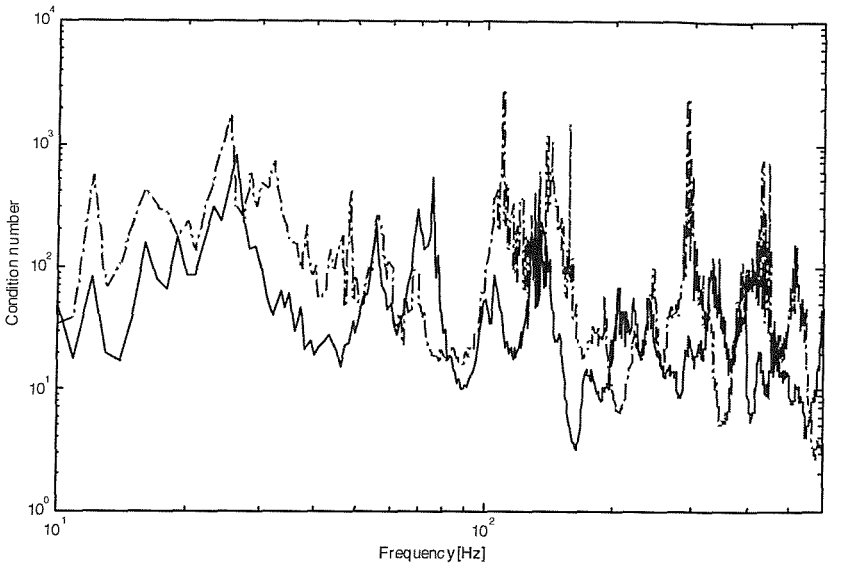

Figure 9.12. Condition numbers of best and worst locations out of available 10 locations as selected by method based on amplification factor. ———— best locations, · — · — · — · worst locations.

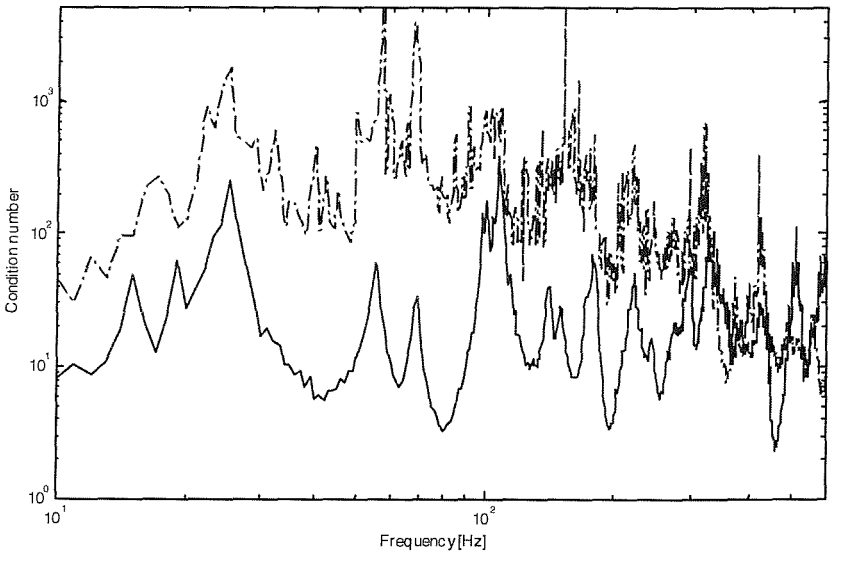

Figure 9.13. Condition numbers of best and worst locations out of available 20 locations as selected by method based on amplification factor. ———— best locations, · — · — · — · worst locations.

Due to the reduction in the condition numbers for the 'best' locations compared with the corresponding cases in the earlier section, the force determination improves considerably, as shown in Figure 9.14 which shows results for the best 4 positions chosen from 20. The results are closer to the exact ones than the 'best' location case by

Gram-Schmidt orthogonalization (Figure 9.3). The 'worst' locations selected in the proposed method give the poorest force reconstruction of all the cases considered here as shown in Figure 9.15 (compare with Figures 9.14, 9.3 and 9.4). Improvements in force determination for the best locations also translate into an improved receiver location response as shown in Figure 9.16. Figure 9.17 shows the response reconstruction for the worst case. In most of the frequency range this reconstruction contains large errors. These results are further confirmed by 1/3 octave band representation of the response as shown in Figures 9.18. However, note that the 'worst' location gives good results around 300 Hz. This can be explained by reference to Figure 9.13 where it can be seen that the condition number of the worst case is actually better than the 'best' case for a limited frequency range around 350 Hz.

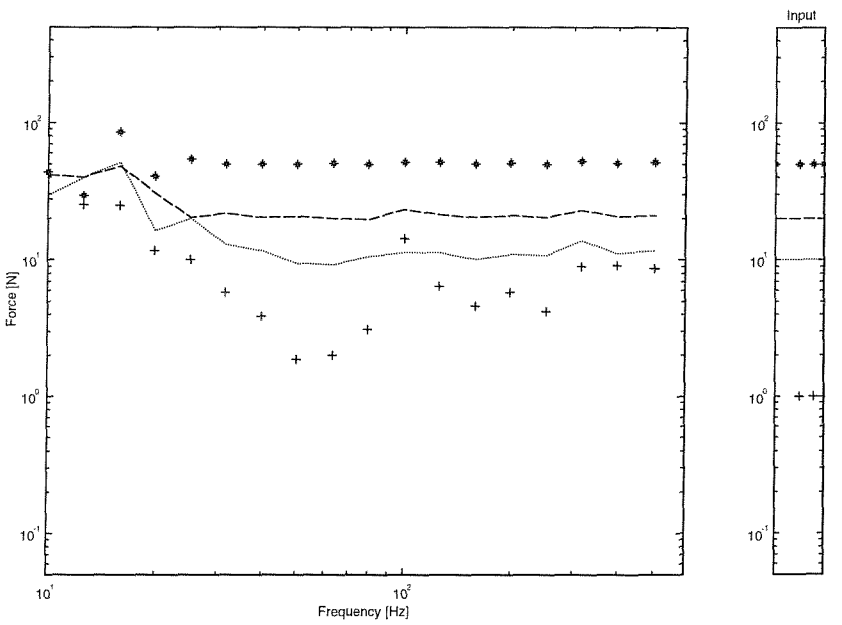

Figure 9.14. Reconstructed forces in 1/3 octave bands for 4 forces and 4 responses. Best locations selected by the method based on amplification factor are used. * * * * * *force 1,* — — — *force 2,* · · · · · · · · *force 3,* + + + + + *force 4.*

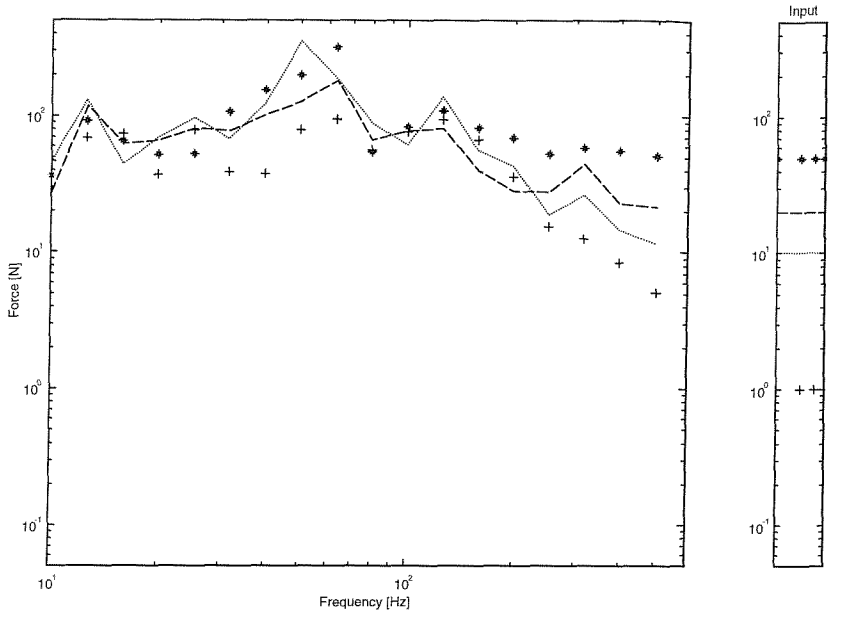

Figure 9.15. Reconstructed forces in 1/3 octave bands for 4 forces and 4 responses. Worst locations selected by the method based on amplification factor are used. * * * * * *force 1,* — — — *force 2,* · · · · · · · · *force 3,* + + + + + *force 4.*

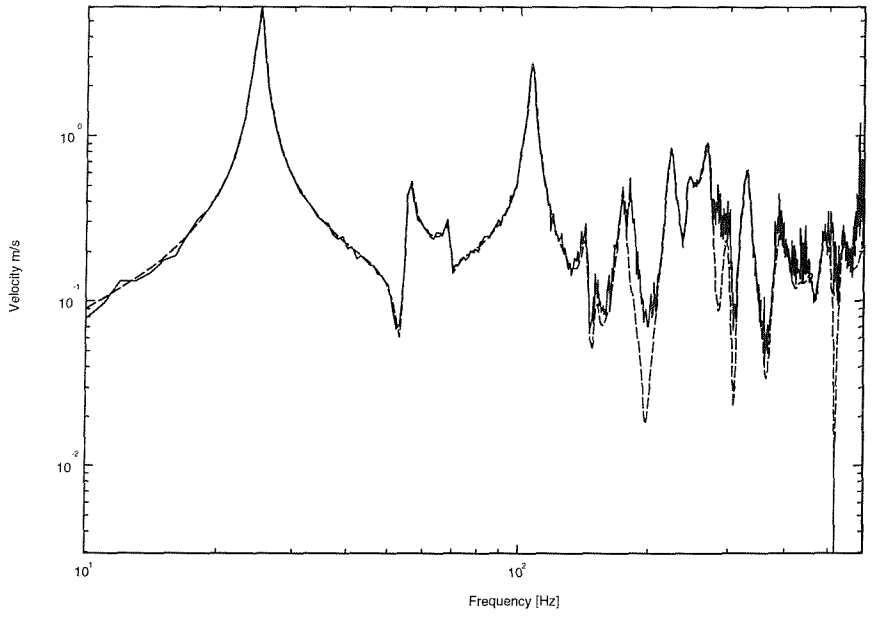

Figure 9.16. Reconstructed receiver location response using forces determined from best location case as selected by the method based on amplification factor. ———— *reconstructed,* — — — *actual.*

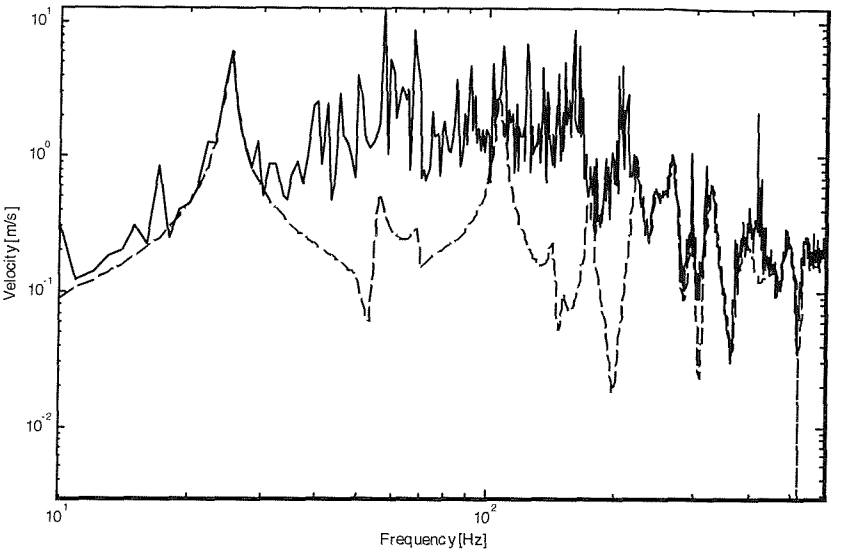

Figure 9.17. Reconstructed receiver location response using forces determined from best location case as selected by the method based on amplification factor. ———— reconstructed, — — — actual.

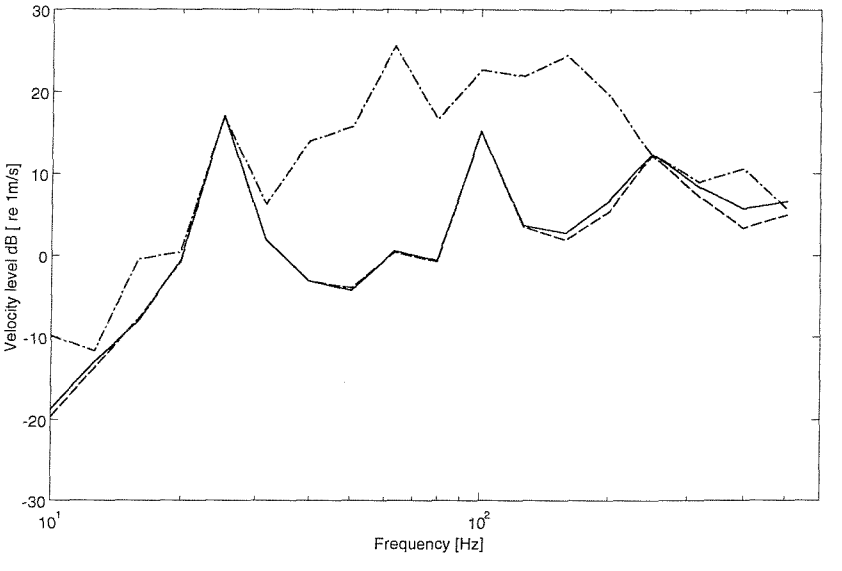

Figure 9.18. Reconstructed receiver location response in 1/3 octave bands using forces determined from best and worst location case as selected by the method based on amplification factor. ———— reconstructed response from best locations, — · — · — · reconstructed response from worst locations — — — — actual response.

9.4 COMPARISON OF AMPLIFICATION FACTOR WITH CONDITION NUMBER

The selection of measurement locations based on the 'amplification factor' needs to be checked for its validity and performance. This can be done by comparing the amplification factor with the actual average of the condition numbers across the frequency range in each case, by constructing the accelerance matrix for each combination. As mentioned earlier, this involves a large number of submatrices. If these two are reasonably well correlated then this will help to justify the use of this method.

Here, this comparison is performed using the experimental data from Chapter 8 measured on a box structure which has additional damping on its sidewalls. Twenty response locations were selected on the structure for FRF measurements. Ten of these locations were nearer to the source on the top plate, while the other ten were distributed on the sidewalls. Measurements of frequency response functions were made from 3 forcing locations to all 20 sensor locations. For this analysis, the first 15 available locations are chosen for the calculations.

In Figure 9.19 the average condition number is plotted against the 'amplification factor' for all combinations of 3 positions chosen from 15. Each point represents the result for one combination of response positions. The general correlation is observed to be quite good despite some scatter in the results. Although the minimum value of amplification factor does not necessarily correspond to the lowest average condition number, it should correspond to a small value of average condition number. Note that the computing time in this case for the estimates based on average condition number is about 10 times that for the amplification factor. This factor increases as the dimension of the matrices increases.

Further information can also be obtained from these plots about the effects of over-determination. This is achieved by varying the number of responses selected. Figure 9.20 shows results for cases where the number of selected responses is varied from 3 to 8, in each case for 3 forces. As the number of responses is increased, there is no large jump in the location of the cluster. Increasing the over-determination does not reduce the minimum condition numbers signficantly although it reduces the possibility of high condition numbers. Based on this, a suitable level of over-determination can be found. In Figure 9.21 the maximum and minimum amplification factor and average condition number are plotted for each number of responses used. These all reduce as the

level of over-determination increases. Also, the range (that is the difference between the maximum and minimum amplification factor or average condition number) reduces as the over-determination increases. In the case considered, little added benefit in the minimum values ensues when more than five responses are used in determining the forces.

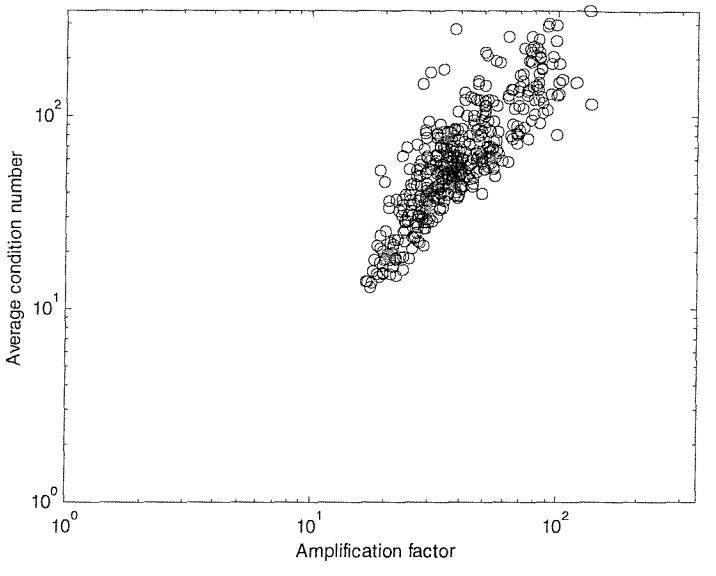

Figure 9.19. Correspondence between the amplification factor and the average condition number of the accelerance matrix for all possible 3×3 matrices chosen from 15 response positions.

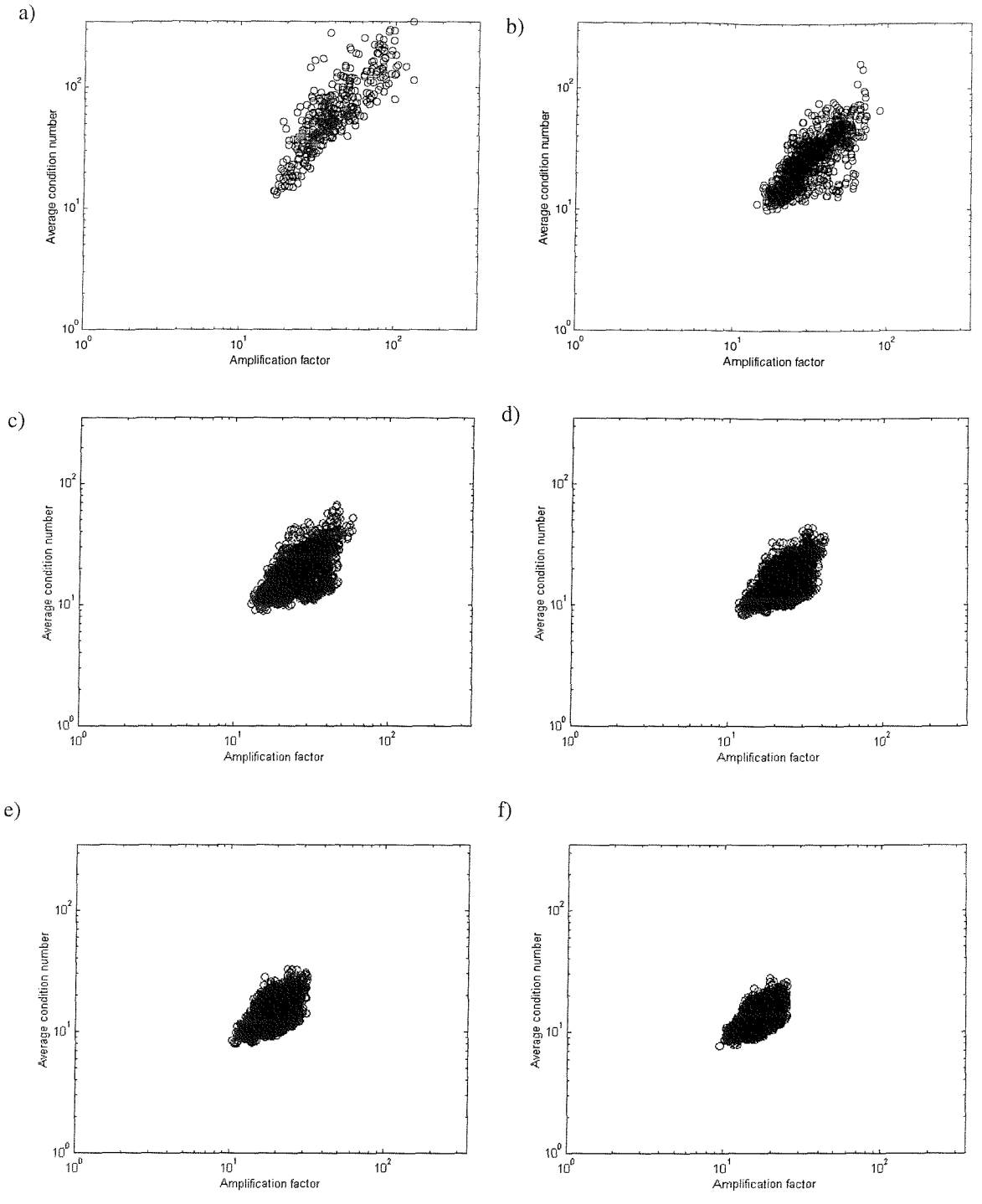

Figure 9.20. Correspondence between the amplification factor and the condition number of the accelerance matrix for different numbers of responses used chosen from 15. a) 3 responses, b) 4 responses, c) 5 responses, d) 6 responses, e) 7 responses and f) 8 responses.

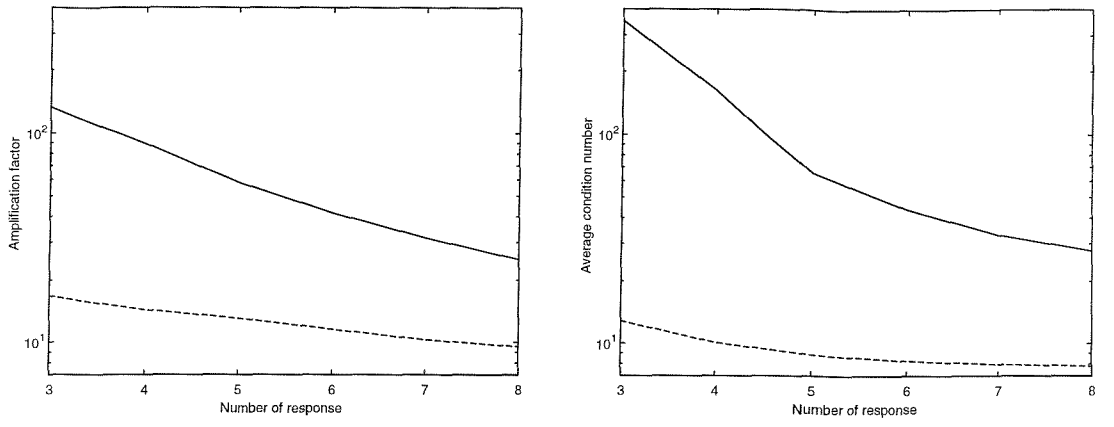

Figure 9.21. a) Variation of amplification factor for different numbers of response positions. b) Variation of average condition number for different numbers of response positions.

——————maximum and — — — —minimum.

9.5 EXPERIMENTAL VALIDATION OF SENSOR LOCATION METHOD

In this section the proposed method of sensor location is applied to the experimental data from the box structure considered in Chapter 8. Using the method of the minimum amplification factor, three positions have been selected from the 10 locations on the top plate, and from the whole set of 20. The locations selected from the experimental data are shown below.

Case 1: Out of 10 locations

Best combination	:	3	6	8
Worst combination	:	7	8	10

Case 2: Out of 20 locations

Best combination	:	3	6	8
Worst combination	:	5	13	19

It may be remarked that the 'best' combination is the same in each case.

The condition numbers for these combinations are shown in Figures 9.22 and 9.23. Comparing the results for the best positions with those for the worst positions, considerable improvement is achieved in the condition numbers for both cases considered. The improvement achieved is consistent, whether 10 or 20 responses are used, which was also observed in the numerical simulations. When more options are available, there is a greater chance of finding a large difference in condition numbers

between best and worst cases, which can be an indication that locations selected are optimal. However, it may be seen that the 'best' set of positions in Figure 9.22 does not always give lower condition numbers than the 'worst' set – see in particular the region around 150 – 200 Hz. Thus the sensor locations are not unique but are determined by the frequency range of interest.

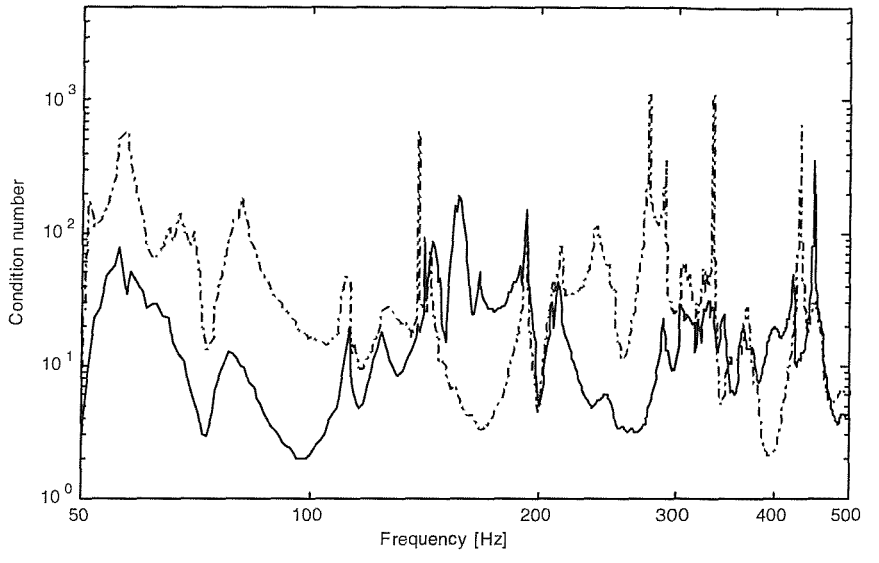

Figure 10.22. Condition numbers of best and worst locations out of 10 available locations from experimental data on box as selected by method based on amplification factor. ———— best locations, · — · — · — · worst locations.

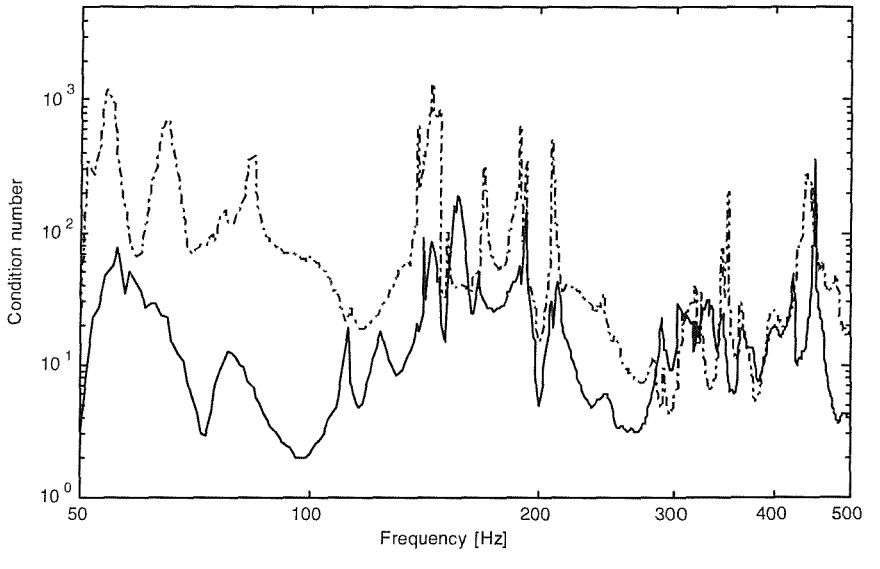

Figure 9.23. Condition numbers of best and worst locations out of 20 available locations from experimental data on box as selected by method based on amplification factor for experimental data. ———— best locations, · — · — · — · worst locations.

Based on the selected locations, operational responses were measured at the best locations 3, 6 and 8 and the worst locations 5, 13 and 19. For comparison, forces transmitted by the source through the three mountings were also measured simultaneously (see Chapter 8).

The forces determined using the worst locations are shown in Figure 9.24 in constant bands of 15 Hz (because the source had a fundamental frequency of 15 Hz). Throughout the frequency range the forces contain large errors when the worst location responses are used in reconstructing the forces. This reconstruction can be compared with that from the best locations as given in Figure 9.25. The forces are much better estimated here, even though no over-determination is applied, although they are over-estimated and appear to have some bias. The more reliable force determination from the 'best' locations appears not to translate into a good reconstruction of the overall receiver location velocity, however, as seen from the plot of differences between reconstructed and actual responses in Figure 9.26. Table 9.4 lists these differences, averaged over all 15 Hz bands. This clearly shows the improvement achieved between worst and best positions in the force estimates. Corresponding results for 4 responses are shown in Table 9.5. Compared with Table 8.1, the choice of the best 4 positions can be seen to result in forces that are as good as or better than most of the regularization techniques applied to a 4×3 matrix consisting of the worst four responses. However, the reconstructed responses are again similar for 'best' and 'worst' cases. This is mainly due to two bands 330 and 450 Hz. The latter is a peak in the condition number (see Figure 9.23). Recall that the worst four responses were used in Chapter 8 to ensure good descrimination between the methods.

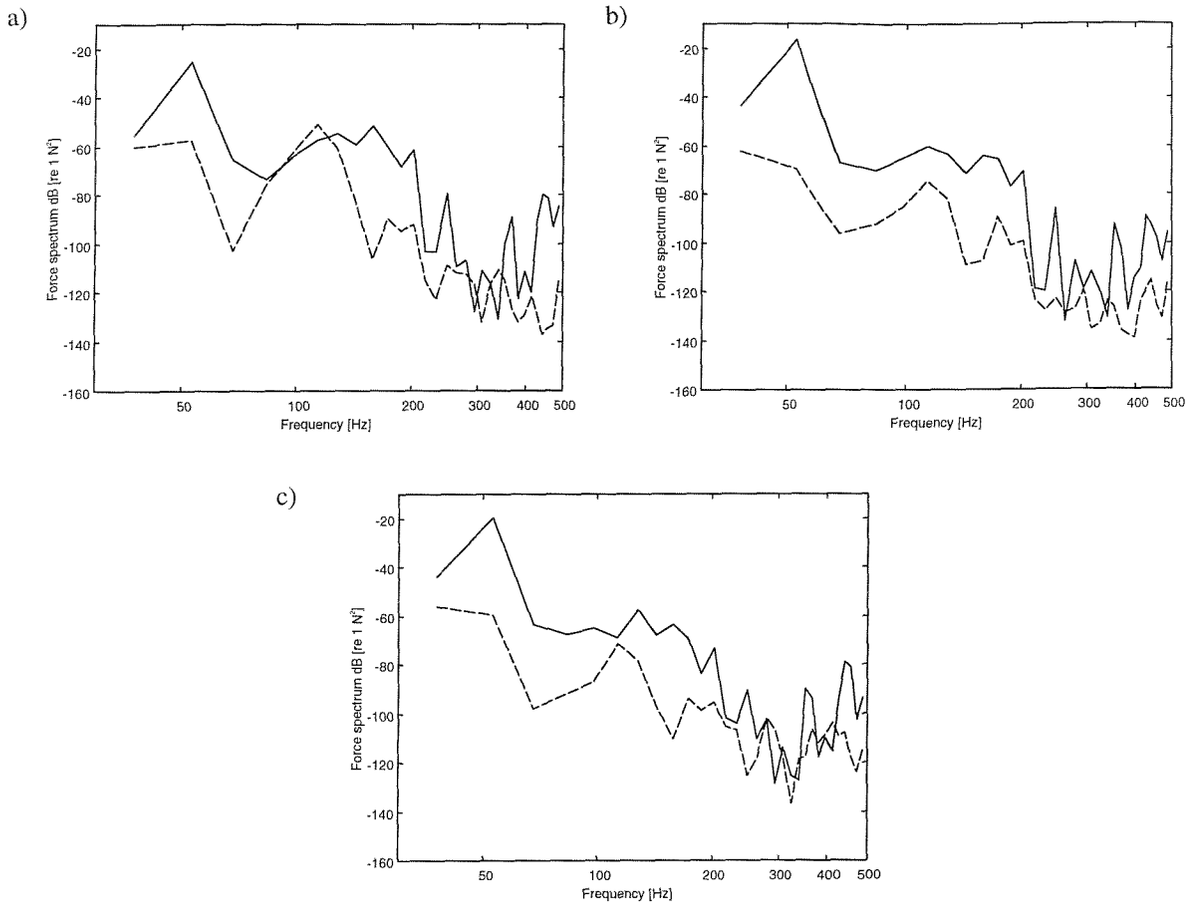

Figure 9.24. Reconstructed forces in constant bands of 15Hz for the worst 3 locations selected out of 20 potential locations from measured data on box. (a) force 1, (b) force 2 and (c) force 3. — — — — measured force, ———— reconstructed force.

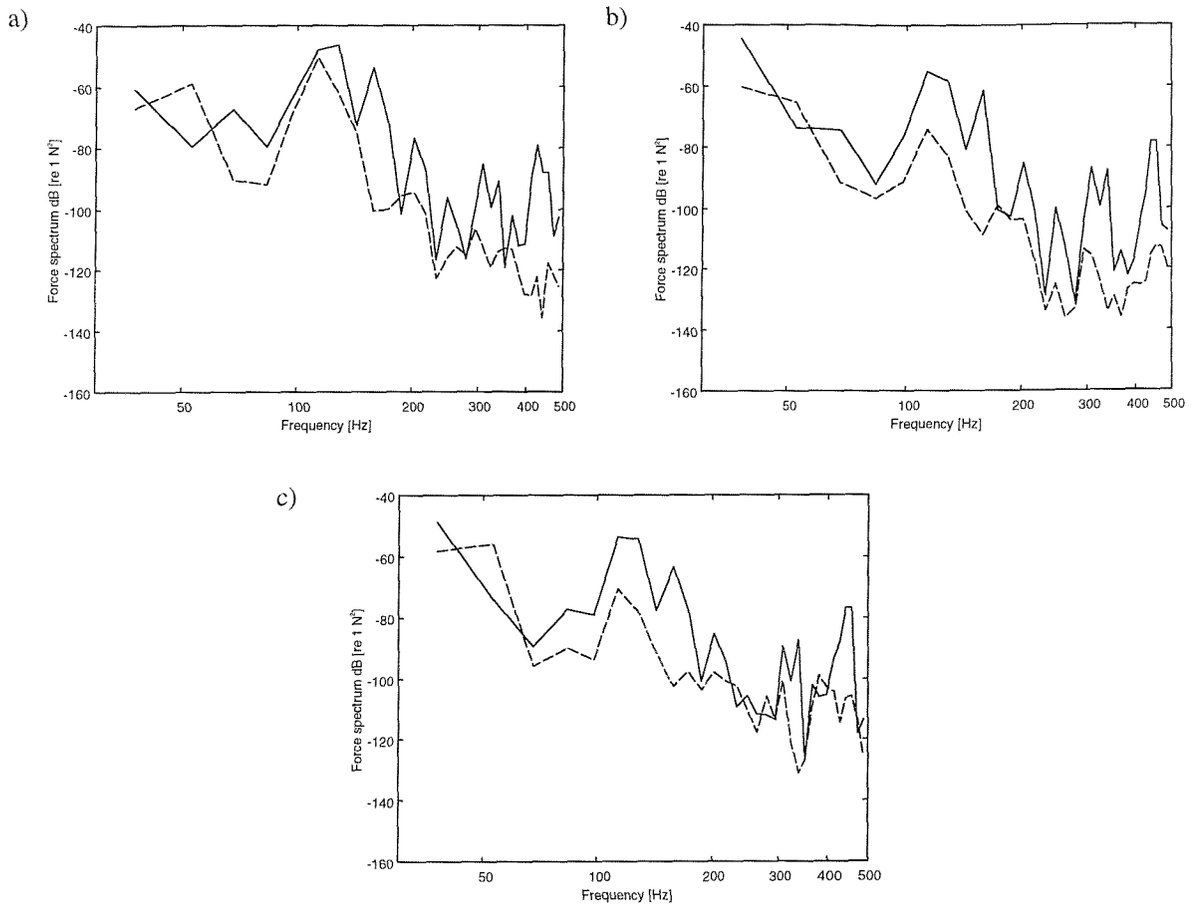

Figure 9.25. Reconstructed forces in constant bands of 15Hz for the best 3 locations selected out of 20 potential locations from measured data on box. (a) force 1, (b) force 2 and (c) force 3. — — — — measured force, ———— reconstructed force.

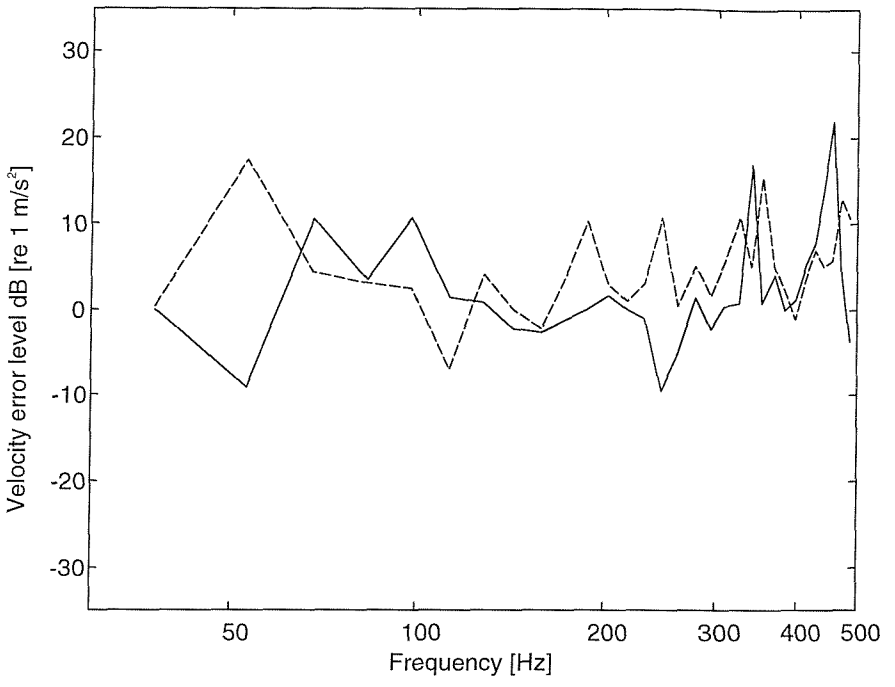

Figure 9.26. Difference between reconstructed and measured receiver response in constant bands of 15Hz for three locations chosen from 20 for experimental data on box. ———— *best locations,* — — — *worst locations.*

Table 9.4. Root mean square errors in constant bands of 15 Hz in dB in reconstructed forces and response for the best and worst case of 3 locations chosen from 20 on box based on experiments

	Force errors			Response error
Method	F1	F2	F3	
Best locations	22.0	21.7	17.4	7.1
Worst locations	27.4	25.2	22.1	7.0

Table 9.5. Root mean square errors in constant bands of 15 Hz in dB in reconstructed forces and response for the best and worst case of 4 locations chosen from 20 on box based on experiments

	Force errors			Response error
Method	F1	F2	F3	
Best locations	16.1	12.5	11.7	4.1
Worst locations	21.7	17.8	13.9	4.0

9.6 CONCLUSION AND DISCUSSION

Methods of sensor location selection from the field of modal testing have been explored. Initially numerical simulations were carried out on a rectangular simply supported flat plate. A method was proposed based on an amplification factor, which is an approximation to the summation of condition numbers of the accelerance matrices across all the frequencies. Numerical simulations were implemented to test this method. Experimental data from Chapter 8 were then used to validate the proposed method. Based on the numerical simulations and experimental validation the following conclusions can be drawn.

1. The Gram-Schmidt orthogonalization method based on impulse responses results in a varying degree of success in selecting good measurment locations. The performance improves when the number of options available is increased. The technique may not always, however, lead to optimal measurement locations. It is also not very reliable at indicating the worst sets of positions for measurements.
2. The other existing method based on experimental data, the test reference identification procedure, was studied theoretically. It was difficult to use this for the application in question since no objective quantification is available to indicate the presence of modes. This shortcoming will significantly affect the high frequency performance where visual differentiation is difficult.
3. The new approximate method based on the amplification factor results in a promising sensor location selection. Although the selection may not always be optimal, it is

generally very close to it. This method is consistent in performance whether or not a large number of optional positions are available.

4. The concept of summing the condition numbers over the frequency range allows an objective comparison to be used for selecting good locations for measuring operational responses. The effectiveness might reduce to some extent when a larger frequency range is used, as the variations in the condition numbers may be averaged out. However, if locations are selected for an over-determined system this should be less significant as over-determination tends to take care of variations at the higher frequency (see Chapter 2). This means that the sum will be influenced more by the condition numbers at low frequencies, which is where modal behaviour is stronger.
5. The proposed approximate method of calculating the amplification factor can be replaced by actual condition numbers if the problem is small enough. However, when many options are available, the selection based on the amplification factor gives results that are almost as good.
6. The amplification factor can also be used efficiently in establishing how much over-determination to apply to a problem.
7. The improvements achieved by the selection of good measurement locations appear to be greater than achieved by some of the regularization techniques studied. The advantage of measurement location selection is that, unlike regularization techniques, it does not introduce bias errors and no assumptions are made. However, for a structure with strong modal behaviour in the structure and very small FRF measurement errors, the regularization techniques may still perform well and should be used to complement the measurement location selection procedure. In this case in the region of the first few modes, selection of any combination of response locations is expected not to improve the matrix condition appreciably.

CHAPTER 10
CONCLUSIONS AND FURTHER WORK

10.1 CONCLUSIONS

The objective of this thesis has been to contribute to advancement in the solution of inverse problems in structural dynamics, specifically by the use of matrix regularization techniques and response location selection methods. For this purpose, using numerical simulations to represent measurements, an assessment has been made of the problems associated with inverse force determination, matrix regularization techniques and the optimal location selection strategies. In each case the test structure is a rectangular plate, and a wide frequency range has been used to include regions of both low and high modal overlap. Later, experiments were conducted on a hanging plate and a built-up structure to validate the findings. The main conclusions of this study are summarised in this section.

In inverse force determination, erratic force predictions may occur at frequencies where the accelerance matrix is ill-conditioned and errors are present in the measurement of operational responses and accelerances.

The condition numbers determine the degree to which noise in the inputs is magnified in the forces reconstructed using inverse methods. The condition numbers are in fact found to depend on the noise level in the FRF's. Larger noise generally reduces the condition numbers at low frequency where the modal density is very small, whereas it can increase the condition numbers at high frequencies. Over-determination of the matrix is observed to help reduce the condition numbers in the high frequency region where the modal density is large. It does not result in significant improvements in the low frequency region.

Full rank inversion or pseudo-inversion of the accelerance matrix is found to be very sensitive to the noise level present in the frequency response functions and the operational responses. They perform worst when the noise level in the FRF's is small (high condition numbers) and the noise level in the responses is large.

Of all the frequency response estimators, the H_1 estimator results in a better force reconstruction across the frequency range in the inversion process. However, this

conclusion might differ slightly depending on the noise model used to corrupt the frequency response functions and the operational responses.

In the strategy of singular value rejection, two types of threshold have been studied which are dependent on FRF errors and response errors respectively. The tolerance in terms of the numbers of standard deviations used in estimating the threshold, was observed to affect the results significantly. Using a range of $\pm$ one standard deviation was found to be more reliable in determining the lower limit for the rejection of the singular values than a larger range. The use of a concept based on the cumulative sum of singular values can generalise the singular value comparison. The performance of singular value rejection based on response errors was found to be more robust to the levels of noise present in the FRF's and the operational responses. However, the performance of this threshold reduces for the case where noise in responses is small and noise in the FRF's is large.

In the experiments on a hanging plate and the box structure, it was found that singular value rejection based on the norm of the accelerance error matrix did not improve the predictions compared with the Moore-Penrose pseudo-inverse, as the coherence corresponding to the FRF estimates was very high, resulting in very few singular values being rejected. The singular value rejection method based on the threshold related to the response error under-estimated the forces at many frequencies for the hanging plate experiment. It resulted in good estimates of forces for the box structure at high frequencies. The performance of these two thresholds, in general, was observed to depend significantly on the noise in the measured data.

A matrix perturbation technique was proposed which was found to perform well when the noise level in the operational responses is small. This method was, however, sensitive to the noise level in the responses. By combining this method with the rejection of singular values a strategy, perturbed singular value rejection, was devised that performs robustly to different noise levels in the FRF's and the operational responses. This method was observed to improve the force estimation for the hanging plate experiment where the noise in the measured responses was small. It failed to perform well for the data based on the box structure as the noise in the measured operational responses was large.

Tikhonov regularization has been explored for its performance in the structural dynamics inverse force determination problem. The weighting of singular values as

performed by Tikhonov regularization with ordinary cross validation gave better results than singular value rejection. However, ordinary cross validation was found to be sensitive to noise levels in the operational responses and FRF's, particularly the combination of small noise in FRF's and large noise in operational responses.

As an alternative to ordinary cross validation, a method referred to as selective cross validation has been proposed in the thesis. This attaches more importance to condition numbers in selecting the regularization parameter. However, as with ordinary cross validation, this was also found to be sensitive to the noise level in the responses and FRF's. To overcome the sensitivity of OCV or SCV to noise levels, biased versions of them have been developed in which a minimum value of regularization parameter is enforced. These methods of selecting the regularization parameter perform robustly for all noise levels, but they can result in some bias for low noise level cases.

Tikhonov regularization with BSCV was observed to perform robustly on the experimental data from the hanging plate and the box structure. In general, this method of regularization was found to be better on both structures than methods considered above.

An alternative means of matrix regularization, the iterative inversion has also been studied. The solution in iterative inversion is based on the principle that when an infinite number of iterations is used in a proper formulation, the solution tends to the usual mean square solution. Generally, the methods considered here to select the iteration number have been found to be robust. Iterative inversion was also found to be robust in force reconstruction based on the experimental data. However, they were found to result in bias at some frequencies. The main disadvantage of iterative inversion is that it takes much more time to execute the problem than Tikhonov regularization based on either BSCV or BOCV.

The location of the sensors on the structure to measure the FRF's and operational responses may influence the condition numbers of the accelerance matrix. A method based on an 'amplification factor' has been developed which minimises the average condition number. The performance of this method has been compared with methods used in modal testing which have been adapted to the structural inverse problem. The method based on the amplification factor appears to be reliable and performs better than

the method based on Gram-Schmidt orthogonalization. Numerical simulations on a simply supported rectangular plate confirmed this.

The improvements achieved by the selection of good measurement locations appear to be greater than achieved by some of the regularization techniques studied. The advantage of measurement location selection is that, unlike regularization techniques, it does not introduce bias errors and no assumptions are made. However, it requires the measurement of many more FRF's and processing of this data before making operational response measurements. Nevertheless it appears to be a promising approach.

10.2 RECOMMENDATIONS FOR FURTHER WORK

Although the error propagation and amplification has been addressed indirectly here, this needs further investigation of how different types of measurement errors, random and bias, interact with the matrix condition numbers resulting in force errors. For this, complete mathematical models need to be developed based on numerical simulations and measurements. This work should categorise in what situation different errors play a significant role depending on the condition numbers of the matrix. Based on this categorisation it will be possible to develop guidelines for a measurement set-up that is least sensitive to the inverse process.

The relation between the 'amplification factor' and the condition number requires a more rigorous analysis, while the summation of condition numbers across the frequency range may not be the best approach to minimising force errors globally. It also does not account for errors that propagate without much amplification. This situation might be crucial where the measurement errors are large at some locations. Alternative strategies need to be developed that are robust in selecting sensor locations which work well for all frequencies under all conditions of the measurements.

In the present work, regularization techniques have been investigated quite extensively for their suitability to inverse force determination. The regularization parameter selection needs further investigation in terms of error amplification and condition numbers. Also, other methods to select the regularization parameter such as the L curve [63] need to be investigated for their performance.

It is recommended that the methods investigated in this thesis should be applied to measurements on built-up structures, covering different damping values and structural

complexities. However for this to provide a useful validation of the techniques, it would be essential that either measured forces or some other means of establishing the 'correct' answer are available.

A range of different techniques has been studied here and it will not always be obvious to a new user which technique would give the best results. Some automation of this decision, or guidelines for the user, would be beneficial. To achieve this wider experience of using the techniques is required.

REFERENCES

1. EC directive 96/267/EC (70.157/EEC) relating to the permissible sound level and the exhaust system of motor vehicles.
2. P Scarth, 2002, Recent advances in diesel engine noise and its effect on whole vehicle noise. European conference on vehicle noise and vibration, IMechE, London.
3. DJ Thompson, 2001, Noise and vibration control I, MSc course material, ISVR.
4. LMS application notes on transfer path analysis 1995. The qualification and quantification of vibro-acoustic transfer paths. LMS International, Leuven, Belgium.
5. I-DEAS Noise path analysis, 1998 MTS system corporation.
6. JW Verheij, 1982, Multi-path sound transfer from resiliently mounted shipboard machinery. PhD Dissertation. TNO, Institute of Applied Physics.
7. JW Verheij, 1997, Inverse and reciprocity methods for machinery noise source characterisation and sound path quantification, Part 1: Sources. International Journal of Acoustics and Vibration, Vol 2, No.1, 11-20.
8. JW Verheij, 1997, Inverse and reciprocity methods for machinery noise source characterisation and sound path quantification, Part 2: Transmission paths. International Journal of Acoustics and Vibration, Vol 2, No3, 103-112.
9. MS Hardy, 2000, A methodology for calculating noise transfer functions for a vehicle cabin. European conference on vehicle noise and vibration, IMechE, London, 285-302.
10. RE Powell and W Seering, 1984, Multi-channel structural inverse filtering. Journal of Vibration, Acoustics, Stress and Reliability in Design, Transactions of the ASME, Vol 106, 22-28.
11. MHA Janssens, JW Verheij and DJ Thompson, 1999, The use of an equivalent forces method for the experimental quantification of structural sound transmission. Journal of Sound and Vibration, 226, 305-328.
12. MHA Janssens and JW Verheij, 2000, A pseudo-forces methodology to be used in characterisation of structure-borne sound sources. Applied Acoustics, 61, 285-308.

13. MHA Janssens, JW Verheij and T Loyau, 2002, Experimental example of the pseudo-forces method used in characterisation of structure-borne sound. Applied Acoustics, 63, 9-34.
14. H Van der Auweraer, K Wyckaert, W Hendricx and P Linden, 1995, Noise and vibration transfer path analysis. Proceedings International Seminar on Applied Acoustics ISAAC 6, Leuven, vol IV, 1-22.
15. D Otte, 1994, Development and evaluation of singular value analysis methodologies for studying multivariate noise and vibration problems. PhD Dissertation. Katholieke Universiteit Leuven.
16. U Fingberg and T Ahlersmeyer, 1992, Noise path analysis of structure-borne engine excitation to interior noise of a vehicle. 17th International Seminar on Modal Analysis, Leuven, Belgium, 143-152.
17. J. Romano and J.A. Lopez, 1996, Practical application of transfer path analysis to resolve structure-borne noise problems in vehicle design. Proceedings of the 21st International Seminar on Modal Analysis, Leuven, Belgium, 527-536.
18. PV Ponseele, D Lowet and F Deblaue, 1998, Psycho-Acoustic modeling and evaluation of engine orders and their transfer paths. Euro-noise 98, Munich, 743-748.
19. PV Ponseele and M Adams, 2000, The integration of sound quality in the virtual car model. European conference on vehicle noise and vibration, IMechE, London, 179-186.
20. VK Singh, Nitin Wani and VD Monkaba, 2002, Powertrain noise path analysis of a truck. European conference on vehicle noise and vibration, IMechE, London.
21. A Gillibrand and D Marshall, 2002, Road noise transfer path analysis with time domain representation. European conference on vehicle noise and vibration, IMechE, London, 157-164.
22. BJ Dobson and E Rider, 1990, A review of the indirect calculation of excitation forces from measured structural response data. Proceedings of Institution of Mechanical Engineers, 204, 69-75.
23. WM To and DJ Ewins, 1995, The role of the generalised inverse in structural dynamics, Journal of Sound and Vibration, 186(2), 185-195.

24. JA Fabunmi, March 1986, Effects of structural modes on vibratory force determination by Pseudo-inverse technique. AIAA Journal, 24 No. 3, 504-509.
25. G Desanghere and R Snoeys, 1985, Indirect identification of excitation forces by modal co-ordinate transformation. Proceedings of International Modal Analysis Conference (IMAC), 685-690.
26. P Mas and P Sas, 1994, Indirect force identification based on impedance matrix inversion: A study on statistical and deterministic accuracy, 19th International Seminar on Modal Analysis, Leuven, Belgium, 1049-1065.
27. W Hendricx, 1994, Accurate vehicle FRF measurements for indirect force determination based upon matrix inversion, 19th International Seminar on Modal Analysis, Leuven, Belgium, 1037-1048.
28. SES Karlsson, 1996, Identification of external structural loads from measured harmonic responses, Journal of Sound and Vibration, 196, 59-74.
29. H Lee and Y Park, 1995, Error analysis of indirect force determination and a regularization method to reduce force determination error. Mechanical Systems and Signal Processing 9(6), 615-633.
30. TJ Roggenkamp, 1992, An investigation of the indirect measurement of broad-band force spectra. PhD Dissertation, Purdue University.
31. TJ Roggenkamp and RJ Bernhard, 1993, Indirect measurement of multiple random force spectra, Proceedings of Inter-noise 93, Leuven, 881-884.
32. M Blau, 1999, Indirect measurement of multiple excitation spectra by FRF matrix inversion: Influence of errors in statistical estimates of FRFs and response, Acustica, 85, 464-479.
33. M Blau, 1999, Error considerations in inverse force synthesis: A closer look at the estimation of response spectra. Sixth International Congress on Sound and Vibration, Copenhagen, 2191-2198.
34. M Blau, 1997, Indirect force spectra identification by FRF Matrix Inversion : A Reliable approach based on quantitative error Models. Proceedings Inter-noise, Budapest, Hungary, 1387-1390.
35. J Biemond, RL Lagendijk and RM Mersereau, May 1990, Iterative methods for Image deblurring. Proceedings of the IEEE, 78 (5), 856-883.

36. BK Kim and JG Ih, 2000, Design of an optimal wave vector filter for enhancing the resolution of reconstructed source field by near-field acoustical holography (NAH). Journal of the Acoustical Society of America, 107 (6), 3289-3297.
37. MR Bai, 1995, Acoustical source characterisation by using Wiener filtering. Journal of the Acoustical Society of America, 97, 2657 - 2663.
38. H Fleischer and V Axelrad, 1986, Restoring an acoustic source from pressure data using Weiner filtering. Research notes, Acustica, 60, 172-175.
39. PA Nelson, 1999, Some inverse problems in acoustics. Sixth International Congress on Sound and Vibration, Copenhagen, Denmark, 7-32.
40. PA Nelson and SH Yoon, 2000, Estimation of acoustic source strength by inverse methods: Part I, conditioning of the inverse problem. Journal of Sound and Vibration 233(4), 643-668.
41. SH Yoon and PA Nelson, 2000, Estimation of acoustic source strength by inverse methods: Part II, Experimental investigation of methods for choosing regularization parameters. Journal of Sound and Vibration 233(4), 669-705.
42. E Williams, 2000, Regularization and Nearfield Acoustical Holography. Proceedings of Internoise 2000, Nice, France, 73-79.
43. GH Golub, M Heath and G Wahba, 1979, Generalized cross-validation as a method for choosing a good ridge parameter. Technometrics, 21(2), 215-223.
44. G Wahba, 1977, Practical approximate solutions to linear operator equations when data are noisy. SIAM Journal of Numerical Analysis, 14, 651-667.
45. DM Allen, 1974, The relationship between variable selection and data augmentation and a method for prediction. Technometrics, 16 (1), 125-127.
46. NP Galatsanos and AK Katsaggelos, 1992, Methods for choosing regularization parameter and estimating the noise variance in image restoration and their relation. IEEE Transactions on Image Processing, 1 (3), 322-336.
47. M Blau, 2000, Inverse force synthesis: State of the art and future research. Proceedings of Internoise 2000, Nice, France, 2401-2407.
48. YR Kim and KJ Kim, 1999, Indirect input identification by modal filter technique. Mechanical Systems and Signal Processing, 13(6), 893-910.

49. C Pezerat, JL Guyader, 2000, Identification of Vibration Sources. Applied Acoustics 61, 309-324.
50. DC Kammer, 1992, Effects of noise on sensor placement for on-orbit modal identification of large space structures. Journal of Dynamic Systems, Measurement, and Control, 15, 334-341.
51. M Papadopoulos and E Garcia, 1998, Sensor placement methodologies for dynamic testing. AIAA Journal, 36, 256-263.
52. P Avitabile and D Heselton, 1997, A new procedure for selecting modal testing reference locations. Sound and Vibration, 24-29.
53. M Saayei, O Onipede and SR Babu, 1992, Selection of Noisy measurement locations for error reduction in static parameter identification. AIAA Journal, 30, 2299-2309.
54. JET Penny, MI Friswell and SD Garvey, 1994, Automatic choice of measurement locations for dynamic testing. AIAA Journal, 32, 407-414.
55. M Blau, 1999, Force spectra identification by FRF matrix inversion: A sensor placement critarion, Journal of the Acoustical Society of America, 105 (2, part 2), pp970 (abstract only).
56. JA Fabunmi and FA Tasker, July 1988, Advanced Techniques for measuring structural mobilities. ASME Journal of Vibration, Acoustics, Stress and Reliability in Design, 110, 345-349.
57. PR White and WB Collis, 1998, Analysis of TLS frequency response function estimator. Proceedings of the 9th International Workshop on Statistical and Array Processing, Portland, Oregan, 156-159.
58. KS Hong and CB Yun, 1993, Improved method for frequency domain identification of structures. Engineering Structures, 15 (3), 179-188.
59. MJ Ratcliffe and NAJ Lieven, 1999, An investigation into the effects of frequency response function estimators on model updating. Mechanical Systems and Signal Processing 13(2), 315-334.
60. MS Kompella, P Davies, RJ Bernhard and DA Ufford, 1994, A technique to determine the number of incoherent sources contributing to the response of a system. Mechanical Systems and Signal Processing, 8(4), 363-380.

61. R Bernhard, 2000, The characterisation of Vibration sources and measurement of forces using multiple operating conditions and matrix decomposition methods. Proceedings of Internoise 2000, Nice, France, 2408-2413.
62. DC Quinn, P Cox and I Edlinger, 2000, Active path tracking - a novel method for rapid identification of structure-borne noise paths important to vehicle noise quality. IMechE European Conference on Vehicle Noise and Vibration, London, 207-215.
63. PC Hansen, Rank-Deficient and Discrete Ill-Posed Problems. SIAM, 1998.
64. CF Gerald and PO Wheatley, 1999, Applied numerical analysis. New York: Addison-Wesley.
65. GW Stewart, 1973, Introduction to Matrix Computations. Academic Press.
66. GH Golub and CF Van Loan 1983 Matrix computations. Oxford: North Oxford Academic, 1st edition.
67. RL Branham, Jr. 1990 Scientific data analysis: An introduction to overdetermined systems. New York: Spinger-Verlag, 1st edition.
68. E Kreyszig, 1979 Advanced Engineering Mathematics. New York: John Wiley and Sons.
69. KG McConnell, 1995 Vibration Testing: Theory and practice. New York: John Wiley and Sons, 1st edition.
70. J.L. Bendat and A.G. Piersol 1993 Engineering application of correlation and spectral analysis. New York : Wiley interscience. 2nd edition.
71. D.E. Newland 1984 An introduction to random vibrations and spectral analysis. 2nd edition, Longman.
72. G.B. Warburton 1976 The dynamical behaviour of structures. Oxford : Pergamon, 2nd edition.
73. D.J. Gorman 1982 Free vibration analysis of rectangular plates. New York: Elsevier, 1st edition.
74. AW Leissa, 1969, Vibration of plates. NASA report SP-160.
75. L. Cremer, M. Heckl / translated and revised by E.E. Ungar 1988 Structure-borne sound: structural vibrations and sound radiation at audio frequencies. Berlin: Springer. 2nd edition.

76. SP Timoshenko and JN Goodier, 1970 Theory of Elasticity. Singapore: McGraw-Hill, 3rd edition.
77. AN Thite and DJ Thompson, May 2000, Study of indirect force determination and transfer path analysis using numerical simulations for a flat plate. ISVR Technical Memorandum no. 851.
78. A Tikhonov and V Arsenin, 1977, Solution of Ill-Posed Problems. Washington DC: Winston.
79. PA Nelson and SJ Elliott, 1992, Active Control of Sound. London: Academic Press, 416-420.
80. AN Thite and DJ Thompson, May 2000, Experimental validation of force identification techniques. ISVR Technical memorandum no. 862.
81. C. Hales, 2000, Vibration isolation demonstration. ISVR undergraduate project report, University of Southampton.

APPENDIX A NORMS AND CONDITION NUMBER

This appendix contains brief theoretical background of matrix algebra that is relevant to this thesis. The commonly used matrix terms such as norms, condition numbers, rank and singular value decomposition are introduced here, taken from well established literature in matrix theory [64-68]. For further reading the book by CF Gerald and PO Wheatley is especially recommended [64].

A1 Vector norm

The norm of a vector can be thought as its length or magnitude. There are several ways of defining the vector norm. The generalised formulation for vector norm is given by

$$\|x\|_p = \left(\sum_{i=1}^{k} x_i^{\ p} \right)^{1/p} \tag{A1}$$

where $x = (x_1, x_2, ..., x_k)$.

When p takes the value of 2, it results in most familiar Euclidean norm or 2-norm.

A2 Matrix norm

The matrix p norm is given by

$$\|A\|_p = \max_{\|x\|_p = 1} \|Ax\|_p \tag{A2}$$

where x is a vector, the p-norm of which is 1. The calculation of the 2-norm is more complicated than other p-norms of the matrix. However, it can be shown [64] that the 2-norm is the square root of the largest eigenvalue of $A^H A$ or the largest singular value of A. Another type of matrix norm is the Frobenius norm, given by

$$\|A\|_F = \sqrt{s_1^{\ 2} + s_1^{\ 2} + ... + s_n^{\ 2}} \tag{A3}$$

where s_1, s_2,....., s_n are the singular values of A (see below). For a vector, the Frobenius norm is equivalent to the 2-norm.

A3 Hermitian transpose

Hermitian transpose of a matrix is given by

$$A^H = A^{*T} \tag{A4}$$

where * indicates the complex conjugate and T represents the transpose operation.

A4 Singular value decomposition

Any matrix can be decomposed [65] into the form

$$A = USV^H \tag{A5}$$

where U and V are unitary matrices containing eigen vectors of AA^H and A^HA respectively, and S is a diagonal matrix containing singular values of the matrix A which are square roots of the eigen values of A^HA. Thus U and V represent 'rotations' in vector space and S represents the magnitude information of the matrix. U satisfies $U^HU = I$ and V satisfies $V^HV = I$.

If A is a square matrix and full rank its inverse is given by

$$A^{-1} = VS^{-1}U^H \tag{A6}$$

Otherwise (A6) represents pseudo-inverse. If singular values are zeros the corresponding elements of S^{-1} should be replaced by 0.

A5 Rank of the matrix

The rank of a matrix is the dimension of the matrix corresponding to the number of linearly independent rows or columns of the matrix, or to the number of nonzero singular values of the matrix. If the rank of a square matrix is less than its dimension the matrix is singular, that is its inverse does not exist, and its condition number is infinite (see below).

A6 Condition number

The condition number of a matrix determines the invertability of the matrix. It is given by

$$\kappa = \frac{\|A\|}{\left\|A^{-1}\right\|} \tag{A7}$$

For the 2-norm equation (A7) becomes

$$\kappa = \frac{s_1}{s_n} \tag{A8}$$

which is the ratio of the largest singular value to the smallest singular value of the matrix. The condition number is always greater than or equal to 1. A large condition number indicates that matrix is nearly singular.

APPENDIX B ORTHOGONALIZATION

B1 GRAM-SCHMIDT ORTHOGONALIZATION

Any set of vectors $[a]$ can be converted into set of orthogonal vectors $[u]$ by the Gram-Schmidt process [66]. The process is given below.

1. Initially the first vector $\{a_1\}$ is normalised and written as the first orthogonalized vector $\{u_1\}$ as below

$$\{u_1\} = \frac{\{a_1\}}{\|\{a_1\}\|_2} \tag{B1}$$

2. All vectors other than the first vector in the matrix $[a]$ are made independent with respect to the first vector by writing $a_{ui} = a_i - \left(a_i u_1^H\right) u_1$ for $i = 2,3,\ldots m$.

3. Then the first vector of $[a_u]$ is normalized as in step 1.

4. Steps 1 to 3 are repeated until all vectors are exhausted in $[a]$. The final result is the set of orthogonal vectors $[u]$ from set of vectors $[a]$.

B2 FISHER INFORMATION MATRIX

The Fisher information matrix M_I is constructed [51] from a modal matrix ψ as below

$$M_I = \psi\psi^T \tag{B2}$$

The matrix ψ contains mode shape coefficients for each co-ordinate (location of response measurement) on its row. The information matrix contains information about the interdependence of the elements of the modal matrix.

APPENDIX C INVERSE FORCE DETERMINATION USING SPECTRAL MATRIX

C1 Spectral matrices

Spectral matrices of operational responses S_{aa} and forces S_{ff} are constructed as, for 3 forces and 3 responses

$$S_{aa} = \begin{bmatrix} S_{a1a1} & S_{a2a1} & S_{a3a1} \\ S_{a1a2} & S_{a2a2} & S_{a3a2} \\ S_{a1a3} & S_{a2a3} & S_{a3a3} \end{bmatrix} \tag{C1}$$

$$S_{ff} = \begin{bmatrix} S_{f1f1} & S_{f2f1} & S_{f3f1} \\ S_{f1f2} & S_{f2f2} & S_{f3f2} \\ S_{f1f3} & S_{f2f3} & S_{f3f3} \end{bmatrix} \tag{C2}$$

These spectral matrices contain auto spectra on the diagonal and cross spectra elsewhere. Given an accelerance matrix A, force and response spectra are related as

$$S_{aa} = AS_{ff}A^H \tag{C3}$$

C2 Full rank inverse

If the accelerance matrix A is square and full rank, then given a response spectral matrix, forces can determined by matrix inversion. The force spectral matrix is therefore given by

$$S_{ff} = A^{-1}S_{aa}\left(A^{-1}\right)^H \tag{C4}$$

C3 Pseudo-inverse

If the accelerance matrix is rectangular i.e. the system is over-determined or it is rank deficient, the pseudo-inverse of the matrix is used to obtain the force spectral matrix. In this case the force spectral matrix is given by

$$S_{ff} = \left(A^H A\right)^{-1} A^H S_{aa}\left(\left(A^H A\right)^{-1} A^H\right)^H \tag{C5}$$

C4 Tikhonov regularization

The corresponding expression for force spectral matrix with the application of Tikhonov regularization is given by

$$S_{ff} = \left(A^H A + I\lambda\right)^{-1} A^H S_{aa} \left(\left(A^H A + I\lambda\right)^{-1} A^H\right)^H \tag{C6}$$

APPENDIX D

DIFFERENT ESTIMATORS OF FREQUENCY RESPONSE FUNCTIONS

The frequency response function between a forcing location and a response measurement location can be estimated in several ways. The estimators developed [56-59] try to improve the accuracy at resonances or anti-resonances or both. Five of these estimators are given below.

D1 H_1 estimator

This is a most popular estimator of the frequency response function and is based on the least square technique to reduce the effect of noise on the output. It is given by [69-71]

$$H_1 = \frac{S_{xy}}{S_{xx}} \tag{D1}$$

where $S_{xx} = \frac{1}{m}\sum_{i=1}^{m} X_i^*(f)X_i(f)$ and $S_{xy} = \frac{1}{m}\sum_{i=1}^{m} X_i^*(f)Y_i(f)$

and $X(f)$ and $Y(f)$ are Fourier transforms of $x(t)$ and $y(t)$ respectively and * indicates conjugation.

H_1 minimizes the effect of noise in the output. Provided that the input is noise-free, the H_1 estimator calculates an un-biased estimate of the frequency response function. At a resonance, as the input strength required for a reasonable response is very low, the noise floor may affect the input measurement. This results in the over-estimation of the auto spectrum of $x(t)$ as noise power also gets added to the signal. Hence, the FRF estimator H_1 is biased and less than the actual result at the resonances. Even at antiresonance H_1 is biased but the amount of bias is very small since the noise in the measured force is much less.

Note : It is assumed that the noise in the input and output are not correlated and hence the cross spectrum is unbiased for a large number of averages.

D2 H_2 estimator

This estimator is calculated based on a least square technique to reduce the effect of noise in the input. It is given by [70]

$$H_2 = \frac{S_{yy}}{S_{xy}} \tag{D2}$$

where $S_{yy} = \frac{1}{m}\sum_{i=1}^{m} Y_i^*(f)Y_i(f)$. H_2 minimizes the effect of noise in the input. Provided that the output is noise-free, the H_2 estimator calculates an un-biased estimate of the frequency response function. At a resonance, as the response is very large, the effect of the noise floor is minimal and hence the estimator approaches the actual FRF. For the estimate to be unbiased, the noise floor should be considerably lower than the response. This condition means that if the response is small enough to be corrupted by the noise floor, even at resonance, the estimate would be biased. At any frequency as the noise power gets added to the actual output, the auto spectrum of the output is over-estimated. This over-estimation depends on the signal-to-noise ratio. The signal-to-noise ratio of the response can be very low at antiresonance. Hence, at antiresonance the H_2 estimator would be biased and would be greater than the actual FRF. Even at resonance the H_2 is biased but the amount of bias is very small since the signal to noise ratio is large.

NB : H_1 always under-estimates the FRF, but at anti-resonance the bias error is low and the FRF approaches the actual one.

H_2 always over-estimates the FRF, but at resonance the bias error is low and the FRF approaches the actual one.

D3 H_v estimator

This estimator evaluates the FRF based on the minimization of the effect of noise on both input and output by a total least squares method and is called an unbiased estimator [57]. The estimator is given by

$$H_v = \frac{S_{yy} - k_f S_{xx} + \sqrt{\left(k_f S_{xx} - S_{yy}\right)^2 + 4k_f S_{xy} S_{yx}}}{2S_{yx}} \tag{D3}$$

where $k_f = \frac{S_{nn}}{S_{mm}}$, is a ratio of input to output noise power. When the noise ratio tends to 0, the estimator approaches H_2 and if it tends to infinity it approaches H_1. In all other cases, where a significant amount of noise exists in both input and output, the estimator

lies between H_2 and H_1. The major disadvantage with this estimator is that the ratio of noises has to be known beforehand, which in general is difficult to estimate reliably.

D4 H_4 estimator

It is also possible to obtain a total least squares-based estimator in terms of H_2 and H_1. The estimator [56] in this case is given as

$$H_4 = \frac{H_2\left[\frac{\gamma^2 F}{|H_1|^2}+1\right]}{\frac{F}{|H_1|^2}+1} \tag{D4}$$

where $F = \frac{\int_{\omega_1}^{\omega_2} |S_{xy}|^2 d\omega}{\int_{\omega_1}^{\omega_2} |S_{xx}|^2 d\omega}$ and the coherence $\gamma^2 = \frac{|S_{xy}|^2}{S_{xx}.S_{yy}}$.The weighting function F is formulated such that higher weight is given to H_2 at the resonances and to H_1 at antiresonances. Reasonably good results are obtained with a constant value of F over a large frequency range [56]. However, further experiments indicated that this cannot give a good estimation either at resonance or antiresonance point. According to [56] rather than using a constant F, the weighting should be such that the ratio of F to H_1 approaches zero for resonance and infinity at antiresonance. The optimal value of F at each natural frequency is found to be inversely proportional to the imaginary part of H_2.

D5 H_s estimator

If the signal-to-noise ratio is small, H_4 tends to have large errors at some frequencies. To overcome this difficulty, in [58] it is suggested to use a different weighing function as given below

$$H_s = H_1(1-W) + H_2 W \tag{D5}$$

where $W = e^{\left(-\left(\frac{\frac{\omega_o}{\omega_n}-1}{\alpha}\right)^2\right)}$ and $\omega_o = 0,1,.....2\omega_n$. Here, the weighting is exponential and has a value 1 at resonance and reduces to zero exponentially at all other points. The exponential decay is inversely proportional to the damping factor [58], which in turn determines the magnitude of α. This estimator can give good results in the region of simple modal behaviour. Under multi-modal behaviour (high modal overlap), finding the weighting function at each frequency would be difficult.

The major assumption in the H_s and H_4 estimators is that H_1 is unbiased at antiresonance and H_2 at resonance. In the majority of the cases where modal behaviour is predominant this assumption may be true. However, when the response at resonance is not so dominant or the force required at antiresonance is not high enough to be well clear of the noise floor, then this assumption would be violated and the estimator would still be biased.

APPENDIX E FORMULATION OF ITERATIVE INVERSION

E1 DERIVATION

Iterative inversion [35] can be applied to force identification as follows. Given a k^{th} estimate of the forces, $\hat{F}_k$, the k+1th estimate is generated as

$$\hat{F}_{k+1} = \hat{F}_k + \beta\hat{A}^H\left(\hat{a} - \hat{A}\hat{F}_k\right)$$

where the term in brackets is the difference between the reconstructed response $\hat{A}\hat{F}$ and the measured response $\hat{a}$ which is multiplied by the convergence factor β and $\hat{A}$. This can be rearranged to give

$$\hat{F}_{k+1} = \beta\hat{A}^H\hat{a} + \left(I - \beta\hat{A}^H\hat{A}\right)\hat{F}_k \tag{E1}$$

where I is the unit matrix. The first approximation for the force vector is taken as

$$\hat{F}_0 = \beta\hat{A}^H\hat{a}$$

Therefore from (E1)

$$\hat{F}_1 = \beta\hat{A}^H\hat{a} + \left(I - \beta\hat{A}^H\hat{A}\right)\beta\hat{A}^H\hat{a} \tag{E2a}$$

and

$$\hat{F}_2 = \beta\hat{A}^H\hat{a} + \left(I - \beta\hat{A}^H\hat{A}\right)\beta\hat{A}^H\hat{a} + \left(I - \beta\hat{A}^H\hat{A}\right)\left(I - \beta\hat{A}^H\hat{A}\right)\beta\hat{A}^H\hat{a} \tag{E2b}$$

and so on. From equation (E2) it can be seen that this forms a geometric series with a geometric ratio of $\left(I - \beta\hat{A}^H\hat{A}\right)$. Therefore, since $1 + n + n^2 + \ldots\ldots + n^k = \dfrac{\left(1 - n^{k+1}\right)}{(1-n)}$ the k^{th} term can be written as

$$\hat{F}_k = \beta\left(I - \left(I - \beta\hat{A}^H\hat{A}\right)\right)^{-1}\left(I - \left(I - \beta\hat{A}^H\hat{A}\right)^{k+1}\right)\hat{A}^H\hat{a} \tag{E3}$$

The solution converges for an infinite number of iterations only when

$$\left(I - \beta\hat{A}^H\hat{A}\right)^{k+1} \to [0] \quad \text{as} \quad k \to \infty$$

In the limiting case (when k tends to infinity), therefore from (E3)

$$\hat{F}_\infty = \beta\left(\beta\hat{A}^H\hat{A}\right)^{-1}\hat{A}^H\hat{a}$$

$$= \left(\hat{A}^H\hat{A}\right)^{-1}\hat{A}^H\hat{a}$$

This is the Moore-Penrose pseudo-inverse (equation (2.13)) which minimizes the mean square error

$$\left|\hat{A}\hat{F}_{\infty} - \hat{a}\right|^2$$

E2 ALTERNATIVE FORMULATION

For simplicity (E3) can also be written as

$$\hat{F}_k = \beta \sum_{r=0}^{k} \left(I - \beta \hat{A}^H \hat{A}\right)^r \hat{A}^H \hat{a} \tag{E4}$$

Using singular value decomposition of the matrix $\hat{A} = USV^H$

$$\hat{F}_k = \beta \sum_{r=0}^{k} \left(I - \beta V \Lambda V^H\right)^r V S^T U^H \hat{a}$$

where $\Lambda = S^T S$. This can be written as

$$\hat{F}_k = \beta \sum_{r=0}^{k} \left(VV^H - \beta V \Lambda V^H\right)^r V S^T U^H \hat{a} \tag{E5}$$

Note that $\left(VV^H - \beta V \Lambda V^H\right)^r = V(I - \beta\Lambda)V^H . V(I - \beta\Lambda)V^H ..... V(I - \beta\Lambda)V^H$

$$= V(I - \beta\Lambda)^r V^H \quad \text{since} \quad V^H V = I$$

Therefore (E5) can be written as

$$\hat{F}_k = \beta \sum_{r=0}^{k} V(I - \beta\Lambda)^r V^H V S^T U^H \hat{a}$$

$$\hat{F}_k = \beta \sum_{r=0}^{k} V(I - \beta\Lambda)^r S^T U^H \hat{a}$$

This equation can be simplified using geometric series as

$$\hat{F}_k = \beta V \left(I - (I - \beta\Lambda)^{k+1}\right)\left(I - (I - \beta\Lambda)\right)^{-1} S^T U^H \hat{a}$$

$$= \beta V \left(I - (I - \beta\Lambda)^{k+1}\right)(\beta\Lambda)^{-1} S^T U^H \hat{a}$$

$$= V \left(I - (I - \beta\Lambda)^{k+1}\right)\beta\left(\beta S^T S\right)^{-1} S^T U^H \hat{a}$$

$$= V \left(I - (I - \beta\Lambda)^{k+1}\right) S^{-1} U^H \hat{a}$$

Multiplication of the term in brackets, and S^{-1}, results in a diagonal matrix and $(m\text{-}n)$ columns of zeros so the above equation can be written as

$$\hat{F}_k = V \left[diag\left(\frac{1 - \left(1 - \beta s_1^2\right)^{k+1}}{s_1}, \ldots \frac{1 - \left(1 - \beta s_n^2\right)^{k+1}}{s_n} \right) \middle| [0]_{n \times m-n} \right] U^H \hat{a} \tag{E6}$$

where n is the rank of the accelerance matrix. Equation (E6) can be further simplified as

$$\hat{F}_k = V[diag(\psi_1,.....\psi_n)|\,[0]_{n\times m-n}]U^H\hat{a} \tag{E7}$$

where $\psi_i = \dfrac{1-(1-\beta s_i^2)^{k+1}}{s_i}$ for i=1,2,.....n (E8)

Comparing this with equation (3.2) reveals that iterative inversion can be seen as an alternative means of regularizing the inverse of $\hat{A}$, replacing s_i^{-1} by $\psi_i(k)$.

E3. BASIS FOR NUMBER OF ITERATIONS

To find the optimum number of iterations in order to minimize the combined error it is necessary to formulate expressions for the bias error and the variance. The expressions can be derived as follows [36]. The reconstructed operational responses derived from the forces determined are given by

$$\begin{aligned}\tilde{a} = \hat{A}\hat{F} &= USV^H V[diag(\psi_1,.....\psi_n)|[0]_{n\times m-n}]U^H\hat{a}\\ &= Udiag(\phi_1,.....\phi_n,0_{n+1},...0_m)U^H\hat{a} \qquad \text{(E9)}\\ &= \delta_k\hat{a} \qquad \text{(E10)}\end{aligned}$$

where $\phi_i = 1-(1-\beta s_i^2)^{k+1}$ with $\delta_k = Udiag(\phi_1,.....\phi_n,0_{n+1},...0_m)U^H$.

Therefore the overall mean square error of the estimation is given by

$$MSE = \varepsilon_k^2 = E[(\tilde{a}-a)^H(\tilde{a}-a)]$$

where $a = AF$ is the exact operational response and E signifies the expected value

$$\begin{aligned}\varepsilon_k^2 &= E[(\delta_k\hat{a}-a)^H(\delta_k\hat{a}-a)]\\ &= E[|\delta_k\hat{a}|^2]+|AF|^2 - E[(\delta_k\hat{a})^H]AF - (AF)^H E[\delta_k\hat{a}]\\ &= E[|\delta_k\hat{a}|^2]+|AF|^2 - 2\,\mathrm{Re}\{E[(\delta_k\hat{a})^H]AF\}\end{aligned}$$

Adding and subtracting $|E[(\delta_k\hat{a})]|^2$ to this equation gives

$$\varepsilon_k^2 = E[|\delta_k\hat{a}|^2]-|E[(\delta_k\hat{a})]|^2+|E[(\delta_k\hat{a})]|^2+|AF|^2-2\,\mathrm{Re}\{E[(\delta_k\hat{a})^H]AF\}$$

Since (assuming the measurement of $\hat{a}$ is unbiased) $E[(\delta_k\hat{a})] = \delta_k AF$, the first two terms in the above equation can be simplified as

$$E[|\delta_k\hat{a}|^2]-|E[(\delta_k\hat{a})]|^2 = E[|\delta_k\hat{a}|^2]+|\delta_k AF|^2-2\,\mathrm{Re}\{(E[\delta_k\hat{a}])^H\delta_k AF\}$$

$$= E\left[(\delta_k \hat{a} - \delta_k AF)^H (\delta_k \hat{a} - \delta_k AF)\right]$$

Similarly the last three terms can be simplified as

$$|E[(\delta_k \hat{a})]|^2 + |AF|^2 - 2\mathrm{Re}\left\{E\left[(\delta_k \hat{a})^H\right] AF\right\} = |\delta_k AF|^2 + |AF|^2 - 2\mathrm{Re}\left\{(\delta_k AF)^H AF\right\}$$
$$= (\delta_k AF - AF)^H (\delta_k AF - AF)$$

Therefore the expression for the MSE can be written as

$$\varepsilon_k^2 = E\left[(\delta_k \hat{a} - \delta_k AF)^H (\delta_k \hat{a} - \delta_k AF)\right] + (\delta_k AF - AF)^H (\delta_k AF - AF)$$
$$= E\left[(\delta_k \{\hat{a} - AF\})^H (\delta_k \{\hat{a} - AF\})\right] + ((\delta_k - I)AF)^H ((\delta_k - I)AF)$$
$$= E\left[trace\left\{(\delta_k \{\hat{a} - AF\})(\delta_k \{\hat{a} - AF\})^H\right\}\right] + (AF)^H (\delta_k - I)^H (\delta_k - I)AF$$
$$= E\left[trace\left\{\delta_k (\hat{a} - AF)(\hat{a} - AF)^H \delta_k{}^H\right\}\right] + (AF)^H (\delta_k - I)^H (\delta_k - I)AF \qquad \text{(E11)}$$

If it can be assumed that same variance σ^2 exists for all the measurement points, this reduces to

$$\varepsilon_k^2 = \sigma^2 \sum_{i=1}^{n} \phi_i + (AF)^H (\delta_k - I)^H (\delta_k - I)AF \qquad \text{(E12)}$$

where ϕ is defined in (E10).

The above equation cannot be quantified since 'F' is unknown. The second term, however, can be simplified as follows. The actual bias error is given by

$$b = (\delta_k - I)AF$$

whilst, the estimated bias error is given by

$$\hat{b} = (\delta_k - I)\hat{a}$$

The variance of the estimated bias error from the true bias error can be obtained (assuming $E[\hat{b}] = b$) as

$$E\left[(\hat{b} - b)^H (\hat{b} - b)\right] = E\left[(\hat{a} - AF)^H (\delta_k - I)^H (\delta_k - I)(\hat{a} - AF)\right] \qquad \text{(E13)}$$
$$= E\left[trace\left\{(\delta_k - I)(\hat{a} - AF)(\hat{a} - AF)^H (\delta_k - I)^H\right\}\right]$$

Again with the assumption that the variance σ^2 is the same for all the acceleration measurements, the above equation can be simplified as

$$E\left[(\hat{b} - b)^H (\hat{b} - b)\right] = \sigma^2 E\left[trace\left\{U(diag(\phi_1, ..\phi_n, 0_{n+1}..0_m) - I)(diag(\phi_1, ..\phi_n, 0_{n+1}..0_m) - I)^H U^H\right\}\right]$$
$$= \sigma^2 E\left[trace\left\{U\left(diag(\phi_1{}^2, ..\phi_n{}^2, 0_{n+1}..0_m) - 2diag(\phi_1, ..\phi_n, 0_{n+1}..0_m) + I\right)^H U^H\right\}\right]$$

$$= \sigma^2 \left(\sum_{i=1}^{n} \phi_i^{\,2} - 2\sum_{i=1}^{n} \phi_i + n \right) \tag{E14}$$

The left hand side of (E14) can also be simplified as

$$E\left[(\hat{b}-b)^H(\hat{b}-b)\right] = E\left[\hat{b}^H\hat{b}\right] + E\left[b^H b\right] - 2\,\mathrm{Re}\left\{E\left[\hat{b}^H b\right]\right\}$$

As it has already been assumed that $E\left[\hat{b}\right] = b$, therefore

$$E\left[(\hat{b}-b)^H(\hat{b}-b)\right] = E\left[\hat{b}^H\hat{b}\right] - b^H b$$

Using (E14)

$$E\left[\hat{b}^H\hat{b}\right] - b^H b = \sigma^2 \left(\sum_{i=1}^{n} \phi_i^{\,2} - 2\sum_{i=1}^{n} \phi_i + n \right)$$

$$\Rightarrow \qquad b^H b = E\left[\hat{b}^H\hat{b}\right] - \sigma^2 \left(\sum_{i=1}^{n} \phi_i^{\,2} - 2\sum_{i=1}^{n} \phi_i + n \right) \tag{E15}$$

Combining the above equation with the earlier expression (E12)

$$\varepsilon_k^2 = \sigma^2 \left(2\sum_{i=1}^{n} \phi_i - n \right) + E\left[\hat{b}^H\hat{b}\right]$$

Since

$$E\left[\hat{b}^H\hat{b}\right] = \hat{b}^H\hat{b} \tag{E16}$$

the mean square error can finally be written as

$$\varepsilon_k^2 = \sigma^2 \left(2\sum_{i=1}^{n} \phi_i - n \right) + \hat{b}^H\hat{b} \tag{E17}$$